Time-Dependent Tensile Properties of ETFE Foils

by

Linda Charbonneau

A thesis
presented to the University of Waterloo
in fulfilment of the
thesis requirement for the degree of
Master of Applied Science
in
Civil Engineering

Waterloo, Ontario, Canada, 2011

I hereby declare that I am the sole author of this thesis. This is a true copy of the thesis, including any required final revisions, as accepted by my examiners.

I understand that my thesis may be made electronically available to the public.

Abstract

The purpose of this thesis is to provide an overview of ETFE foil, as it applies to pneumatic cushion cladding, with a focus on creep behavior of the material.

Characteristics of ETFE, including weight, optics, insulation, flexibility, environmental properties, fire performance, cushion span and other features are discussed, and, where possible, are compared to the characteristics of glass panels used in similar applications. Relevant chemical and mechanical properties of ETFE are given. Load carrying concepts of tension structures and inflated cushions are discussed, as well as structural design methods for ETFE cushions. Several prominent structures constructed using ETFE foil are introduced and benefits and design issues associated with these structures are reviewed.

When used in cushion applications, ETFE films are placed in constant tension, and are therefore subject to creep. Quantifying this creep is desirable so that it can be predicted during the design phase. Therefore, this thesis summarizes the findings of other researchers in the area of creep of ETFE as well as the general mechanical behavior of the material, and presents the results of uniaxial creep tests done for the purpose of this study. These tests included 24 hour uniaxial creep tests done at four stress levels on both the transverse and longitudinal directions of three different brands of film. Two thicknesses of the third film were acquired and both were tested. The stress levels were chosen to coincide with typical design tensile stresses for ETFE film, and to be similar to the levels tested by other researchers. The effects of the different stresses, brands, directions and thicknesses are evaluated and discussed. Three seven day creep tests were also done on one of the films, each at a different stress level.

Constitutive viscoelastic and viscoplastic models were developed to represent the 24-hour creep data. The viscoelastic models were based on a four-element Kelvin model and the viscoplastic models were based on a power-law model. The model parameters were determined from the data using linear least squares fitting. Models were also developed for the seven day creep data. Several of these models were based only upon the first 24 hours of data, and were used to determine the applicability of the 24-hour creep models to long-term behavior. It was found that while a viscoelastic model appears to fit long-term creep most closely, the 24-hour models are inadequate for modeling longer time frames. Another method is required for predicting long-term creep. Nonlinear fitting of the parameters is recommended as a possible alternative for creating more accurate models. Longer-term creep tests are also recommended.

Tensile tests were also done on the films to confirm mechanical properties supplied by the film manufacturers. Good agreement to the given values was found in the test data.

Acknowledgements

I would like to acknowledge the guidance of Professor Maria Anna Polak, which made this thesis possible. Her knowledge and experience were extremely valuable during all the phases of researching, testing and writing.

I would like to thank Professor Alexander Penlidis of Chemical Engineering for sharing his personal wealth of knowledge on polymers, guiding me to appropriate resources, and assisting me in procuring test samples.

The work of past and present members of the "Creeps Group" at the University of Waterloo has also been an important resource for the writing of this thesis.

The University of Waterloo Civil Engineering lab technicians were a great help in the testing phase of this research. I would particularly like to thank Richard Morrison for his extensive help with the planning, setting-up and conducting of experiments.

I would also like to thank the individuals and companies that kindly provided samples of ETFE film to this research: Dr. Peter Scott of Dyneon USA, the late Dr. Tuyu Xie, and Drs. John Richards and John Congalidis of Dupont USA, Christian Hartz of the Technische Universität Berlin and Nowofol Germany.

I greatly appreciate the support and care of my family over my entire academic career and especially over the last two years. I would like to thank Mum and Dad for always encouraging me to do my best, Paul, Jenny and Michael for helping me to relax when I need to, and all the Waddens, Chabonneaus and Sneddons for all their motivation, dedication and love. I would also like to thank my wonderful friends for their positivity and support during the past few years.

Finally I would like to thank my husband Matt for his unfailing optimism and love and for always having time to listen.

Table of Contents

List of Figures

List of Tables

Chapter 1 Introduction and Background

In the traditional design process associated with buildings, architects create the initial design for a structure, and then structural engineers design the supporting elements for the building. Generally, the processes carried out by the two parties are separate and are carried out in sequence rather than in conjunction with each other. This is because the structural and architectural elements of a building are viewed as separate entities in most cases. However, in the case of tension structures, the supporting elements, such as fabrics, cables, or films, are integral parts of the appearance of the building and are therefore also major architectural elements. These elements cannot be designed purely for aesthetics, though, because their form directly affects their functionality as structural components. Therefore it is important that the structural engineers be a part of the design right from the beginning, collaborating with the architects in a form-finding process, until a design with the desired aesthetic and required structural capabilities is achieved. One of the ways in which structural considerations affect the appearance of tension structures is through mechanical processes, such as creep. Creep is the phenomenon by which a material subjected to constant stress continues to strain over time, beyond its initial elastic response. Tension structures are particularly susceptible to creep, because, by definition, their structural elements are continually subjected to tension. Structures made from ethylene tetrafluoroethylene (ETFE) films, on which this thesis focuses, are said to only achieve their final shape some two to three years after their completion (LeCuyer, 2008). Because of this, a good understanding of the creep behaviour of ETFE is crucial to their design.

1.1 Overview of ETFE

Ethylene tetrafluoroethylene (ETFE) is a copolymer of ethylene and fluoroethylene. It is used for a range of applications including structural cladding, which will be the focus of this thesis. ETFE can be extruded into large thin sheets, referred to as foils or films, which can be used in single or multi-layer cladding applications. Films currently in production range in thickness from 50μm to 300μm. In single-layer applications the foils would be stretched over a structural frame of some sort, and used as a canopy in areas that do not experience high levels of loading. Multi-layer ETFE cladding is created by clamping and sealing two or more layers of foil together at the edges and inflating the space between the foils with air. These cladding systems are called cushions. Several variations of cushion constructions are shown in cross section in Figure 1.1 (Hafner & Moritz, 2010). ETFE cushions are typically used in skylight and atria applications where glass would traditionally be used. However, ETFE has several advantages over glass for these types of applications, which are outlined in the following subsections.

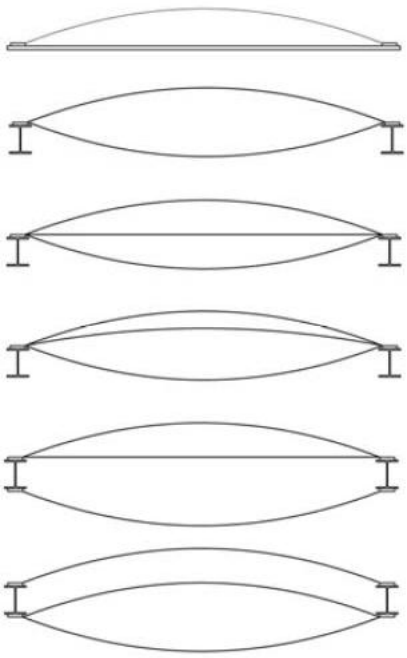

Figure 1.1 - Various configurations of one, two and three-layer ETFE foil cushions (Hafner & Moritz, 2010)

1.1.1 Weight

ETFE cushions are much lighter than glass. The density of ETFE is 1.75 g/cm^3 (Moritz, 2007b), meaning that the minimum weight per square metre of a cushion, made from two layers of 50 μm foil, would be about 1.72 N/m^2. The maximum weight per square metre of a cushion, made from five layers of 300 μm foil, would be about 25.75 N/m^2, however this cushion would likely never exist in practice since such thick foils are typically only used for outer layers, while the inner layers act primarily for insulation purposes and are usually made from thinner foils. A typical cushion would be a three-layer cushion with thicker foils, such as 300 μm, forming the outer layers, and a thinner foil, such as a 50 μm foil, used for the middle layer. This cushion would weigh about 11.16 N/m^2. The self-weight of a double-glazed glass panel is about 149.1 N/m^2 (15.2 kg/m^2) for two 3 mm panes (Glass Association of North America, 2008). Therefore ETFE allows for a much lighter and thus less expensive support structure.

1.1.2 Optics

ETFE allows a 90-97% transmission of visible light (Cripps, Kolokotroni, Robinson-Gayle, & Tanno, 2001; Tanno, 1997; Moritz, 2007b; Hafner & Moritz, 2010; Barthel, Burger, & Saxe, 2003), whereas untreated glass only allows for about 81% (All Weather Windows, n.d.). ETFE also allows more UV light to pass than glass – 85% compared to only 58% for untreated double-glazed glass panels – making it preferable for plant growth conditions (Tanno, 1997; All Weather Windows, n.d.). UV rays also inhibit growth of bacteria, so ETFE is an ideal solution for swimming pool enclosures and animal housing as well. ETFE does, however, have a slightly milky appearance, which increases with increasing film thickness. Also, due to the curvature of their surfaces, images viewed through ETFE cushions will appear somewhat distorted.

1.1.3 Insulation

ETFE cushions are better insulators than glass panels, owing to the still air pockets contained between the layers of foil. For example, a typical triple-layer ETFE cushion has a U-value of approximately 1.95 W/m^{2}K (Tanno, 1997), whereas an uncoated double-glazed air-filled glass panel has a U-value of approximately 2.84 W/m^{2}K (All Weather Windows, n.d). A lower U-value is an indication of greater insulation. Additional layers of ETFE foil increase insulation levels due to the increased number of air pockets. Insulation levels can be further improved by separating foil layers within the frames with an insulating material such as rubber (Hafner & Moritz, 2010).

1.1.4 Flexibility

ETFE is a flexible material, meaning that under dynamic loading it is less susceptible to failure than glass. In the event that an ETFE cushion does fail the damage it causes will be minimal compared to a failed glass panel, due to its ductile mode of failure and its light weight.

1.1.5 Environmental Benefits

In addition to its improved insulation over glass, ETFE cushions are environmentally preferable for several other reasons. The embodied energy, a value that takes into account all of the energy used to produce a material, for ETFE is roughly 10% of the corresponding value for glass, when put in terms of MJ/m^2 (Cripps et al., 2001). ETFE is also a recyclable material (Hafner & Moritz, 2010). Damaged foils can be added to virgin resin to be reprocessed into new material (Cripps et al., 2001).

1.1.6 Fire Performance

The performance of ETFE under fire conditions is unique in that it shrinks away, allowing smoke and fire to be vented to the exterior. Instead of melting and dripping onto building occupants, material fragments are swept up with the plume. The material is self-extinguishing, so fire will not spread across it. However, all cushions exposed to fire or extreme temperatures will need to be replaced (Vector Foiltec, 2011c). ETFE cushions are rated fire class B1 classified according to DIN 4102 (Moritz, 2007a) or class I/A according to ASTM E 84 (BLDG) (Hafner & Moritz, 2010).

1.1.7 Span

Typically glass panels are limited to spans of 2 m x 4 m (Tanno, 1997). ETFE cushions, however, can have much larger spans. In their long direction, they are virtually unlimited in span. In their short direction there are varying opinions on maximum span. Tanno (1997) suggests a maximum width of 3.5 m, as do Architen Landrel (n.d.), while Schöne (2007) suggests 4 m is the largest practical span, and Moritz (2007a) recommends 4.5 m. In practice, cushions as large as 11 m diameter hexagons and 5 m by 17 m rhombuses have been constructed (LeCuyer, 2008). Even larger spans can be achieved with the use of secondary support systems such as cable nets. Also, since ETFE cushions have a lower self-weight than glass panels, larger clear spans of supporting members can be achieved.

1.1.8 Other Features

In addition to the aforementioned qualities, ETFE has other features, which can assist architects and engineers in creating innovative designs. Due to the fact that it allows a high level of light to pass through it, solar heat gain can pose a problem with ETFE structures. To counteract this, films can be printed with shading patterns. These patterns can be variable, which allows different levels of shading at different points throughout the day. This is achieved by having inverse patterns printed on inner and outer layers of the cushions, and "closing" or "opening" the inner layer to adjust the level of shading, as shown in Figure 1.2.

(a)

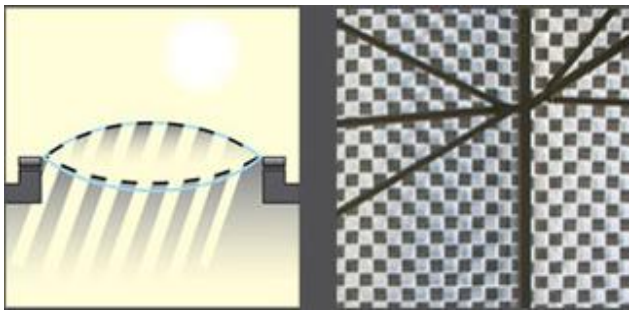

(b)

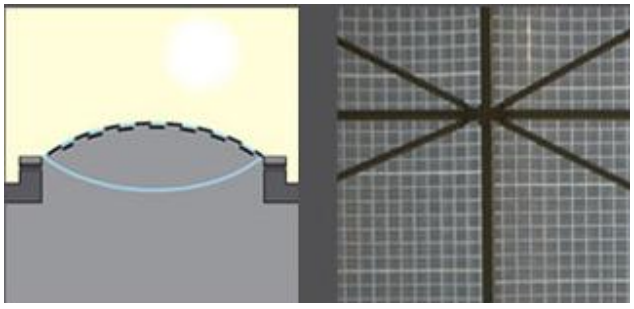

Figure 1.2 - Open (a) and closed (b) inner layer of printed ETFE cushion (Vector Foiltec, 2011g)

This feature has been used effectively in many structures, including the Kingsdale School in London, England, discussed in section 1.3.5.

Cushioned structures can also be equipped with sensors that detect events such as heavy snowfall or high winds, and increase the pressure in the cushions accordingly. This allows for energy savings during times of lesser loading conditions. This is a contrast to conventional structures, which are set up at all times to withstand the maximum load, although they will likely only encounter it on rare occasions.

From a visual perspective, ETFE is a versatile material because it can be tinted to any colour, printed with any pattern, or fitted with lights to display varying colours, images or messages. Several examples of how these features can be employed are found in section 1.3.

Due to the fact that ETFE films are very thin, they provide very little sound insulation. In some cases this is preferable to materials that reflect a high level of sound, as echoing of voices and footsteps in large spaces with

ETFE roofs or walls will be minimized. However it also means that outdoor noises such as traffic will be audible from within the building. The sound of rainfall on an ETFE roof is amplified by the drum-like form of the cushions. To counteract this effect, rain suppressors have been developed to be fitted on the outside of ETFE cushion roofs where rain noise poses a significant problem. These consist of a wire mesh grid which traps a layer of water on the surface of the cushion and dampens the sound of the raindrops (LeCuyer, 2008).

1.1.9 Processing

To process ETFE, the resin is heated to temperatures above 380°C, where it reaches a molten state. Films can be created by either extrusion or blowing. Extrusion, which results in a higher quality product, involves passing the resin through rollers to create thin films up to 2200 mm wide (LeCuyer, 2008). Blown film is created by passing the molten resin over a ring, causing it to be formed into a tube, which is expanded by inflating it with air. The tube is then cut lengthwise to form flat sheets (Seidel, 2009). Figure 1.3 and Figure 1.4 show a schematic representation of the processes used for blowing and for extrusion (Moritz, 2007b).

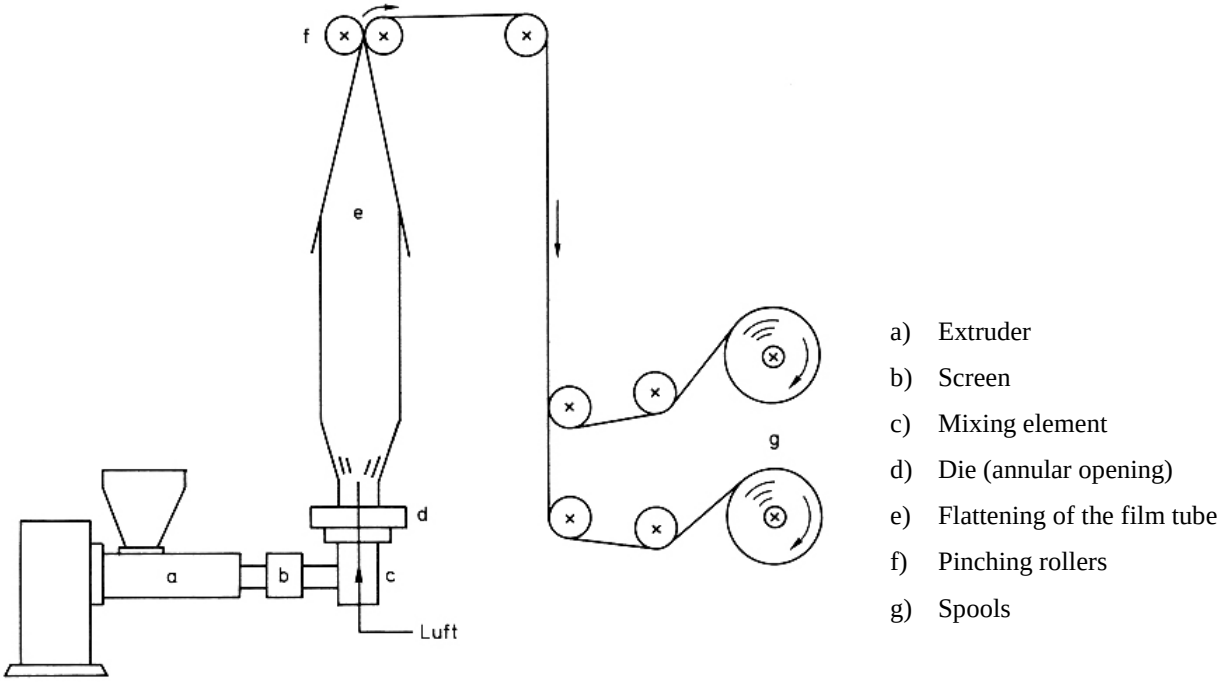

Figure 1.3 - Schematic representation of procedure for manufacturing blown film (Moritz, 2007b)

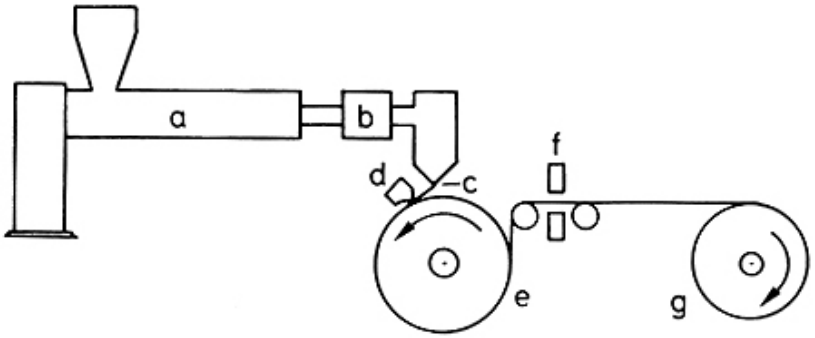

a) Extruder
b) Screen
c) Die
d) Air brush
e) Cooling roller
f) Thickness control
g) Spool

Figure 1.4 - Schematic representation of procedure for manufacturing extruded film (Moritz, 2007b)

Blowing is a less expensive process than extrusion, but extrusion produces higher transparency, crystallinity, stiffness, homogeneity in the longitudinal and transverse directions and thickness tolerance (Seidel, 2009). Therefore, for architectural applications, extruded films are more commonly used (LeCuyer, 2008).

Films are cut by a rotating blade as opposed to a laser, since the high operating temperatures of lasers would cause ETFE to emit toxic fumes. When required cushion widths are larger than film widths, sections of film can be welded together using a melt bond welding process which applies heat and pressure to the two sheets to fuse them together. The shapes of the films used in cushions are chosen using computer simulations that flatten the three-dimensional forms of the cushion layers into two-dimensional shapes (LeCuyer, 2008). This means that, for example, a cushion with a square plan will not necessarily have square film layers, as the diagonal lengths of the films will likely be longer to accommodate the rise at the centre of the inflated cushion. The most common edge detail for ETFE cushions is a PVC or polyester rope factory-welded into a folded-over sleeve of ETFE, which is slipped or clamped into the extruded aluminum frame on site. Two examples are shown in Figure 1.5.

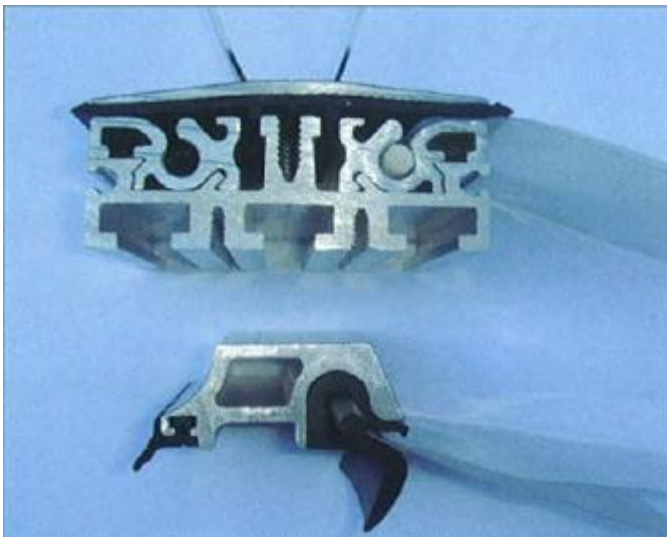

Figure 1.5 – Two possible edge details for ETFE cushions, both with PVC or polyester rope slipped in aluminum extrusion (Schmid, 2009)

Injection-moulded ETFE air valves are installed into the foils in the factory as part of the manufacturing process.

Figure 1.6 - Air valve in ETFE cushion (Buitink Technology, n.d.)

Cushions are folded for transportation to site, where they are installed in their frames and inflated (LeCuyer, 2008).

1.2 Load-Carrying Concepts of ETFE

ETFE cushions are a type of pneumatic membrane structure. The term "membrane" indicates that all stresses generated in the material act parallel to the local surface only, and are constant throughout the thickness of the

surface (Koch, 2004). In the case of ETFE, as well as other tensile surface structures, these stresses are intended to be solely tensile stresses. Most membrane structures must be designed with consideration of material direction. In fabrics, there are two primary material directions, corresponding to the directions of the weave: warp and fill, where the warp is the direction along the length of the roll and fill is the direction perpendicular to the length of the roll. Ideally, fabric structures should be designed such that the warp and fill directions of the material correspond to the directions of principal curvature of the surface. In ETFE foil, or other types of extruded films, the equivalent directions to warp and fill are the longitudinal and transverse direction of the film (Koch, 2004). Due to the nearly isotropic nature of ETFE, it is not as crucial to consider the material directions in design, but it is still good practice to have the longitudinal and transverse directions of film coincide with the primary directions of curvature, as the manufacturing process can result in molecules being aligned in the direction of extrusion (ASM International, 2003).

The term "pneumatic" refers to the use of gas, liquid, foam, or bulk materials to create a pressure difference to stabilize the membrane (Roland, 1970). In the case of ETFE and in most other building applications, air pressure is used for membrane pretension.

The most common forms of pneumatic membrane structures are large spaces enclosed by domed or semi-spherical shaped membranes stabilized by higher-than-atmospheric air pressure within the entire closed space. These structures must remain under airlock to maintain constant internal pressure. Under internal pressure alone, the membrane develops tensile prestress. In a sphere or spherical segment, the membrane stress, σ_M, for a membrane under internal pressure alone, is found using the following formula:

$$\sigma_M = \tfrac{1}{2}pr \qquad \textbf{(1-1)}$$

where p is the internal pressure and r is the radius of curvature (Roland, 1970).

In theory, when a pneumatic structure is loaded, for example with wind or snow, the membrane stresses decrease, and could go to zero in the case where the external loading equals the internal air pressure. In this type of building it is not the structure itself carrying the loading, but the enclosed volume of air itself (Otto, 1967). This theory neglects the fact that the external load acts vertically, but the air pressure acts parallel to the surface, meaning that in practice the membrane stresses will never completely disappear, but this helps to illustrate the concept of how an inflated membrane structure carries load (Roland, 1970).

Cushion-type structures, such as ETFE cushions, operate under a similar principal. They usually consist of two or more layers of the membrane material, cut into shapes, such as rectangles, triangles or hexagons, and clamped along the edges into an interconnecting system of framework which can clad roofs or entire buildings. Air is pumped between the layers of membrane (or foil, in the case of ETFE) to inflate them into cushions. The air causes prestress to form in the foils, as with any pneumatic structure. When externally loaded, the exterior layer of foil is the first to bear the load. When the load is directed inwards (or downwards, in the case of roofs), then this load is passed to the air pocket by causing the cushion to compress. This results in an increase in air pressure, which transfers an increased load to the lower layer of foil. For two-layer (single-pocket) cushions, this is the last layer to bear the load,

but in cushions with three or more layers (multi-pocket) the load is subsequently transferred to the next air pocket, and so on. When the last layer of foil is reached, the load is transferred to the frame through tension in the bottom layer or the cushion. When the load is outwards (or upwards, for roofs), then the load is primarily borne in by tension in the top layer of the cushion. This load case accompanies a decrease in pressure within the cushion, and a corresponding unloading of the lower layers of foil. The primary difference between cushion structures and internally pressurized single-membrane structures is that cushion structures do not rely on the air to carry the entire load, but rather to increase the load-carrying capacity of the membrane, which transfers the load to a structural frame. Fully pneumatic buildings do not require conventional structural frames, as the loads are transferred to the ground through air pressure alone.

1.3 Structures using ETFE

ETFE was first used in construction in 1982 as a replacement for failed fluorinated ethylene propylene (FEP) film on the roof of the Burger's Zoo Mangrove Hall in Arnhem, Netherlands (LeCuyer, 2008). This structure remains in service today. Since the introduction of ETFE as a construction material, its popularity has grown rapidly, with usage spreading to nearly every continent. However, applications of ETFE remain substantially more frequent in Western Europe, especially the United Kingdom and Germany. Recently, though, the number of projects in the United States, Asia, and Australia has been climbing. The first ETFE structure in Canada, a portion of the new roof for BC Place Stadium, is currently under construction in Vancouver.

This section outlines several major ETFE structures that have been built, or are being built, around the world. Where available, information on the project teams, including architects, structural engineers, ETFE suppliers and contractors, is given to indicate who some of the major experts in ETFE are worldwide.

1.3.1 DomAquarée, Berlin, Germany

DomAquarée is a mixed-used development designed by NPS Tchoban Voss architects and Leonhardt, Andrä und Partner structural engineers, and built in 2003. It contains a hotel, offices, retail and residential apartments (Leonhardt, Andrä und Partner, n.d.). The centrepiece of the development is a 16 m high cylindrical salt water aquarium – the largest in the world. Three separate atrium areas in the development are covered with steel-supported ETFE cushion roofing (Vector Foiltec, 2011a). The complex was originally designed with glass roofs, but concern over the threat caused to the aquarium by failed glass panels falling from the roof prompted the switch to lighter-weight ETFE. The roof over the aquarium area, shown in Figure 1.7, is made of four-layer cushions printed with a variable pattern to control light and resulting heat gain. Closing the pattern, as described in section 1.1.8, reduces light transmission from 50% to 35%. Since the number of air pockets can be varied, insulation levels of the roof can also be adjusted as necessary (LeCuyer, 2008). The retail strip connecting the two main buildings of the complex is covered by an arched roof of two-layer cushions printed with a lighter fritted pattern to control glare, but still allow enough light to pass to create the illusion of an outdoor street. The third ETFE roof covers an atrium in the office area and is printed with the same fritted pattern as the retail strip (Vector Foiltec, 2011a), but contains three-layer

cushions for added insulation (LeCuyer, 2008). All three ETFE roofs are shown from above in Figure 1.8. The ETFE cushions were supplied and engineered by Vector Foiltec.

Figure 1.7 - DomAquarée aquarium atrium (Vector Foiltec, 2011a)

Figure 1.8 - The three ETFE roofs at DomAquarée (Vector Foiltec, 2011a)

1.3.2 Allianz Arena, Munich, Germany

The Allianz Arena, constructed in 2005, is home to Munich's two football clubs and was one of the stadiums used to host the 2006 FIFA World Cup. The stadium has a capacity of up to 66,000 spectators. The façade, including the

walls and the roof covering the spectator seating areas, is clad with 66,500 m^2 of ETFE cushions that are fitted with fluorescent lights allowing them to change from white to blue to red to suit the home team using the stadium. Figure 1.9 shows the facade illuminated with white lights. The area directly above the pitch is open, allowing rainwater and sunlight onto the field. The stadium was designed by architects Herzog & De Meuron. Arup completed the competition design scheme for the structural design of the entire building and the construction design for the bowl portion. The construction design of the roof was completed by Sailer Stephan und Partner, the facade structural design was done by R+R Fuchs and the pneumatic skin design calculations were done by Engineering + Design. The ETFE cushions were manufactured by KfM GmbH (LeCuyer, 2008).

Figure 1.9 - Allianz Arena (Mi Modern Architecture, 2009)

The wall cushions are printed with a variable dot pattern which is densest at the base, reducing the intensity of the lighting at the eye level of drivers and pedestrians. The roof cushions are clear, allowing sunlight onto the pitch even when the sun is not directly overhead (LeCuyer, 2008).

Since its construction, the Allianz Arena has provided examples of potential performance issues that can arise with ETFE cushions. The large, low slope roof was initially unable to deal with heavy snow loads, leading to the failure of some cushions. To accommodate the heavy loads, inflation pressure can now be increased four times, from 200 Pa to 800 Pa. Some of the roof cushions have also been fitted with drain tubes through their centres to drain water and snow from the roof. However, air loss can occur at the O-ring separating the ETFE from the tube, resulting in deflation and inversion of the cushions, allowing water to pond, ultimately leading to failure of the cushions (LeCuyer, 2008).

1.3.3 Eden Project, Cornwall, England

Set in a former clay quarry, the Eden Project is a series of ETFE clad steel geodesic domes completed in 2001 (Figure 1.10). These domes contain simulated Mediterranean and tropical climates to support the growth of plant life native to those climates (Arup, n.d.a). The Eden Project is the world's largest self-supported transparent envelope. The domes are made of 667 tonnes of steelwork and contain 536 tonnes of air (Vector Foiltec, 2011b). The largest dome is 110 m in diameter at the base and 45 m high on the inside. The ETFE cushions are mostly

hexagonal and up to 11 m in diameter (SKM, 2009). Of the 831 ETFE panels on the domes, 230 are "intelligently controlled", meaning that their inflation levels are automatically adjusted according to the varying climate conditions, and are operable to allow natural ventilation (Vector Foiltec, 2011b). During heavy snowfall, the inflation pressure of the cushions can be increased from 250 Pa to 400 Pa (LeCuyer, 2008). The outer layer of foil is comprised of two vacuum laminated thin foils instead of one thick foil, since thick foils can be apt to fail in a brittle manner. This was done to counteract the governing load case of wind suction on the cushions (LeCuyer, 2008). At the intersections of the domes, snow loads are higher due to drifting, so a cable net is used to reinforce the cushions at these locations (LeCuyer, 2008). The Eden Project was designed by Grimshaw Architects (Arup, n.d.b) and the structural engineering was done by Anthony Hunts and Associates (SKM, 2009), who are now known as SKM Anthony Hunts (Broughton, T., 2007). ETFE supply and engineering was done by Vector-Foiltec (Vector Foiltec, 2011b).

Figure 1.10 - Eden Project (Vector Foiltec, 2011b)

1.3.4 National Aquatics Centre, Beijing, China

China's National Aquatics Centre (Figure 1.11), commonly known as the Water Cube, hosted aquatic events during the 2008 summer Olympic Games. The centre contains five swimming pools, a restaurant, seating for 17,000 spectators, and all facilities associated with those components (Arup, n.d.b). The entire stadium is covered in over 100,000 m^2 of ETFE foil cushions, making it the largest ETFE structure in the world to date. The blue-tinted ETFE cushions, which are further illuminated by blue LED lights, are enclosed in aluminum frames, which are supported on the lightweight tubular steel superstructure (Vector Foiltec, 2011f). The shape of the ETFE cushions was inspired by the natural formation of soap bubbles (Arup, n.d.b).

The walls and roof are all clad with two distinct envelopes of ETFE cushions, separated by 3.6m of steel structure on the walls and 7.2m on the roof. The walls are comprised of two tiers of three-layer cushions and the roof is comprised of two tiers of four-layer cushions. High levels of insulation are achieved, owing to the thickness of the envelope. Additionally, the envelope can adapt to changes in season. During spring and fall, vents are opened in the outer tier, allowing air to enter the envelope to be heated passively by solar radiation. The air is then supplied to the pool area of the building through vents in the inner tier. During the summer, vents at grade and in the roof of the outer tier are opened. Air that is cooled by passing over a moat surrounding the building is drawn into the envelope

at ground level. As the air warms, it rises and is vented from the roof, allowing cooler air to enter again at ground level. In the winter all layers of the envelope are closed to minimize air loss and maximize insulation (LeCuyer, 2008).

The large, flat roof poses a risk of ponding causing cushions to invert and fail. To avoid this, each cushion is surrounded by a gutter, into which drains are incorporated at regular intervals. The inner air pocket in each roof cushion is supplied by a separate air inflation tube from the outer pockets, to ensure it remains at a higher pressure, and also providing a backup inflation system should one fail. Backup electrical supply systems were also put in place in case the primary one fails. However, if ponding and inversion still occur in spite of these safeguards, all layers of the cushions are designed to act as one strong tension membrane, preventing ultimate failure (LeCuyer, 2008).

The natatorium, which was designed by China Construction Design International and Peddle Thorp Walker, was completed in 2007. The ETFE foils were supplied and engineered by Vector Foiltec (Vector Foiltec, 20011f). Arup provided structural engineering services for the project. The structural design required consideration of the seismic activity in Beijing. ETFE works well for seismic design because of its ability to undergo significant deflections without being damaged (Arup, n.d.b).

Figure 1.11 - The National Aquatics Centre (Vector Foiltec, 2011f)

1.3.5 Kingsdale School, London, England

The original Kingsdale School building was constructed in the 1950s, and prior to its £12 million renovation in 2003, it was in very poor shape. Student performance and behaviour was similarly poor (Vector Foiltec, 2011d). Renovation of the school was part of the Architecture Foundation's School Works initiative, which sought to observe the impact of architectural environment on student performance. The initiative was funded by the Department for Education and Skills. De Rijke Marsh Morgan Architects were awarded the contract to redesign the school and Michael Hadi Associates performed the structural engineering for the project. The school contained a

large 80 m long by 40 m wide courtyard at its centre; it was decided that a major component of the renovation would be to cover this courtyard with an ETFE roof, with foils supplied and engineered by Vector Foiltec. Shallow tubular steel arches span the courtyard and support the ETFE cushions. The light weight of the cushions and their support structure means they are easily supported by the structure of the existing building without extensive reinforcement. The courtyard is covered with three layer cushions with patterns printed on the top two layers, blocking varying amounts of light depending on which chambers of the cushions are inflated (Kennet, 2004). The maximum light transmittance into the courtyard is 50%, when both air chambers in the three-layer ETFE cushions are inflated (Figure 1.12), and the minimum light transmittance is 5%, when only the upper chamber is inflated (Figure 1.13) (Kennet, 2004).

Figure 1.12 - Kingsdale School courtyard, with both chambers of the ETFE cushions inflated (Vector Foiltec, 2011d)

Figure 1.13 - Kingsdale School courtyard, with only one chamber of the ETFE cushions inflated (Vector Foiltec, 2011d)

The use of Variable Skin cushions allows for more heat gain in the winter than the summer, regulating the temperatures in the courtyard. The ground level target temperatures for the courtyard were no less than 14^{o}C in winter and no more than 30^{o}C in summer. Temperature control is assisted by the installation of six 12 m by 2.5 m ETFE flaps at either end of the roof, which are controlled automatically by pistons to open and close depending on weather and temperature conditions (Kennet, 2004).

1.3.6 Khan Shatyry Entertainment Centre, Astana, Kazakhstan

Khan Shatyry is a multi-use entertainment centre completed in 2010 in Astana, Kazakhstan, which includes an indoor park, shopping, recreation and a resort. The building, shown in Figure 1.14, is a tent-shaped cable structure clad in lightly printed ETFE foil cushions. It has a 200 m elliptical base and a 150 m tall mast, from which the vertical cables are suspended (Vector Foiltec, 2011e). At this height, it is currently the world's tallest tensile structure (Foster + Partners, n.d.). The vertical cables are designed to resist wind pressures, while horizontal cable hoops resist wind suction (LeCuyer, 2008). Sir Norman Foster & Partners were the project architects and Buro Happold were the structural engineers (Foster + Partners, n.d.). Vector Foiltec supplied and engineered the ETFE foil cushions (Vector Foiltec, 2011e).

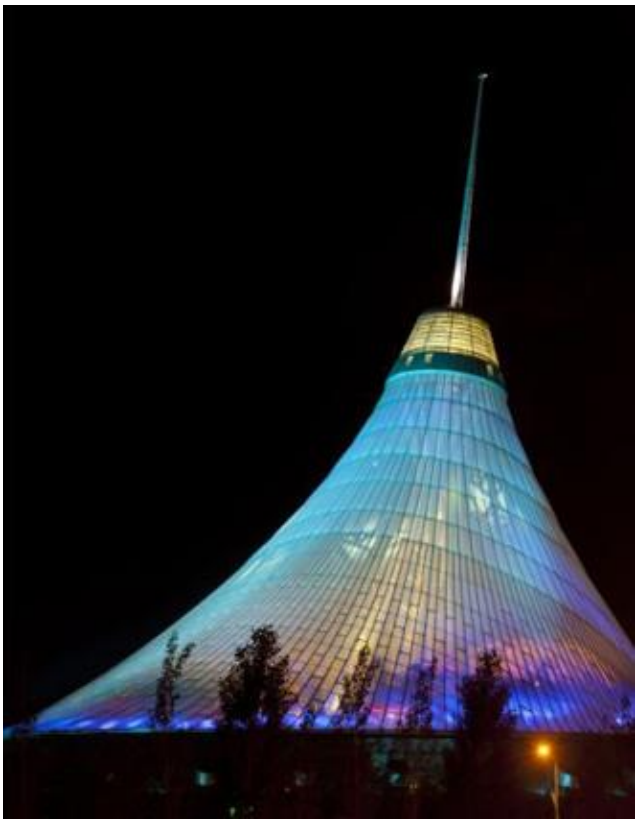

Figure 1.14 - Khan Shatyry Entertainment Centre (Vector Foiltec, 2011e)

1.3.7 BC Place Stadium, Vancouver, Canada

The first use of ETFE film on a building in Canada will be the new roof of BC Place Stadium in Vancouver, British Columbia, under construction at the time of writing this thesis. Figure 1.15 and Figure 1.16 show renderings of the planned structure. The new roof will be made primarily of woven PTFE fabric panels supported by a post-tensioned radial cable truss encircled by a steel compression ring and 36 steel masts around the perimeter of the new roof (Campbell, 2010). At the centre of the new roof will be a retractable section made of an ETFE-coated woven fabric called Tenara formed into two-layer inflated cushions (PCL, n.d.).

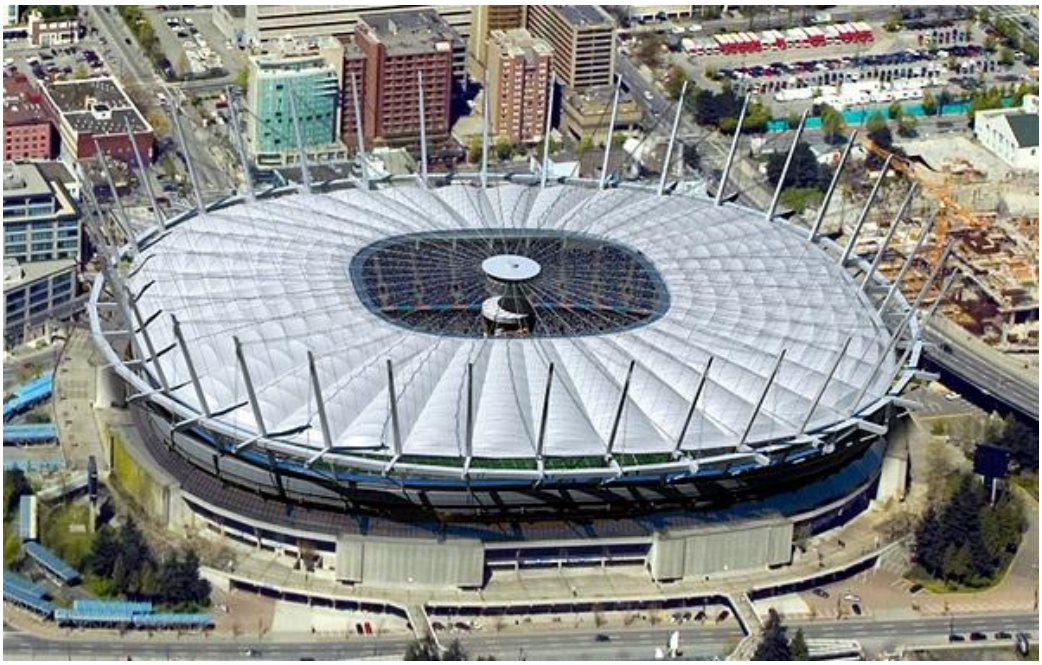

Figure 1.15 - Rendering of the new BC Place fabric roof, with the centre portion retracted (Cygniak, 2011)

Just below the fabric roof, but above the existing structure, will be a facade of 6500 m^2 of pre-stressed single-layer 250 μm thick ETFE panels (PCL, n.d.). The film will be prestressed to 2.2 MPa in the horizontal direction and 2.6 MPa in the vertical direction.

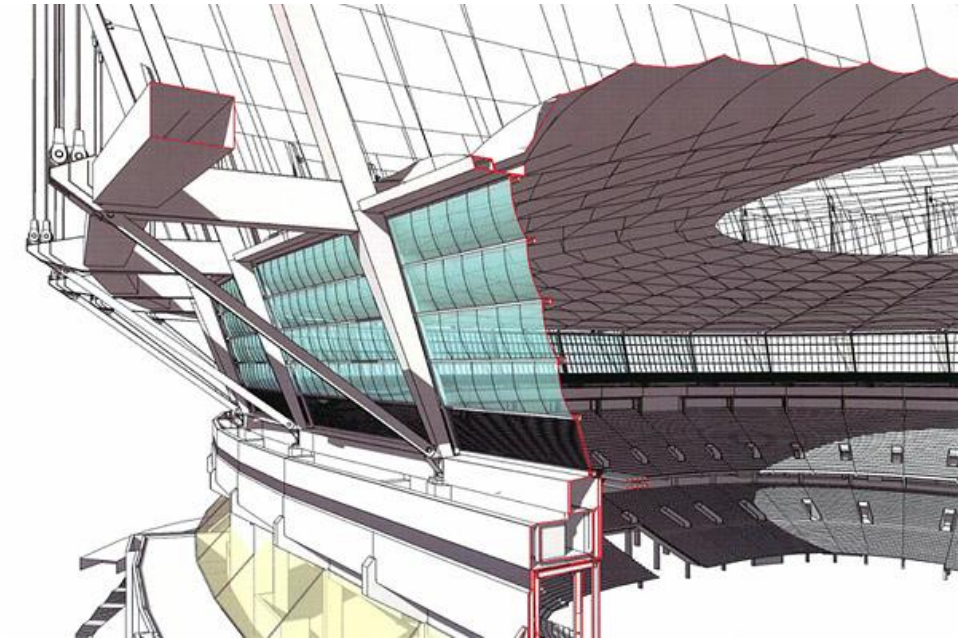

Figure 1.16 - Rendering of the ETFE facade on the new BC Place roof (Cygniak, 2011)

The project is expected to be completed in September 2011 (Cyganiac, 2011). Hightex is supplying the ETFE as well as the Tenara fabric (PCL, n.d.). PCL Constructors West Coast Inc. are providing construction services, and

Stantec Architecture are providing the architectural design. The structural engineering is being done by Geiger Engineers, with consultation from Schlaich Bergermann and Partner (Cygniac, 2011).

1.4 Chemical Properties of ETFE

Polymers are long chain (macro) molecules made up of n identical repeating units, called monomers. A copolymer is a polymer that contains two different repeating units on its chain. ETFE is a copolymer of ethylene, shown in Figure 1.17, and tetrafluoroethylene, shown in Figure 1.18. The ethylene and tetrafluoroethylene molecules occur in an alternating pattern along the ETFE polymer chain, shown in Figure 1.19 (Polymers: a Properties Database, n.d.).

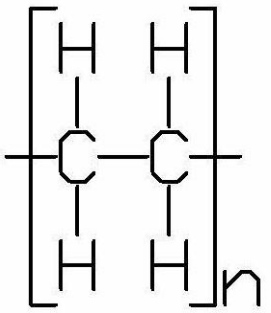

Figure 1.17 - Polyethylene molecular structure

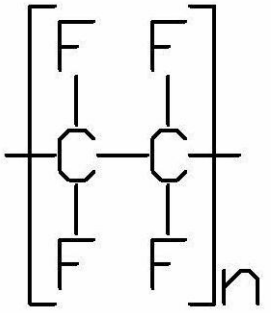

Figure 1.18 - Polytetrafluoroethylene molecular structure

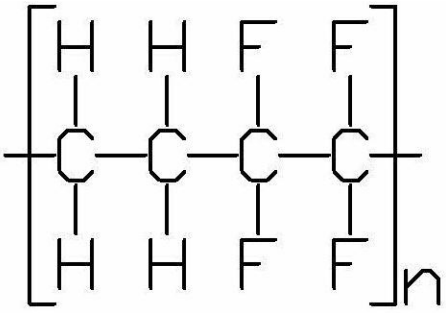

Figure 1.19 - Poly(ethylene tetrafluoroethylene) molecular structure

Ethylene consists of a backbone of two carbon atoms, each attached to two hydrogen atoms with a double bond. Tetrafluoroethylene also has two carbon atoms as its backbone, but each is attached to fluorine atoms instead of hydrogen. The ETFE molecule contains repeating units of alternating ethylene and tetrafluoroethylene monomers.

Fluoropolymers are polymers that contain carbon, hydrogen and fluorine. Polymers that contain only carbon and fluorine, such as polytetrafluoroethylene, are called perfluoropolymers. Fluoropolymers that also contain hydrogen are called partially fluorinated polymers. ETFE is a partially fluorinated polymer. The addition of hydrogen increases hardness and toughness but decreases thermal stability (Ebnesajjad & Khaladkar, 2005).

Polymers can be either thermoplastic or thermosetting. Thermoplastic polymers can be heat-softened, and therefore are melt-processable. Thermosets contain crosslinking between polymer chains, making them resistant to heat-softening, so they cannot be melt-processed (Fried, 1995). All fluoropolymers, including ETFE, are thermoplastic (Ebnesajjad & Khaladkar, 2005). ETFE film can therefore be formed by extrusion, as described in section 1.1.9.

ETFE is a semi-crystalline polymer, meaning that it has both crystalline and amorphous phases (Ebnesajjad & Khaladkar, 2005). In the crystalline phase, the polymer chains are folded in a regular pattern, forming crystalline lamellae. In the amorphous phase, the chains are randomly coiled and intertwined. Symmetric polymer chains, such as polyethylene, tend to favour a crystalline structure, whereas very asymmetrical polymers, such as those with heavy side groups and a high degree of branching, tend to favour an amorphous structure. Most polymers contain a combination of crystalline and amorphous phases (Fried, 1995). Semi-crystalline polymers have a degree of crystallinity somewhere between 30 and 70%. ETFE is about 33% crystalline (Moritz, 2007b). Figure 1.20 represents a semi-crystalline microstructure, where the straight, parallel lines represent crystalline regions, called lamellae, and the random curved lines represent amorphous regions.

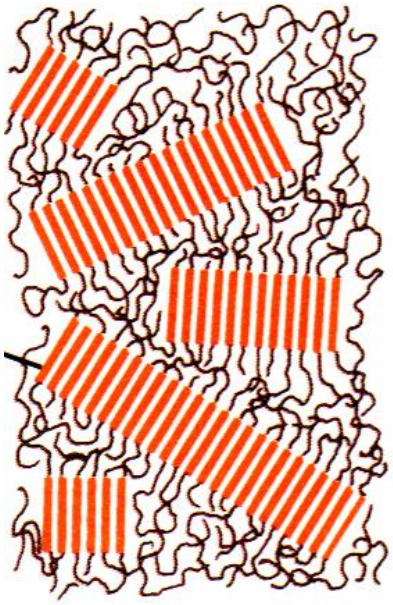

Figure 1.20 - Visualization of a semi-crystalline microstructure (Winkler, 2009)

As a polymer is stretched, such as when creep is occurring, the lamellae will align themselves in the direction of loading, as shown in Figure 1.21.

Figure 1.21 - Semi-crystalline microstructure, oriented in the loading direction (Winkler, 2009)

A polymer's microstructure affects its mechanical properties. For example, degree of crystallinity is inversely related to flex life, the number of fatigue cycles required to fail an element, meaning that highly crystalline polymers are less resistant to fatigue than amorphous ones. In terms of creep, perfluoropolymers are more susceptible to it than partially fluorinated polymers (Ebnesajjad & Khaladkar, 2005). Also, the crosslinking of thermosets inhibits creep (ASM International, 2003). Studies have shown that density can be related to creep in that higher density polymers will exhibit less creep than lower density polymers (Bobovitch, Gutman, Mogilansky, & Unigovski, 2011).

1.5 Mechanical Properties of ETFE

Academic and industrial literature contains many references to the mechanical properties of ETFE. Table 1.1 provides some of the values for mechanical properties of ETFE obtained from these sources.

Table 1.1 - Mechanical properties of ETFE obtained from the literature

Source	Tensile Strength (MPa)	Yield Stress (MPa)	Elongation at Break (%)	Tear Resistance (MPa)	Tensile Modulus of Elasticity (MPa)	Melt Temperature (°C)	Maximum Service Temperature (°C)	Minimum Service Temperature (°C)
Lehnert and Schween (2006)	50	-	>350	400	700	-	-	-160
Drobny (2001)	44	-	-	-	826	271	-	-
Tanno (1997)	-	20	200-300	-	-	-	150	-200
Moritz (2007b)	53	30	300	440	900-1000	265-278	150	-190
Schöne (2007)	52.5	-	600	-	300-750	265		
Barthel, Burger and Saxe (2003)	-	-	400-600	-	650-700	-	150	-200
Ebnesajjad and Khaladkar (2005)	45	-	150-300	-	827	-	-	-

The tensile strength of ETFE is estimated by the various sources as ranging from 44 MPa to 53 MPa. Only two values are available for yield strength; 20 and 30 MPa. The elongation at break varies from 150% to 600%, which is a large range. It is probable that such a large range of elongations can be demonstrated consistently with ETFE foils as elongation depends on a number of factors, including specimen size, shape, orientation and loading speed. Two values for tear strength are available; 400 and 440 MPa. Values given for tensile modulus of elasticity (E) also have a large variation, ranging from 300 to 1000 MPa. If the low and high values are excluded, all other values vary from 650 to 827 MPa, which is a much narrower range. All the given melt temperatures are within 265 to 278 °C. The three maximum service temperatures given are all 150 °C, and the minimum service temperatures range from -200 to -160 °C. A number of experimental results on ETFE are reviewed in section 1.7, so additional data on the mechanical properties of ETFE can be found there as well.

1.6 Structural Design Methods for ETFE Cushions

A structure or a structural member is considered to be geometrically linear when the actual displacements are directly proportional to the applied loading and geometrically nonlinear when they are not (Koch, 2004). Tension structures exhibit geometrically linear behaviour for small displacements, but nonlinear behaviour for large displacements (Lewis, 2003). Membrane structures have relatively large surface movements under applied loading in order to allow them to effectively carry the loads, meaning that any analysis must account for nonlinear behaviour (Koch, 2004).

According to Frei Otto (1967), there are two main issues to solve in the static analysis of pneumatic or other pre-stretched structures: 1) determining the necessary inflation pressure to counteract the expected applied loads, and 2) establishing the maximum tensile stresses that will occur in the system at the given internal pressure and applied load. Due to the geometric nonlinearity of the system, the determination of the inflation pressure must be an iterative process. For simple shapes of ETFE cushions, such as rectangles, this can be done by hand, although the procedure is cumbersome. For more complex shapes, three-dimensional analysis is required, so modeling in a finite element computer program is necessary (Koch, 2004).

Several procedures for simplified analysis of pneumatic cushions have been proposed, and these are discussed in the following sections.

1.6.1 Huntington Method

In order to determine the initial prestress under internal pressure, a cable model, as presented by Craig G. Huntington (2004), can be employed as follows:

- A cable spanning a distance l, with a sag of h, under uniform load w, has end reactions V and H, in the horizontal and vertical directions, respectively, calculated as follows:

$$V = \frac{wl}{2} \quad \textbf{(1-2)}$$

$$H = \frac{wl^2}{8h} \quad \textbf{(1-3)}$$

- For uniform loads perpendicular to the cable, such as internal pressure, the tensile force in the cable, F, is found using the following equation:

$$F = \frac{w(l^2 + 4h)}{8h} \quad \textbf{(1-4)}$$

- The unloaded arclength of the cable is found as follows:

$$A = 2\left[\frac{l^2}{4} + \frac{4}{3}h^2\right] \quad \textbf{(1-5)}$$

- The change in the arclength under loading, δA, is computed with the following formula:

$$\delta A = \frac{FA}{E} \quad \textbf{(1-6)}$$

  where E is the modulus of elasticity,

- The new arclength is then calculated by:

$$A' = A + \delta A \quad \textbf{(1-7)}$$

- The corresponding new sag in the cable is calculated as follows:

$$h' = \frac{\sqrt{3}}{4}\sqrt{A'^2 + l^2} \quad \textbf{(1-8)}$$

- Inputting h' into the original equation for F yields F'. Iterating through all of the formulas until F' converges allows the determination of the final cable geometry.

To use this method for foils instead of cables, a unit width of foil can be assessed.

1.6.2 Wagner Method

Rosemarie Wagner (2007) developed an analytical method for solving stresses in inflated cushions, which is also based on the cable concept. Under internal pressure alone the cushion parameters are specified in Figure 1.22.

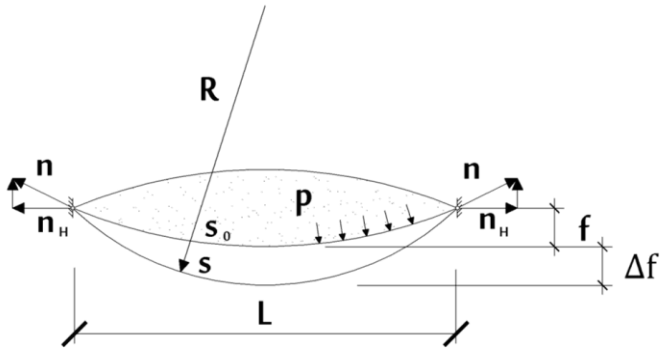

Figure 1.22 - Cushion under internal load (Wagner, 2007)

The initial length of the foil, s_o, increases to s when the cushion is inflated. The new length, s, is found using the following equation:

$$s = L\sqrt{1 + \frac{16(f + \Delta f)^2}{3L^2}} \tag{1-9}$$

This can be simplified using a Taylor series expansion as:

$$s \cong L\left[1 + \frac{8(f + \Delta f)^2}{3L^2}\right] \tag{1-10}$$

The total sag in the cushion, f+Δf, is found as follows:

$$f + \Delta f = R - R\sqrt{1 - \frac{L^2}{4R^2}} \tag{1-11}$$

which can also be simplified using a Taylor series expansion, creating the following equation.

$$f + \Delta f \cong \frac{L^2}{8R} \tag{1-12}$$

It follows that:

$$R = \frac{L^2}{8(f + \Delta f)} \tag{1-13}$$

So that the stress in the foil, n, is described as:

$$n = p \cdot R \cong p \cdot \frac{L^2}{8(f + \Delta f)} \tag{1-14}$$

Also, the foil length, s, can be calculated in terms of n, using the following equation:

$$s = L\left(1 + \frac{p^2L^2}{24n^2}\right) \cong s_o + \Delta s = s_o + \frac{ns_o}{EA} \quad \textbf{(1-15)}$$

To solve for the stress, n, the following cubic equation must be solved:

$$n^3 + EAn^2\left(1 + \frac{L}{s_o}\right) = \frac{EAp^2L^3}{24s_o} \quad \textbf{(1-16)}$$

A cushion under internal pressure and external load has the parameters shown in Figure 1.23.

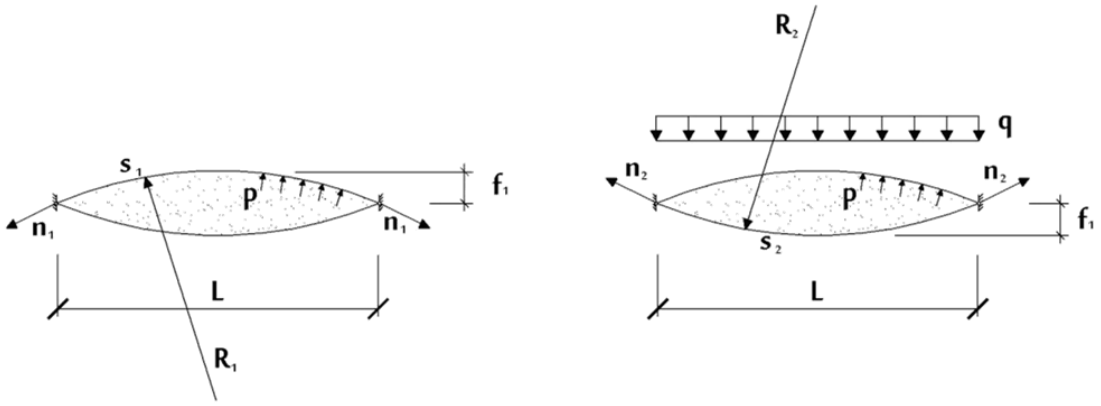

Figure 1.23 - Cushion under external load (Wagner, 2007)

The following assumptions must be made to use the simplified nonlinear equations employed in this case:

- The geometry of the surface is a shape of equilibrium defined by internal pressure
- The cushion is only singly curved (i.e. it has no curvature in the third dimension)
- The orientation of the fabric is in the direction of curvature
- The external load is similar to the internal, avoiding strain less deformations
- The boundaries are fixed (Wagner, 2007).

In the following procedure, the subscript "o" refers to the inflated, unloaded state. The length of the upper membrane is found as follows:

$$s_1 = s_{1,o+}\Delta s_1 \cong L_1\left(1 + \frac{8(f_1 - \Delta f_1)^2}{3L_1^2}\right) \quad \textbf{(1-17)}$$

The stress in the upper membrane is found as follows:

$$n_1 = (p - q) \cdot R_1 = (p - q) \cdot \frac{L^2}{8(f_1 - \Delta f_1)^2} \quad \textbf{(1-18)}$$

The elastic strain in the upper membrane is calculated using the following equation:

$$\Delta s_1 = \frac{(n_1 - n_{1,o})s_{1,o}}{E_1 A_1} = \frac{(n_1 - \frac{p_o L^2}{8f_{1,o}})s_{1,o}}{E_1 A_1} \quad \textbf{(1-19)}$$

The deformed length of the upper membrane is obtained by adding the initial length to the elastic strain, as follows:

$$s_1 \cong s_{1,o} + \Delta s_1 = s_{1,o} + \frac{(n_1 - \frac{p_o L^2}{8f_{1,o}})s_{1,o}}{E_1 A_1} \quad \textbf{(1-20)}$$

To determine the stress in the upper membrane, n_1, the following cubic equation can be solved:

$$n_1^2\left(n_1 - \frac{p_o L_1^2}{8f_{1,o}}\right) + E_1 A_1 n_1^2\left(1 - \frac{L_1}{s_{1,o}}\right) = \frac{E_1 A_1 (p-q)^2 L_1^3}{24 s_{1,o}} \quad \textbf{(1-21)}$$

Similarly, the stress in the lower membrane, n_2, can be found from:

$$n_2^2\left(n_2 - \frac{p_o L_2^2}{8f_{2,o}}\right) + E_2 A_2 n_2^2\left(1 - \frac{L_2}{s_{2,o}}\right) = \frac{E_2 A_2 p^2 L_2^3}{24 s_{2,o}} \quad \textbf{(1-22)}$$

The undeformed and deformed volumes of air inside the cushion are found as follows:

$$V_o = \frac{2}{3}(L_1 f_{1,o} + L_2 f_{2,o}) \cdot b \quad \textbf{(1-23)}$$

$$V = \frac{2}{3}(L_1 f_1 + L_2 f_2) \cdot b \quad \textbf{(1-24)}$$

Using these equations for the volumes and the ideal gas pressure-volume relationship, $p_o V_o = pV$, the third equation necessary for solving n_1, n_2, and p, is developed:

$$(p_o + p_{atm})\left(L_1 f_{1,o} + L_2 f_{2,o}\right) = (p_o + p_{atm})(L_1^3 \cdot \frac{p-q}{8n_1} + L_2^3 \frac{p}{8n_2}) \quad \textbf{(1-25)}$$

If p_o, $f_{1,o}$ and $f_{2,o}$ are known, then p, n_1 and n_2 can be found by solving Equations (1-21), (1-22) and (1-25).

1.6.3 Borgart Method

Borgart (2007) proposed a similar method for the analysis of rectangular cushions. Figure 1.24 shows the cushion characteristics used in his equations.

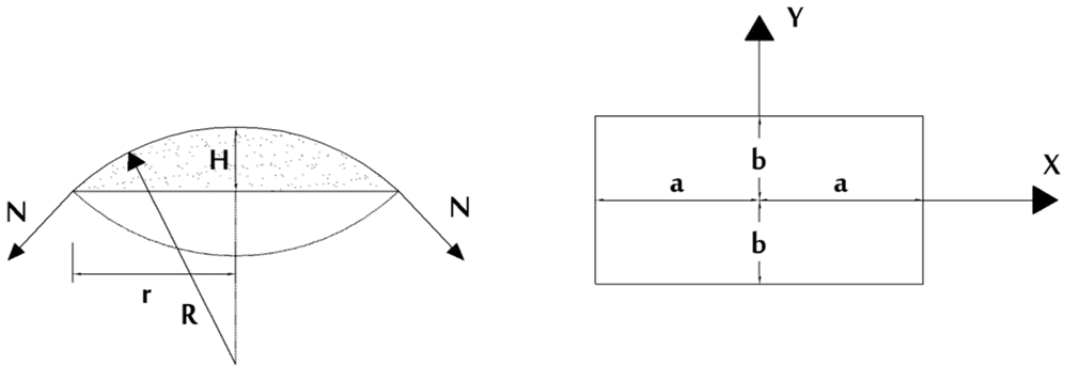

Figure 1.24 - Inflated rectangular cushion (Borgart, 2007)

The radius of one of the inflated foil layers is found as follows:

$$R = \frac{H^2 + r^2}{2H} \tag{1-26}$$

The membrane forces in the x and y directions, respectively, are given by the following equations:

$$N_{xx} = \frac{-5b^2 Q R_x}{4(a^2 + b^2)} \tag{1-27}$$

$$N_{yy} = \frac{-5a^2 Q R_y}{4(a^2 + b^2)} \tag{1-28}$$

For square cushions, the strain in the material is described by

$$\varepsilon = \frac{5PR}{8K} \tag{1-29}$$

where P is the internal air pressure, R is the cushion radius, K is the in plane stiffness, which equals Ed(1+v), where d is the foil layer thickness and v is the contraction coefficient. The lengths of the uninflated and inflated membrane are given by l and l_{o1}, respectively, in the equations below:

$$l = \frac{6r^2 + 4H^2}{3r} \tag{1-30}$$

$$l_{o1} = \frac{16KH_1(6r^2 + 4H_1^2)}{3r(5PH_1^2 + 5Pr^2 + 16KH_1)} \tag{1-31}$$

Based on Boyle's gas law, the pressures before and after loading an inflated cushion with an external load can be related:

$$P_1 = \left(\frac{H_1 + H_2}{H_{11} + H_{21}}\right) P_o \quad \textbf{(1-32)}$$

In the above equation, Po is the internal air pressure before loading, P_1 is the internal air pressure after loading, H_1 and H_2 are the cushion heights before loading of the upper and lower layers, respectively, and H_{11} and H_{21} are the cushion heights after loading. To determine the deformed length of the cushion membrane, and the membrane forces, the following three equations can be solved:

$$l_{11} = l_{o1}(1 + \varepsilon) \quad \textbf{(1-33)}$$

$$\left[1 + \frac{5\left(\left[\frac{H_1 + H_2}{H_{11} + H_{21}}\right] P_o - P_o - P_w\right)(H_{11}^2 + r^2)}{16 H_{11} K}\right] \cdot l_{o1} - \frac{6r^2 + 4H_{11}^2}{3r} = 0 \quad \textbf{(1-34)}$$

$$\left[1 + \frac{5\left(\left[\frac{H_1 + H_2}{H_{11} + H_{21}}\right] P_o - P_w\right)(H_{21}^2 + r^2)}{16 H_{21} K}\right] \cdot l_{o2} - \frac{6r^2 + 4H_{21}^2}{3r} = 0 \quad \textbf{(1-35)}$$

1.6.4 Computer Analysis Methods

The above methods are applicable only for very simple cushion shapes and constant distributed loadings. The mathematics, even in these basic cases, is still very cumbersome and it is useful to have a computer program capable of solving complex systems of equations to arrive at a solution. For more unusual cushion shapes, or for non-uniform loadings, it is necessary to use computer methods. Standard finite element analysis programs must be adapted to include the enclosed volume of air within the cushions, the pressure of which changes with the applied loading (Koch, 2004). Koch (2004) suggests the following basic adaptation of the ideal gas law for this purpose:

- Using a finite element program, determine the necessary inflation pressure, P_o, to create the desired prestress in the membrane,
- Calculate the corresponding volume of enclosed air at this stage, V_o, using the ideal gas law,
- Estimate a final internal pressure, P_i, after loading,
- Run a load analysis of the system until P_i converges, and calculate corresponding V_i,
- Compare P_oV_o with P_iV_i; if they are not equal, adjust P_i iteratively until they are equal, and
- Calculate the membrane stress at this pressure and volume to determine if it is acceptable.

In order to model the nonlinear behaviour of membranes, Lewis (2003) suggests using one of three methods; the transient stiffness method, the force density method, and the dynamic relaxation method. All are described in full detail in her book, *Tension Structures: Form and Behaviour*, and all require the use of computer modeling for complex structures, such as cushions.

1.7 Prior Research

1.7.1 General Research on Mechanical Behaviour of ETFE

Mechanical research on ETFE has been underway since the material was first developed. This section will outline some of the more prominent and recent research undertaken in the area, excluding creep research, which will be covered in a subsequent section.

1.7.1.1 Ansell, 1985

In 1985, at the University of Bath, M.P. Ansell performed mechanical tests on ETFE on behalf of Buro Happold Consulting Engineers. His test program involved studying the effects of temperature on the mechanical behaviour of ETFE films (Ansell, 1985).

Uniaxial short-term tensile tests were done on 300 μm thick foils with sample widths of 12.5 mm, at room temperature (23°C) as well as at temperatures of 21°, 37°, 63°, 84°, 93°, and 105° C. At 23°C five samples were tested in each direction at a displacement rate of 5 mm/min. The average maximum stresses from the tests are reported by Ansell to be 17.59 MPa and 16.56 MPa, in the longitudinal and transverse directions, respectively. It is unclear whether these values represent ultimate break stresses, yield stresses or stresses for failure due to excessive deformation. Table 1.2 gives the maximum stresses for the other temperatures. All of these tests were performed in the longitudinal direction of the material (Ansell, 1985).

Table 1.2 - Maximum stresses at different temperatures, as per Ansell (1985)

Sample	Temperature (°C)	Maximum Stress (MPa)	Comments from Ansell
1	21	18.62	Flowed
2	21	18.57	
3	37	14.60	
4	37	14.37	
5	63	~7.7	Samples do not achieve maximum stress, yield is recoverable
6	63	~7.7	
7	84	~3.9	
8	93	~3.9	
9	105	~2.8	

Once again, it is unclear what exactly these stress values represent, but it is obvious that there is a marked decline in their values as the temperature increases, indicating a loss in strength of the material at higher temperatures. This is shown visually in Figure 1.25.

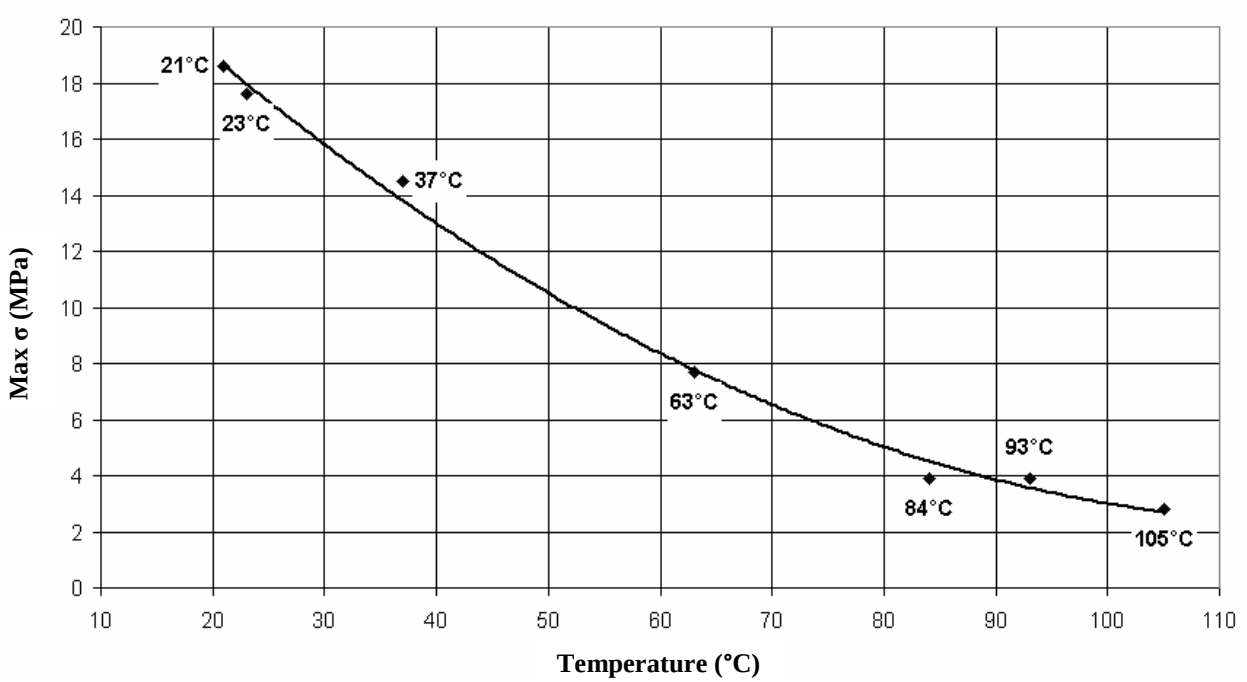

Figure 1.25 - Maximum stress versus temperature, as per Ansell (1985)

The relationship between maximum stress and temperature is clearly an inverse one, with dramatically lower values achieved for stress at the higher test temperatures (Moritz, 2007b).

Ansell also performed short-term tensile tests on samples that were stored in 105°C distilled water for a period of time. The samples were all 300 μm thick and were tested in the longitudinal direction. The tests were all done at 23°C. Table 1.3 shows the maximum stresses of all the tested samples, as well as the averages over each set stored for the same number of days.

Table 1.3- Maximum stresses of samples held in boiling water, as per Ansell (1985)

Sample	Maximum Stress (MPa)	Average Maximum Stress (MPa)	Number of Days in 105°C Water
A4	19.18		
A5	20.19	19.41	9
A6	18.87		
B4	18.95		
B5	18.46	18.50	19
B6	18.10		
C4	17.56		
C5	20.24	19.54	29
C6	20.83		
D4	19.03		
D5	19.11	18.90	36
D6	18.57		
E4	20.81		
E5	19.31	20.33	42
E6	20.88		
F4	20.21		
F5	18.77	19.11	50
F6	18.36		
G4	18.93		
G5	18.21	18.74	56
G6	19.08		

Based on these results it appears that length of time spent in 105°C water has no effect on the maximum stress of the ETFE samples. Ansell also noted that there was no colour change in the samples after they were held in hot water.

Ansell also performed uniaxial short-term tensile tests on specimens that were exposed to ultraviolet (UV) radiation for 51 days. The samples were placed under two filtered xenon arc lamps with power outputs of 1000 W/m^2 used to simulate solar radiation in the visible and UV range with wavelengths between 300 and 830 nm. Table 1.4 shows the results of the tensile tests in the longitudinal direction of the film, after exposure, for five samples of 300 μm thick foil.

Table 1.4 - Effect of UV radiation on maximum stress of ETFE, as per Ansell (1985)

Sample	Maximum Stress (MPa)	Average Maximum Stress (MPa)
UV 1	19.06	
UV 2	20.73	
UV 3	19.06	19.43
UV 4	19.34	
UV 5	18.95	

Ansell concluded that exposure to UV radiation also had no effect on maximum stress.

To determine the yield stress, yield strain and elastic modulus of ETFE, Ansell conducted tensile tests. He found the modulus to be about 460 MPa, the yield stress to be about 13.08 MPa and the yield strain to be about 2.87%. These values are all much lower than those reported more recently by others, given in Table 1.1. He also loaded an unyielded specimen to 11.6 MPa (90% of the yield stress he determined) twenty times and found that the strain in this range was completely recoverable (Moritz, 2007b).

Tear tests were performed on production-fresh samples of 300 μm ETFE film, that were 50 mm by 50 mm and slotted in the centre. The results are shown in Table 1.5.

Table 1.5 - Tear strength of production-fresh samples of ETFE foil, as per Ansell (1985)

Sample	Direction (L=Logitudinal, T=Transverse)	Tear Force F (N)	Tear Strength F/d (d=0.3 mm) (MPa)	Average Tear Strength (MPa)
300 L2T	L	217.78	725.7	
300 L3T	L	217.78	725.7	
300 L4T	L	213.86	712.6	699.5
300 L5T	L	204.05	680.0	
300 L6T	L	198.16	660.3	
300 T1T	T	196.20	653.7	
300 T2T	T	197.18	657.0	
300 T3T	T	197.18	657.0	657.0
300 T4T	T	198.16	660.3	
300 T5T	T	196.20	653.7	

Tear tests were then completed on 100 μm thick 50 mm by 50 mm samples which, prior to testing, were held in 105°C water for 44 days. The results of these tear tests are shown in Table 1.6.

Table 1.6 - Tear strength of ETFE samples held in boiling water for 44 days, as per Ansell (1985)

Sample	Direction (L=Logitudinal, T=Transverse)	Tear Force F (N)	Tear Strength F/d (d=0.1 mm) (MPa)	Average Tear Strength (MPa)
100 L1T	L	77.08	770.8	865.9
100 L2T	L	81.70	817.0	
100 L3T	L	81.59	815.9	
100 L4T	L	91.40	914.0	
100 L5T	L	95.91	959.1	
100 L6T	L	92.18	921.8	
100 T1T	T	70.22	702.2	707.1
100 T2T	T	71.78	717.8	
100 T3T	T	66.00	660.0	
100 T4T	T	71.78	717.8	
100 T5T	T	74.33	743.3	
100 T6T	T	69.82	698.2	

The third and final set of tear tests were done on bent samples. Prior to the tear tests, the samples were bent in half and held in place for ten seconds with a ten kilogram mass. The samples were then bent in the other direction and held in place for another ten seconds. They were then bent and held one more time in each direction so that they had been bent a total of four times before the tear tests. All samples were tested in the longitudinal direction. The first three samples were 100 μm thick and the last three were 300 μm thick. All samples were tested in the longitudinal direction. Table 1.7 gives the results of the tear test.

Table 1.7 - Tear strength of bent ETFE samples, as per Ansell (1985)

Sample	Direction (L=Logitudinal, T=Transverse)	Tear Force F (N)	Tear Strength F/d (d=0.1 mm, d=0.3 mm) (MPa)	Average Tear Strength (MPa)
100 L7T	L	91.53	915.3	885.6
100 L8T	L	84.86	848.6	
100 L9T	L	89.47	894.7	
300 L7T	L	229.55	765.5	735.8
300 L8T	L	224.65	748.8	
300 L9T	L	207.97	693.2	

The samples that were held in boiling water exhibited higher tear strengths than the production fresh samples. The bent samples also display higher tear strengths than the production fresh samples, and similar values to those held in boiling water. At the time when Ansell completed these tests, no standardized testing methods were available for tear tests, so his values differ from more recent data conducted using standardized methods. Therefore, Ansell's results are valuable for comparing the relative tear strengths of production-fresh, heated and bent samples, but additional resources should be consulted when seeking absolute values for tear strengths.

Ansell also conducted uniaxial creep tests at different temperatures which are discussed in Section 1.7.2.2.

1.7.1.2 DSET Laboratories, 1979-1989

Researchers at DSET Laboratories in Phoenix, Arizona, performed long-term tests on ETFE foils over a period of ten years. The 200 μm thick samples were exposed to the Arizona climate continually and their mechanical properties were tested after 1, 2, 3, 5, 7 and 10 years. The total amount of solar radiation experienced by the foils over the ten-year period was 78.1 MJ/m^2. Table 1.8 summarizes the results of these tests.

Table 1.8 - Mechanical properties of ETFE film after exposure to Arizona environment, as per DSET test results (Moritz, 2007b)

Property	Units	Years of Exposure						
		Original	1	2	3	5	7	10
Longitudinal (L) Direction Tensile Strength	MPa	46.7	45.6	46.2	44.9	46.0	48.4	52.4
Transverse (T) Direction Tensile Strength	MPa	42.3	43.8	45.5	42.6	44.8	42.4	44.6
Stress at 10% Strain (L)	MPa	22.6	22.5	25.0	22.3	23.2	22.8	22.5
Stress at 10% Strain (T)	MPa	21.8	21.4	22.0	-	22.3	21.0	21.5
Break Strain (L)	%	330	340	310	345	315	325	340
Break Strain (T)	%	390	405	390	390	420	390	405
Tear Strength (L)	N/mm	420	430	415	445	440	525	-
Tear Strength (T)	N/mm	435	425	420	480	430	530	-
Light Transmission (Total)	%	95	96	94	95	96	96	96
Light Transmission (Scattered)	%	8	8	11	9	11	11	8
Light Transmission (Direct)	%	87	88	83	86	85	85	88

These data are shown visually in Figures 1.26 - 1.28. Figure 1.26 plots tensile strength (σ_B), break strain (ε_B), and stress at 10% strain ($\sigma_{\varepsilon=10\%}$), in each direction (T and L).

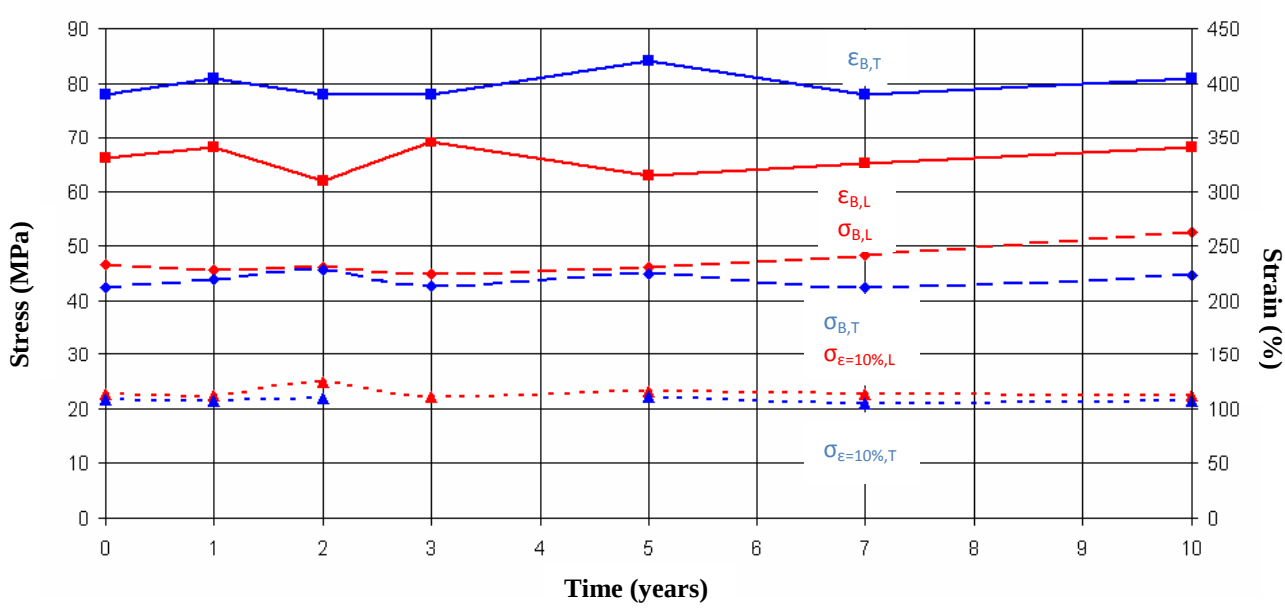

Figure 1.26 - Tensile strength, break strain and stress at 10% strain at various years of exposure to environment, as per DSET test results (Moritz, 2007b)

From this graph it is evident that no significant changes occurred in any of these mechanical properties over the course of the ten years. Figure 1.27 plots tear strength of the material in both directions, where "E" indicates the longitudinal direction and "Q" indicates the transverse direction.

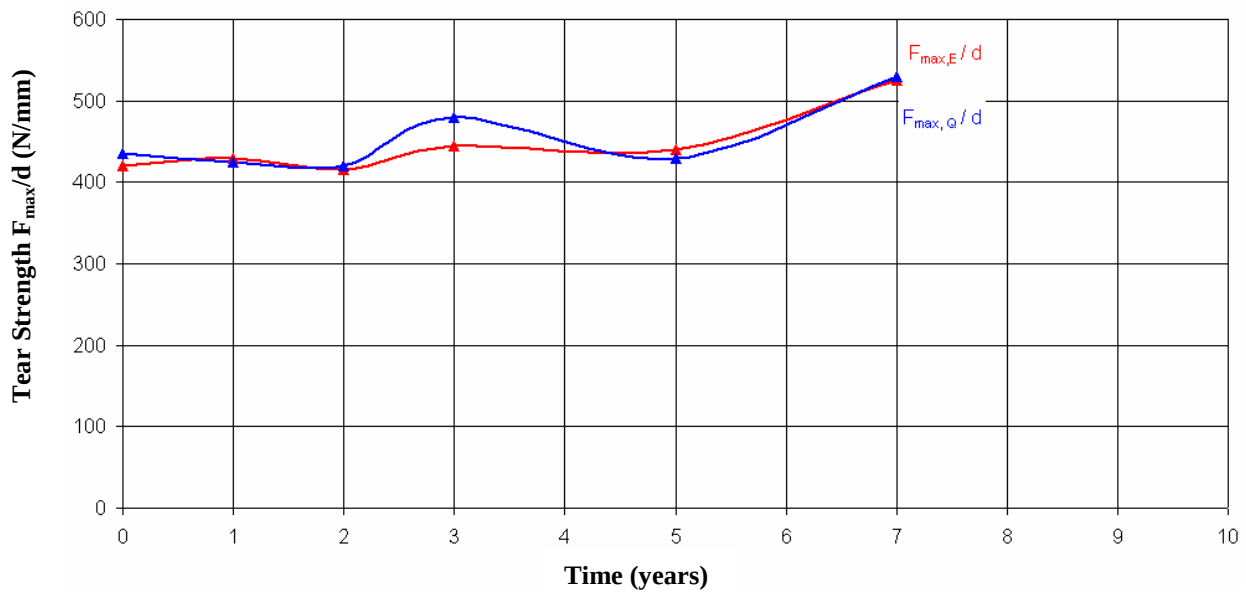

Figure 1.27 - Tear strength at various years of exposure to environment, as per DSET test results (Moritz, 2007b)

Over the seven-year period where tear strength was tested, it increased by about 25% in both directions. However, since the increase occurred predominantly between five and seven years, and prior to five years the tear strength fluctuated above and below its original value, it is difficult to draw any definitive conclusions regarding the effects

of environmental exposure on tear strength based on these results. Figure 1.28 shows the light transmission over the ten year exposure period, where t_t is total light transmission, t_d is direct light transmission and t_s is scattered light transmission.

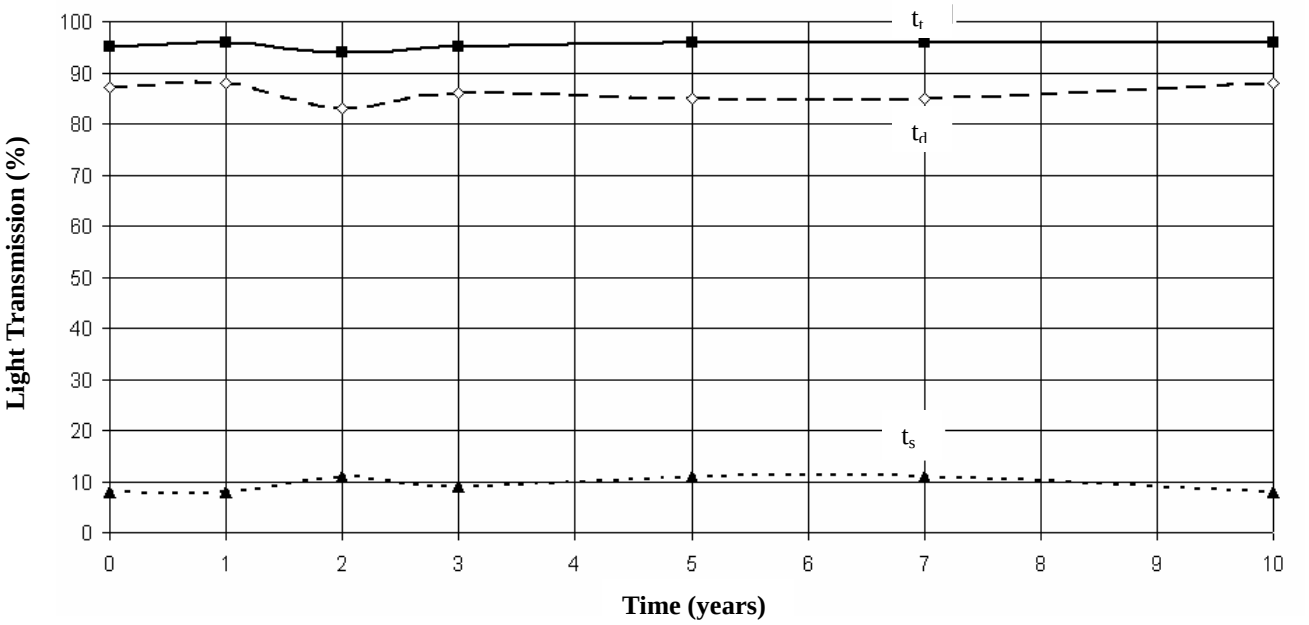

Figure 1.28 - Light transmission of ETFE foils at various years of exposure to environment, as per DSET test results (Moritz, 2007b)

There are no obvious changes in any of the light transmission levels over the ten year exposure period.

Based on the results of the DSET tests, exposure to an Arizona-type environment, which is generally fairly dry and hot, with high levels of solar radiation, appears to have little impact on the mechanical properties of ETFE over a ten year period.

1.7.1.3 Barthel, Burger and Saxe, 2003

Researchers Barthel, Burger and Saxe at the University of Duisburg-Essen in Germany undertook a test program on ETFE films which included uniaxial and biaxial short-term tensile tests, cyclic load tests and uniaxial creep tests. All tests were conducted on Nowoflon ET 6235 film with a thickness of 225 microns, at 23°C. The uniaxial short-term tensile tests loaded the 200 mm long and 100 mm wide strips at a rate of 0.2 (kN/m)/s. They found the material to have a yield strength of 39.1 MPa in the longitudinal direction and 40.3 MPa in the transverse direction, and an average elongation at break of 340% (Barthel, Burger, & Saxe, 2003; Moritz, 2007b).

Biaxial tensile tests were also done, where the material was loaded to 26.7 MPa, then the load was released and the material was allowed to rest for 24 hours before it was loaded again to 26.7 MPa. The following figure shows a load-strain diagram for a biaxially loaded sample. The vertical axis gives the load on the film in kN/m, where 26.7 MPa is equivalent to 6 kN/m. The horizontal axis gives the engineering strain in percentage of original length. The

red line with circular points represents the curve in the longitudinal direction and the blue line with square points represents the curve in the transverse direction (Barthel, Burger, & Saxe, 2003; Moritz, 2007b).

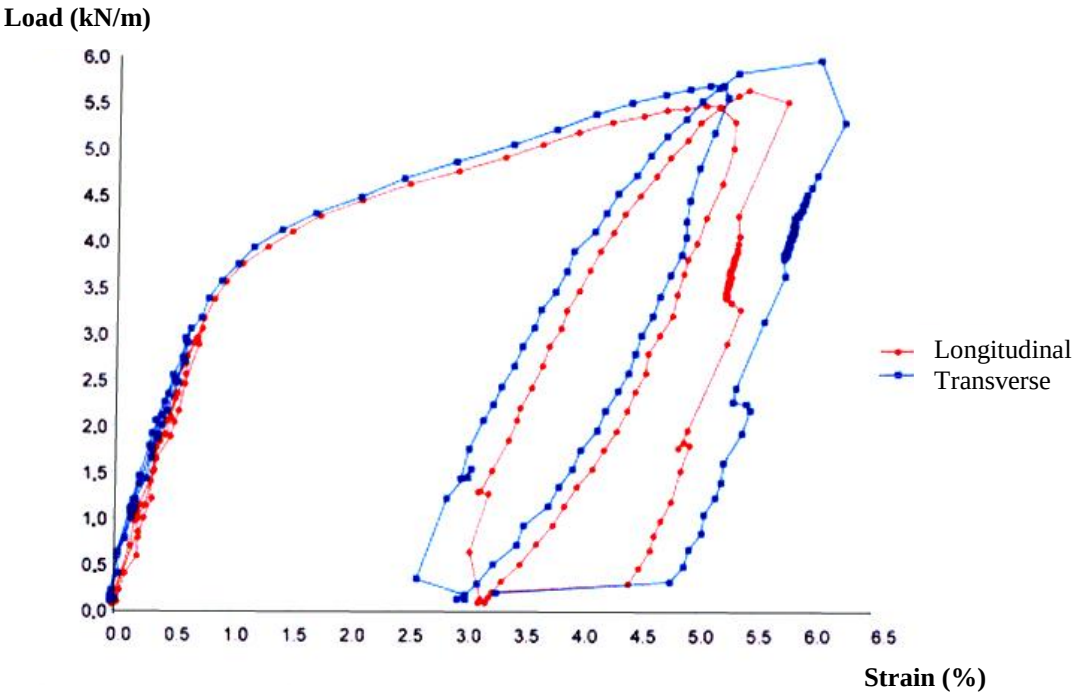

Figure 1.29 - Load-strain curve for biaxially loaded specimens, as per test data from Barthel, Burger and Saxe (Moritz, 2007b)

Figure 1.29 shows that the material is nearly isotropic, particularly at lower stress levels. Linear elastic behaviour is noticeable up to about 13.3 MPa (3 kN/m on the graph), after which the curve begins to flatten. The relationship between load and strain from about 17.8 (4 kN/m) to the maximum load is also fairly linear. After unloading and reloading, higher strains are evident for the same levels of stress. From this test, the Poisson's ratio was determined to be 0.45. The test also showed that modulus of elasticity is dependent upon load history, as the material is initially stiffer than after it has been loaded. Using linear regression of the results, the researchers found the modulus of pre-loaded ETFE to be approximately 600 to 750 MPa (Moritz, 2007b).

The uniaxial cyclic tests loaded the material five times to 17.8 MPa, allowed it to rest for a period of 24 hours, then loaded it to the same stress level another five times, and then discharged the load for a period of 72 hours after which residual strains were measured. The samples had the same dimensions as those used for the uniaxial short-term tensile tests and they were also loaded at a rate of 0.2 (kN/m)/s at a temperature of 23°C. The maximum extension of the specimens increased with each cycle, but at a decreasing rate. After unloading, the residual strains in the transverse direction of the material were found to be higher than those in the longitudinal direction (Moritz, 2007b).

Barthel, Buger and Saxe (2003) also performed uniaxial creep tests, which will be discussed in Section 1.7.2.3.

1.7.1.4 De Vries, 2003

In 2003 J.W.J de Vries completed a graduate thesis at the Delft University of Technology on the use of ETFE foil in construction. As part of his research he conducted uniaxial and biaxial short-term tensile tests at different stresses.

De Vries (2003) used the uniaxial tests to determine testing parameters for the biaxial tests. He tested five samples in each direction – transverse, longitudinal and 45° to these two directions. The samples were 50 mm wide, 200 µm thick and had gauge lengths of 200 mm. De Vries identified two points of interest on the stress-strain curves – the proportional limit, which he defines as the end of linear-elastic behaviour, and the strain acceleration point, which he defines as the point where the ratio of increasing strain to increasing stress becomes very high. These two points are shown on Figure 1.30, and are labelled as P and S, respectively.

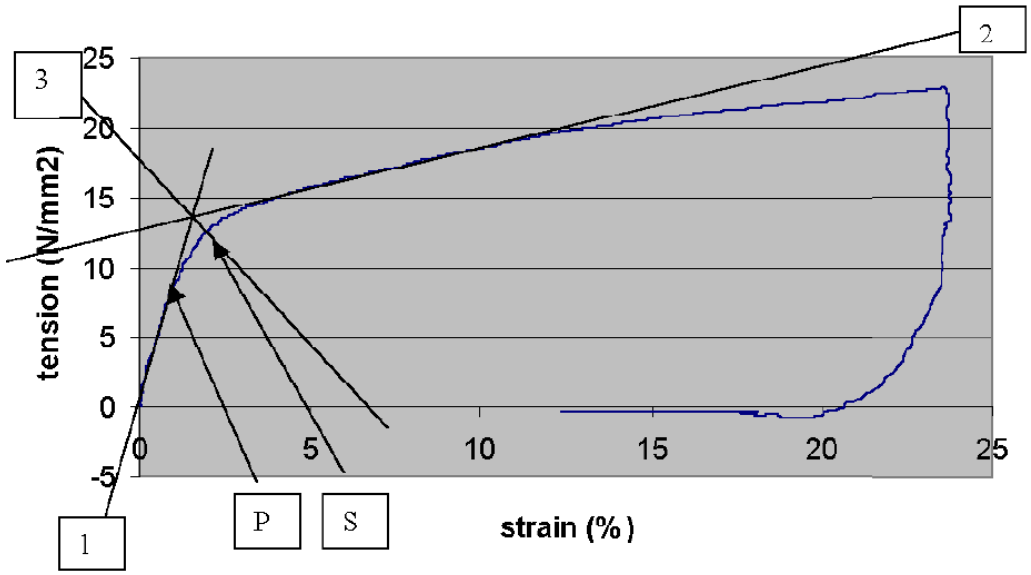

Figure 1.30 - Stress-strain curve showing proportional limit and strain acceleration point, as per de Vries (2003)

Table 1.9 gives the stress and strain proportional limit as well as the modulus of elasticity for the uniaxial tests.

Table 1.9 - Results of uniaxial tests on ETFE, as per de Vries (2003)

Direction	Proportional Limit (MPa)	Strain (%)	Modulus of Elasticity (MPa)
Longitudinal	10.7	0.7	1427
Transverse	11.4	0.94	1305
Diagonal (45°)	12.1	0.95	1285

De Vries (2003) also performed uniaxial tests on welded specimens. He found that all specimens yielded before the welds failed, but that the welded samples failed at lower stresses than the non-welded samples.

The dimensions of the biaxial specimens tested by de Vries are shown in Figure 1.31.

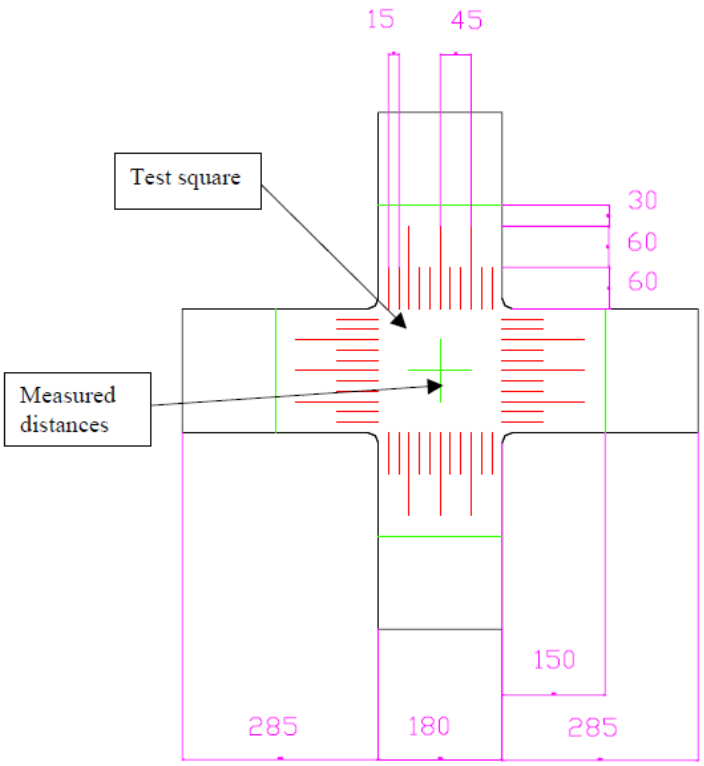

Figure 1.31 - Dimensions of biaxial specimens tested by de Vries (2003)

The biaxial tests were done with a range of load ratios between the two directions from 1:0 to 1:5. The samples were prestressed to about 1.3 MPa (50 N) in both directions and loaded at a rate of 2.75 N/s. Figure 1.32 shows a typical result for the stress-strain behaviour of a sample loaded at a 1:1 ratio (de Vries, 2003).

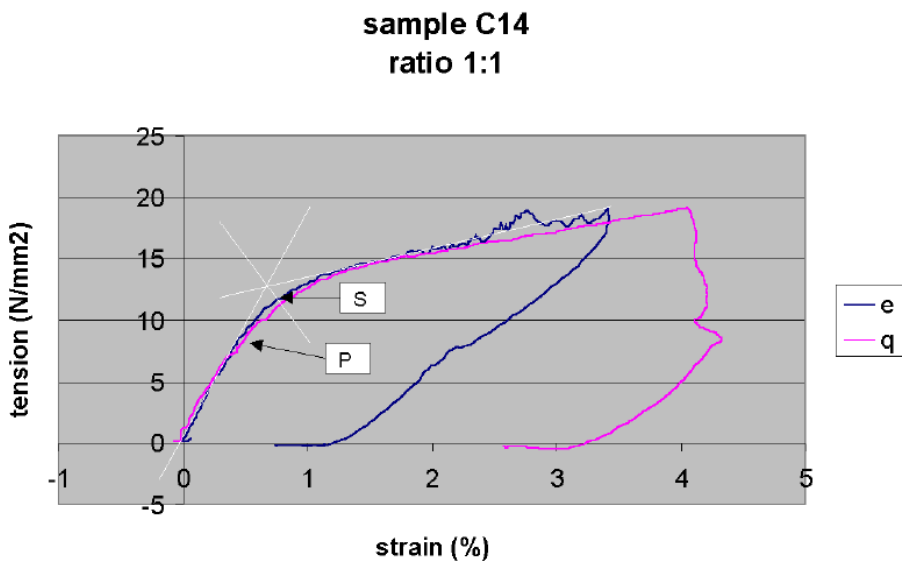

Figure 1.32 - Typical stress-strain curves for a 1:1 biaxial test, as per de Vries (2003)

In this figure there is little difference between the stress values of the two directions at the proportional limit, strain acceleration point and at failure, but the longitudinal direction (labelled "e") exhibits less strain at unloading than the transverse direction (labelled "q"). This can be explained by the asymmetries in testing discussed below.

The two graphs in Figure 1.33 show values for the proportional limit and for the strain acceleration stress point. The horizontal axes (labelled "Q" and "q") represent the transverse material direction and the vertical axes (labelled "E" and "e") represent the longitudinal material direction. The different points represent the stresses at different loading ratios in the longitudinal and transverse directions.

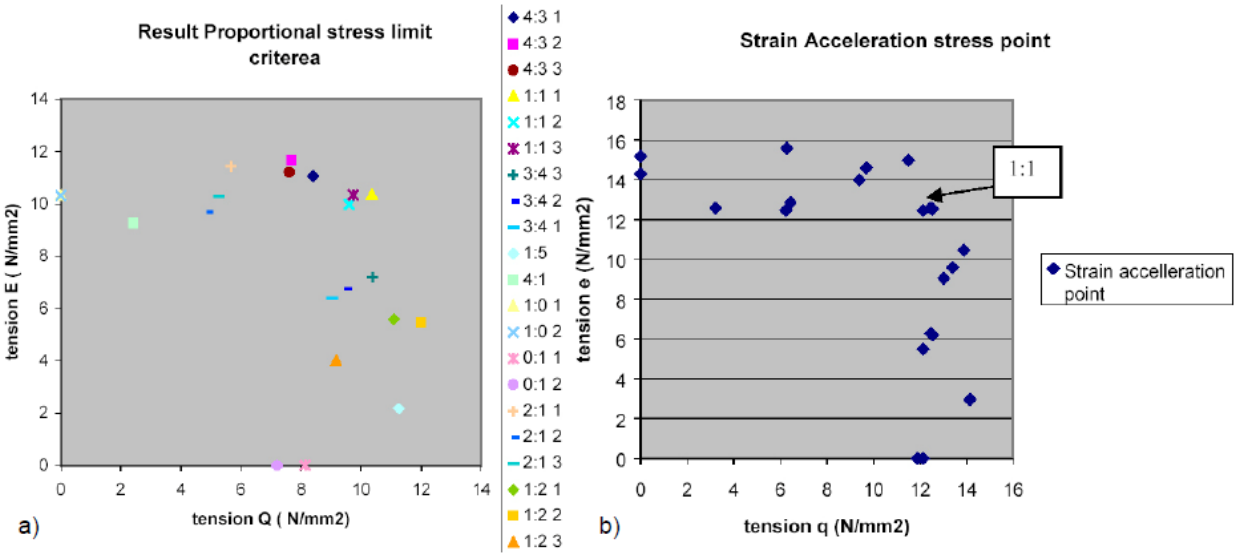

Figure 1.33 - Measured values of biaxial stress at the proportional limit (a) and the yield point (b), as per de Vries (2003)

It is evident from Figure 1.33 that stress of the material in one direction is not greatly affected by the stress in the other direction. For example, the proportional limit of the foil at a ratio of 1:0 (longitudinal: transverse) is nearly the same as for all ratios where the stress in the longitudinal direction is greater than or equal to that in the transverse direction. This indicates that mechanical properties, such as yield, determined through uniaxial tests should give the same results to those determined through biaxial tests.

De Vries (2003) also did several biaxial load repetition tests where, after the sample had yielded, he would unload it at the same speed as it was loaded, and then repeat the loading after the stress dropped below 3 MPa. This cycle was repeated several times on the sample. A typical results graph is shown in Figure 1.34.

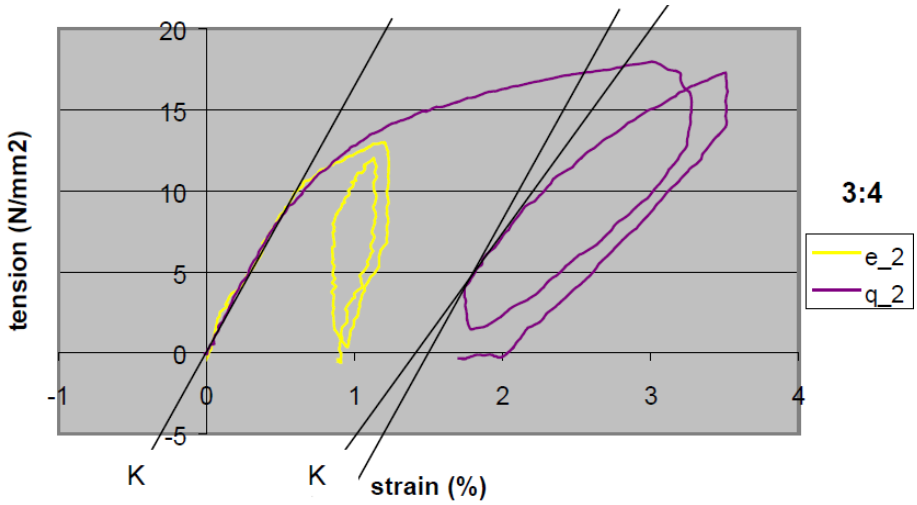

Figure 1.34 - Typical stress-strain curves for repeated loading biaxial test, as per de Vries (2003)

The proportional limit does not appear to change significantly from one repetition to the next, but the secant modulus at the proportional limit appears to be less for the second loading (de Vries, 2003).

De Vries encountered several problems in his testing. For the biaxial tests, skewing of the samples occurred as shown in Figure 1.35.

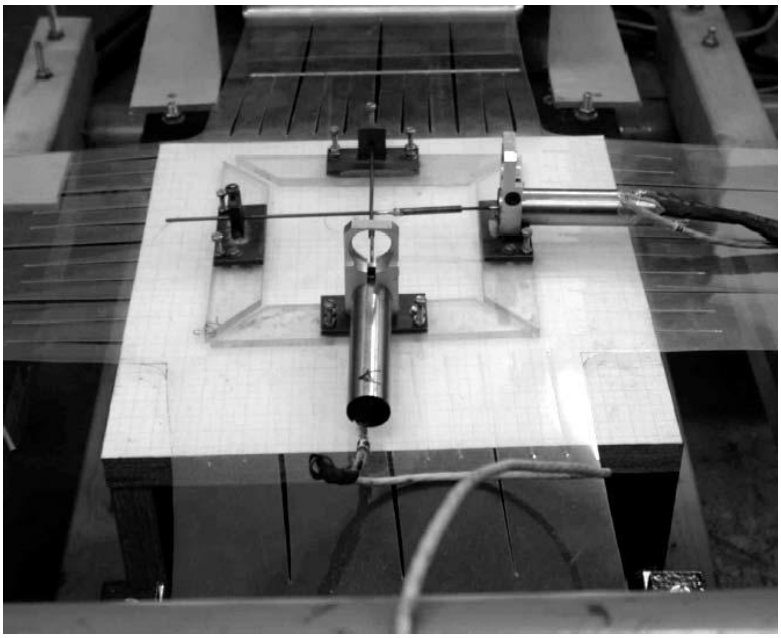

Figure 1.35 - Skewed sample during biaxial test by de Vries (Moritz, 2007b)

De Vries gives several possible reasons for this, including asymmetries in the samples due to manual preparation, friction losses at the clamps, and possible asymmetry of the testing apparatus. Because of the asymmetry, the samples flowed in an anisotropic manner (de Vries, 2003).

1.7.1.5 Moritz, 2007

As part of the PhD dissertation at the Technische Universität München, *ETFE-Folie als Tragelement* (ETFE Foil as a Structural Element), Karsten Moritz analyzed the results of a series of mechanical tests on ETFE foils (2007b). These tests included uniaxial and biaxial short term tensile tests, Dynamic Mechanical Analysis (DMA) tests and burst tests.

For the uniaxial short term tensile tests, Moritz analyzed data collected by Moritz, Abstreiter, and Grützmann in 2000. A total of 123 samples were tested; 108 plain samples ranging in thickness from 100 μm to 250 μm, and 15 welded samples of 200 μm film. Tensile tests were done in both the longitudinal and transverse directions at 23°C. The strain rate for the experiments was 100 mm/min for strains less than or equal to 0.2 and 500 mm/min for strains greater than 0.2. Figure 1.36 shows the average stress strain curves for the different film thicknesses and directions.

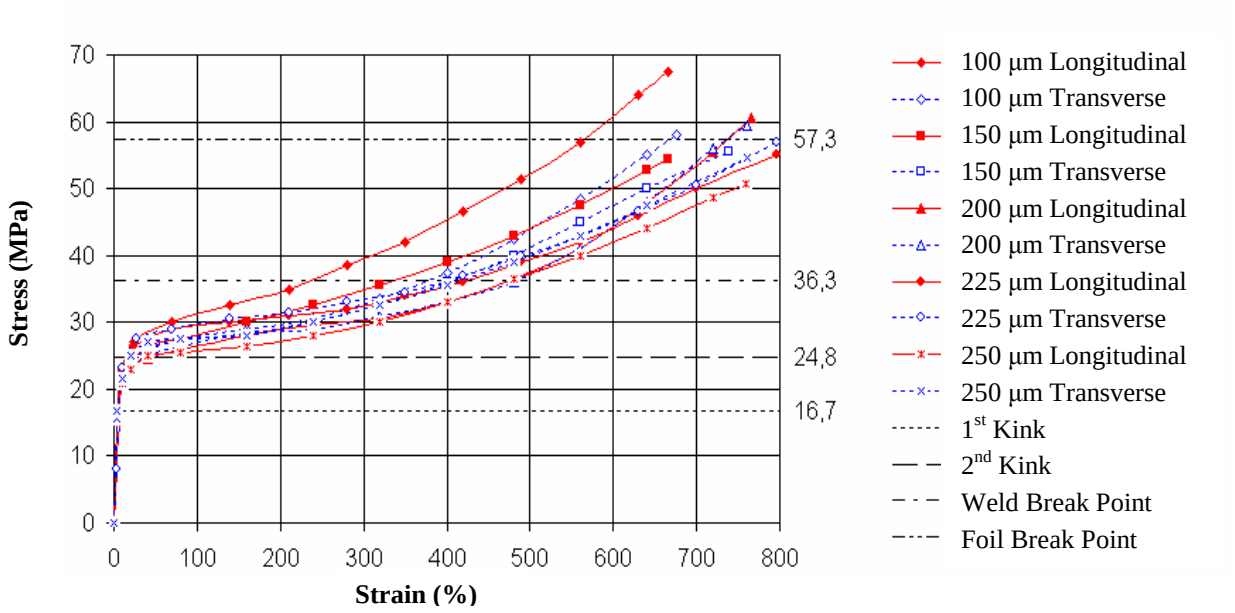

Figure 1.36 - Stress-strain behaviour of multiple ETFE film samples, as per Moritz (2007b)

The horizontal dashed lines in the figure show the so-called first yield, which is roughly the end of the linear-elastic region, at 16.7 MPa, the second yield, where plastic deformation begins, at 24.8 MPa, the average breaking stress of the welded samples at 36.3 MPa, and the average breaking stress of the plain samples at 57.3 MPa. Moritz also created Figure 1.37 from the data to show the relationship between film thickness, direction and break stress.

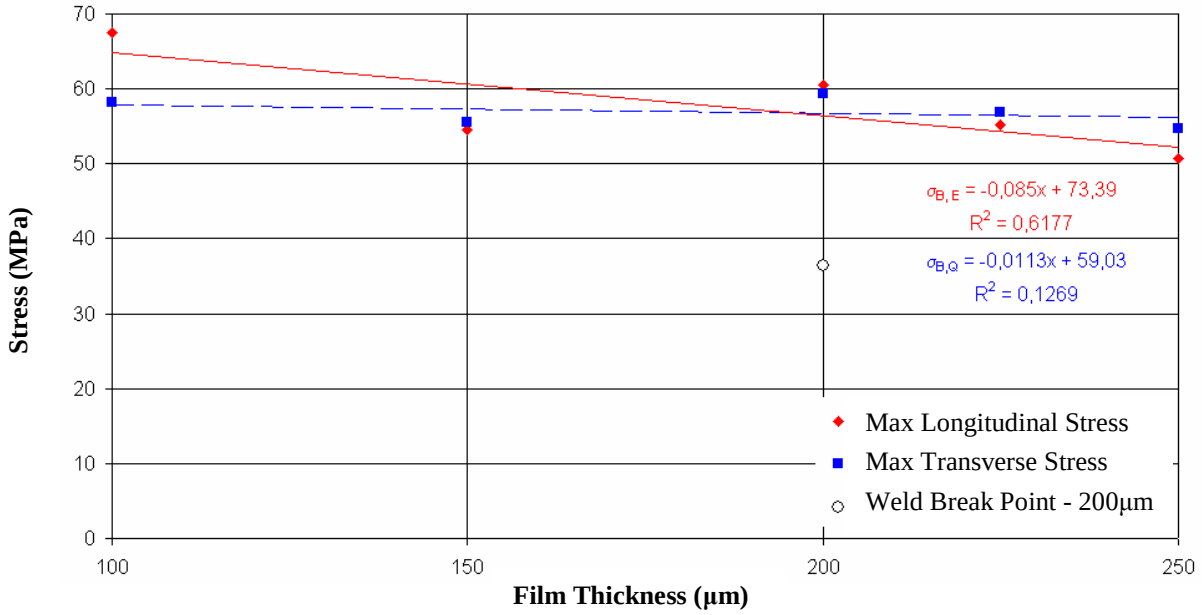

Figure 1.37 - Film thickness vs. breaking stress for both film directions, as per Mortiz (2007b)

From Figure 1.37, it appears that for the specimens in this test, break stress decreased somewhat for greater foil thicknesses. Also, isotropic behaviour was evident only at the mid-level thicknesses of foil, with the 100 µm film appearing to have greater strength in the longitudinal direction and the 250 µm film appearing to have slightly

greater strength in the transverse direction. The break strength of the welded sample is also shown on the figure as the hollow circular point on the 200 μm line. From this, and from Figure 1.36, it is clear that the welds are the first points of failure in the samples, causing failure to occur at much lower stresses than the actual break stress of the foils.

For the biaxial tests, Moritz (2007b) analyzed data collected in 2004 by Saxe and Knop. The samples were cyclically loaded at temperatures of -25°C, 0°C, 23°C and 35°C. The samples were loaded to eight different stress levels, where the transverse direction (direction I) was the principal stress direction, and the longitudinal direction (direction II) carried the lower stress level. Figure 1.38 shows the stresses in the two film directions at each of the eight loading levels for a 250 μm sample at 23°C.

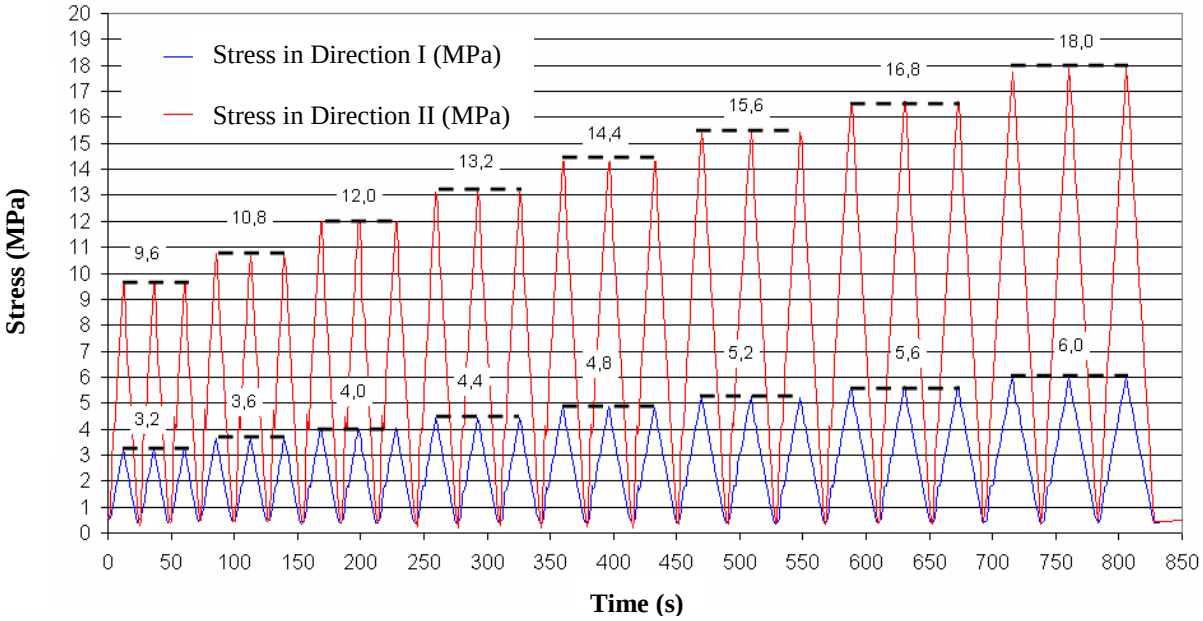

Figure 1.38 - Stress vs. time for three cycles at each of eight biaxial loading levels for 250 μm sample at 23°C, as per Moritz (2007b)

Figure 1.39 shows the stress strain curves for the samples at each of the four temperature levels.

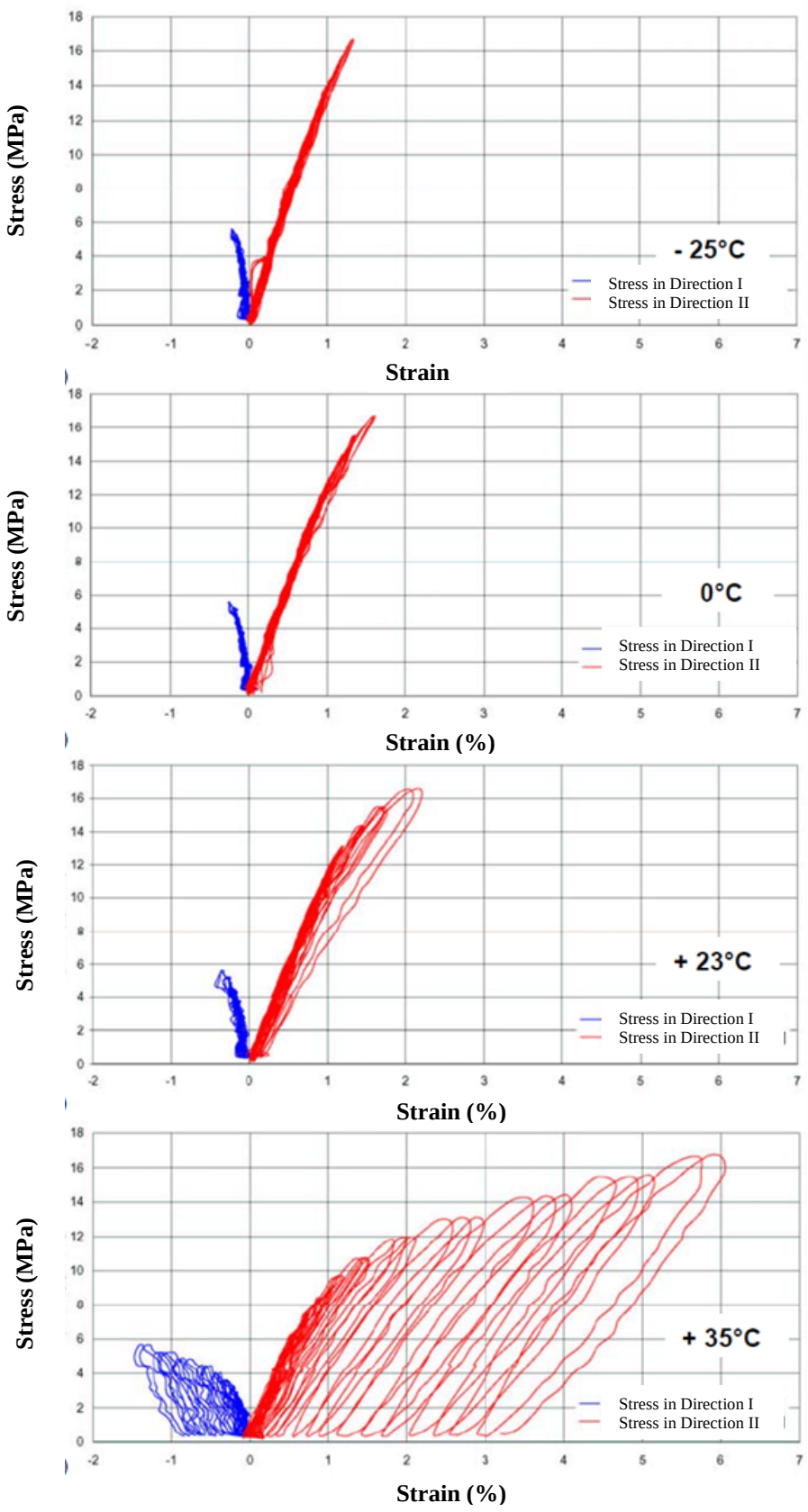

Figure 1.39 - Stress-strain curves for cyclic biaxial tests at different temperatures, as per Moritz (2007b)

From Figure 1.39, it can be seen that as temperature increases, the instantaneous strain remaining in the sample after each loading cycle increases. At -25°C it appears that nearly all strain is recovered immediately after each cycle, but at +35°C the remaining strain in the sample increases after every cycle. A detailed analysis of the effects of temperature on these tests can be found in Moritz's thesis (Moritz, 2007b).

Moritz also analyzed the data obtained by Saxe and Knop from their biaxial experiments at different loading speeds. All of these tests were done at 23°C. The samples were cyclically loaded three times to the same stress level at the first loading rate, and then again at the second rate and then finally at the third rate. The three rates were 0.02, 0.2, and 0.96 (kN/m)/s in the longitudinal direction (direction II), corresponding to approximate rates of 0.007, 0.07, and 0.32 (kN/m)/s in the transverse direction (direction I). Figure 1.40 shows the stress and strain in both directions of the sample, over time.

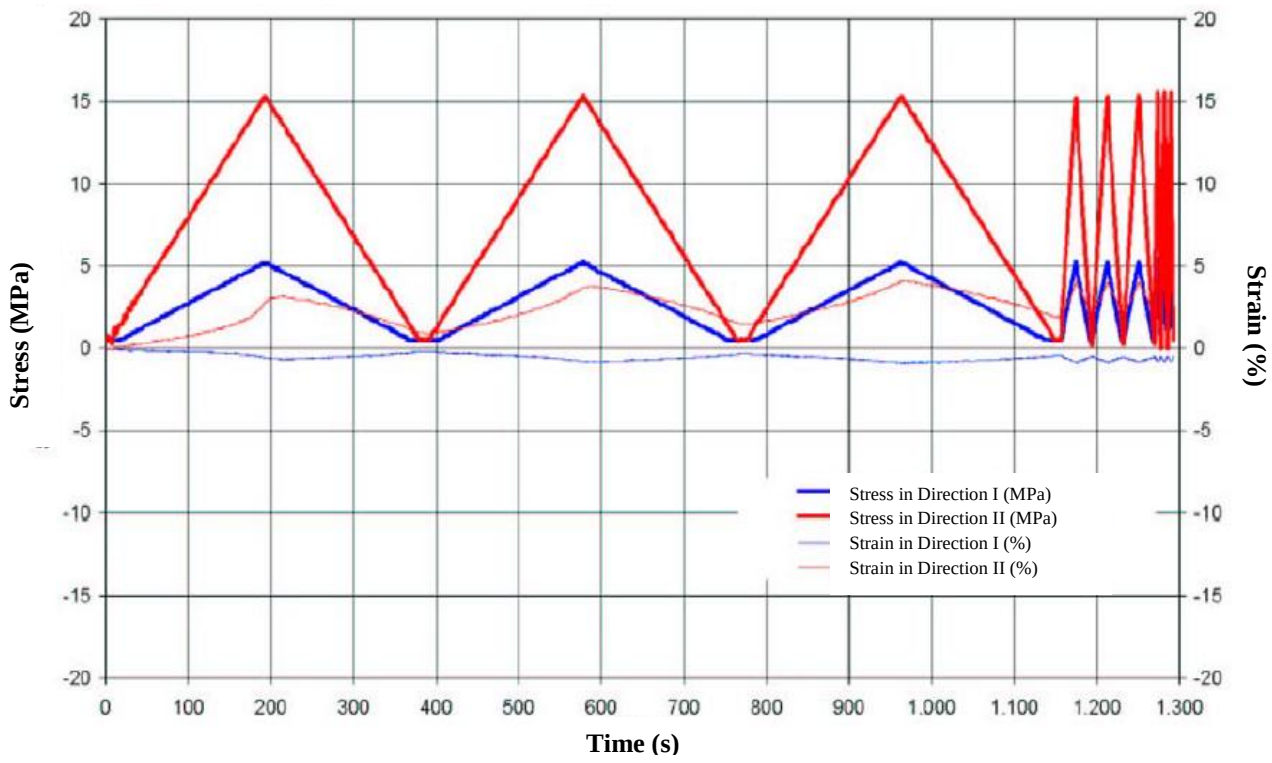

Figure 1.40 - Biaxial cyclic test of ETFE film, with increasing loading speed, as per Moritz (2007b)

The actual stress strain diagram for the three different loading speeds is shown in Figure 1.41.

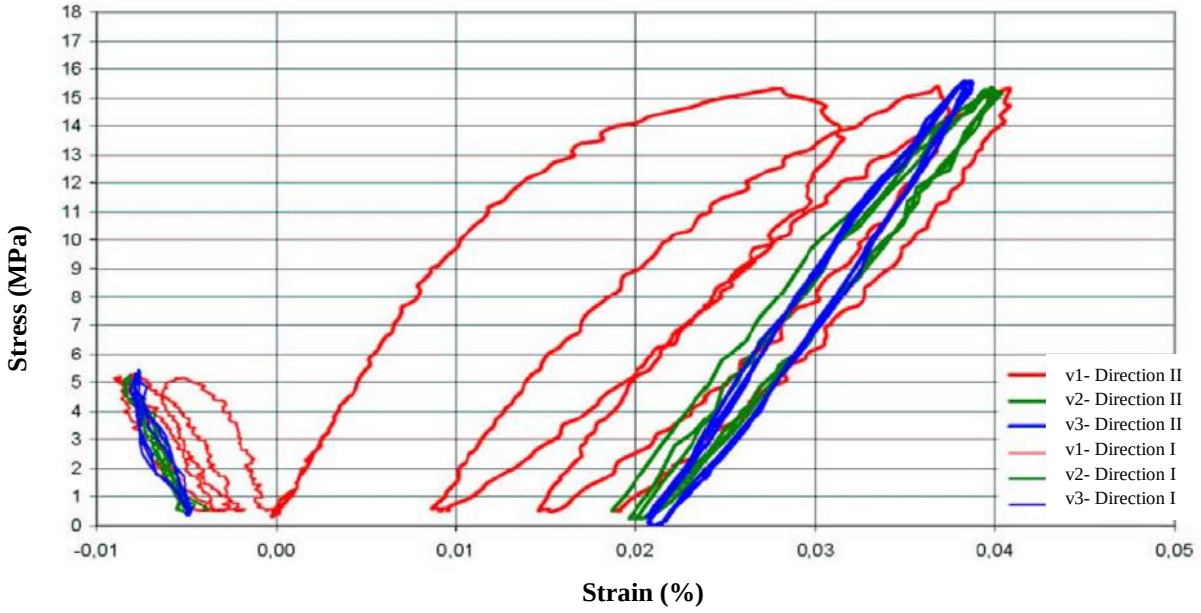

Figure 1.41 - Stress-strain diagram for cyclic loading of ETFE at three different loading speeds, as per Moritz (2007b)

If the residual strains that remain instantaneously after each loading cycle are removed, Figure 1.42 describes the result.

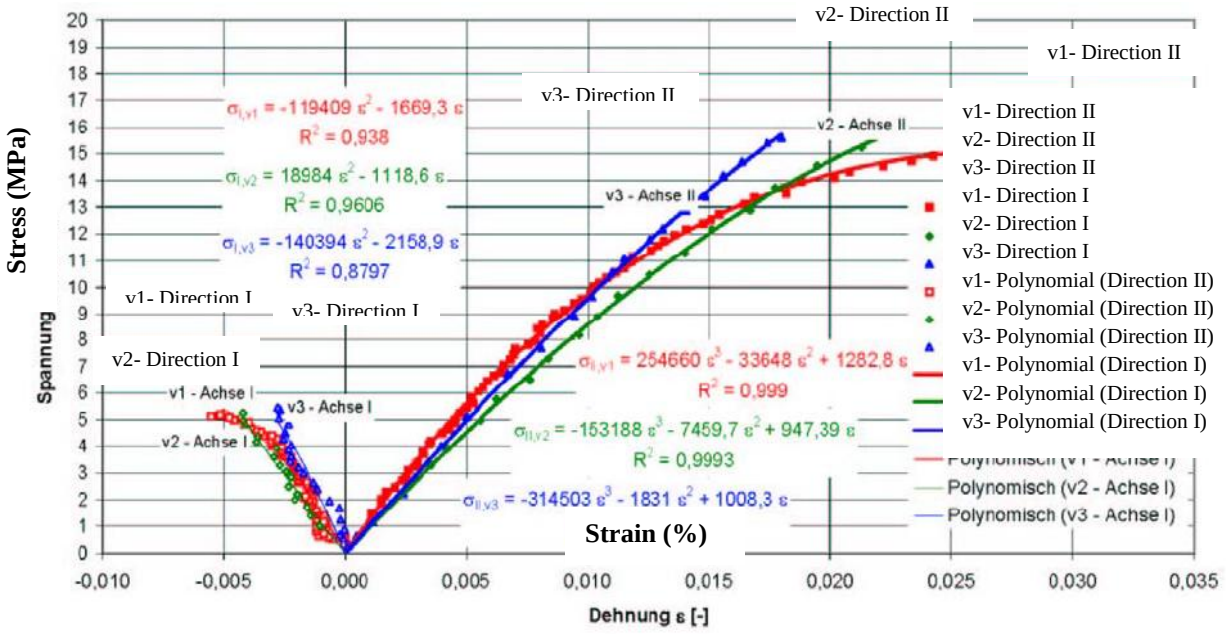

Figure 1.42 - Stress-strain diagram for cyclic loading of ETFE at three different loading speeds, with residual strains removed, as per Moritz (2007b)

The specimens tested at the two higher loading speeds (v2=0.2 (kN/m)/s and v3=0.95 (kN/m)/s) display nearly linear behaviour and do not exhibit a yield point. However, the specimens tested at the lower loading speed (v1=0.02 (kN/m)/s) display nonlinear stress-strain behaviour. This is likely because time-dependent creep, which is

nonlinear in nature, is occurring simultaneously with the elastic strain and the slower loading speeds allow for more creep to occur.

DMA tests can be used to determine the degree of viscoelasticity of a polymer. The concept of viscoelasticity is discussed in detail in section 3.1. A sinusoidal stress is applied to a sample and the resulting strain is measured. In a perfectly elastic material the stress and strain will occur simultaneously. In a purely viscous material, there will be a 90 degree phase lag, δ, between stress and strain. Values of δ between 0 and 90 will occur for viscoelastic materials. The phase angle, tanδ, is related to the tensile storage and loss moduli, E' and E'', respectively, as follows:

$$\tan\delta = \frac{E''}{E'} \tag{1-36}$$

where,

$$E' = \frac{\sigma_0}{\varepsilon_0}\cos\delta \tag{1-37}$$

$$E'' = \frac{\sigma_0}{\varepsilon_0}\sin\delta \tag{1-38}$$

and σ_0 and ε_0 are the initial stress and strain, respectively (Chawla & Meyers, 1999). The storage modulus, E', represents the elastic response, as it relates to the stored energy, whereas the loss modulus, E'', represents the viscous response, as it relates to the energy lost to heat. Temperature can be varied during DMA tests to investigate its effects on the viscosity of the material. This can indicate the point where the glass transition temperature occurs, and can also give other general information regarding the effects of temperature on the viscoelastic properties of a polymer. The DMA tests analyzed by Moritz were conducted by Dyneon. They were done at three different frequencies – 1, 10 and 100 Hz – and over a temperature range of 0 to 250°C. The strain was pulsated in the range of 0.01 to 0.1% while the temperature was increased at a rate of 2°C/minute (Moritz, 2007b). Figure 1.43 shows the results from these tests.

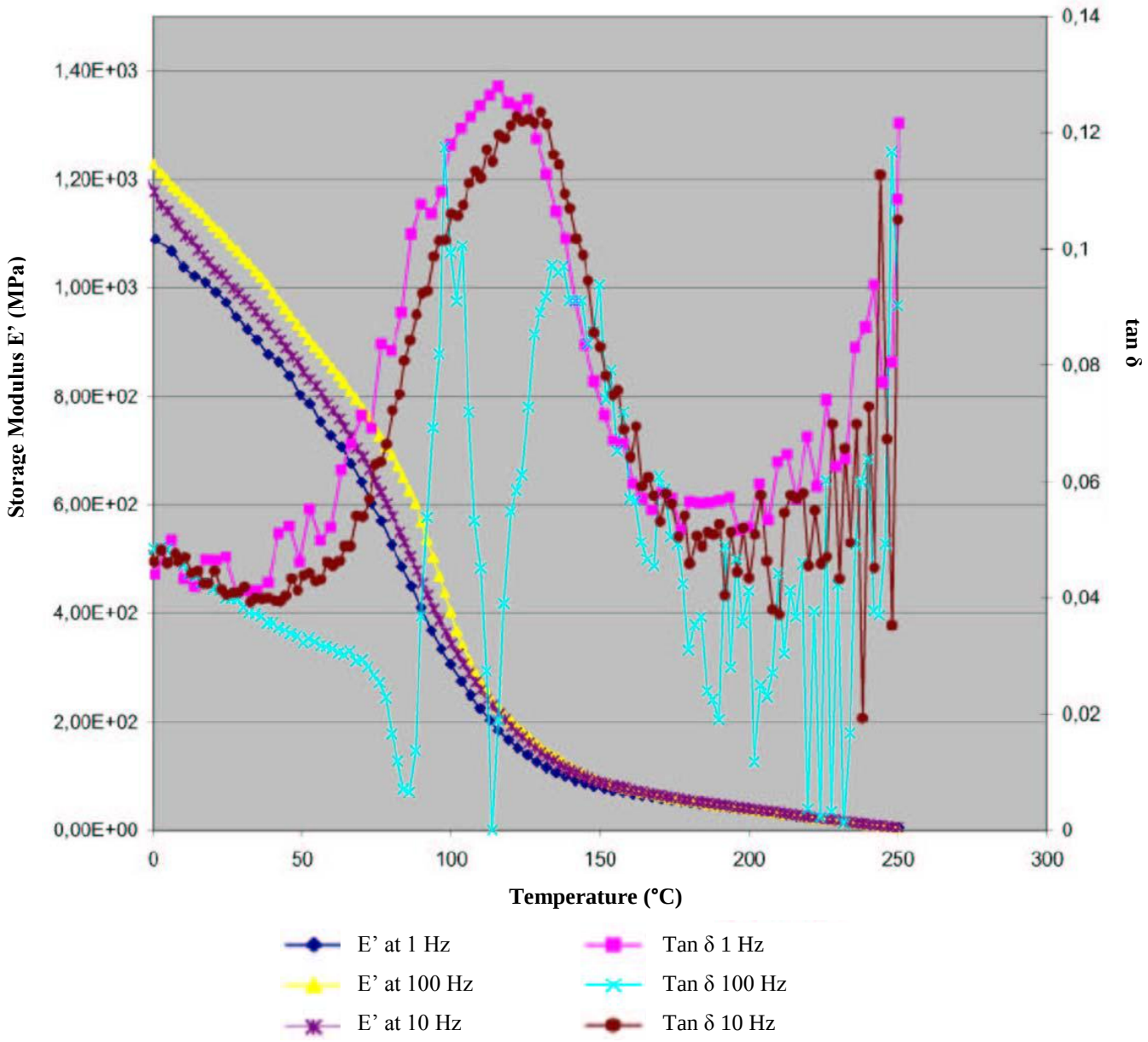

Figure 1.43 - Results of DMA tests on ETFE, as per Moritz (2007b)

The storage modulus decreases as the temperature increases, indicating a reduction in elasticity and an increase in viscosity. The phase angle, tan δ, has local maxima for 1 Hz and 10 Hz at around 120°C. This indicates that softening occurs in this vicinity, suggesting that the glass transition temperature of ETFE is around 120°C (Moritz, 2007b). For the 100 Hz excitation, the glass transition temperature is not clearly visible from the results.

Moritz also analyzed burst test data from Bauer, Steigenberger et al. collected for ETFE manufacturer Skyspan in 2003, using finite element analysis to replicate the test results. The burst tests were done on 3.8 m by 5 m cushions made from 250 micron film. The film was cut such that the pre-inflation camber (vertical distance from horizontal

plane of cushion to centre of foil, labelled in Figure 1.44 as f_0) was 0.592 m, which increased to 0.6 m when the internal pressure was increased to 400 Pa. Figure 1.44 shows the initial geometry of the cushion.

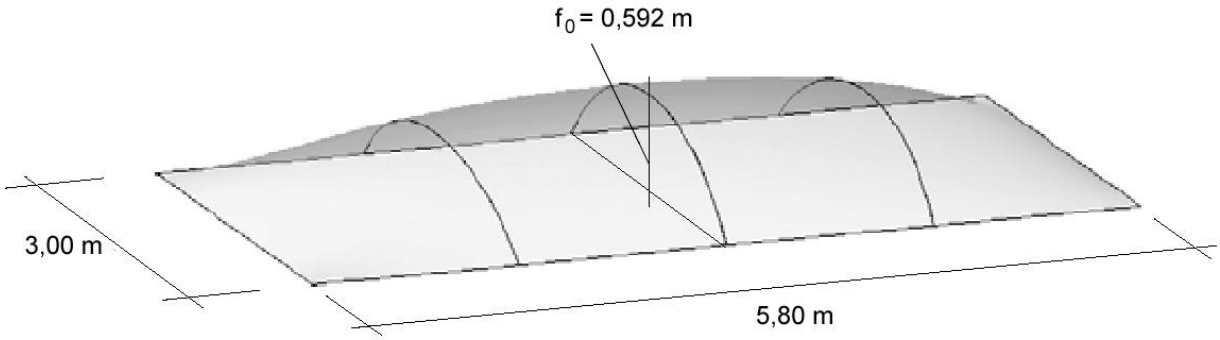

Figure 1.44 - Initial geometry of ETFE cushion used in burst tests by Bauer, Steinberger et al. (Moritz, 2007b)

In the burst tests failure occurred at an internal pressure of approximately 4.8 kPa, corresponding to a camber of about 890 mm. The failure occurred near the centre of the cushion, along a weld boundary.

Moritz divided the film into 3200 approximately square finite elements for her analysis. She used finite element models to investigate the effects of different cutting methods on the final form and stress distribution in the cushion, and compared the results to the results of the physical tests. Moritz also used finite element models to determine the principal stress in the film at the point where it failed during testing, under an internal pressure of 4.8 kPa. The maximum principal stress in the cushion was determined by the model to be 34.79 MPa. This is very similar to the results of the aforementioned biaxial tensile tests on welded specimens, which had an average break strength of 36.3 MPa.

1.7.1.6 Wu, Mu and Liu, 2008

Researchers at Tongji University in Shanghai, China published a paper in 2008 entitled "Cycle Loading and Creep Tests of ETFE Foil" (Liu, Mu, & Wu, 2008). They performed cyclic loading tests on ETFE samples, as well as 24 hour creep tests. The creep tests are discussed in section 1.7.2.4. The ETFE samples were 250 μm thick and were 150 mm by 15 mm, but a gauge length of 100 mm was used for testing. The cyclic loading tests were conducted at a strain rate of 3 mm/minute and at a temperature of 24 +/- 1° C. The first set of samples were loaded to stresses of 6 MPa or 12 MPa, then unloaded for a total of five cycles, and then loaded to 40 to 50% strain. The stress-strain curves from these cycles are shown in Figure 1.45.

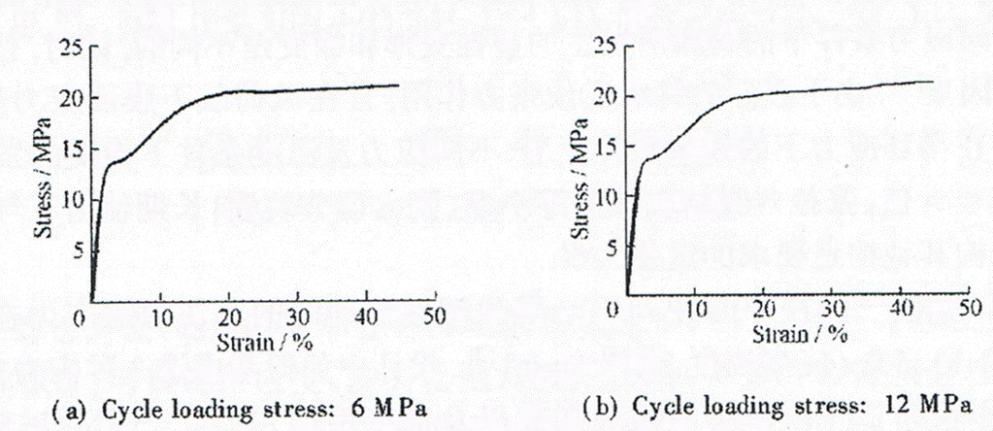

Figure 1.45 - Stress-strain curves for cyclic loading to 6 MPa (a) and 12 MPa (b), as per Liu et al. (2008)

No residual strain developed in this range. The second set of samples was loaded to 17 or 20 MPa, roughly in the range of the elastic limit of the material, and the same procedure was followed. Results are shown in Figure 1.46.

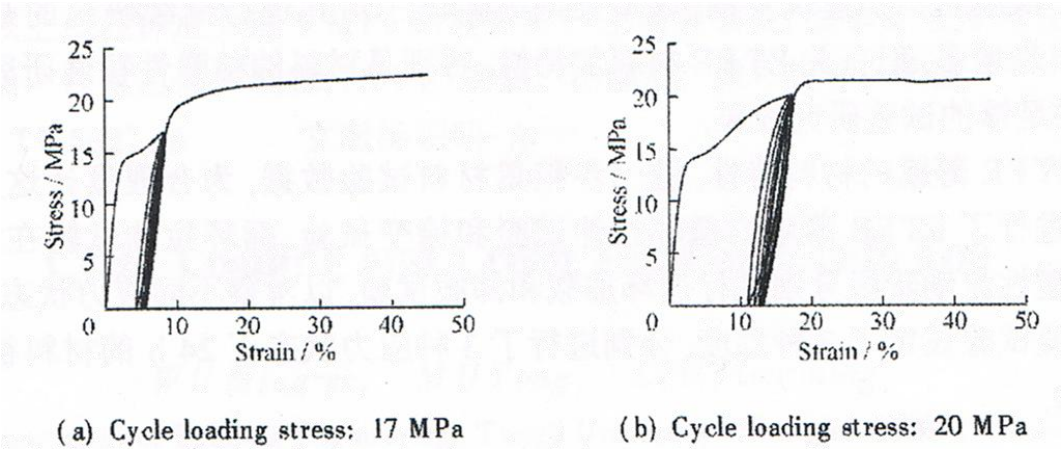

Figure 1.46 - Stress-strain curves for cyclic loading to 17 MPa (a) and 20 MPa (b), as per Liu at al. (2008)

Samples were also cyclically loaded to the elastic limit by using strain instead of stress as the controlling parameter. These samples were strained to 10 or 15% for five repetitions and then were loaded to 40 to 50% strain in the same manner as the previous tests. The results are shown in Figure 1.47.

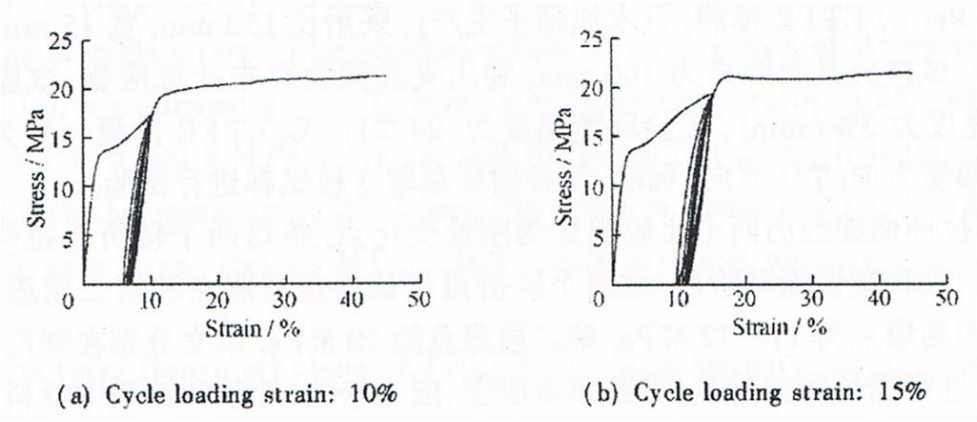

Figure 1.47 - Stress-strain curves for cyclic loading to 10% (a) and 15% (b), as per Liu et al. (2008)

It is evident from Figures 1.46 and 1.47 that not all strain was recovered after unloading, so plastic deformation occurred in this range. Also, from the data presented in Figure 1.47, some stress relaxation can be observed. The stress levels in the samples at 10 and 15% strain decreased by 5 to 10% after five loading cycles. Finally, samples were cyclically loaded in the plastic range, to 21 MPa and to 30% strain. The results are shown in Figure 1.48.

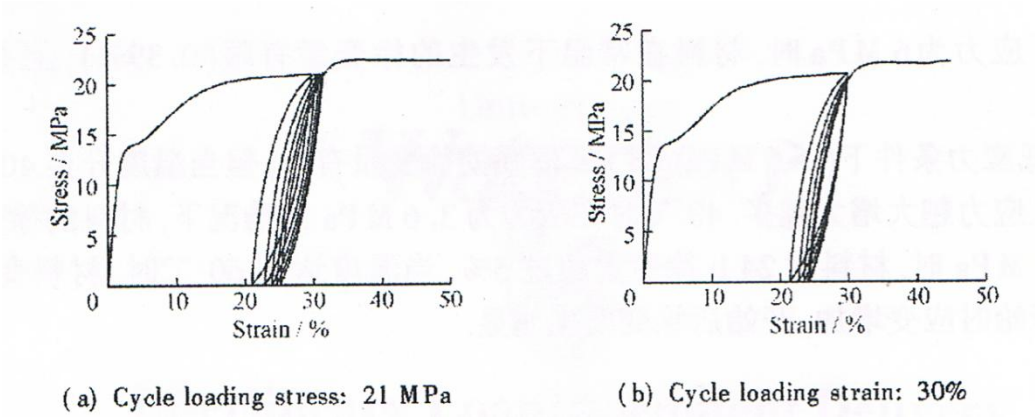

Figure 1.48 - Stress-strain curves for cyclic loading to 21 MPa (a) and 30% strain (b), as per Liu et al. (2008)

Significant residual strain is evident in this range. Again, stress relaxation occurs in the strain-controlled sample.

1.7.1.7 Schiemann, Hinz and Stephani, 2009

At the 2009 International Conference on Textile Composites and Inflatable Structures L. Schiemann, S. Hinz, and M. Stephani presented research on burst tests of ETFE foils. The tests were done on circular samples of approximately 50 cm diameter, clamped by a locking ring onto a rigid base plate. The foils were inflated and their 3D deformation was recorded by strategically positioned cameras (Hinz, Schiemann, & Stephani, 2009). The researchers were primarily concerned with the methodology associated with conducting burst tests on transparent material, so the full results of the mechanical tests were not presented.

1.7.1.8 Galliot and Luchsinger, 2010

In 2010 C. Galliot and R.H. Luchsinger of the Center for Synergetic Structures at the Swiss Federal Laboratories for Materials Science and Technology presented results on mechanical tests of ETFE films at the TensiNet Symposium in Sofia, Bulgaria. Their research included uniaxial stress-strain tests on ETFE films in the longitudinal and transverse directions as well as at 45° to both directions. Figure 1.49 is a set of sample curves from their results. The graph on the left shows the full stress-strain curves, while the graph on the right shows the first 30% of the strain, displaying the yield point and modulus of elasticity with more clarity.

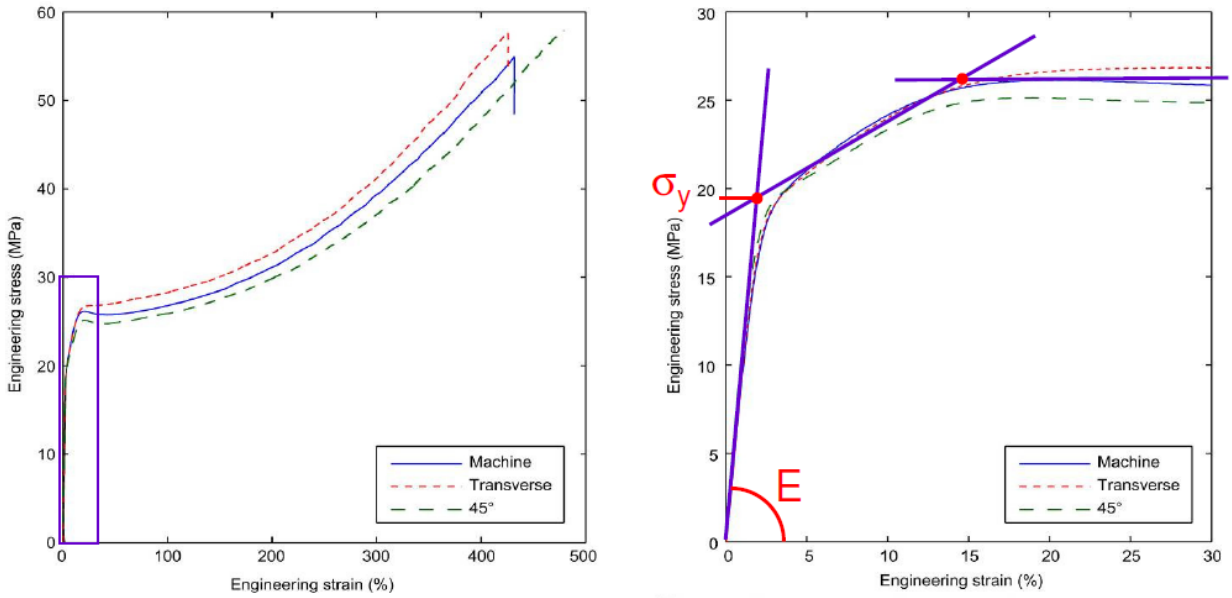

Figure 1.49 - Stress-strain curves for uniaxial tests by Galliot and Luchsinger (2010)

From both curves it appears that the transverse direction has the highest yield point and ultimate strength, followed by the longitudinal (machine) direction and then the 45° direction. Galliot and Luchsinger tested at different strain rates to determine the effect on yield stress and modulus of elasticity. Their findings indicate that an increase in strain rate corresponds to an increase in both yield stress and modulus of elasticity (Galliot & Luchsinger, 2010).

Galliot and Luchsinger also performed biaxial tests on ETFE film, in which cruciform specimens were loaded to failure at a strain rate of 4% per minute, with a 1:1 load ratio in the two directions. Figure 1.50 shows the resulting stress-strain curve.

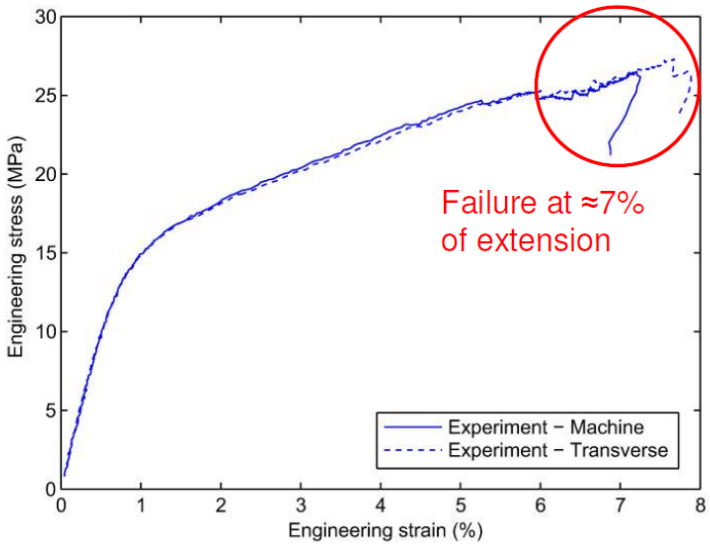

Figure 1.50 - Stress-strain curve for biaxial tests by Galliot and Luchsinger (2010)

As shown in Figure 1.50, the specimen failed in both directions at approximately 7% engineering strain, with the longitudinal (machine) direction failing slightly sooner than the transverse direction (Galliot & Luchsinger, 2010).

The final experiments on ETFE performed by Galliot and Luchsinger were burst tests of inflated circular films. Figure 1.51 shows the stress-strain curve obtained from these tests.

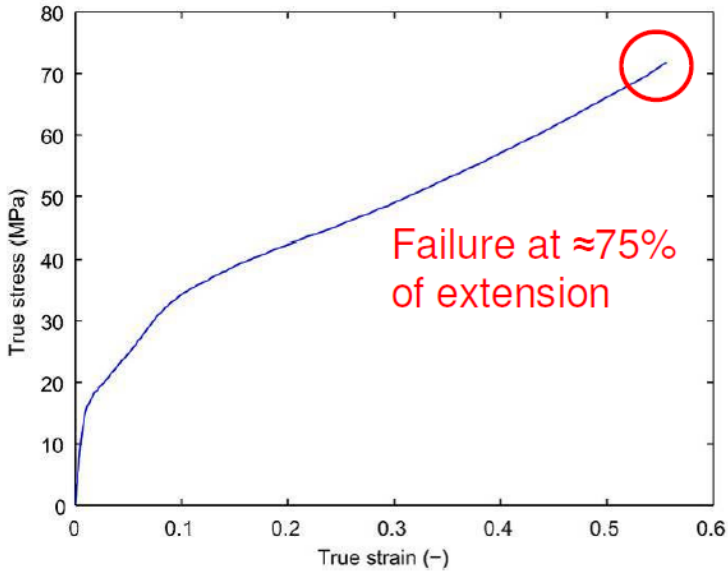

Figure 1.51 - True stress-true strain curve for burst tests by Galliot and Luchsinger (2010)

A comparison stress-strain chart for all three tests is given in Figure 1.52.

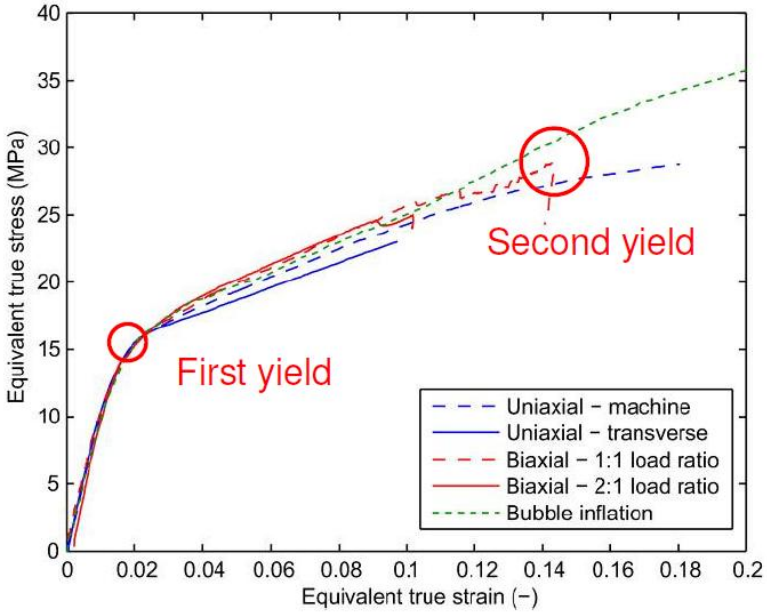

Figure 1.52 - Comparison stress-strain curves from Galliot and Luchsinger (2010)

Figure 1.52 shows a similar initial yield point is obtained for all three test types, but a much higher failure point is observed for the burst (bubble inflation) tests than for the other types. Based on these results, Galliot and Luchsinger suggest that uniaxial tests provide sufficient information on the mechanical behaviour of ETFE foils, except where failure is concerned (Galliot & Luchsinger, 2010).

1.7.2 Research on Creep of ETFE

Little research has been published to date on the creep behaviour of ETFE, particularly in the academic sector. However, nearly all manufacturers and suppliers of ETFE state that it has good creep resistance, although very few provide data to support this claim. This section covers the available results of creep tests done by academic and commercial researchers.

1.7.2.1 DuPont

DuPont has published results on creep tests on its Tefzel ETFE, some of the few data available on the subject. For deformation of ETFE under a 1000 psi (6.9 MPa) load over a 24 hour period, they report a strain of 0.2-0.3% (DuPont, n.d.). They also published the following curves for flexural creep of 5" x 0.5" x 0.125" (127 mm x 12.7 mm x 3.175 mm) injection moulded bars, reprinted here from the *DuPont Tefzel Fluoropolymer Resin Properties Handbook* (n.d.).

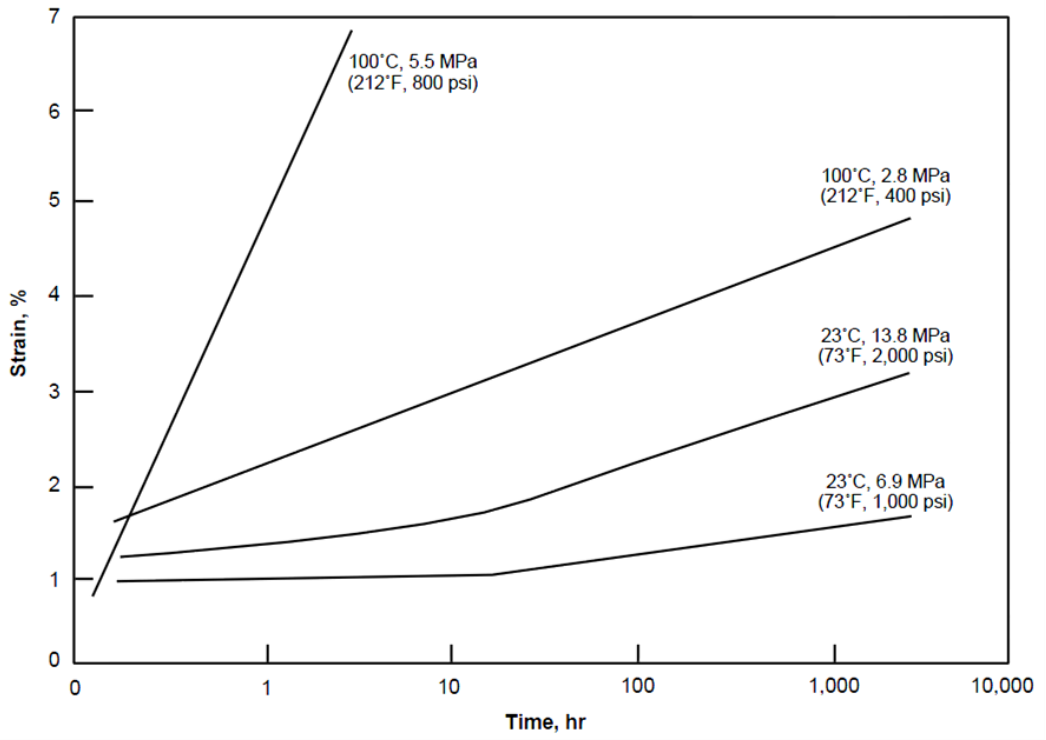

Figure 1.53 - Flexural creep of DuPont Tefzel 200 ETFE (DuPont, n.d.)

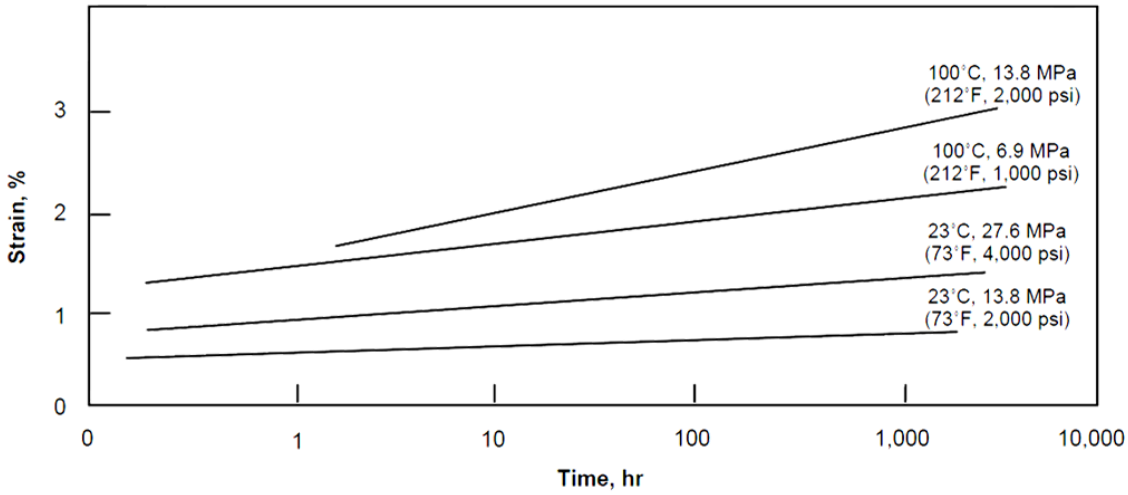

Figure 1.54 - Flexural creep of DuPont Tefzel HT-2004 glass-fibre reinforced ETFE (DuPont, n.d.)

Figure 1.53 is for Tefzel 200, a general-purpose grade of ETFE, used primarily for electrical applications, such as sleeves and switches. The lower curves on the graph show creep results at 23°C, for 6.9 and 13.8 MPa. The upper curves on the graph show creep results at 100°C, for 2.8 MPa and 5.5 MPa. Significantly higher levels of creep are evident at the higher temperature, even though the samples were tested at lower stress levels. Figure 1.54 is for Tefzel HT-2004, a glass-fibre reinforced ETFE resin, used for injection moulding. Again, creep curves are shown at

23°C and 100°C, at stress levels of 13.8 and 27.6 MPa, and 6.9 and 13.8 MPa, respectively. The glass fibre reinforcement appears to add significantly to the creep resistance of the material, as the strain levels are much lower than for the Tefzel 200 ETFE, even for higher stresses (DuPont, n.d.).

1.7.2.2 Ansell, 1985

Ansell conducted uniaxial creep tests on ETFE foil at temperatures of 40, 60 and 100 °C. The 60 and 100° tests were done under dry conditions but the 40° tests were done under conditions of approximately 100% relative humidity. A stress of 5 MPa was applied to the samples and held for the entire testing period. The tests done at 40 °C lasted for 46 days (1104 hours), the tests done at 60 °C lasted 19 days (456 hours), and the tests done at 100 °C lasted for only four hours due to excessive flow in the material. The film samples were 100 and 300 µm thick and had a gauge length of 250 mm. Two samples were tested in each direction at each temperature (Ansell, 1985).

Table 1.10 shows the results of the creep tests.

Table 1.10 - Results of uniaxial creep tests at 40, 60 and 100 °C, as per Ansell (1985)

		Strain (%)			
	Time (Hours)	**Longitudinal 100 µm**	**Transverse 100 µm**	**Longitudinal 300 µm**	**Transverse 300 µm**
40 °C 100% Relative Humidity	0	0.00	0.00	0.00	0.00
	48	1.20	3.20	2.00	2.80
	216	0.80	2.40	1.60	2.20
	696	0.80	2.80	1.60	2.40
	1104	0.60	2.80	1.80	2.60
	Time (hours)	**Longitudinal 100 µm**	**Transverse 100 µm**	**Longitudinal 300 µm**	**Transverse 300 µm**
60 °C Dry Air	0	0.00	0.00	0.00	0.00
	120	15.49	32.50	18.00	28.50
	140	16.40	34.40	18.40	29.60
	264	17.00	36.40	19.60	30.40
	456	17.60	37.20	20.60	32.10
	Time (hours)	**Longitudinal 100 µm**	**Transverse 100 µm**	**Longitudinal 300 µm**	**Transverse 300 µm**
100 °C Dry Air	2	13.20	11.6	39.6	31.2
	4	Quick Flow			

In the results from the 40° tests, the 48 hour strain is greater than the subsequent values. Ansell attributed this to experimental errors of some sort, and left the 48 hour values off Figure 1.55. Also, since the 100° tests were only measured at one point in time, they were also not included on the graph as no strain-time relationship could be determined. Figure 1.55 shows the strain vs. time plots for the remaining points, displayed on a log time scale (Ansell, 1985).

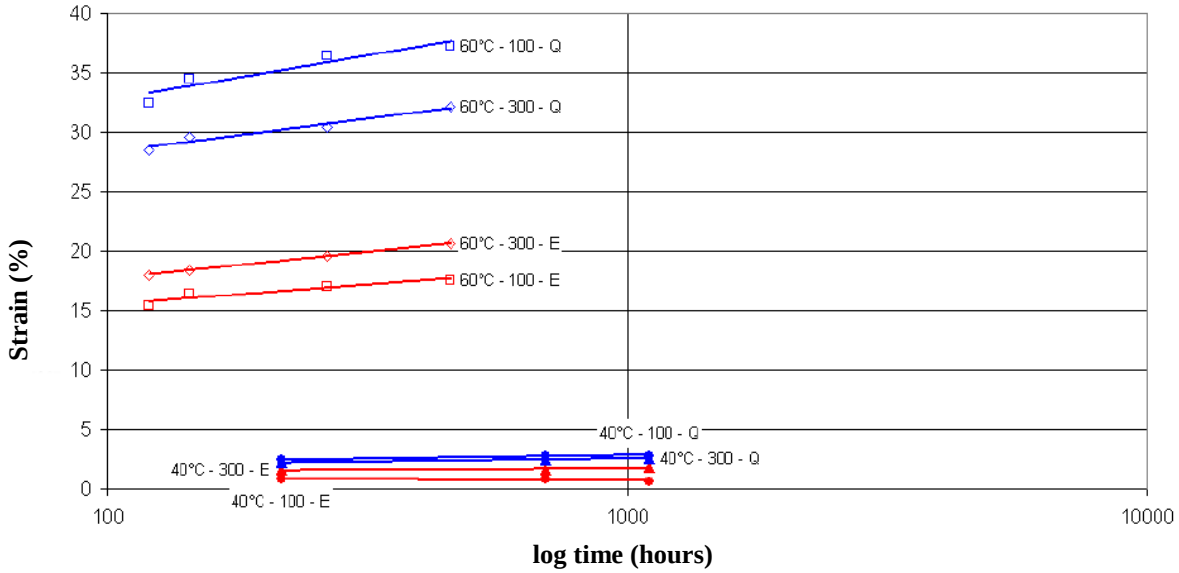

Figure 1.55 - Strain vs. time for creep tests at 40 and 60°C, as per Ansell (1985)

From the chart in Figure 1.55, the effect of temperature on creep of ETFE film is quite pronounced, with the films tested at 60°C creeping much more than those tested at 40°C. Also, it appears that the film creeps more in the transverse direction (Q on the graph) than the longitudinal direction (E on the graph) at both temperatures. The thickness of the film does not appear to have any consistent effects on creep.

1.7.2.3 Barthel, Burger and Saxe, 2003

Barthel, Burger and Saxe (2003) performed 1000 hour creep tests on 225 µm ETFE film. The tests were done at approximately 23°C and the samples were 100 mm wide and 200 mm long. The samples were loaded to 5.3, 8.0 and 10.7 MPa stress levels, which were maintained for 1000 hours, then discharged and the strain recovery was recorded over a period of 96 hours (Moritz, 2007b). They found that the strain always approached a constant value, but that this value differed in accordance to stress level. The increase in strain from one stress level to the next was, however, not proportional to the increase in stress. The strains that occurred were a combination of elastic and plastic deformations. After the load was removed some of the elastic strain recovered instantaneously, but some exhibited a delayed recovery, occurring over an extended period of time. At a stress level of about 40% of the elastic limit, all strain was recoverable after some time (Barthel, Burger & Saxe, 2003).

1.7.2.4 Wu, Mu and Liu, 2008

The creep tests done by Liu et al. were done on samples with the same dimensions as those used in the cyclic loading tests. They were uniaxial tests, done at stress levels of 3, 6 and 9 MPa and temperatures of 25, 40 and 60°C. The samples were again loaded at a rate of 3 mm/minute, until the desired stress level was achieved, and then the stress was maintained for 24 hours (Liu et al., 2008). Table 1.11 shows the strains for the different stress levels at three points in time and for three temperatures. Time 0 refers to the time when the desired load was first reached.

Table 1.11 - Strain (%) at start, 12 hours and 24 hours of creep testing at 3, 6 and 9 MPa and 25, 40 and 60 °C, as per Liu et al. (2008)

Temperature	Stress: 3 MPa			Stress: 6 MPa			Stress: 9 MPa		
(°C)	0 h	12 h	24 h	0 h	12 h	24 h	0 h	12 h	24 h
25	0.35	0.44	0.49	0.73	0.94	1.12	1.13	2.24	2.58
40	0.39	0.89	0.98	0.92	2.43	2.72	1.45	6.71	7.10
60	0.83	2.55	2.66	1.85	6.36	6.65	5.76	12.68	13.21

At low stresses and normal (typical ambient) temperatures, very little creep is observed in the 24 hour time period. The full creep of the specimen tested at 3 MPa and 25 °C is only 0.49%. However as stress and temperature are increased, creep becomes much more significant. The full creep of the specimen tested at 9 MPa and 60 °C is 13.21%.

1.7.2.5 Winkler, 2009

In terms of academic research, the most comprehensive work available on creep of ETFE foil is the graduate thesis of Jan Winkler of the Institut fur Bauingenieurwesen at the Technische Universitat Berlin, *Kriechverhalten von ETFE-Foilen im konstruktiven Ingenieurbau* (Creep Behaviour of ETFE Foils in Structural Engineering) (Winkler, 2009). Winkler performed 1000 hour biaxial creep tests at 4, 8 and 14 MPa stress levels.

Samples with thicknesses of 200 μm were tested. The specimens were cross-shaped with the dimensions (in mm) shown in Figure 1.56. The shaded areas were held by clamps. The overall testing apparatus is shown Figure 1.57. The sample was clamped in the centre of the apparatus, and pulled in four directions by cables attached to equal weights.

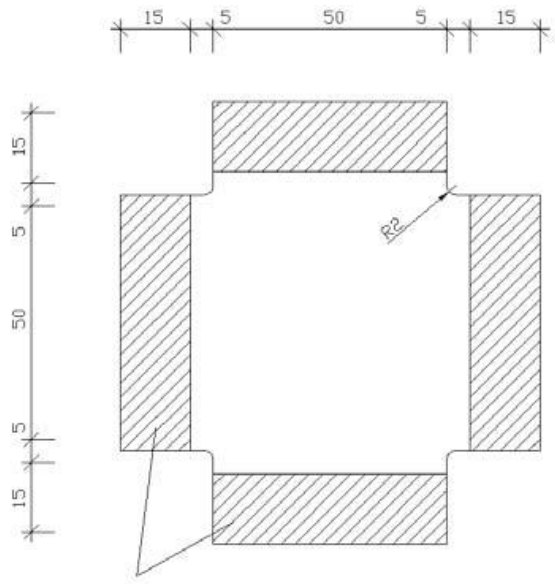

Figure 1.56 - Dimensions of samples used in biaxial creep tests by Winkler (2009)

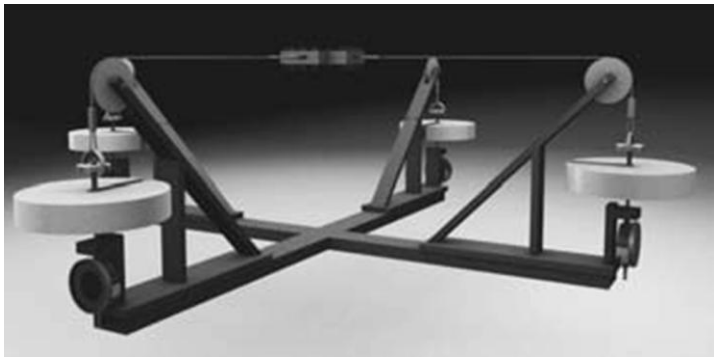

Figure 1.57 - Testing apparatus used by Winkler (2009)

The temperature was held at 20°C, and the relative humidity was 65%. Three samples were tested at each stress level. Figure 1.58 shows the results of the 4 MPa tests in the longitudinal direction.

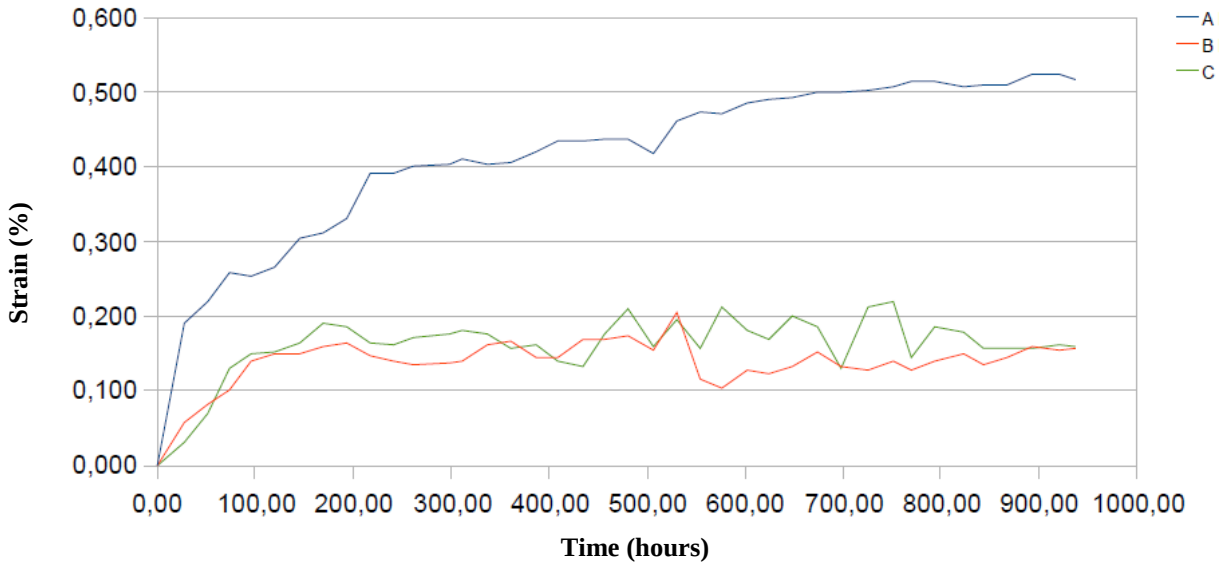

Figure 1.58 - Strain vs. time curves for longitudinal direction of biaxial creep tests at 4 MPa, as per Winkler (Bögle & Hartz, 2008)

Figure 1.59 shows the results of the 4 MPa tests in the transverse direction.

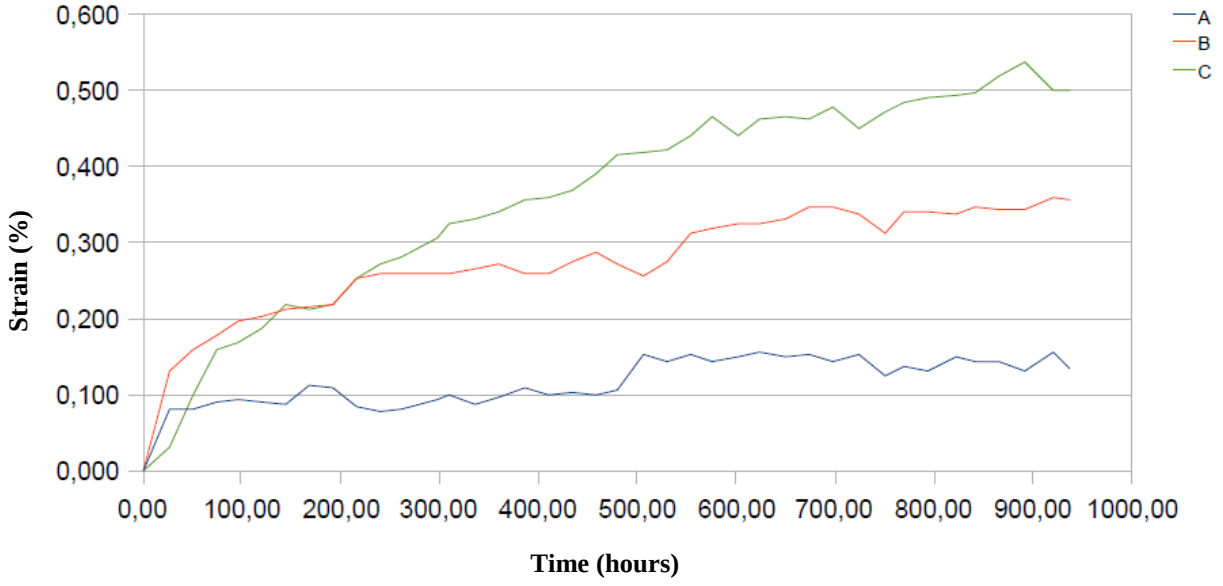

Figure 1.59 - Strain vs. time curves for transverse direction of biaxial creep tests at 4 MPa, as per Winkler (Bögle & Hartz, 2008)

In both directions, a large scatter is observed. There is also no obvious difference in results between the longitudinal and transverse directions (Winkler, 2009). Winkler developed a logarithmic function to fit the data, so that creep after a longer period of time could be determined. The resulting function from all the 4 MPa data is shown in Figure 1.60.

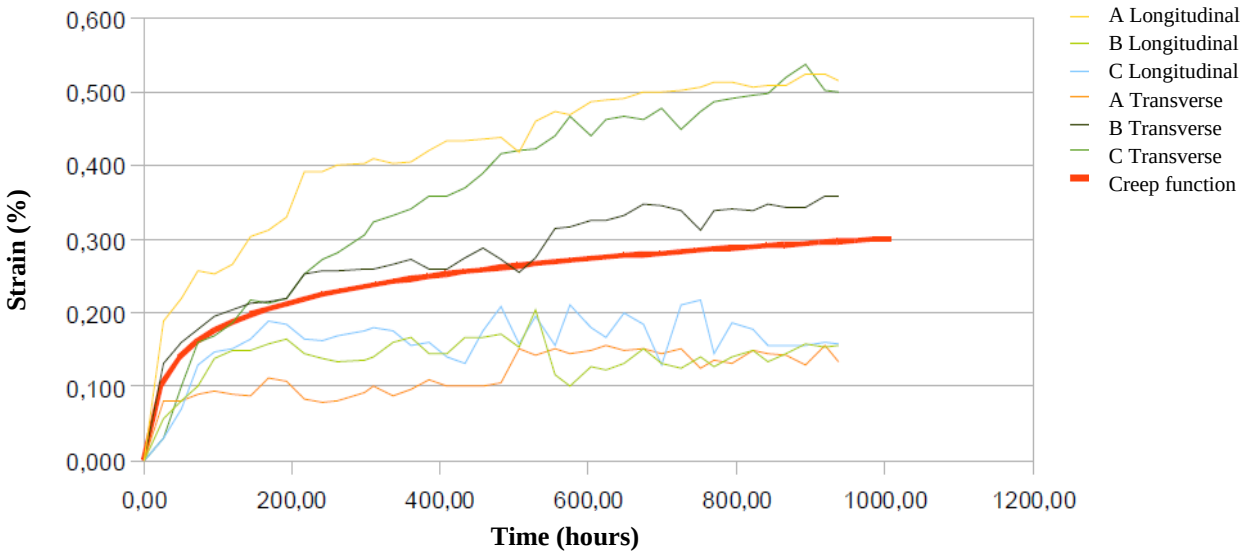

Figure 1.60 - Average creep function for all 4 MPa data, as per Winkler (Bögle & Hartz, 2008)

Based on this function, the expected 1000 hour creep strain would be about 0.3 %. After 25 years the expected creep strain would be about 0.6% (Winkler, 2009).

Figure 1.61 shows the results of the 8 MPa tests in both the longitudinal and transverse directions.

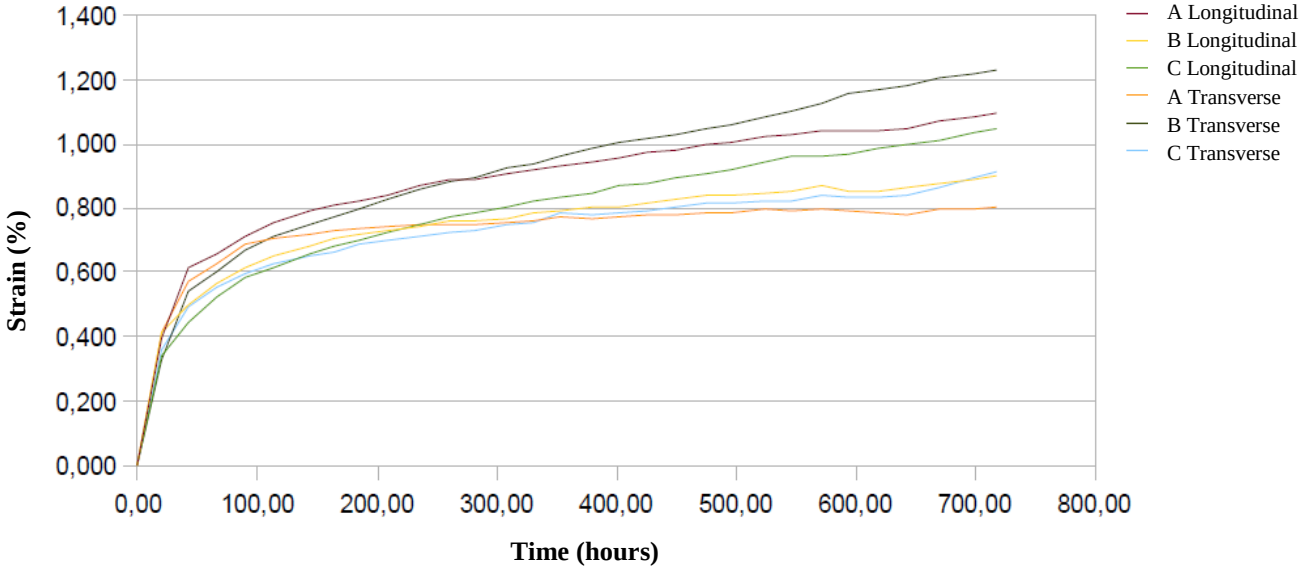

Figure 1.61 - Strain vs. time curves for longitudinal and transverse directions of biaxial creep tests at 8 MPa, as per Winkler (Bögle & Hartz, 2008)

At this stress level less scatter occurred, making the creep behaviour more obvious. The tests were stopped short of 1000 hours due to technical difficulties, but 700 hours of data is available for each sample. Again, a characteristic function was created for this stress level and is shown in Figure 1.62.

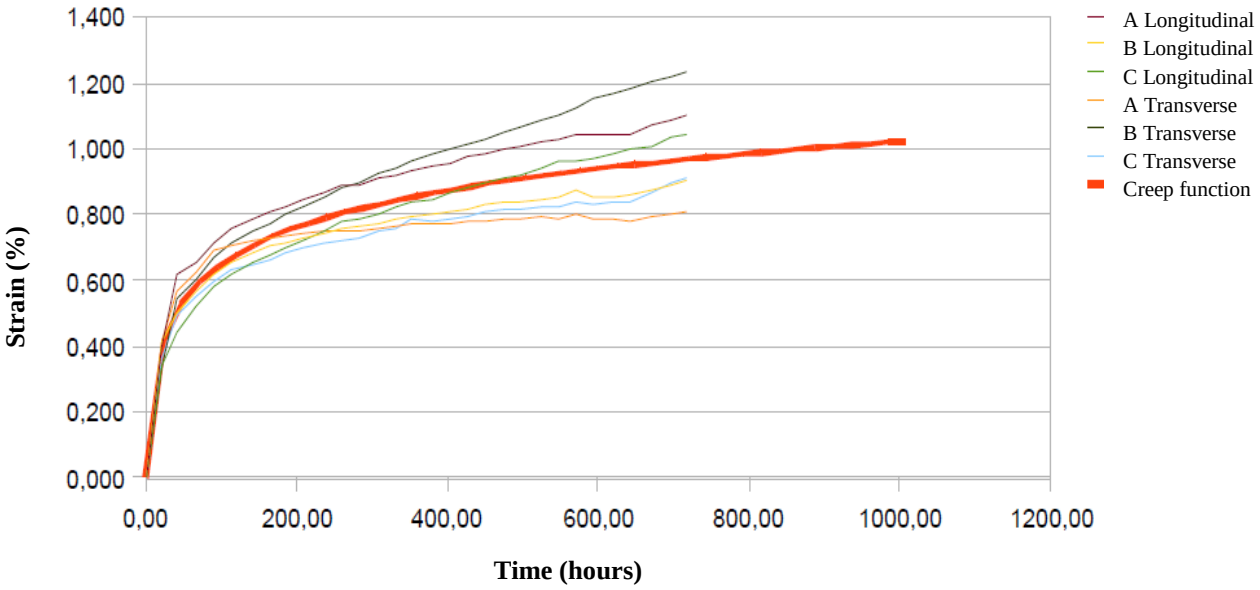

Figure 1.62 - Average creep function for all 8 MPa data, as per Winkler (Bögle & Hartz, 2008)

After 1000 hours at 8 MPa the predicted elongation is about 1%. After 25 years it is about 1.9%.

The results of the 14 MPa tests are shown in Figure 1.63 for both material directions.

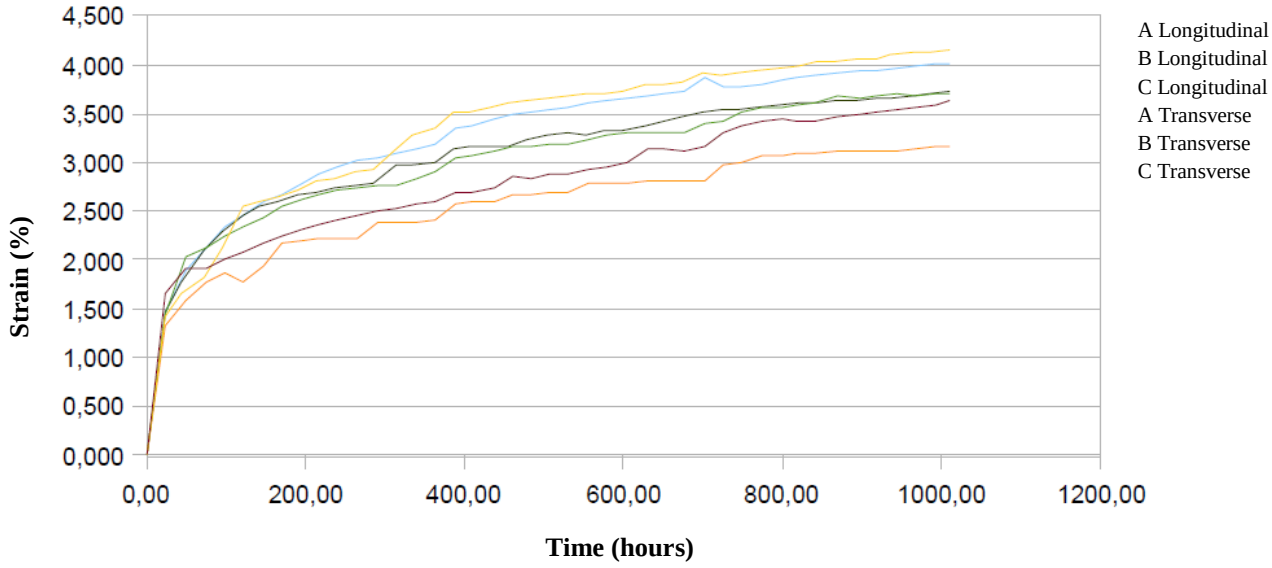

Figure 1.63 - Strain vs. time curves for longitudinal and transverse directions of biaxial creep tests at 14 MPa, as per Winkler (Bögle & Hartz, 2008)

The creep curves are even more pronounced at this stress level, due to a further decrease in scattering in the data. The average creep function for 14 MPa is shown in Figure 1.64.

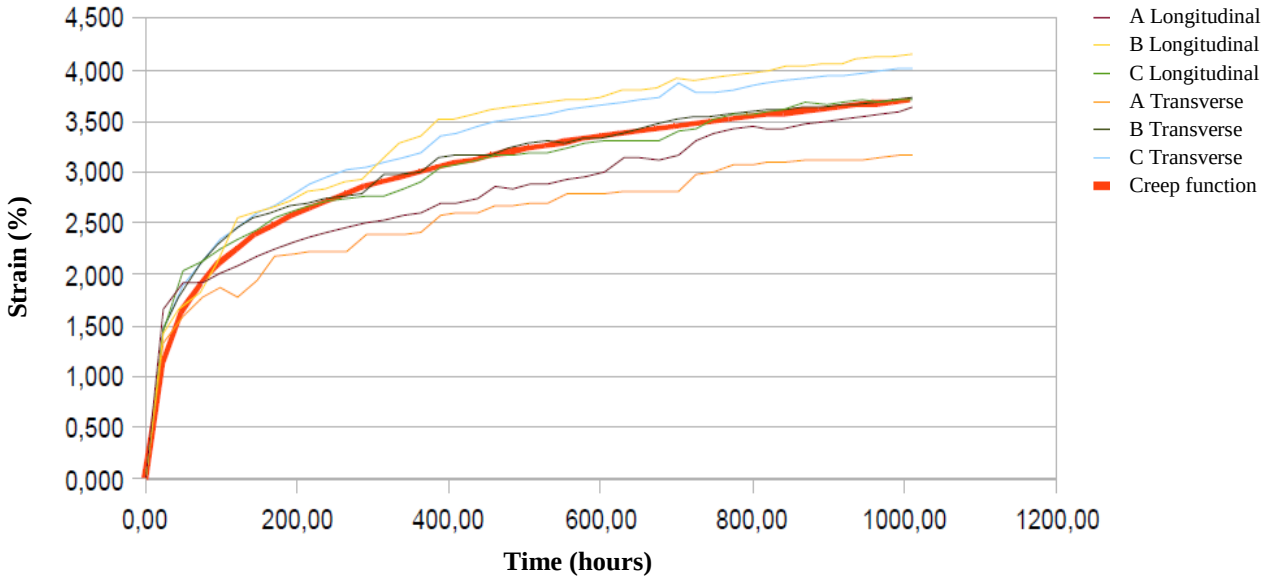

Figure 1.64 - Average creep function for all 14 MPa data, as per Winkler (Bögle & Hartz, 2008)

After 1000 hours at 14 MPa, the function predicts a creep strain of about 3.7%. After 25 years it predicts a creep strain of about 7.4% (Winkler, 2009).

Chapter 2 Laboratory Tests

2.1 Outline of Research done for this Study

The research done for this thesis involved a series of 24-hour uniaxial creep tests, as well as several seven-day creep tests. Uniaxial tests were selected instead of biaxial creep tests for the following reasons:

- The available equipment was readily equipped for uniaxial creep tests, but would have required significant modifications for biaxial tests,
- Uniaxial tests allow behaviour in different material directions to be isolated,
- Research done by others has indicated that uniaxial tests of ETFE provide sufficient information on material behaviour, except where failure is concerned (Galliot, & Luchsinger, 2010).

The creep tests were performed at 2, 8, 12 and 14 MPa constant stress levels. Three different brands of ETFE were tested; two had a thickness of 50 microns and the third came in two thicknesses – 150 and 300 microns. In addition, tensile tests were done on each material involved in the creep tests.

Constitutive models were developed for the results of the creep tests. Viscoelastic and viscoplastic models were both applied to the data. Several different modeling techniques were used on the seven-day test results, which included models based on the first 24 hours of data and models based on the full seven days of data.

Tensile tests were also done on the films in order to compare the results to published manufacturer data, and relate the creep behaviour to other mechanical properties. These tests were done in accordance with ASTM D882-09, and generated values for yield and failure stresses of the ETFE samples in both film directions.

2.2 Films Used in Laboratory Tests

Three brands of ETFE foil were tested. All brands were received in the form of extruded foil in rolls or sheets. The brands are referred to here as A, B and C, with numbers designating the different thicknesses of foil. Table 2.1 gives the names assigned to the foils along with the associated thicknesses.

Table 2.1 - Thickness of foils

Foil	Thickness (μm)
A	50
B	50
C1	150
C2	300

Some of the mechanical properties for the three brands of ETFE film tested for this thesis are given in Table 2.2. All of these properties were obtained by the film manufacturers (DuPont, n.d.; Dyneon, 2003).

Table 2.2 - Mechanical properties of tested films

Film Brand	Tensile Strength (MPa)	Yield Stress (MPa)	Elongation at Break (%)	Melt Temperature (°C)	Maximum Service Temperature (°C)	Density (g/cm^3)
A	46 (at 23°C)	22 (at 23°C)	425	267	150	-
B	41 (at 25°C)	-	250 (Minimum)	250-270	-	1.73-1.77
C	46 (at 23°C)	22 (at 23°C)	425	267	150	-

Films A and C were made from the same resin, and therefore have the same properties. However, they were extruded by different film manufacturers, so the finished products may differ somewhat. Tensile tests were done to verify some of the mechanical properties given above. The results of these tests can be found in section 2.6.

2.3 Test Procedure for Creep Tests

The specimens were cut into 50 mm wide strips in both the longitudinal and transverse directions of the material. A utility knife and rigid metal ruler were used to cut the 50 micron film while it was held in place with tape against a firm cardboard cutting surface, while the thicker films were cut with a paper cutter while being held in place with tape. The strips were cut to lengths of approximately 200 mm to accommodate a 124 mm gauge length. Exceptions to this were film B tested at the two higher stress levels in the transverse direction and at the highest stress level in the longitudinal direction, film C1 tested at the highest stress level in both directions and C2 tested at the highest level in the longitudinal direction and the two higher stress levels in the transverse direction. These cases required a shorter gauge length of 63 mm for the extensometer and test frame to accommodate the higher levels of creep they exhibited compared to the other tests.

Stress levels of 2, 8, 12 and 14 MPa were selected for the creep tests. The methodology for selecting these stress levels can be found in section 2.3.1. The films were held in place during testing with MTS 100 N Vise-Action Grips. The uniaxial creep tests were performed by attaching a specimen in the top grip and tightening the gripping mechanism. The bottom of the specimen was then placed loosely through the bottom grip and pulled taut from the bottom. The bottom grip was then tightened as well to hold the specimen securely in place. Permanent marks were placed on the specimen just on the inside of the grips to show whether any slippage was occurring within the grips during the test. The placement of the specimen in the grips is shown in Figure 2.1.

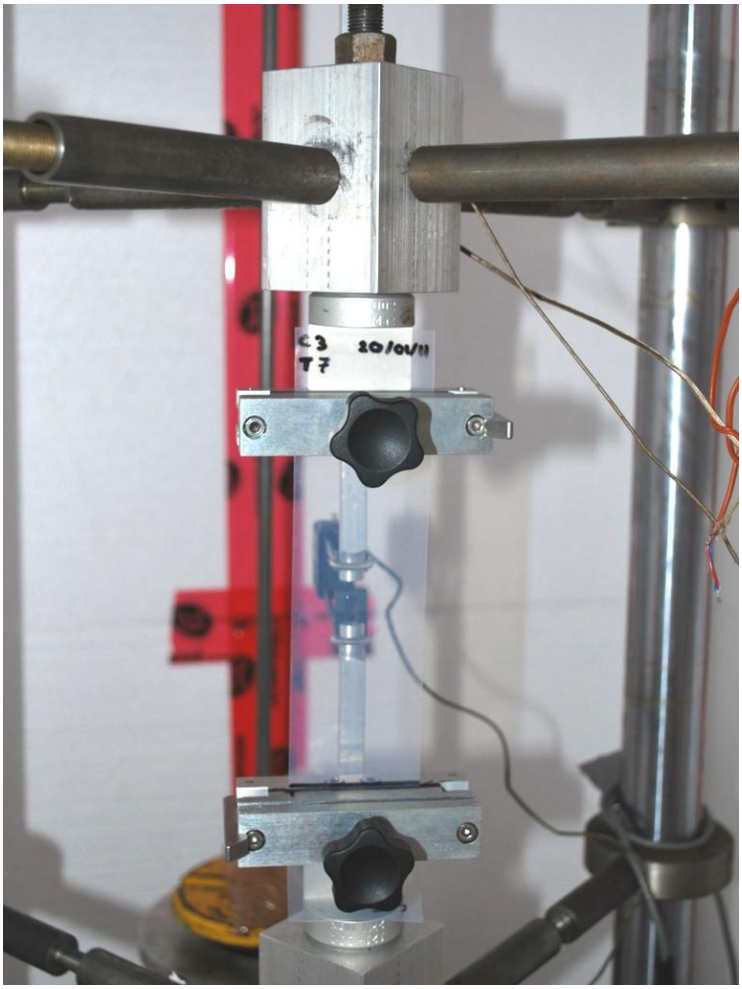

Figure 2.1 - ETFE specimen in grips

An extensometer was attached to the grips by means of aluminum bars, as shown in Figure 2.2. The extensometer could not be attached directly to the specimen because the foils were not sufficiently rigid, but an effort was made to place it as close as possible to the tested specimens.

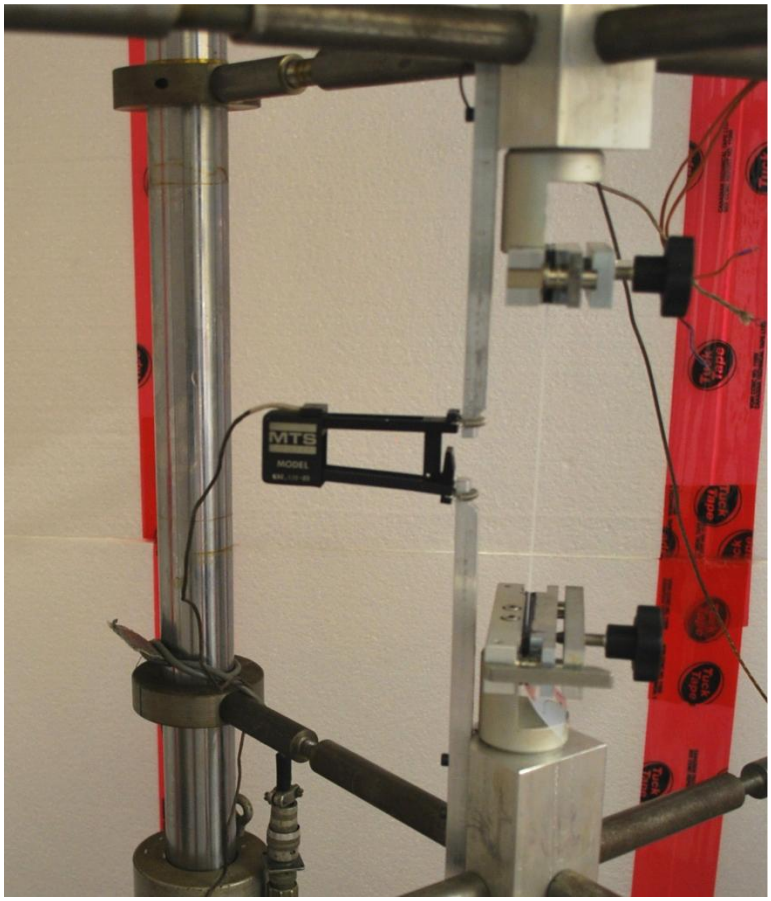

Figure 2.2 - Extensometer used for measuring elongation of specimens

The specimens were loaded by means of placing a mass on a platform connected to the grips by a lever arm, as shown in Figure 2.3.

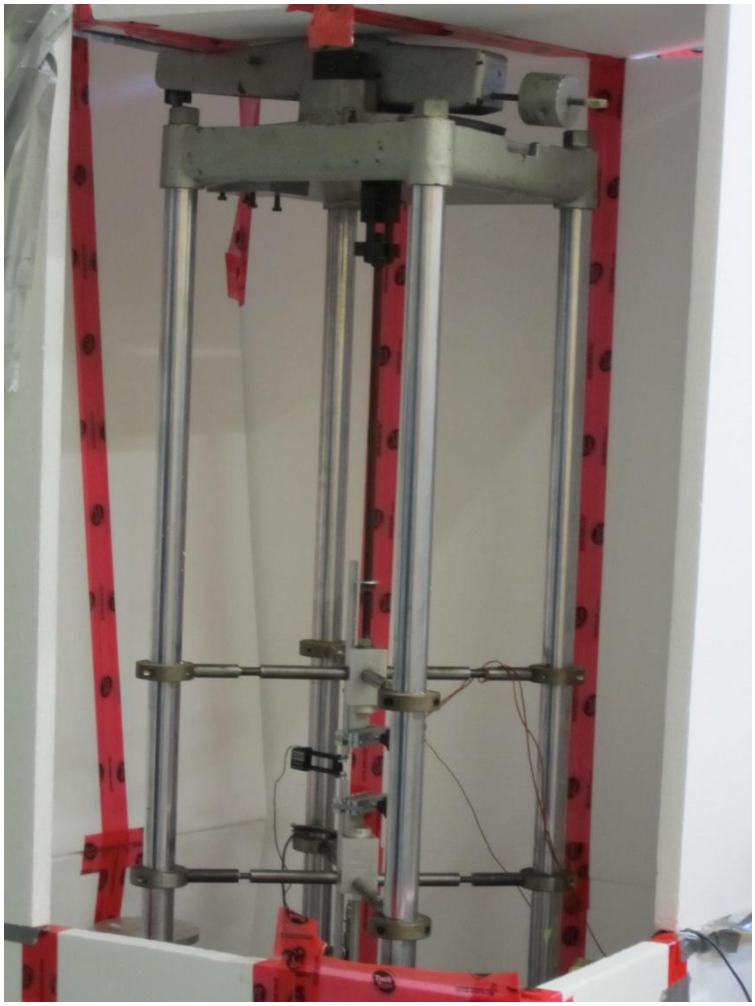

Figure 2.3 - Frame used for creep tests

The load was placed all at once, so as to give an accurate recording or the initial elastic response of the material. The load was left on the specimen for a period of 24 hours, during which the extensometer recorded the grip extension at the approximate time intervals cited in Table 2.3.

Table 2.3 - Extension recording intervals

Time From Start of Test	Recording Interval
< 1 minute	0.25 seconds
1 minute – 1 hour	1 second
1 hour – 4 hours	30 seconds
4 hours – 24 hours	1 minute

Steel and lead shot in resealable plastic bags in combination with pre-fabricated steel weights were used for the masses. The loads used to provide the four stress levels for the different thicknesses of foil are given in Table 2.4.

Table 2.4 - Applied mass for creep tests

Foil Thickness (µm)	Stress (MPa)	Mass (g)
50	2	50.9
	8	203.5
	12	305.2
	14	356.1
150	2	152.6
	8	610.5
	12	915.7
	14	1068.4
300	2	305.2
	8	1221.0
	12	1831.5
	14	2136.7

The entire test frame was enclosed in a structure made from 1 ½ inch (approximately 38 mm) thick expanded polystyrene (EPS) insulation, as shown in Figure 2.4. Joints between insulation boards were sealed using tape, with the exception of a few of the joints along the front and one side of the frame which were left unsealed so that the enclosure could be opened to switch the samples and add or remove the weights.

Figure 2.4 - Insulation enclosure for test frame

The insulation enclosure served to regulate the temperature of the foils during testing and to protect the test apparatus from air gusts which could cause the specimen or the load to move. During winter, when the ambient temperature of the laboratory dropped below acceptable levels, a ceramic heater with a fan was used to heat the enclosure. A proportional temperature controller was used to regulate the output of the heater, maintaining the temperature of the enclosure at 23°C +/- 0.2°C. The mechanical behaviour of the foils is extremely temperature-dependent, so maintaining a consistent temperature for all tests was important for comparative purposes.

Each film was tested a minimum of two times in each direction at each stress level. Two independent replications, being the minimum one can do, might be a relatively insufficient number to do a statistical analysis of the data, but due to time constraints no more could be completed at this time. Future work should aim to further replicate the tests outlined here and subject the data to a more rigorous statistical analysis.

2.3.1 Selection of Stress Levels for Creep Tests

The stress levels used in testing were determined based on an estimate of the range of expected stresses of typical ETFE cushions in service. Craig G. Huntington's (2004) method for determining the stress in cables loaded with a

perpendicular uniform load, presented in section 1.6.1 was applied. Low and high estimates for stress were determined by varying the cushion width, the camber and the inflation pressure. For the low estimate, a single-curvature cushion of one metre width, with a ten percent camber of 0.1 metres, and an inflation pressure of 200 Pa was assumed. Equation (1-4) can be applied as follows:

$$F = \frac{w(l^2 + 4h)}{8h}$$

$$F = \frac{0.0002\text{N/mm}^2[(1000\text{mm})^2 + 4 \cdot 100\text{mm}]}{8 \cdot 100\text{mm}}$$

$$F = 0.2501\text{N/mm}$$

The stress in the foil is then determined by dividing out the foil thickness. Here, a typical structural foil thickness of 200 microns has been selected.

$$\sigma = \frac{F}{t}$$

$$\sigma = \frac{0.2501}{0.2\text{mm}}$$

$$\sigma = 1.25\ \text{MPa}$$

Therefore, the lowest applied stress chosen for testing was 2 MPa, just above this approximation. For the high estimate, a single-curvature cushion of four metres width, with a 20% camber of 0.8 metres, and an inflation pressure of 1000 Pa was assumed. Applying Equation (1-4) yields a tensile force of 2.5 N/mm and a stress of 12.5 MPa, when a thickness of 200 microns is used. Therefore, the highest stress selected for testing was 14 MPa, just above this estimate. The remainder of the stress levels were selected at intermediate values between 2 and 14 MPa. The differences between the chosen stresses decreases as the stresses increase, since the effect of stress on creep was found to be more pronounced at higher levels of stress.

The chosen stresses also fall into the range of those used by other researchers who performed creep tests on ETFE (Moritz, 2007a; Barthel et al., 2003; Liu et. al, 2008; Winkler, 2009). Additionally, actual stress levels for two buildings using single-layer, mechanically prestressed ETFE foils are known. The exhibition and conference building of the German Federal Environmental Foundation was constructed with a single-layer roof prestressed to 4.4 MPa and 3.6 MPa in the two different film directions (Barthel, et al., 2003). The ETFE facade on the new BC Place Stadium is designed to be prestressed to 2.2 MPa in one direction and 2.6 MPa in the other. The stress values in the films would increase when loaded, and, in the case of cushions, could be increased to accommodate higher loads. These values all fall into the range of tested stresses in this thesis.

2.4 Results of Creep Tests

2.4.1 Film A Data

Figures 2.5 - 2.6 plot the strain versus time for the 24 hour creep tests done on film A. Figure 2.5 is for tests done in the longitudinal (L) direction of the film. All stress levels are shown on the same graph here, but each stress level is plotted on a separate graph in Appendix A, using different scales for strain.

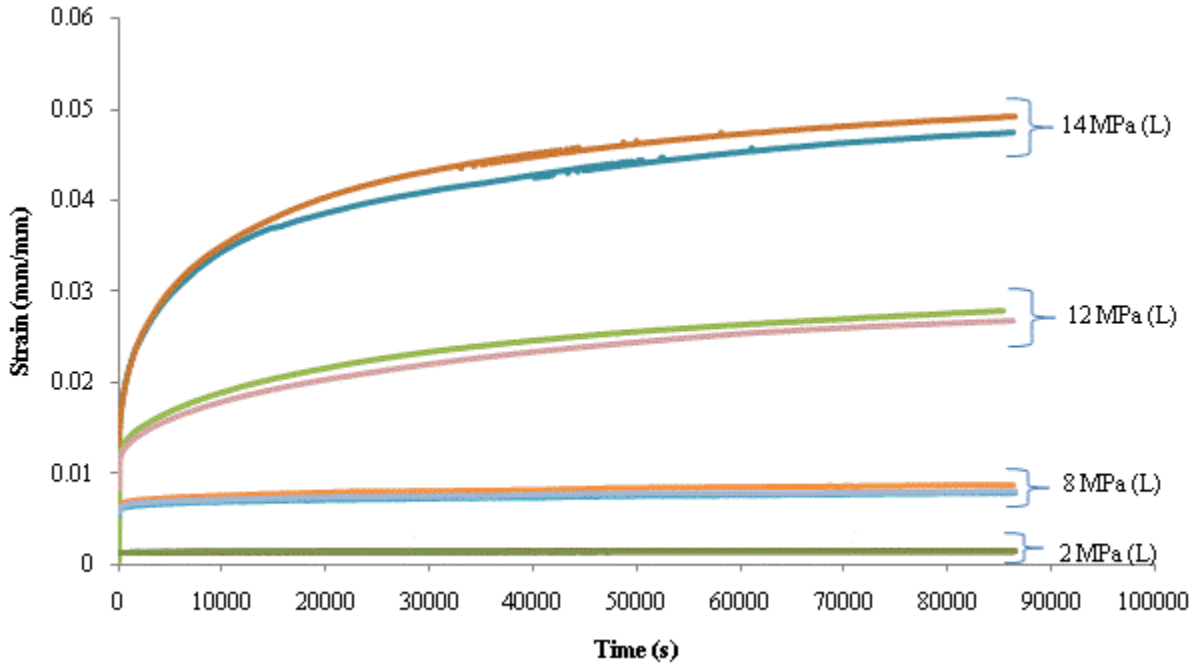

Figure 2.5 - Comparison of all strain vs. time curves for longitudinal samples of film A

In Figure 2.5 the creep curves appear to have a similar shape to the other curves at the same stress level. However, in some cases the strain for one of the trials begins at a lower value than the other, suggesting that its initial elastic strain was lower. What likely occurred is not an actual difference in the elastic strain, but a small slippage, either between the specimen and the grips, or between the extensometer and the aluminum bars, during the loading of the first specimen. This is especially evident on the 2 MPa graph (Figure A. 1) shown in Appendix A. Such a slippage would be too small to see with the naked eye, as it would be in the range of about 0.02 mm, but, as the overall creep strain under 2 MPa is also very small, it is apparent on the graph.

Figure 2.6 is for film A tested in the transverse direction.

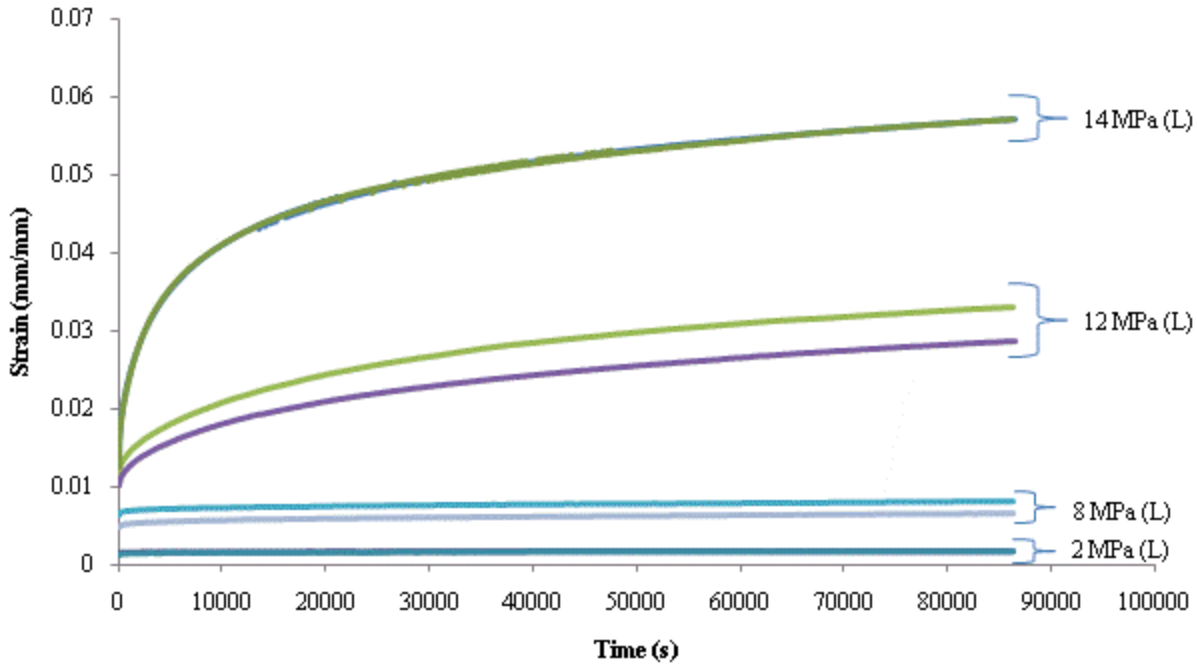

Figure 2.6 - Comparison of all strain vs. time curves for transverse samples of film A

As with the longitudinal tests, a small difference in the initial elastic strain is evident between some of the transverse trials. Again, this is likely due to a small amount of slippage of the specimen or the extensometer.

2.4.2 Film B Data

Figures 2.7 – 2.8 are for creep tests on film B. Plots for individual stress levels can be found in Appendix B.

Figure 2.7 shows all of the strain-time curves for film B tested in the longitudinal direction on the same scale for comparison purposes.

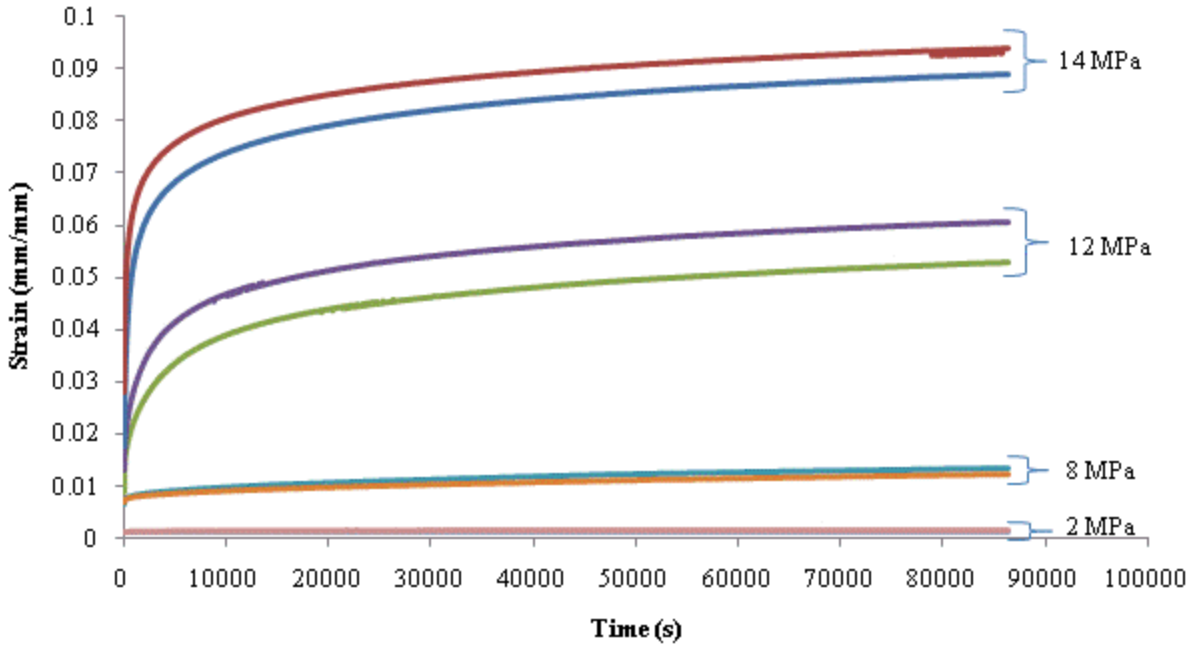

Figure 2.7 - Comparison of all strain vs. time curves for longitudinal samples of film B

Figure 2.8 plots all of the film B transverse curves on the same scale.

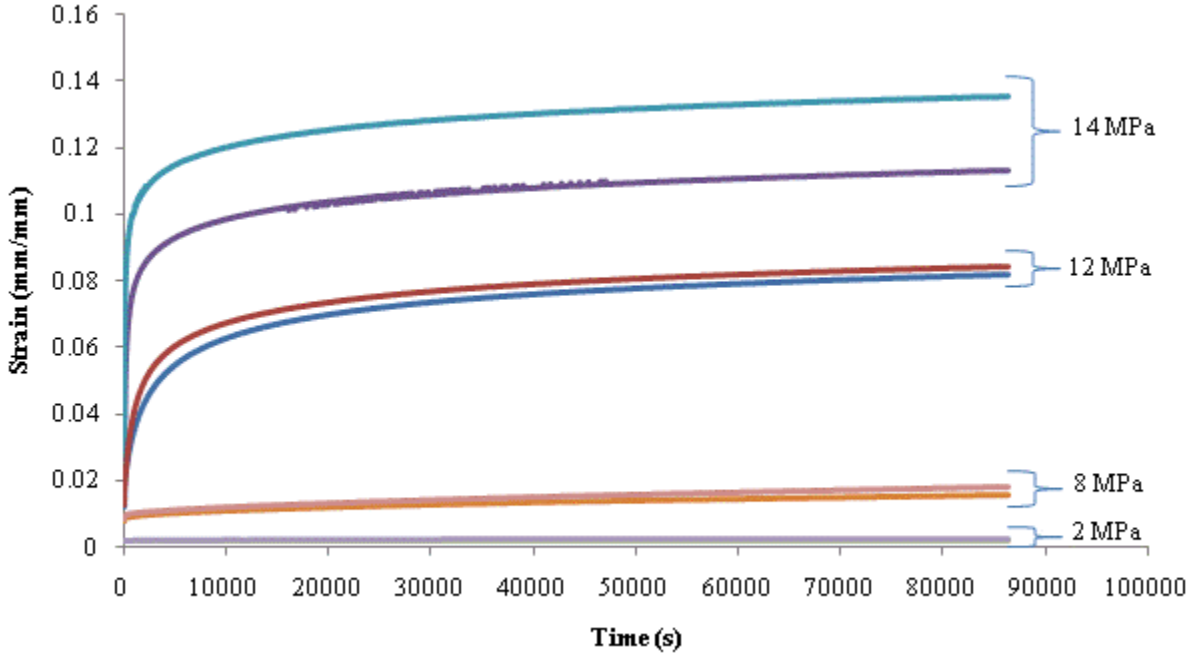

Figure 2.8 - Comparison of all strain vs. time curves for transverse samples of film B

As with many of the 2 MPa tests, a vertical shift exists between the curves from the two 14 MPa trials. Both curves have the same shape, however, so it is likely that a slip has occurred here as well.

2.4.3 Film C1 Data

Figures 2.1 – 2.10 are strain-time curves for film C1. Curves for individual stress levels are given in Appendix C.

Figure 2.9 shows all of the creep curves for film C1 tested in the longitudinal direction.

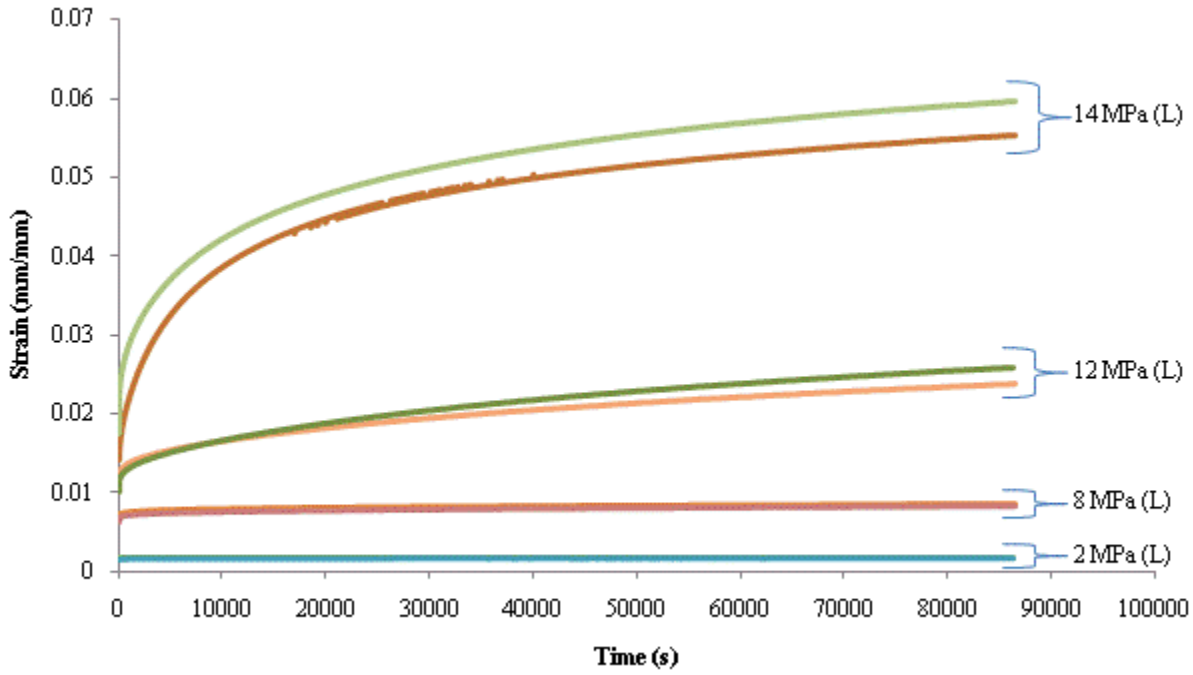

Figure 2.9 - Comparison of all strain vs. time curves for longitudinal samples of film C1

Figure 2.10 shows all of the creep curves for film C1 tested in the transverse direction on the same scale.

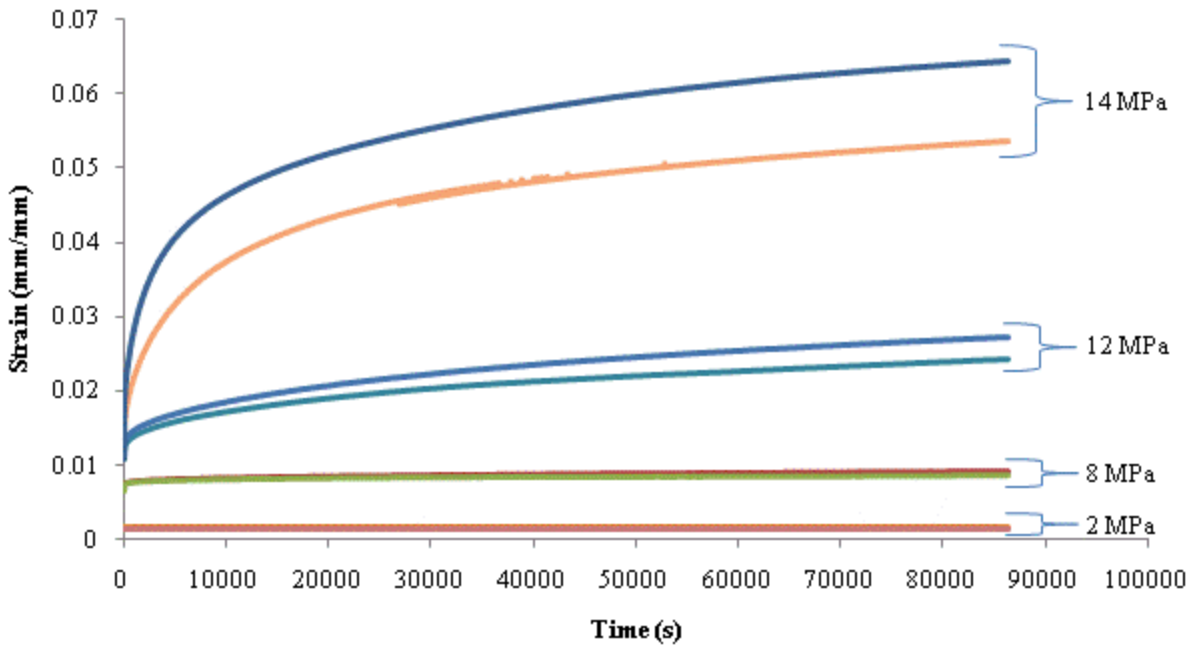

Figure 2.10 - Comparison of all strain vs. time curves for transverse samples of film C1

A slip has also likely occurred during the first trial at 14 MPa, since the two 14 MPa curves have different magnitudes but the same shape.

2.4.4 Film C2 Data

Figures 2.11 – 2.12 contain data for film C2. Curves for individual stress levels are given in Appendix D.

Figure 2.11 shows the creep curves for all stress levels of tests on film C2 in the longitudinal direction on the same scale.

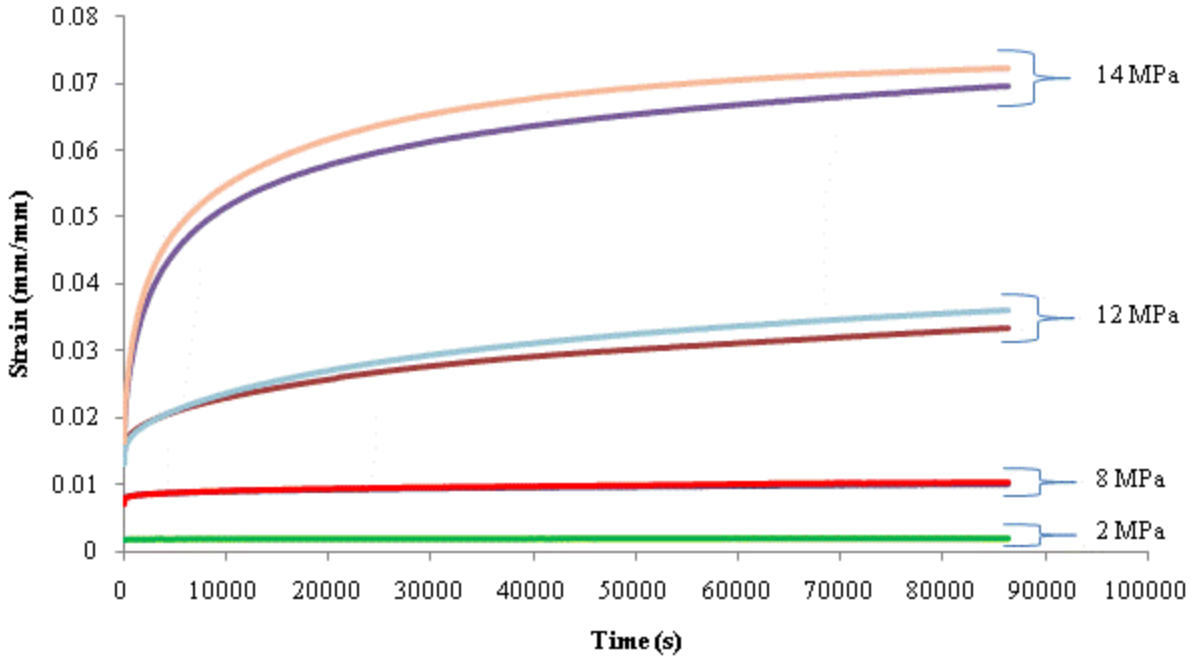

Figure 2.11 - Comparison of all strain vs. time curves for longitudinal samples of film C2

Figure 2.12 plots all of the creep curves for C2 tested in the transverse direction on the same scale.

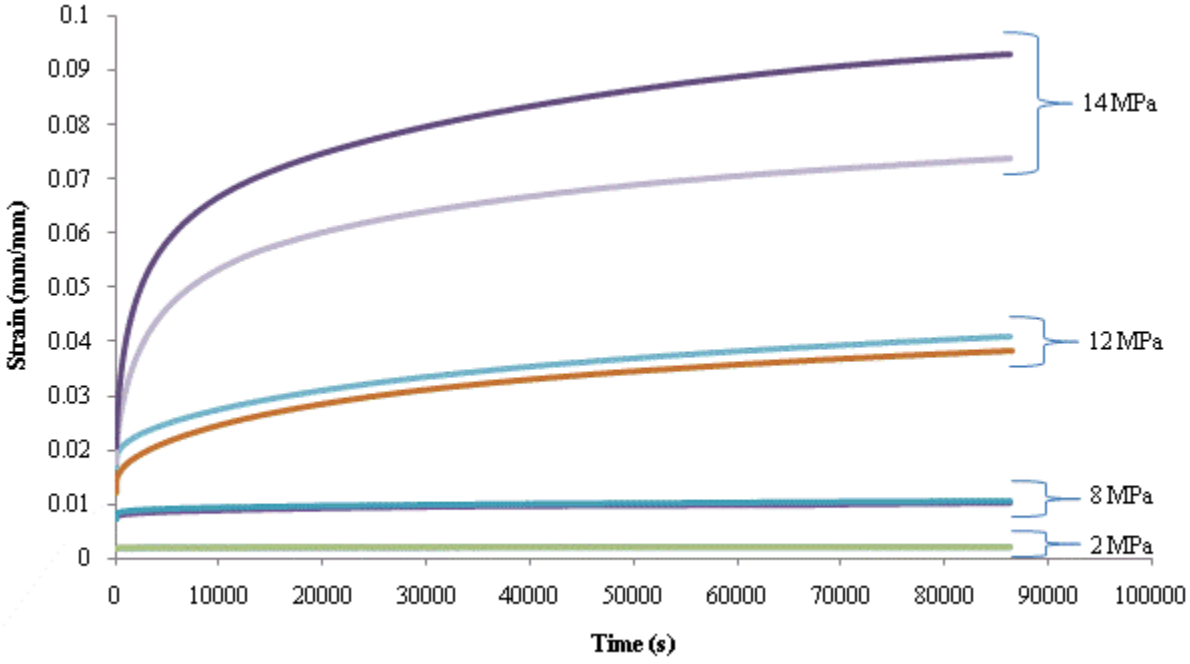

Figure 2.12 - Comparison of all strain vs. time curves for transverse samples of film C2

2.4.5 Results Summary

Table 2.5 summarizes the results of all of the 24 hour creep tests. The average values from the replicated trials are given.

Table 2.5 - Summary of results from all 24-hour creep tests

Film	Stress (MPa)	Average Strain for all Trials (%)					
		Initial at t=0		Total at t=24 hours		Creep at t=24 hours (Total - Initial)	
		Longitudinal	Transverse	Longitudinal	Transverse	Longitudinal	Transverse
A	2	0.125	0.133	0.144	0.166	0.020	0.033
	8	0.574	0.639	0.822	0.879	0.248	0.240
	12	0.930	1.024	2.737	3.090	1.807	2.066
	14	1.248	1.346	4.833	5.717	3.586	4.371
B	2	0.117	0.186	0.146	0.217	0.029	0.031
	8	0.684	0.810	1.293	1.691	0.610	0.881
	12	1.103	1.249	5.688	8.330	4.586	7.081
	14	2.324	2.073	9.142	12.428	6.818	10.355
C1	2	0.155	0.147	0.170	0.165	0.015	0.018
	8	0.642	0.664	0.845	0.899	0.203	0.235
	12	1.063	1.181	2.481	2.582	1.418	1.401
	14	1.581	1.270	5.754	5.908	4.172	4.638
C2	2	0.163	0.170	0.183	0.197	0.021	0.027
	8	0.737	0.768	1.019	1.066	0.282	0.298
	12	1.345	1.442	3.469	3.972	2.124	2.530
	14	1.577	1.910	7.099	8.348	5.522	6.437

2.4.6 Long-Term Creep Test Data

Several longer term creep tests were also done on ETFE film, where the stress was maintained for a period of seven days (604,800 seconds) rather than 24 hours. These tests were all done on film C1 in the longitudinal direction, and were done at 2 MPa, 8 MPa and 14 MPa. The creep curve from the 2 MPa test is shown in Figure 2.13.

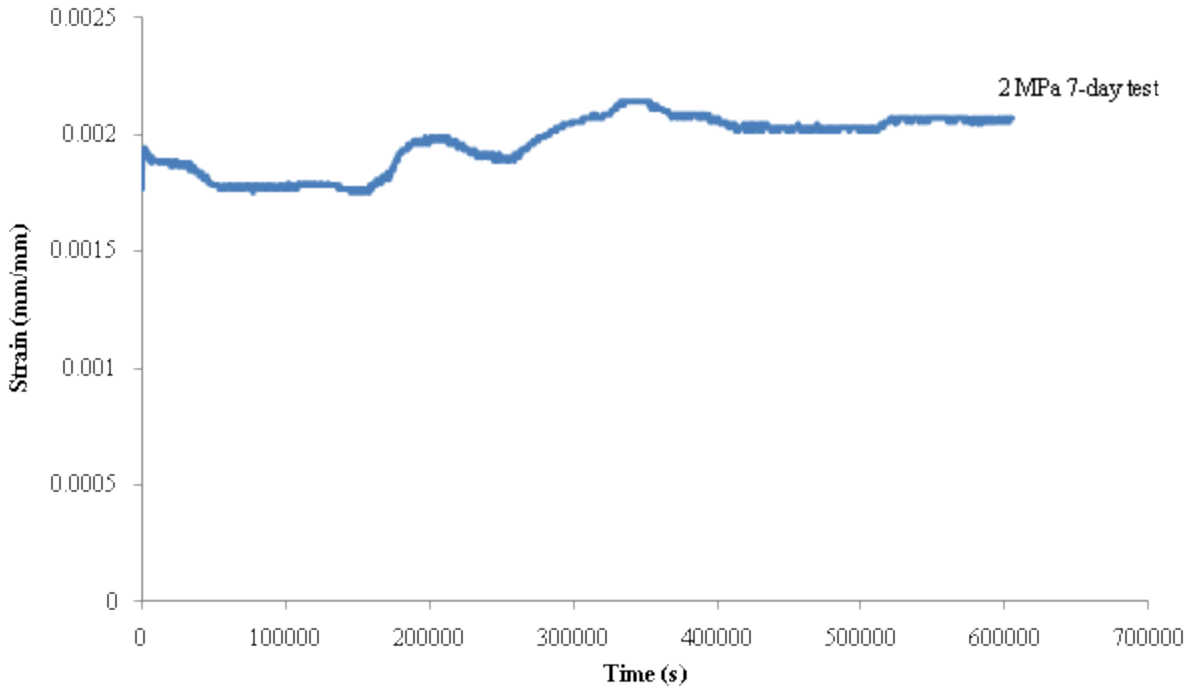

Figure 2.13 - Strain vs. time for film C1 subjected to 2 MPa in the longitudinal direction for 7 days

During the course of this test the heater used to maintain a constant temperature in the testing enclosure failed, causing a drastic effect on the results. This will be discussed in more detail in section 2.4.7.5. Due to time constraints this test could not be repeated.

The creep curve for the 8 MPa test is shown in Figure 2.14.

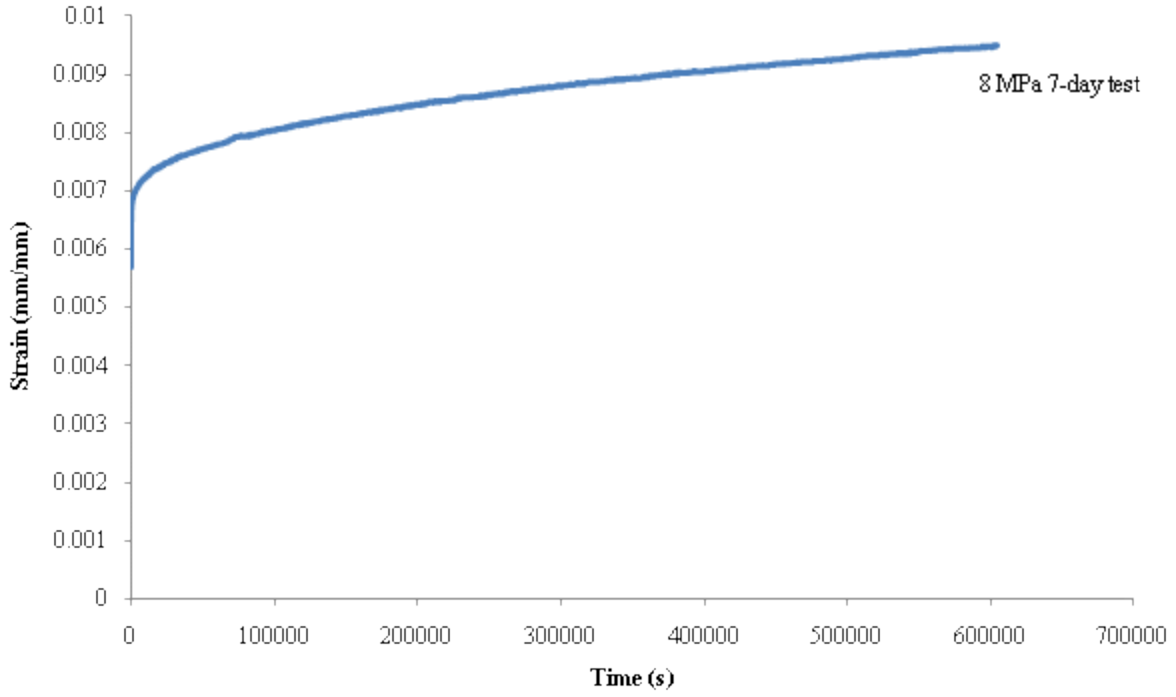

Figure 2.14 - Strain vs. time for film C1 subjected to 8 MPa in the longitudinal direction for 7 days

The 14 MPa seven day creep curve is shown in Figure 2.15.

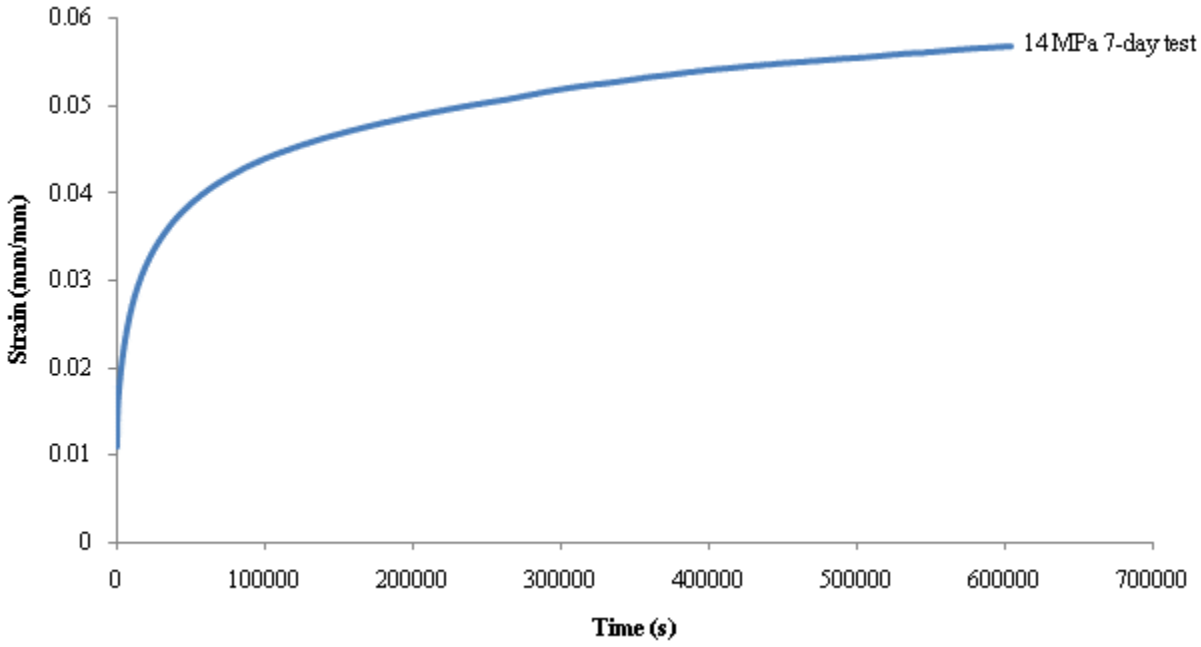

Figure 2.15 - Strain vs. time for film C1 subjected to 14 MPa in the longitudinal direction for 7 days

2.4.7 Discussion of Results

In the interest of clarity, the comparative graphs in the following section will not show all repetitions for each film and stress level, but will instead show only the most representative sample for comparison purposes.

2.4.7.1 General

For all of the films, creep tests done at higher stress levels produced higher levels of strain. This includes both the initial elastic strain response of the material, which increased with increasing stress levels, and the delayed creep strain, which occurred gradually over the entire test period, but also increased in magnitude with increasing stress. The curves also became smoother as stress levels increased. This is primarily because the extensometer used for measuring displacement is designed for extensions of up to 12 mm. The lower stresses, especially 2 MPa, produced deformations as low as 0.2 mm over the total 24 hour period, meaning that the measurements were at the extreme low end of the extensometer's range, so noise affected the readings.

As mentioned several times previously, some slippage may have occurred between the specimens and the grips or the extensometer and the aluminum bars during the initial loading phase of some of the tests. In general, it had a very minor impact on the results, but was especially noticable for the 2 MPa tests, as their strain ranges were quite small.

Although the strain rate of the films slowed over time, they continued to creep for the full 24 hours or seven days of every test. In no case did the strain become a constant value before the end of the test.

2.4.7.2 Effect of Film Direction

All of the films were tested at all stress levels in both the longitudinal and transverse directions of the material. In nearly every case, more strain was observed in the transverse direction than the longitudinal direction. As an example, Figure 2.16 shows the 12 MPa curves for film A in both directions.

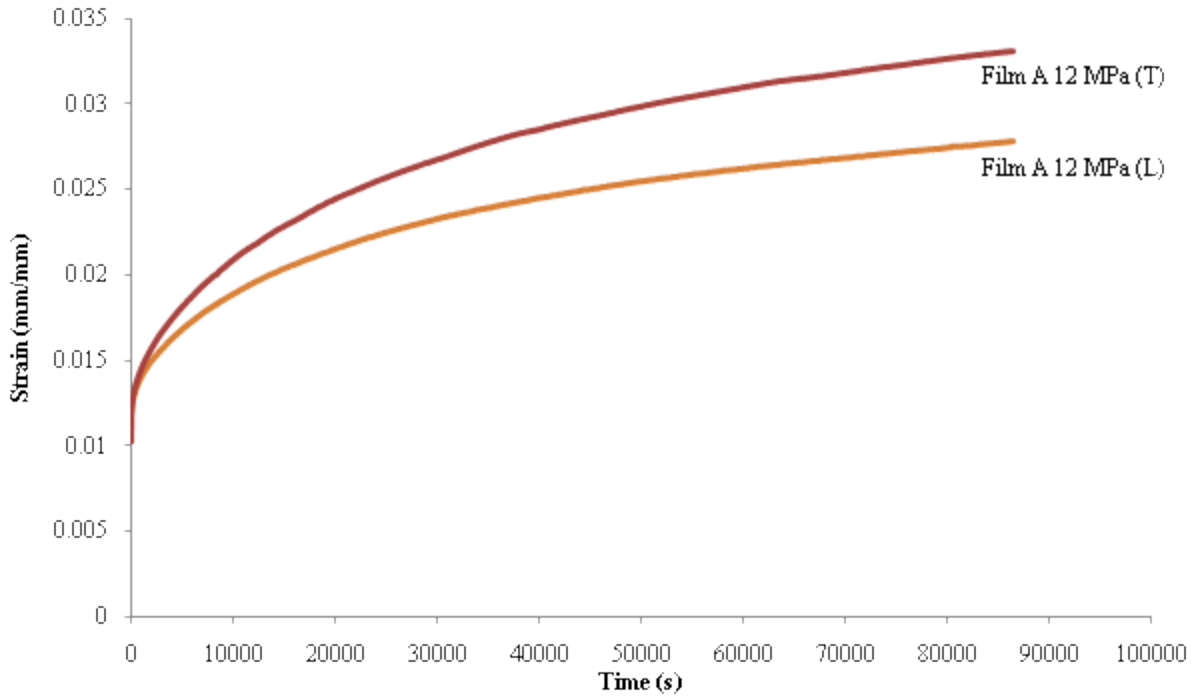

Figure 2.16 – Creep curves for film A tested at 12 MPa in both directions

A difference between the tensile behaviour of ETFE in the two directions has been observed by others as well. Ansell (1985) found a higher average tear strength in samples tested in the longitudinal direction, as shown in Table 1.5 through Table 1.7. Ansell also found that long term creep in the transverse direction is higher than in the longitudinal direction, except at 100°C in dry air, as shown in Table 1.10 (Ansell, 1985). DSET reported a higher tensile strength in the longitudinal direction after each year of exposure, as shown in Table 1.8. However, no major differences are evident between the tear strengths in the two directions in this test (Moritz, 2007b). Conversely, Galliot and Luchsinger (2010) found that uniaxial tensile tests showed a slightly higher yield and ultimate strength for the transverse direction.

The extrusion process by which ETFE film is created could be responsible for this anisotropic behaviour because it causes the molecules to be stretched in the direction of extrusion such that they are aligned in the longitudinal direction. It could also be due to the crystal structure of the molecule, i.e. the degree of crystallinity, the location of the crystalline regions and the orientation of the crystals, or to thermally activated relaxation processes that occur during film processing (Hadley &Ward, 1993).

2.4.7.3 Effect of Film Brand

Three brands of film were tested, and are referred to in this thesis as A, B and C. Films A and C are structural-grade films extruded by different manufacturers from the same resin. Film B is a general-purpose film. Mechanical properties supplied by the resin manufacturers were given in Table 2.2. In general, films A and C displayed similar levels of creep, as would be expected given that they are manufactured from the same resin. Film B generally

displayed higher levels of creep than the other films. Figure 2.17 shows, as an example, a representative 8 MPa longitudinal curve for each film.

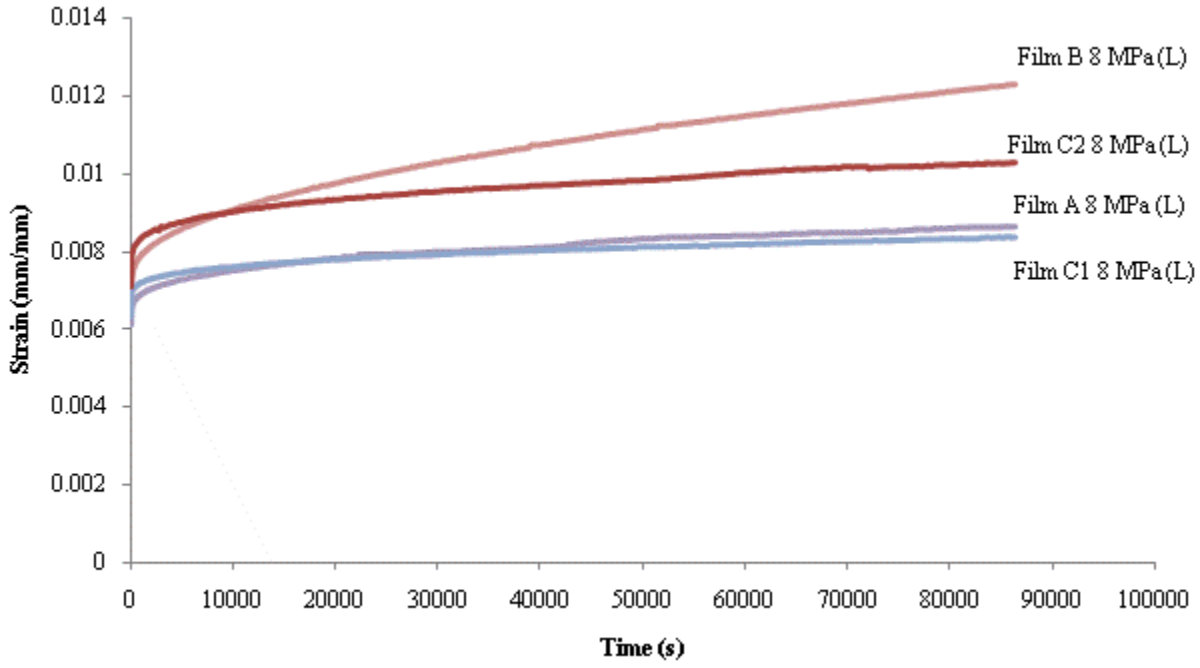

Figure 2.17 - Creep curves for all brands tested at 8 MPa in the longitudinal direction

The curves for film A, film C1 and film C2 all take on a very similar shape. The curves for A and C1 are nearly identical in magnitude as well, but the curve for C2 is higher. It is possible that this is due to a slip between the grips and the specimen or between the extensometer and the aluminum bars, or there could be an actual difference between the elastic responses of films C1 and C2. The effect of film thickness on creep behaviour will be discussed in more detail in section 2.4.7.4. The curve for film B, on the other hand, takes on an entirely different shape than the other three, and achieves a higher 24-hour value. The curve is much steeper than the others, indicating that the creep is continuing at a higher rate, and will likely not level off as quickly as the others.

2.4.7.4 Effect of Film Thickness

Having two thicknesses of film C (150 μm and 300 μm) allows for an analysis of the effects of film thickness on creep. In all cases C2 showed more creep in 24 hours than C1. For instance, Figure 2.18 shows the creep curves for a C1 and a C2 sample tested in the transverse direction at 12 MPa,

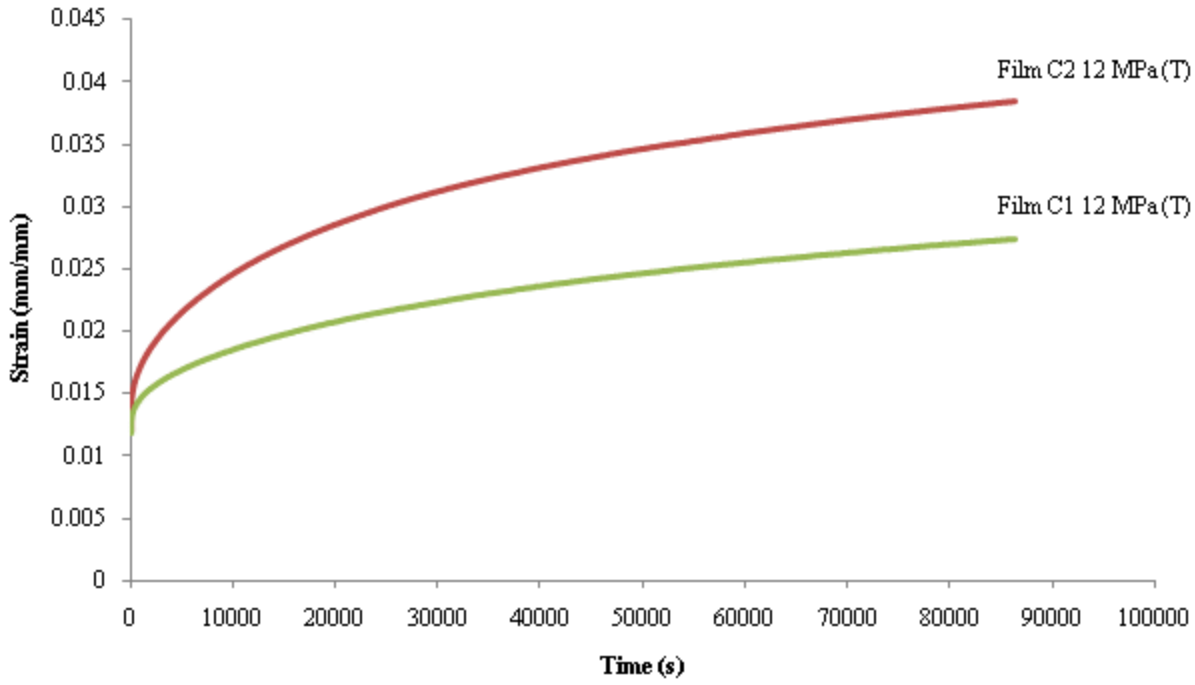

Figure 2.18 - Creep curves for both thicknesses of film C tested at 12 MPa in the transverse direction

Differences in tensile properties of different thicknesses of the same film have been found by others as well. Ansell (1985) found that 100 μm bent film samples had higher average tear strength than 300 μm bent film samples of the same variety. Also, Moritz (2007b) observed a slightly higher ultimate tensile strength for thinner film samples, based on the data from Moritz, Abstreiter, and Grützmann, as shown in Figure 1.37. Moritz also discussed the effect of film thickness on tensile test data obtained by the film manufacturer Nowoflon. The data shows a general decrease in tensile strength, stress at 10% strain, and tear strength, as film thickness increases. However, break strain increased along with thickness (Moritz, 2007b). Moritz suggested that because the cross-sectional areas of the samples were decreasing considerably as they were strained, the given values for engineering stress and strain are misleading. The thicker samples failed at a higher engineering strain, indicating that their cross-sections were reduced by a greater percentage than the thinner samples. This means that the engineering stress for the thicker samples likely exceeds the true stress by a greater amount than that for the thinner samples, and the true stresses may actually be nearly equal for all thicknesses (Moritz, 2007b). This could also apply to the creep results. The thicker samples are at a higher engineering strain after 24 hours, so their cross-sections are accordingly reduced. The actual stress the samples are experiencing would have increased with decreasing cross-section, meaning that the thicker samples would have been undergoing increasingly higher stress values than the thinner ones, causing further reductions in cross-section.

2.4.7.5 Effect of Temperature

Although the effects of temperature on creep were not explicitly investigated in this study, certain occurrences allowed for the existence of temperature-dependent creep behaviour to be observed. When testing began, the test

frame was not insulated nor was the temperature regulated. Temperature fluctuations were quite large, with the daytime high temperature reaching about 22°C in the laboratory, and the night time low temperature dropping to about 10°C. Samples tested under these conditions consistently displayed less creep in 24 hours than those that were tested at a regulated temperature of 23°C. The results of the tests done under uncontrolled temperature conditions are not presented in this thesis. An additional insight into the temperature dependent creep behaviour of ETFE foils came during the seven day creep test on film C1 at 2 MPa. The heater failed to operate consistently when switched on by the controller, so the temperature fluctuated by several degrees over the course of this test. The results of the creep test are shown on the graph below, in conjunction with the temperature divided by 10,000, so that it would appear on the same scale.

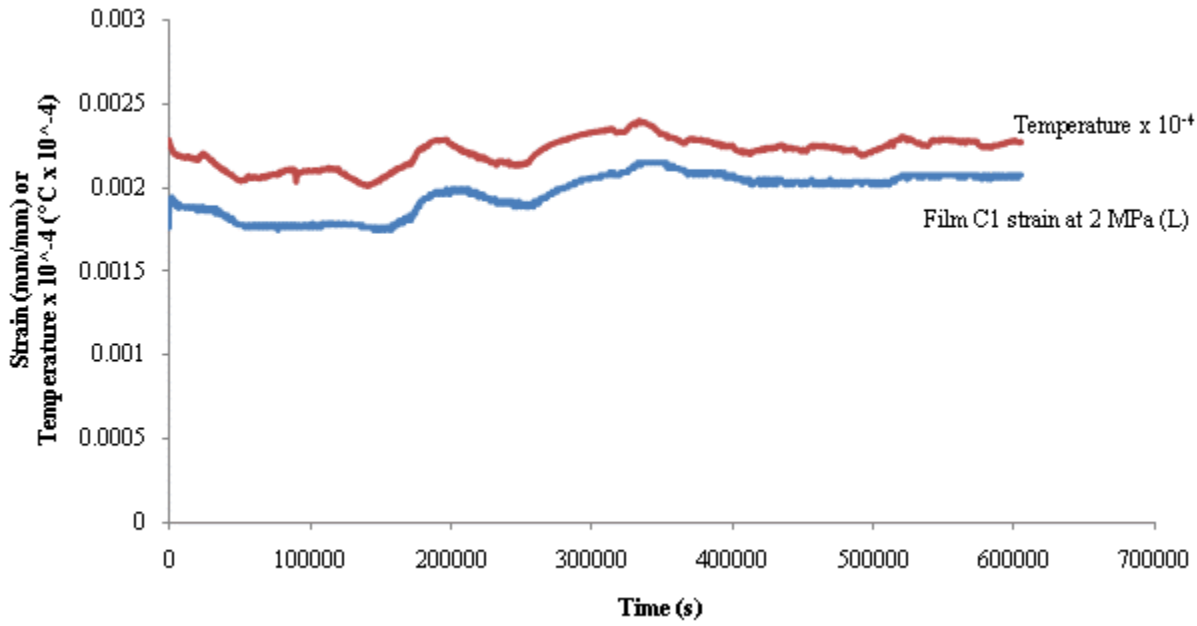

Figure 2.19 - Seven-day strain and temperature comparison for film C1 tested at 2 MPa in the longitudinal direction

It is obvious that the strain does not increase in the same manner as on the other creep curves, but instead fluctuates along with the temperature. At this low stress level, it appears that small temperature fluctuations can have a greater impact on strain than the stress itself does. Since real-life applications of ETFE film, such as in cushions on buildings, can involve large temperature fluctuations from day to night or from one day to the next, future research should be considered where film is subjected to fluctuating temperatures during creep tests, instead of held at constant elevated or lowered temperatures.

2.5 Test Procedure for Tensile Tests

Tensile tests were carried out according to ASTM D882-09 *Standard Test Method for Tensile Properties of Thin Plastic Sheeting*. These were done to verify the yield and failure stress values provided by the film manufacturers.

Five specimens of each film were tested in each direction. The Instron 4465 tensile testing frame shown in the following figure was used for all tests.

Figure 2.20 - Instron 4465 tensile test frame

The MTS grips used for the creep tests were used for the tensile tests as well. The specimens were cut to a width of 25 mm and a length of 150 mm so as to accommodate a gauge length (initial grip separation) of 50 mm. The grips were separated at a rate of 500 mm/min, while their separation distance and the corresponding applied load were recorded at regular intervals. The specimens were elongated until failure.

2.6 Results of Tensile Tests

Figures 2.21 – 2.24 show the results of the tensile tests in terms of stress-strain curves. It is important to note here that due to the high levels of elongation of the specimens, and the consequential decrease in the cross-sectional

areas, these are engineering stress and strain values, not true stress or strain values. Figure 2.21 shows the stress-strain curves for all trials of film A in both directions.

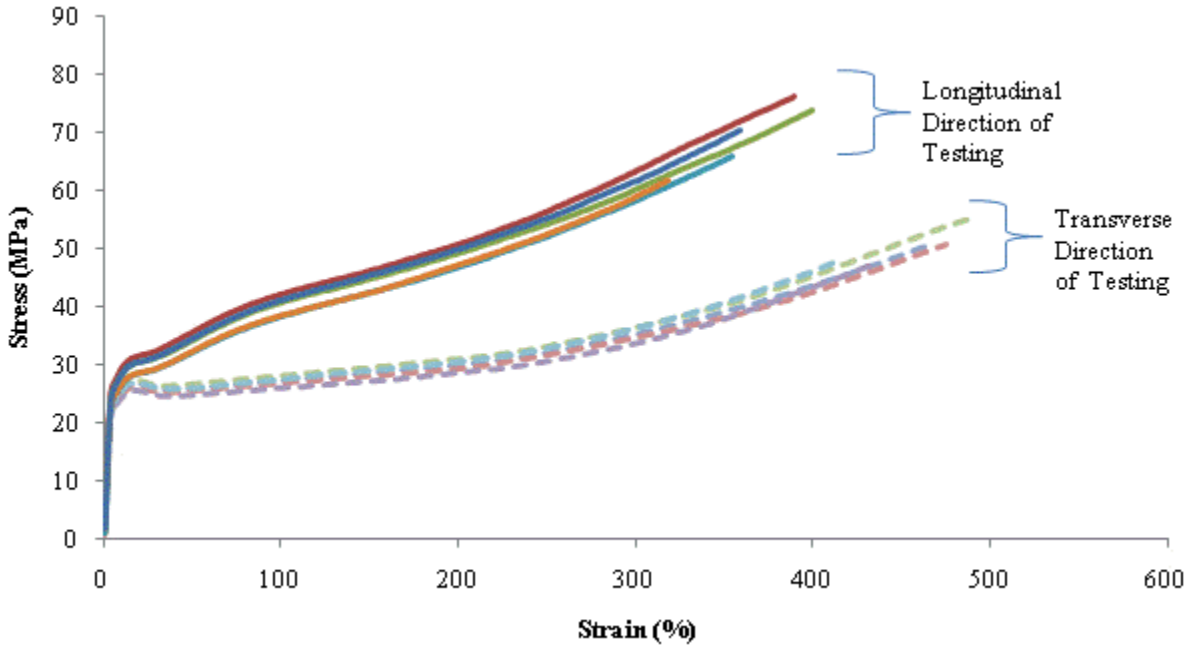

Figure 2.21 - Stress-strain curves for film A tested in tension in both directions

The film initially strained in a fairly linear fashion, but yielded at between 20 and 35 MPa of engineering stress, where the curves exhibit local maxima, then continue on with increasing slope until the failure point.

The films tested in the longitudinal direction had higher failure stress levels than those tested in the transverse direction, but failed at lower strains. The film is highly ductile in both directions, making failure stress of greater importance than failure strain when choosing primary stress direction of the film in applications. The film also yielded at a slightly higher stress in the longitudinal direction than in the transverse direction.

Figure 2.22 shows the stress-strain curves for film B tested in both directions.

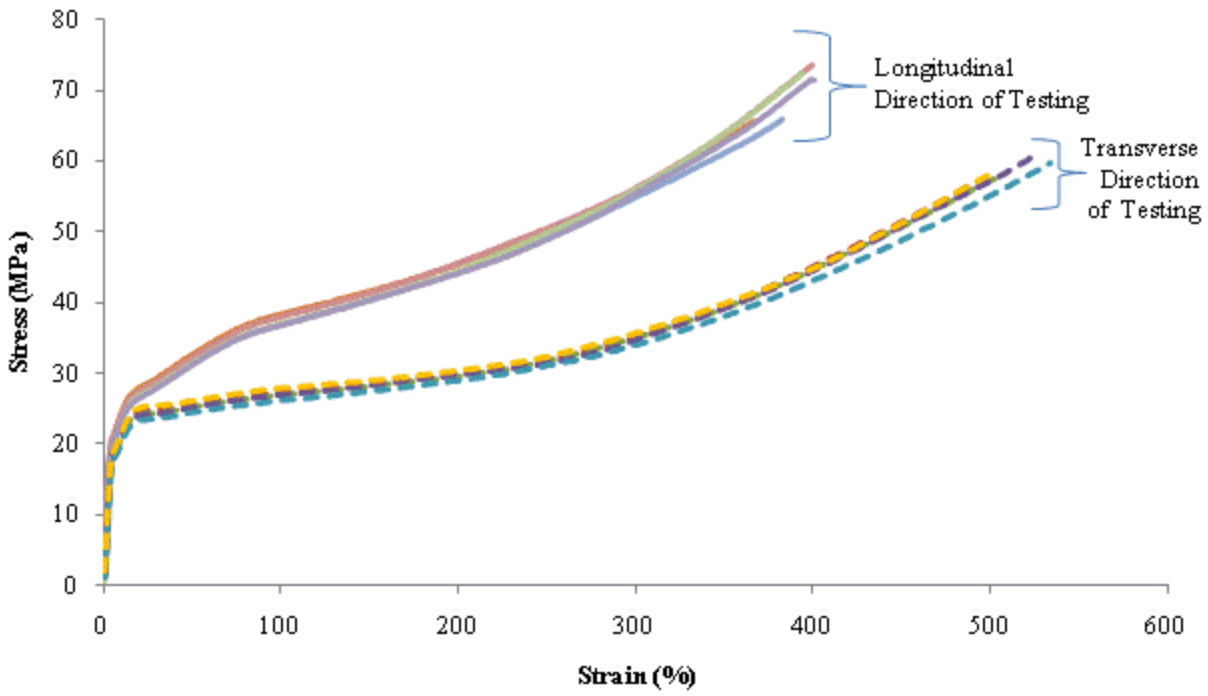

Figure 2.22 - Stress-strain curves for film B tested in tension in both directions

Again, early local maxima on the curves show the yield point of the film, which is slightly higher in the longitudinal direction. Film B also had a higher failure stress and lower failure strain in the longitudinal direction than in the transverse direction.

Figure 2.23 shows the stress-strain curves for film C1 tested in both directions.

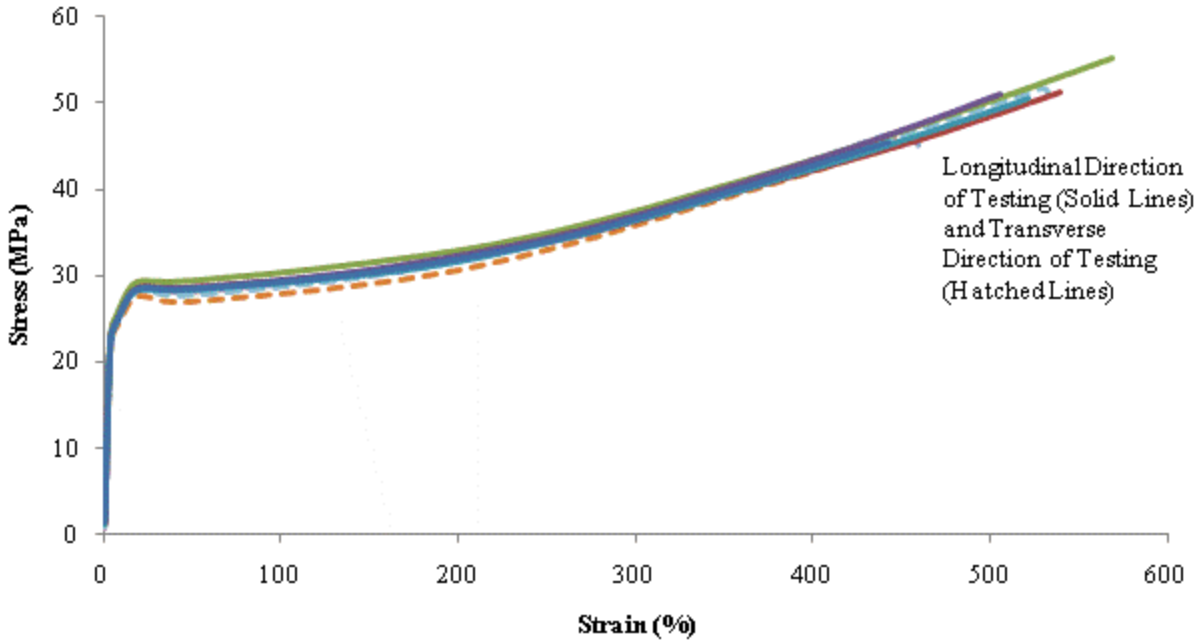

Figure 2.23 - Stress-strain curves for film C1 tested in tension in both directions

Film C1 displayed nearly identical behaviour in both directions. The curves closely resemble those exhibited by the other films.

The final stress-strain curve is for film C2 tested in both directions (Figure 2.24).

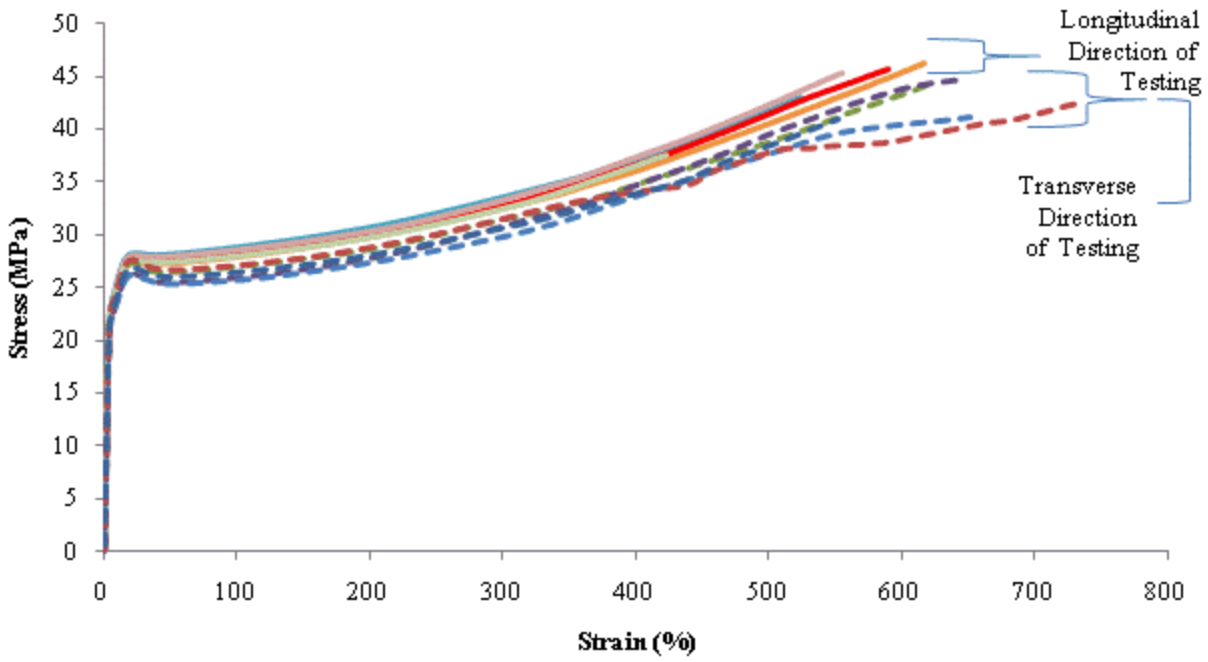

Figure 2.24 - Stress-strain curves for film C2 tested in tension in both directions

Film C2 showed less variation between the transverse and longitudinal directions than films A or B, but more than film C1. Here, the film yielded and failed at slightly higher stresses in the longitudinal directions, but the difference in ductility was less obvious.

Table 2.6 summarizes the average values of yield stress and failure stress and strain for the four films in both directions, and compares them to the values provided by the manufacturers. The yield stresses were taken as the values of the initial peaks of the curves. There are many ways to determine yield stress from stress-strain curves, so the manufacturers' values may have been determined using another method.

Table 2.6 - Summary of tensile test data, with comparison to manufacturer data

	Experimental Data			Manufacturer Data		
	Break		Yield	Break		Yield
	Strain (%)	Stress (MPa)	Stress (MPa)	Strain (%)	Stress (MPa)	Stress (MPa)
AL	363.93	69.69	28.02	425	46	22
AT	455.78	50.27	26.60	425	46	22
BL	388.12	69.73	25.92	250	41	-
BT	501.67	57.60	24.44	250	41	-
C1L	515.34	50.64	28.73	425	46	22
C1T	478.54	47.94	28.46	425	46	22
C2L	541.67	43.60	27.84	425	46	22
C2T	641.05	42.71	26.75	425	46	22

In nearly every case the measured values were at least as great as the manufacturers' values. The only cases where the experimental data were lower were the break strain of film A in the longitudinal direction, and the break stress of film C2 in both directions. However, these values were close enough to state that the mechanical properties provided by the manufactures are good design values for the films.

Chapter 3 Viscoelastic and Viscoplastic Modeling of ETFE

In elastic theory of material behaviour, no consideration is given to time-dependence. When a load is applied to an elastic material, its initial strain response is directly proportional to the stress that has been applied, and increases linearly with stress, in proportion to the elastic modulus, E. However, if the stress is held constant for a period of time, instead of the strain remaining at a constant value, the material will "creep", meaning that the strain will continue to increase. The theory of viscoelasticity considers this time dependence. Viscoelastic and viscoplastic constitutive models have been developed to model the creep response of ETFE during the lab tests. This section presents the basic theory behind these models as well as the actual models that were used.

3.1 Theory of Viscoelasticity

A linear elastic solid is a material in which the stress at any point X and time t, $\sigma(X,t)$, is a function of the strain at that point and time, $\varepsilon(X,t)$. A linear viscous fluid is a material in which $\sigma(X,t)$ is a function of the current strain rate, $\partial\varepsilon(X,t)/\partial t$. It has no "memory" of past deformation, except where it can be expressed in terms of the current strain rate. Linear viscoelastic materials remember deformations more generally. The stress, $\sigma(X,t)$, depends on all strains $\varepsilon(X,\tau)$ for all times τ, up to and including t (Lockett, 1972).

Materials are considered to be linear when the creep compliance, ε/σ, is independent of stress, meaning that it can be described by the same curve for all stress levels. In practice, most materials, including ETFE, are nonlinear, meaning that the compliance is a function of stress and a different curve is required to describe it at each stress level, so nonlinear models must be used to describe creep behaviour (Ahmad, Emery, Krishnaswamy, & Tuttle, 1992).

3.1.1 Spring and Dashpot Representations

Viscoelastic materials can be modeled by combinations of spring and dashpot elements. By building up these elements and considering the resulting behaviour, constitutive equations for viscoelastic materials can be developed.

A spring element is represented by a helical spring, as shown in Figure 3.1, which elongates by a certain amount u when a tensile force P is applied to both ends.

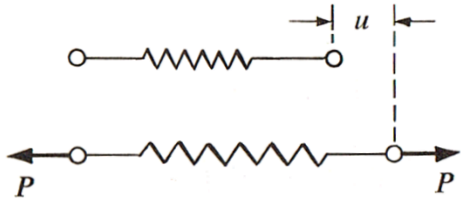

Figure 3.1 - Spring model (Flugge, 1967)

This is the behaviour exhibited by an elastic bar in tension. If the bar material is liner-elastic, the stress-strain relation is as follows:

$$\sigma = E\varepsilon \quad \textbf{(3-1)}$$

where E is Young's modulus. This relationship is known as Hooke's law.

A dashpot element, shown in Figure 3.2, is represented by a piston moving inside a cylinder with a perforated bottom to prevent air from being trapped in it, and a viscous lubricant between the walls of the piston and the cylinder. Because of the lubricant, a force P is required to displace the piston. The higher P is, the faster the movement of the piston will be.

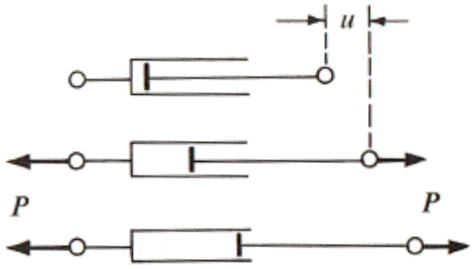

Figure 3.2 - Dashpot model (Flugge, 1967)

If the relationship between force and displacement speed of the piston is linear, then it follows that:

$$P = k\left(\frac{du}{dt}\right) \quad \textbf{(3-2)}$$

where k is a constant depending on the viscosity of the lubricant. Tension bars made of viscous materials will follow a similar model, where the time rate of change of elongation d(el)/dt is proportional to the applied force. Their deformation is entirely plastic, meaning that none of it is recoverable after the force is removed. In terms of stress and strain, this relationship is described by Equation (3-3).

$$\sigma = F\left(\frac{d\varepsilon}{dt}\right) \quad \textbf{(3-3)}$$

Viscoelastic materials behave in a way described by a combination of Equations (3-1) and (3-3). There are many ways to combine the basic spring and dashpot models to describe different material behaviour (Flugge, 1967). A series of Kelvin solid elements is the most common representation, and was the one chosen for the viscoelastic model for these tests. A single Kelvin solid element consists of a spring and dashpot connected in parallel, as shown in Figure 3.3.

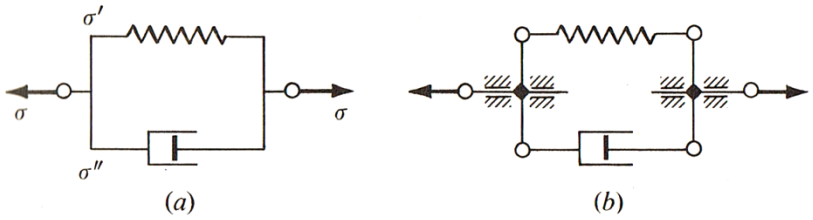

Figure 3.3 - Kelvin solid model (Flugge, 1967)

Figure 3.3 (a) is how a Kelvin element is typically displayed, but in reality it behaves more like it is shown in Figure 3.3 (b), such that the strain is the same for both the spring and dashpot (Flugge, 1967). A chain can be formed by any number of elements connected in series. The use of the model will be discussed in more detail in section 3.2.1.

3.2 Modeling

The constitutive modeling procedure used here is based on that developed by Hongtau Liu (2007) for modeling creep behaviour of polyethylene. The final constitutive equations and the basic modeling approach will be presented in the following sections, but full derivations of the equations and explanations of the procedure can be found in Liu's thesis, *Material Modelling for Structural Analysis of Polyethylene* (2007).

3.2.1 Viscoelastic Model

In a viscoelastic model, the material will experience an instantaneous elastic response as soon as it is loaded. The strain will then continue to increase slowly until it reaches an asymptote, resulting in a constant strain from that point forward. The model is represented by Kelvin elements arranged in series, as shown in Figure 3.4, where the spring provides the elastic response and the dashpot provides the viscous response.

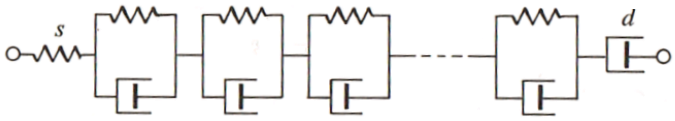

Figure 3.4 - Kelvin chain (Flugge, 1967)

A material following this model would, if unloaded, experience an instantaneous recovery of the elastic strain, followed by a gradual recovery of the remaining viscous strain.

For a constant stress σ_C, the constitutive strain equation for a viscoelastic material is

$$\varepsilon(t) = \sigma_C \left\{ \frac{1}{E_0} + \sum_{i=1}^{N} \frac{1}{E_i} \left[1 - \exp\left(-\frac{t}{\tau_i} \right) \right] \right\} \quad \textbf{(3-4)}$$

where E_0 is the elastic modulus of the material, determined from the initial linear portion of the creep curve, and t represents the time from loading. E_0 is represented in the model by the elastic modulus of the single spring. This

model applies to N Kelvin elements, each with its own relaxation time τ_i and defining material constant E_i. The E_i values correspond to the elastic moduli of the springs in each of the Kelvin elements, and the relaxation times are equivalent to η_i/E_i, where η_i is the viscosity of each dashpot element (Cheng, 2008).

The relaxation times are selected for the model such that the entire time spectrum of the test is well represented. Essentially, each Kelvin element will provide a strain curve to fit the data in the vicinity of its relaxation time, but its curve will be fairly linear prior to this point and will be constant after it. Figure 3.5 illustrates the effect of different relaxation times on strain-time curves.

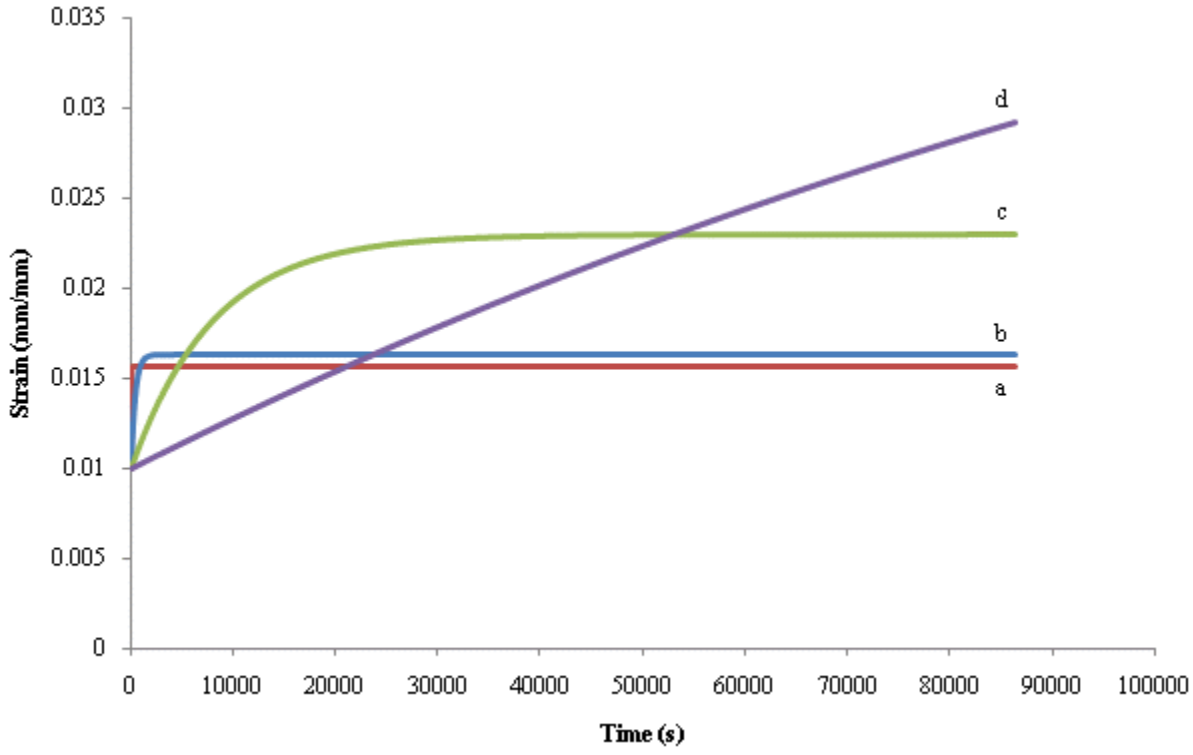

Figure 3.5 - Effect of relaxation times on creep curves

Each of the above curves is fitted for only one relaxation time, but each curve from a through d has a higher relaxation time than the last: 20, 400, 8000, and 160,000 seconds, respectively. Curves a and b have very low relaxation times with respect to the total time scale shown, and so become constant very quickly. Curve c has a relaxation time partway along the time scale and exhibits an approximately linear portion prior to becoming horizontal. Curve d has a relaxation time that is greater than the maximum time shown, so it remains linear for the entire scale. If a series of relaxation times are used together in one function, the resulting curve will be capable of reflecting the strain value accurately at all points in time.

For the creep data obtained for ETFE, a four-element Kelvin chain model was selected. One, two and three-element models were also attempted, but these models failed to provide an accurate fit along all points of the curve. The

three-element model was usually a very good approximation, but in several cases resulted in negative values for one or more of the E_i's. This, although mathematically possible, is physically impossible since it means that the sample would compress when placed in tension. Therefore, four elements were selected to avoid this scenario. The relaxation times chosen were 20 seconds, 400 seconds, 8,000 seconds and 160,000 seconds, or $\tau_i=20^i$. These times were selected because they cover the full 24 hour range of the creep tests and are concentrated at the lower end of the time scale, where strain is increasing at a higher rate. The exact values are more or less arbitrary, and multiple possible options for relaxation times likely exist that will provide a reasonable fit for the data. Some researchers, such as Cheng, Penlidis and Polak (2010) have also suggested setting the relaxation times as parameters in the model, which subsequently becomes nonlinear in the parameters. The relaxation times would then be estimated along with the other parameters using non-linear regression. This approach is effective for providing a good fit to the data for any time scale, but due to the necessary rigour involved, it was not used for this thesis.

The remaining elements required to define the viscoelastic creep function for the tests are the stress-dependent material constants, E. These were determined from the test data. E_0 was evaluated directly from the elastic response portion of the data curves as

$$E_0 = \frac{\sigma_C}{\hat{\varepsilon}_0} \tag{3-5}$$

where $\hat{\varepsilon}_0$ is the instantaneous jump in strain that occurs at t=0. The E_i values were found using linear least-squares fitting, in terms of their inverses, $x_i=1/E_i$. Following the method outlined by Liu (2007), a set of simultaneous linear equations can be created as follows:

$$[A]_{NxN}\{x\}_{Nx1} = \{F\}_{Nx1} \tag{3-6}$$

where [A] is an NxN matrix and {x} and {F} are Nx1 vectors, defined by

$$A_{ij} = \sum_{p=1}^{M_k} \left\{ \sigma_C \left[1 - \exp\left(-\frac{t_p}{\tau_j} \right) \right] \left[1 - \exp\left(-\frac{t_p}{\tau_i} \right) \right] \right\}, i, j = 1, \dots, N \tag{3-7}$$

and

$$F_i = \sum_{p=1}^{M_k} \left\{ \left(\hat{\varepsilon}_p - \frac{\sigma_C}{E_0} \right) \left[1 - \exp\left(-\frac{t_p}{\tau_i} \right) \right] \right\}, i = 1, \dots, N \tag{3-8}$$

where $\hat{\varepsilon}_p$ is the measured strain at time $t=t_p$ and M_k is the total number of strain measurements taken during the creep test.

An example of the curve-fitting procedure used to develop the viscoelastic models is given in Appendix G.

3.2.1.1 Viscoelastic Modeling Results

A graph is presented here for each brand which shows the measured 24-hour creep data at each stress and in each direction, along with a fitted curve corresponding to each data set. Individual fitted curves are shown in Appendix E.

The seven-day curves follow the 24-hour curves, and are presented individually by stress level and curve-fitting methodology.

3.2.1.1.1 Film A 24 Hour Viscoelastic Models

Figure 3.6 shows the fitted viscoelastic models for strain along with the measured strain data for film A tested at all stresses.

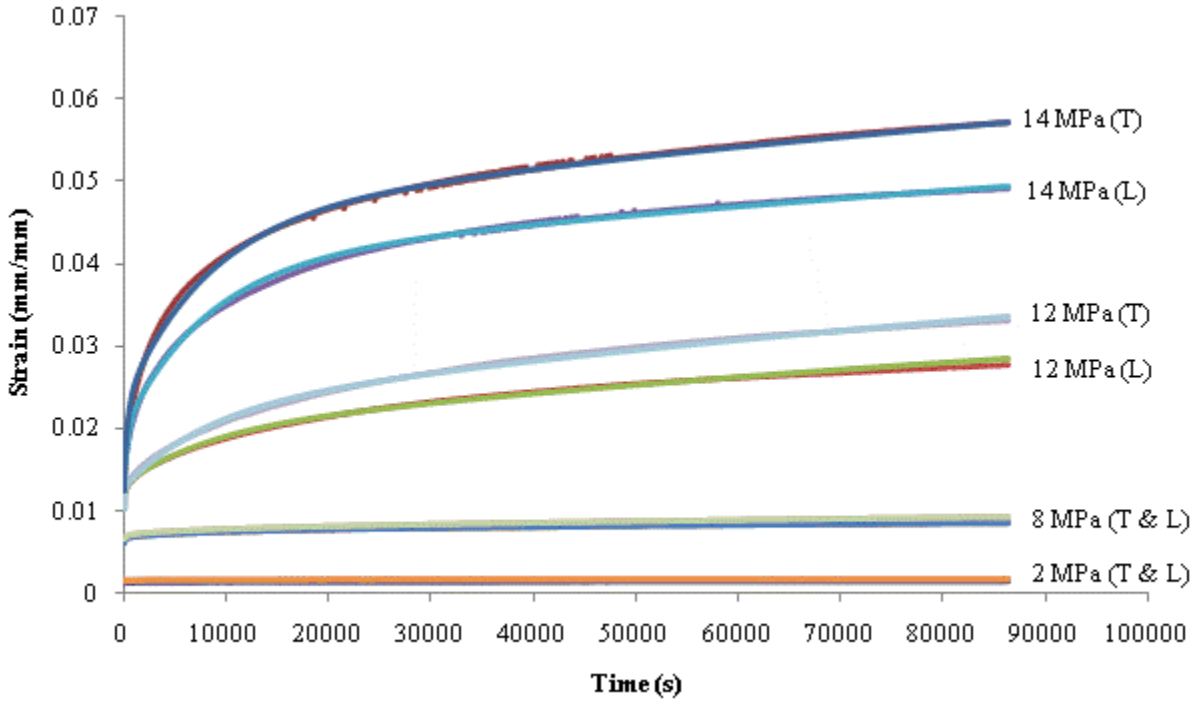

Figure 3.6 – Measured data and fitted viscoelastic curves for all 24-hour creep tests on film A

It is difficult to distinguish the measured curves from the fitted ones as the models provide a very close fit to the data.

3.2.1.1.2 Film B 24 Hour Viscoelastic Models

Figure 3.7 shows the fitted viscoelastic models for strain along with the measured strain data for film B tested at all stresses.

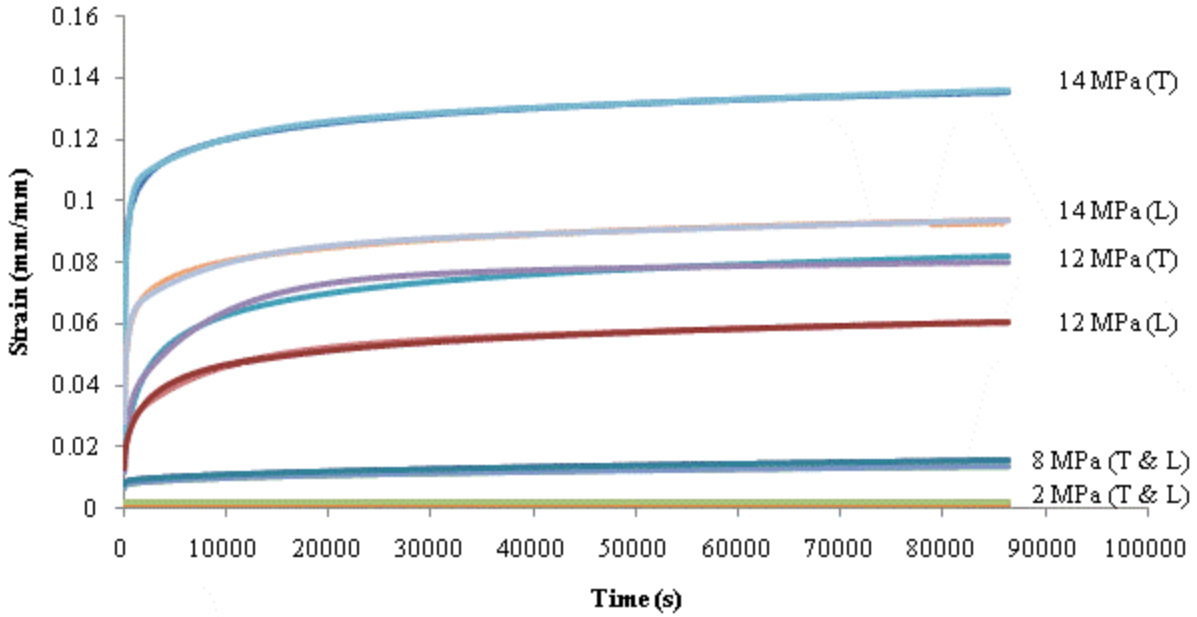

Figure 3.7 - Measured data and fitted viscoelastic curves for all 24-hour creep tests on film B

Once again, the models provide an exceptionally close fit to the data, making it difficult to distinguish between the measured and fitted curves.

3.2.1.1.3 Film C1 24 Hour Viscoelastic Models

Figure 3.8 shows the fitted viscoelastic models for strain along with the measured strain data for film C1 tested at all stresses.

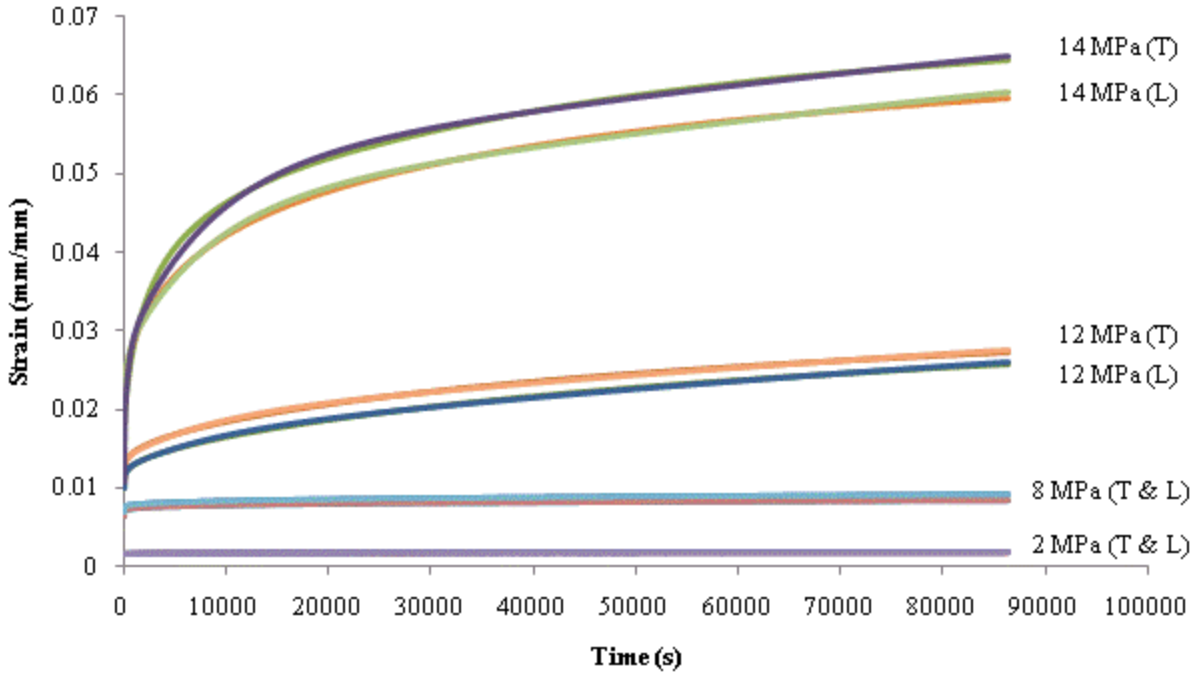

Figure 3.8 - Measured data and fitted viscoelastic curves for all 24-hour creep tests on film C1

The viscoelastic models also fit the C1 data very closely.

3.2.1.1.4 Film C2 24 Hour Viscoelastic Models

Figure 3.9 shows the fitted viscoelastic models for strain along with the measured strain data for film C2 tested at all stresses.

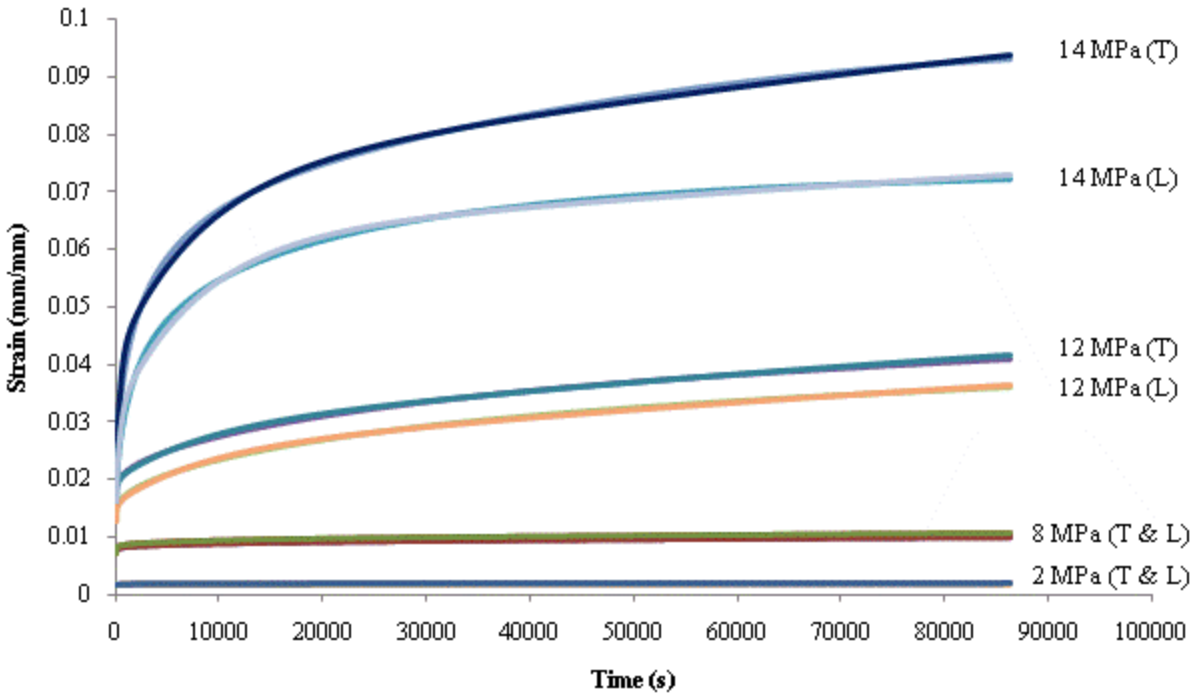

Figure 3.9 - Measured data and fitted viscoelastic curves for all 24-hour creep tests on film C2

The C2 data are also very well represented by the viscoelastic models.

3.2.1.1.5 Summary of Numerical Parameters for 24 Hour Viscoelastic Models

Tables 3.1 – 3.8 present the numerical parameters determined for the viscoelastic models shown above. They are presented in order of brand, then direction.

Table 3.1 - Viscoelastic modeling parameters for 24 hour test on film A in the longitudinal direction

Number of Kelvin elements:		**4**			
Stress	**E_0**	**τ_1** **20**	**τ_2** **400**	**τ_3** **8000**	**τ_4** **160000**
		E_1	**E_2**	**E_3**	**E_4**
2 MPa	1,698.63	528,820.73	28,752.16	46,210.72	7,407.41
8 MPa	1,308.62	20,790.02	23,180.34	11,048.50	3,091.19
12 MPa	1,171.11	6,596.31	10,031.10	1,923.08	564.97
14 MPa	1,148.17	7,501.88	2,341.92	708.72	605.33

Table 3.2 - Viscoelastic modeling parameters for 24 hour test on film A in the transverse direction

Number of Kelvin elements:				**4**	
Stress	E_0	τ_1 **20**	τ_2 **400**	τ_3 **8000**	τ_4 **160000**
		E_1	E_2	E_3	E_4
2 MPa	1,417.14	14,952.15	1,443,418.01	23,696.68	10,695.19
8 MPa	1,227.72	82,712.99	17,448.96	11,865.21	2,092.05
12 MPa	1,168.89	5,330.49	28,074.12	1,285.18	439.95
14 MPa	1,115.68	5,656.11	1,704.74	630.52	493.58

Table 3.3 - Viscoelastic modeling parameters for 24 hour test on film B in the longitudinal direction

Number of Kelvin elements:				**4**	
Stress	E_0	τ_1 **20**	τ_2 **400**	τ_3 **8000**	τ_4 **160000**
		E_1	E_2	E_3	E_4
2 MPa	1,600.00	58,754.41	36,995.93	19,204.92	8,396.31
8 MPa	1,181.10	9,794.32	12,347.20	4,666.36	904.16
12 MPa	916.26	6,939.63	914.91	501.00	572.41
14 MPa	500.28	1,160.09	593.47	669.79	623.44

Table 3.4 - Viscoelastic modeling parameters for 24 hour test on film B in the transverse direction

Number of Kelvin elements:				**4**	
Stress	E_0	τ_1 **20**	τ_2 **400**	τ_3 **8000**	τ_4 **160000**
		E_1	E_2	E_3	E_4
2 MPa	976.38	28,490.03	1,499,700.06	16,079.76	6,765.90
8 MPa	1,017.81	14,259.23	12,065.64	4,528.99	659.63
12 MPa	986.95	6,123.70	587.20	293.86	1,014.71
14 MPa	707.30	300.48	368.46	710.23	492.13

Table 3.5 - Viscoelastic modeling parameters for 24 hour test on film C1 in the longitudinal direction

Number of Kelvin elements:		**4**			
Stress	**E_0**	**τ_1** **20**	**τ_2** **400**	**τ_3** **8000**	**τ_4** **160000**
		E_1	**E_2**	**E_3**	**E_4**
2 MPa	1,265.31	107,307.65	53,191.49	35,663.34	14,130.28
8 MPa	1,223.24	11,540.68	30,892.80	15,923.57	6,357.28
12 MPa	1,200.00	7,923.93	11,617.10	3,041.36	523.29
14 MPa	802.55	2,464.88	3,591.95	751.31	398.72

Table 3.6 - Viscoelastic modeling parameters for 24 hour test on film C1 in the transverse direction

Number of Kelvin elements:		**4**			
Stress	**E0**	**τ1** **20**	**τ2** **400**	**τ3** **8000**	**τ4** **160000**
		E1	**E2**	**E3**	**E4**
2 MPa	**1,252.53**	**44,247.79**	**47,348.48**	**46,860.36**	**19,932.23**
8 MPa	**1,162.95**	**10,848.34**	**32,637.08**	**14,894.25**	**3,863.99**
12 MPa	**1,011.56**	**10,000.00**	**12,189.18**	**2,513.19**	**568.18**
14 MPa	**1,296.62**	**2,070.39**	**1,424.50**	**610.13**	**399.36**

Table 3.7 - Viscoelastic modeling parameters for 24 hour test on film C2 in the longitudinal direction

Number of Kelvin elements:		**4**			
Stress	**E_0**	**τ_1** **20**	**τ_2** **400**	**τ_3** **8000**	**τ_4** **160000**
		E_1	**E_2**	**E_3**	**E_4**
2 MPa	1,221.67	77,101.00	30,637.25	23,752.97	14,332.81
8 MPa	1,046.41	26,427.06	20,008.00	12,026.46	3,121.10
12 MPa	857.96	6,289.31	9,124.09	1,853.91	507.61
14 MPa	854.79	10,623.61	993.05	469.48	511.77

Table 3.8 - Viscoelastic modeling parameters for 24 hour test on film C2 in the transverse direction

Number of Kelvin elements:				**4**	
Stress	**E_0**	**τ_1** **20**	**τ_2** **400**	**τ_3** **8000**	**τ_4** **160000**
		E_1	**E_2**	**E_3**	**E_4**
2 MPa	1,158.88	47,147.57	22,815.42	32,637.08	9,523.81
8 MPa	1,107.14	8,340.28	17,711.65	10,082.68	2,831.26
12 MPa	709.19	6,261.74	9,532.89	1,460.07	380.52
14 MPa	677.94	17,102.79	699.30	464.04	261.85

3.2.1.1.6 Seven Day Viscoelastic Models

Seven day creep tests were run on film C1 in the longitudinal direction at 2 MPa, 8 MPa and 14 MPa. As mentioned previously, the results of the 2 MPa test were dominated by temperature effects, so constitutive models were not developed for the data. However, the 8 MPa and 14 MPa tests were successful, and several methods for developing viscoelastic and viscoplastic models were attempted. The first viscoelastic modeling method used was developing a fitted curve based only on the first 24 hours of data, using the relaxation times used for the other 24 hour models, and then extending the model for the rest of the time period. This modeling method provides an indication of how well the models that were developed based on the 24 hour creep tests will predict creep behaviour in the long term. The results of this modeling method are shown in Figure 3.10 and Figure 3.11.

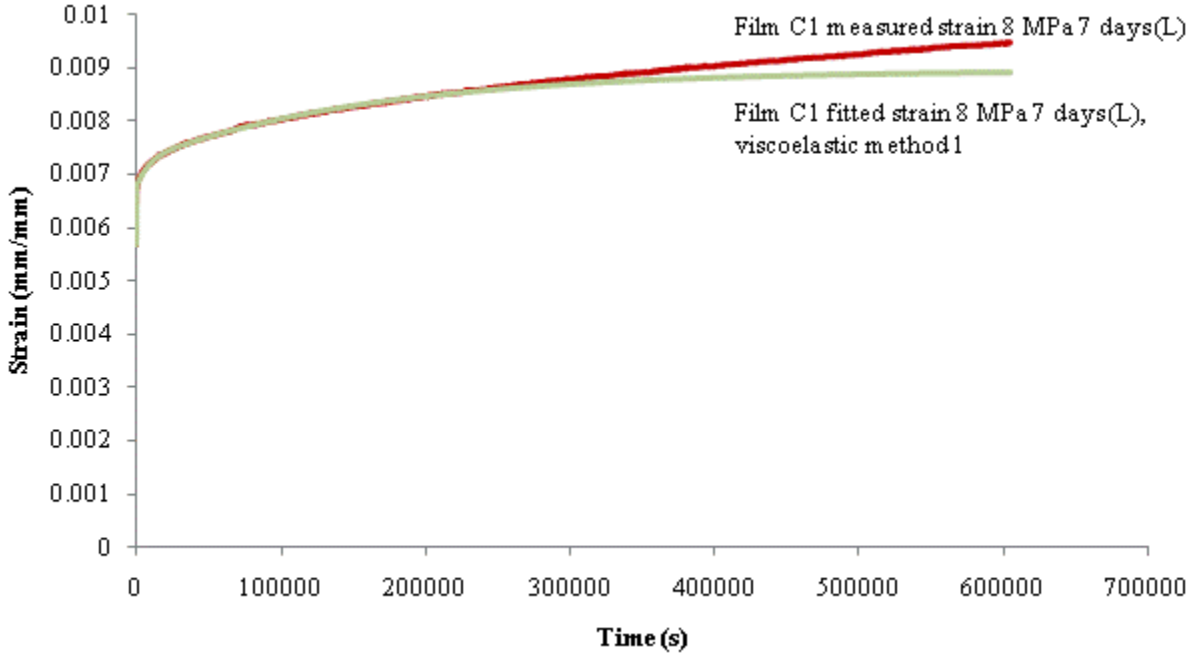

Figure 3.10 - Fitted viscoelastic model for C1 tested in the longitudinal direction at 8 MPa for 7 days, based on first 24 hours of data

From Figure 3.10 it can be seen that the model underestimates creep over the seven day period. After the initial 24 hours, the fitted curve begins to level off, but the measured curve continues to grow.

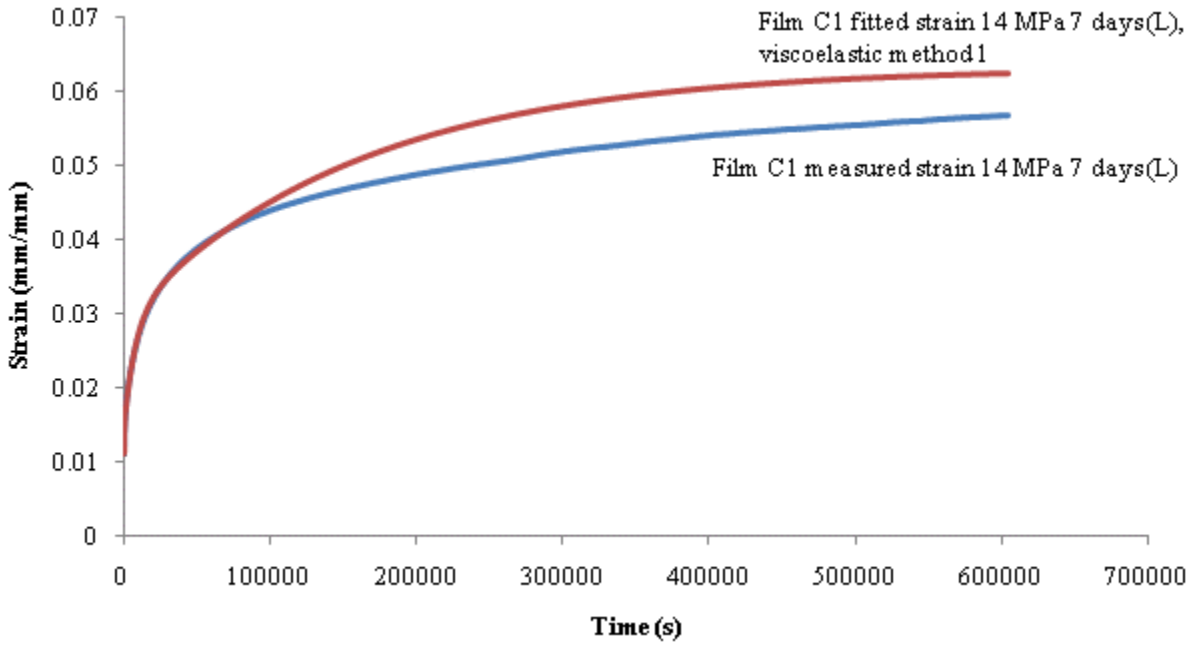

Figure 3.11 - Fitted viscoelastic model for C1 tested in the longitudinal direction at 14 MPa for 7 days, based on first 24 hours of data

From Figure 3.11 it can be seen that the model overestimates the data. It provides a close fit for the initial 24 hour period, but continues to increase at the same rate as the measured strain at 24 hours before beginning to level off, whereas the actual data begins to strain at a lower rate more quickly. However, as the model appears to be approaching a constant value, and the actual strain is increasing, if the curves were extended for a longer time period they would probably meet and eventually cross, whereby the model would underestimate the data, as in Figure 3.10.

The second modeling method attempted was to once again develop a model based on only the first 24 hours of data, but instead of extending the logarithmic equation over the full seven day time period, the slope of the fitted curve at 24 hours was calculated and a straight line was extended from this point using that slope. The results of this modeling method are shown in Figure 3.12 and Figure 3.13.

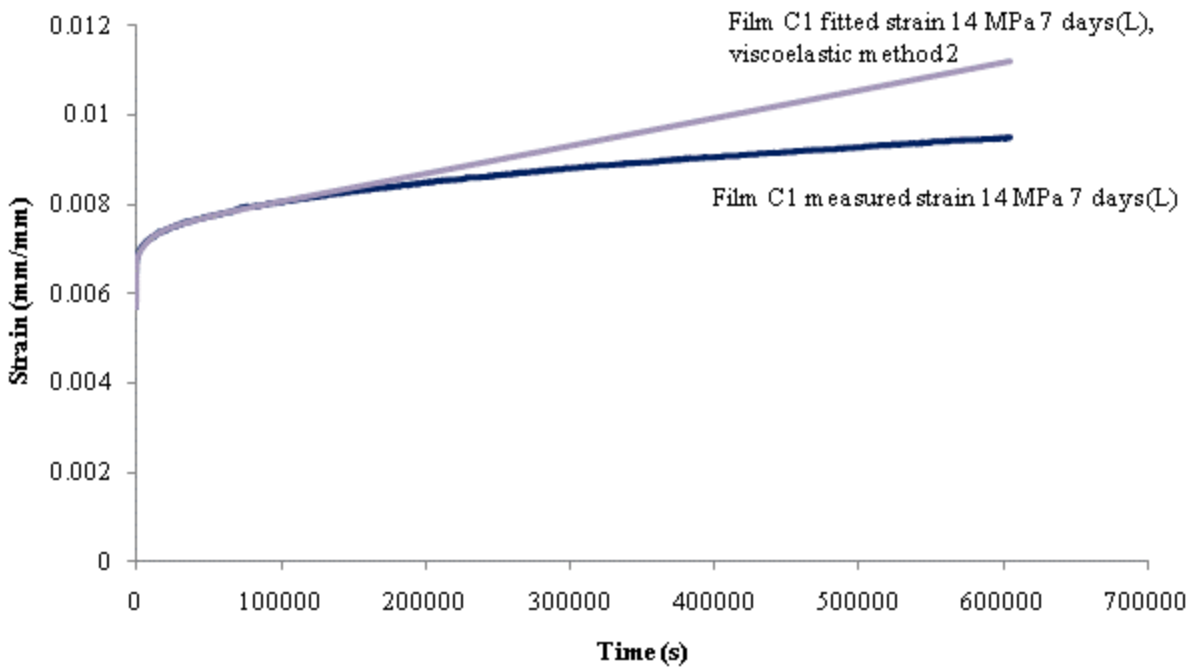

Figure 3.12 - Fitted viscoelastic/linear model for C1 tested at 8 MPa in the longitudinal direction for 7 days, based on first 24 hours of data and a straight line

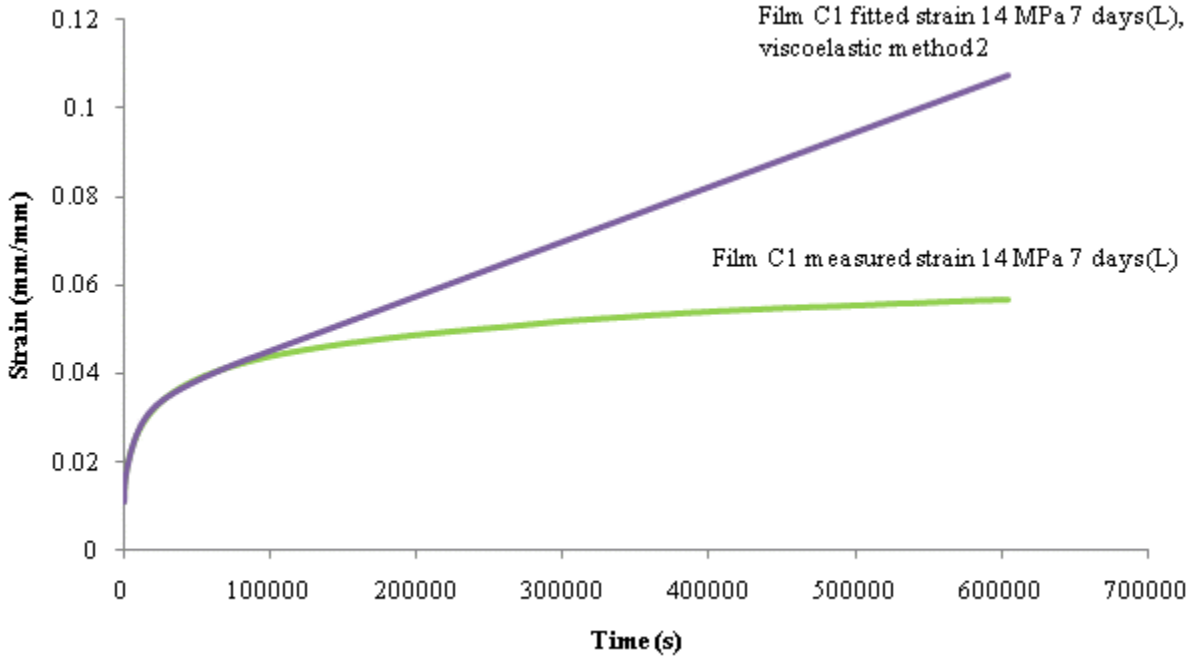

Figure 3.13 - Fitted viscoelastic/linear model for C1 tested at 14 MPa in the longitudinal direction for 7 days, based on first 24 hours of data and a straight line

This method greatly overestimates the seven day strain, because in reality the strain does not increase at a constant rate after the first 24 hours.

The third and final viscoelastic modeling method that was attempted was to adjust the relaxation times to suit the full seven day test period. The selected times were 30, 900, 27,000, and 810,000 seconds, or $\tau_i=30^i$. The corresponding models are shown in Figure 3.14 and Figure 3.15.

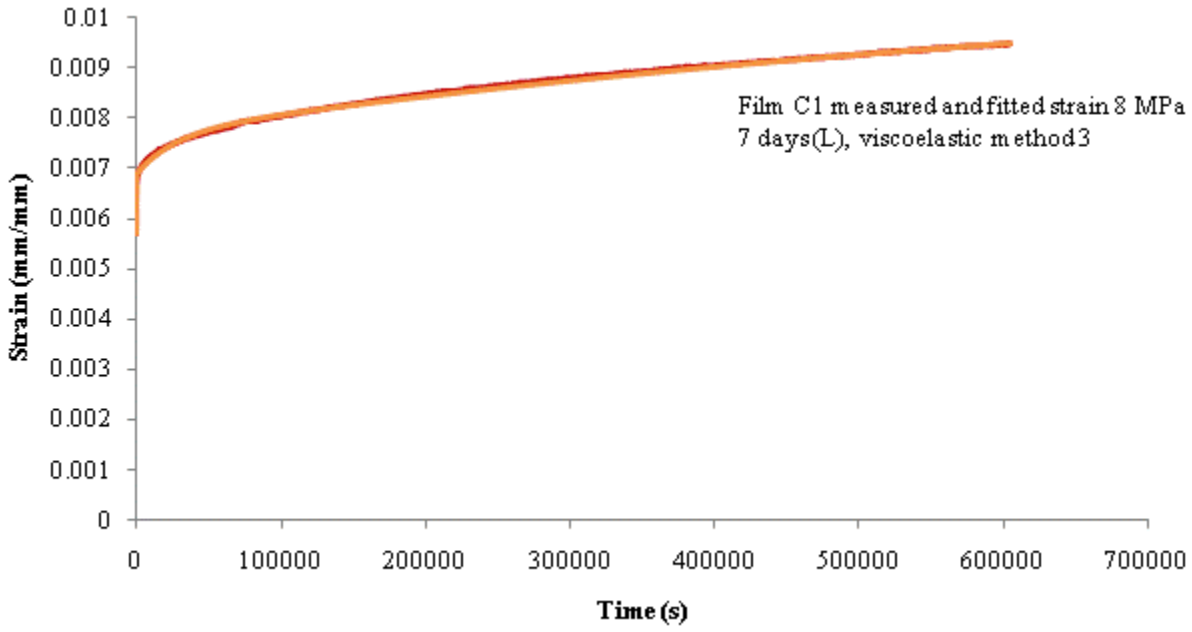

Figure 3.14 - Fitted viscoelastic model for C1 tested at 8 MPa in the longitudinal direction for 7 days, based on full 7 days of data

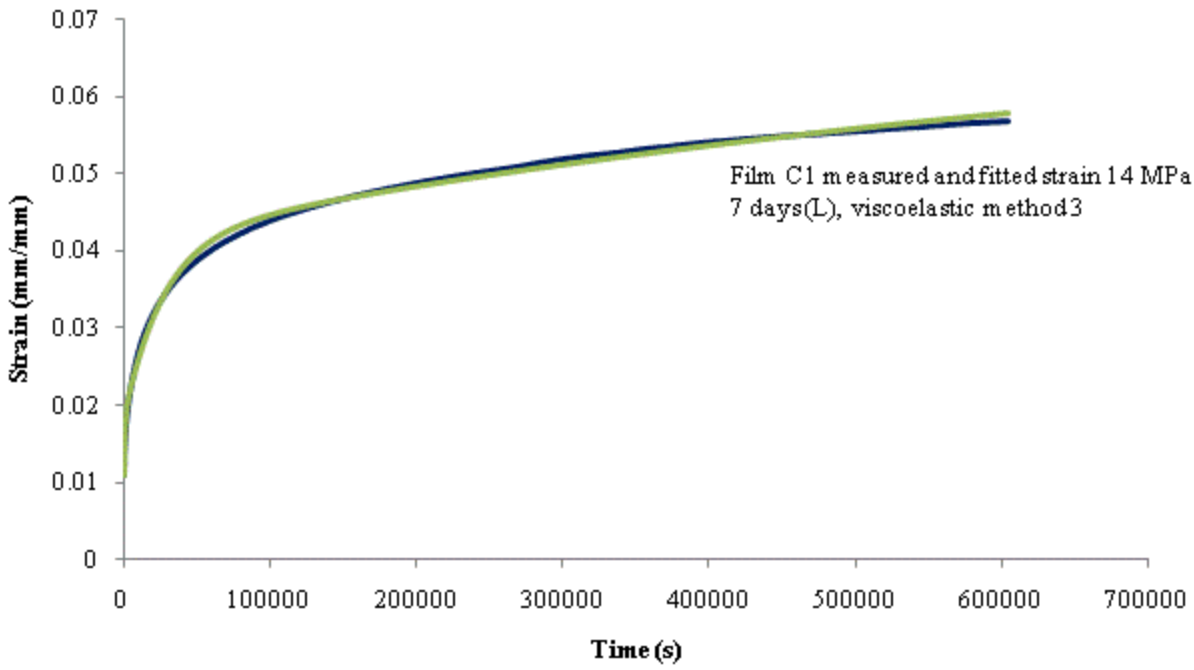

Figure 3.15 - Fitted viscoelastic model for C1 tested at 14 MPa in the longitudinal direction for 7 days, based on full 7 days of data

This method clearly gives the best fit to the full range of data. The applicability of all three methods will be discussed further in section 3.3.

3.2.2 Viscoplastic Model

In a viscoplastic model, the material experiences the same instantaneous elastic strain as with the viscoelastic model, however the strain continues to increase after this point without ever reaching an asymptote. If the stress is removed, the elastic strain will be recovered, but there will be a plastic portion of strain that will remain permanently. Power-law functions are therefore used to model viscoplastic materials.

The constitutive equation for the viscoplastic model applied to the ETFE creep data is the following power-law function:

$$\varepsilon(t) = \frac{\sigma_C}{E_0} + \sigma_C C_0 t^{C_1} \quad \textbf{(3-9)}$$

where C_0 and C_1 are material constants used for modeling. To determine these constants, the constitutive equation is transformed into the following form:

$$\ln\left(\frac{\varepsilon(t)}{\sigma_C} - \frac{1}{E_0}\right) = \ln C_0 + C_1 \ln t \quad \textbf{(3-10)}$$

which is a linear function, where lnt and $\ln(\varepsilon(t)/\sigma_c - 1/E_0)$ are the x and y variables, respectively, and $\ln C_0$ and C_1 are the parameters, which can be determined from linear least-squares fitting. An example of the curve-fitting procedure used to develop the viscoplastic models is given in Appendix H.

3.2.2.1 Viscoplastic Modeling Results

As with the viscoelastic results, a graph is presented in this section for each film brand, showing the results of the 24-hour creep tests at all stress levels and in both directions. The corresponding fitted viscoplastic curves will be shown on the same graphs. Individual fitted curves are shown in Appendix F. The seven-day curves follow the 24-hour curves, and are once again presented individually by stress level and curve-fitting methodology.

3.2.2.1.1 Film A 24 Hour Viscoplastic Models

Figure 3.16 shows the fitted viscoelastic models for strain along with the measured strain data for film A tested at all stresses.

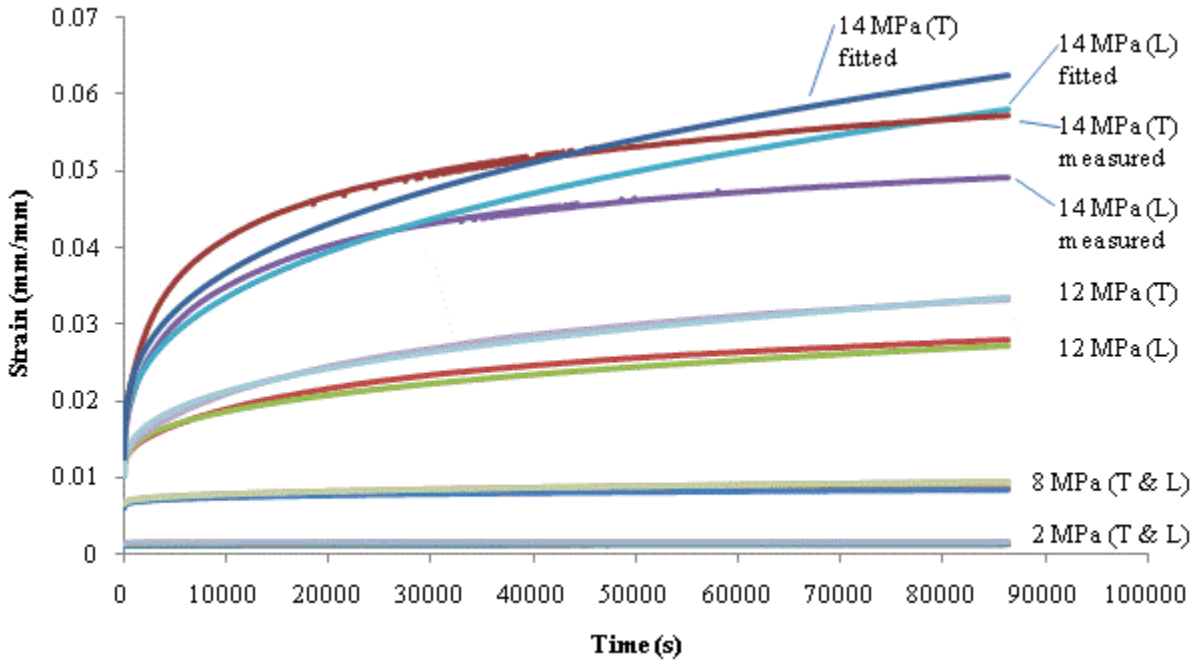

Figure 3.16 – Measured data and fitted viscoplastic curves for all 24-hour creep tests on film A

At the lower stress levels the fitted curves are a very close match to the data, but the 14 MPa models diverge somewhat from the measured results.

3.2.2.1.2 Film B 24 Hour Viscoplastic Models

Figure 3.17 shows the fitted viscoplastic models for strain along with the measured strain data for film B tested at all stresses.

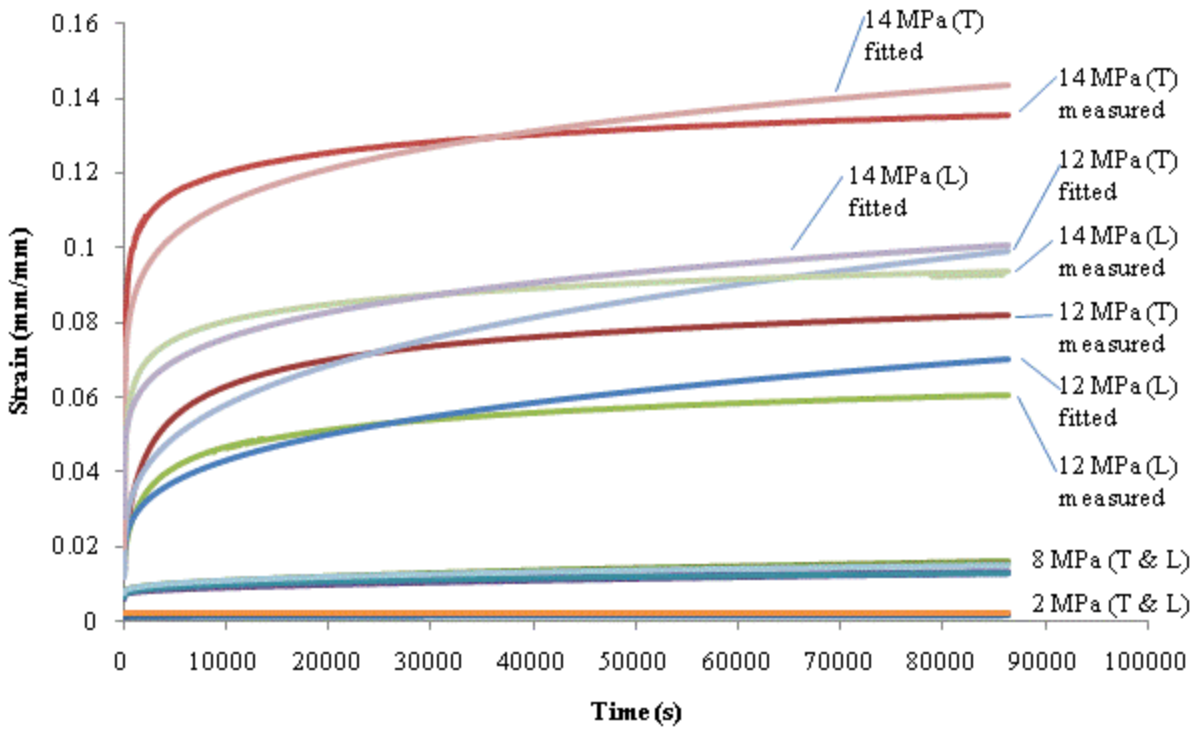

Figure 3.17 - Measured data and fitted viscoplastic curves for all 24-hour creep tests on film B

Once again, the models fit the creep data for the lower stresses well, but diverge from the creep data at the higher stress levels.

3.2.2.1.3 Film C1 24 Hour Viscoplastic Models

Figure 3.18 shows the fitted viscoplastic models for strain along with the measured strain data for film C1 tested at all stresses.

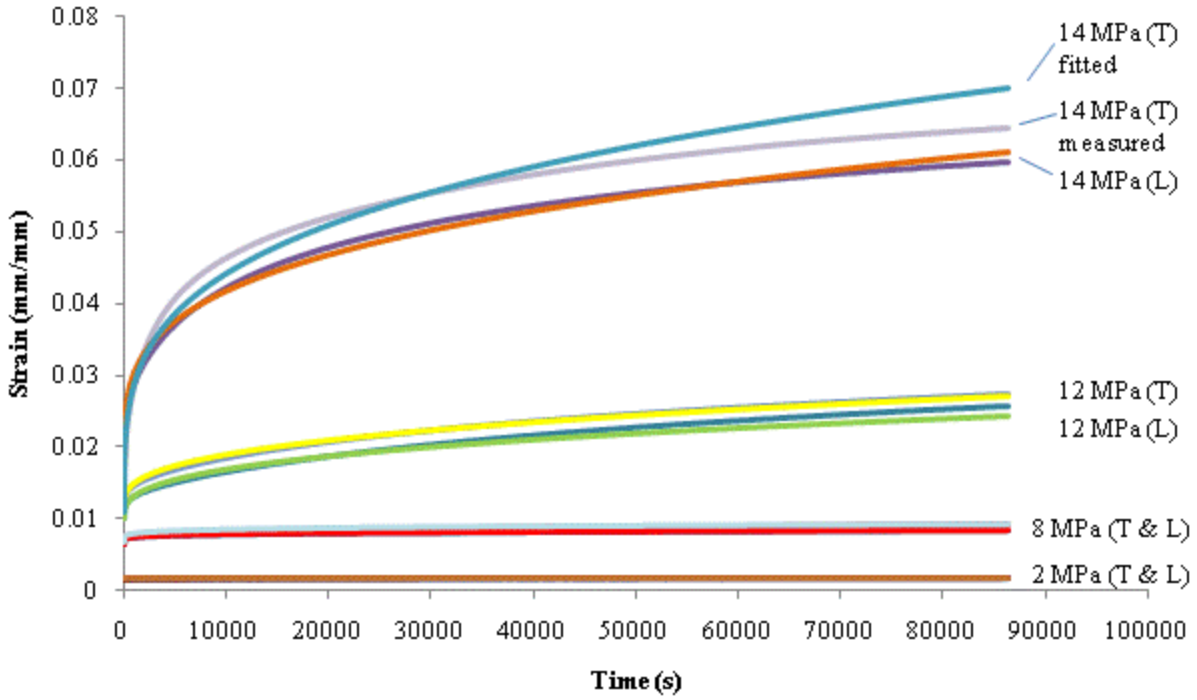

Figure 3.18 - Measured data and fitted viscoplastic curves for all 24-hour creep tests on film C1

The viscoplastic models for C1 generally fit the data quite well, but divergence is still evident from the 14 MPa results.

3.2.2.1.4 Film C2 24 Hour Viscoplastic Models

Figure 3.19 shows the fitted viscoplastic models for strain along with the measured strain data for film C2 tested at all stresses.

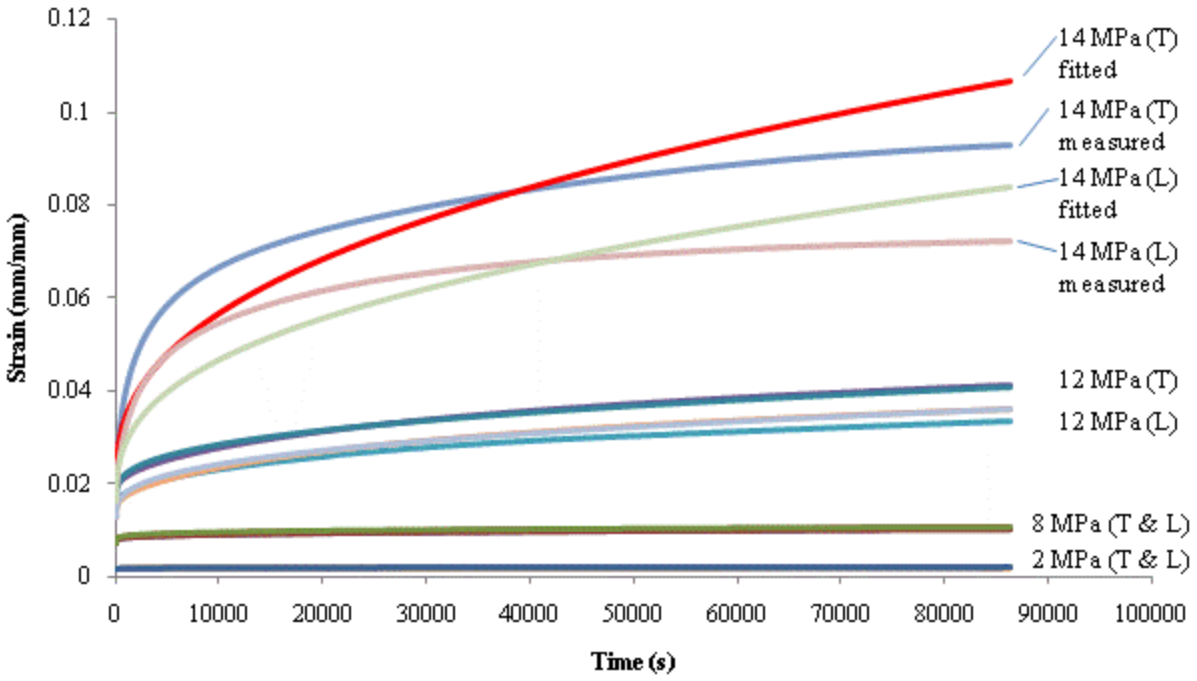

Figure 3.19 - Measured data and fitted viscoplastic curves for all 24-hour creep tests on film C2

The viscoplastic models represent the C2 data well at the lower stresses, but at 14 MPa the modeled curves are higher than the measured ones.

3.2.2.1.5 2 MPa 24 Hour Viscoplastic Models

3.2.2.1.6 Summary of Numerical Parameters for 24 Hour Viscoplastic Models

Tables 3.9 – 3.16 present the numerical parameters determined for the viscoplastic models shown in Figures 3.16 – 3.19. They are presented in order of brand, then direction.

Table 3.9 - Viscoplastic modeling parameters for 24 hour test on film A in the longitudinal direction

Stress	E_0	C_0	C_1
2	1,698.63	2.25E-06	0.348
8	1,308.62	1.75E-05	0.251
12	1,171.11	3.48E-05	0.326
14	1,148.17	5.92E-05	0.353

Table 3.10 - Viscoplastic modeling parameters for 24 hour test on film A in the transverse direction

Stress	E_0	C_0	C_1
2	1,417.14	2.97E-05	0.139
8	1,227.72	4.48E-06	0.384
12	1,168.89	3.81E-05	0.346
14	1,115.68	7.83E-05	0.336

Table 3.11 - Viscoplastic modeling parameters for 24 hour test on film B in the longitudinal direction

Stress	E_0	C_0	C_1
2	1,600.00	7.06E-06	0.268
8	1,181.10	2.66E-05	0.300
12	916.26	1.64E-04	0.296
14	500.28	5.78E-04	0.193

Table 3.12 - Viscoplastic modeling parameters for 24 hour test on film B in the transverse direction

Stress	E_0	C_0	C_1
2	976.38	9.05E-06	0.2518
8	1,017.81	1.43E-05	0.3653
12	986.95	2.54E-04	0.2949
14	707.30	1.88E-03	0.1365

Table 3.13 - Viscoplastic modeling parameters for 24 hour test on film C1 in the longitudinal direction

Stress	E_0	C_0	C_1
2	1,265.31	4.41E-06	0.263
8	1,223.24	4.37E-05	0.150
12	1,200.00	2.48E-05	0.341
14	802.55	1.45E-04	0.270

Table 3.14 - Viscoplastic modeling parameters for 24 hour test on film C1 in the transverse direction

Stress	E_0	C_0	C_1
2	1,252.53	1.25E-05	0.171
8	1,162.95	4.40E-05	0.164
12	1,011.56	2.35E-05	0.351
14	1,296.62	2.05E-04	0.266

Table 3.15 - Viscoplastic modeling parameters for 24 hour test on film C2 in the longitudinal direction

Stress	E_0	C_0	C_1
2	1,221.67	7.03E-06	0.253
8	1,046.41	1.43E-05	0.268
12	929.89	4.50E-05	0.330
14	854.79	7.25E-05	0.369

Table 3.16 - Viscoplastic modeling parameters for 24 hour test on film C2 in the transverse direction

Stress	E_0	C_0	C_1
2	1,158.88	9.94E-06	0.235
8	1,107.14	5.70E-05	0.173
12	709.19	4.08E-05	0.341
14	677.94	6.40E-05	0.402

3.2.2.1.7 Seven Day Viscoplastic Models

The methods for developing the viscoplastic models for the seven day test results are essentially the same as those used to develop the viscoelastic seven day models. The first method was to develop the model based on the first 24 hours of data, then to extend the curve for the full seven day period. The results of this modeling method are shown in Figure 3.20 and Figure 3.21.

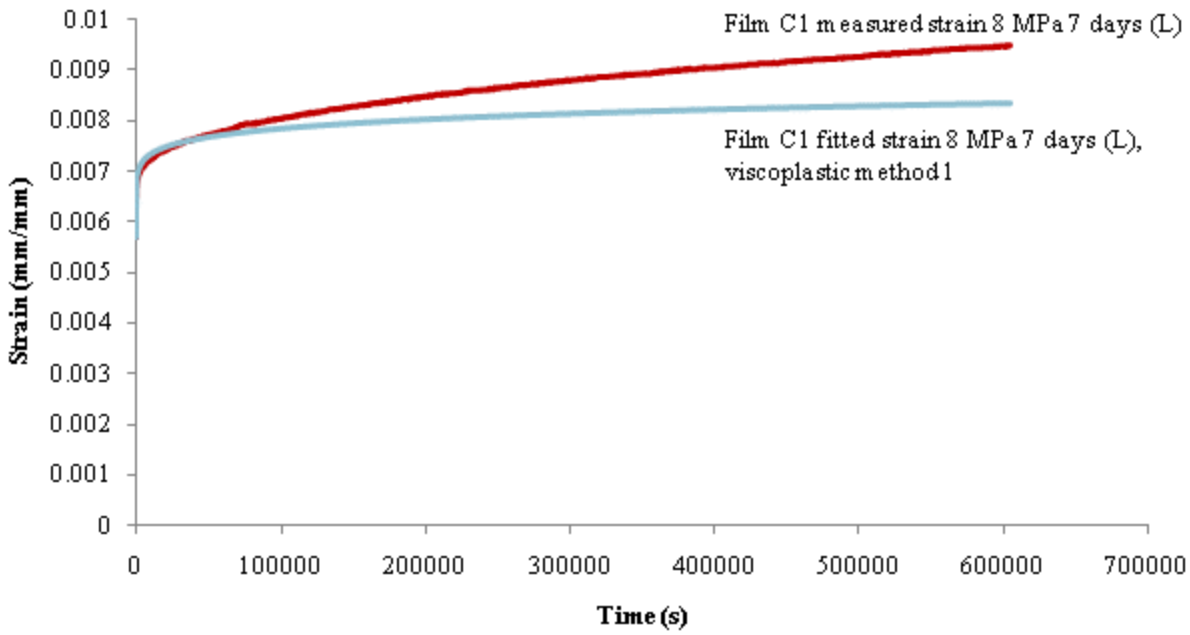

Figure 3.20 - Fitted viscoplastic model for C1 tested at 8 MPa in the longitudinal direction for 7 days, based on first 24 hours of data

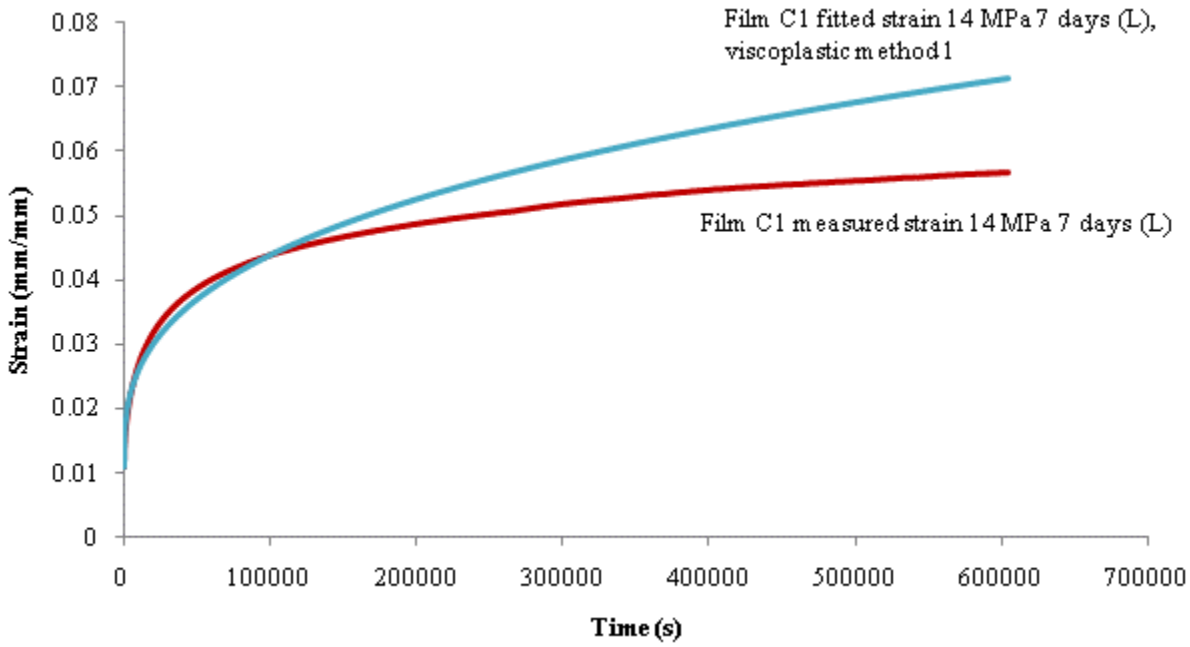

Figure 3.21 - Fitted viscoplastic model for C1 tested at 14 MPa in the longitudinal direction for 7 days, based on first 24 hours of data

For the 8 MPa test, this method provides a drastic underestimation of the seven day strain, however for the 14 MPa test, this method greatly overestimates the seven day strain.

The second method was again to take the fitted curve for the first 24 hours of data, then to find the slope of the curve at 24 hours and create a straight line with that slope for the remainder of the seven days. This method resulted in the following curves in Figure 3.22 and Figure 3.23.

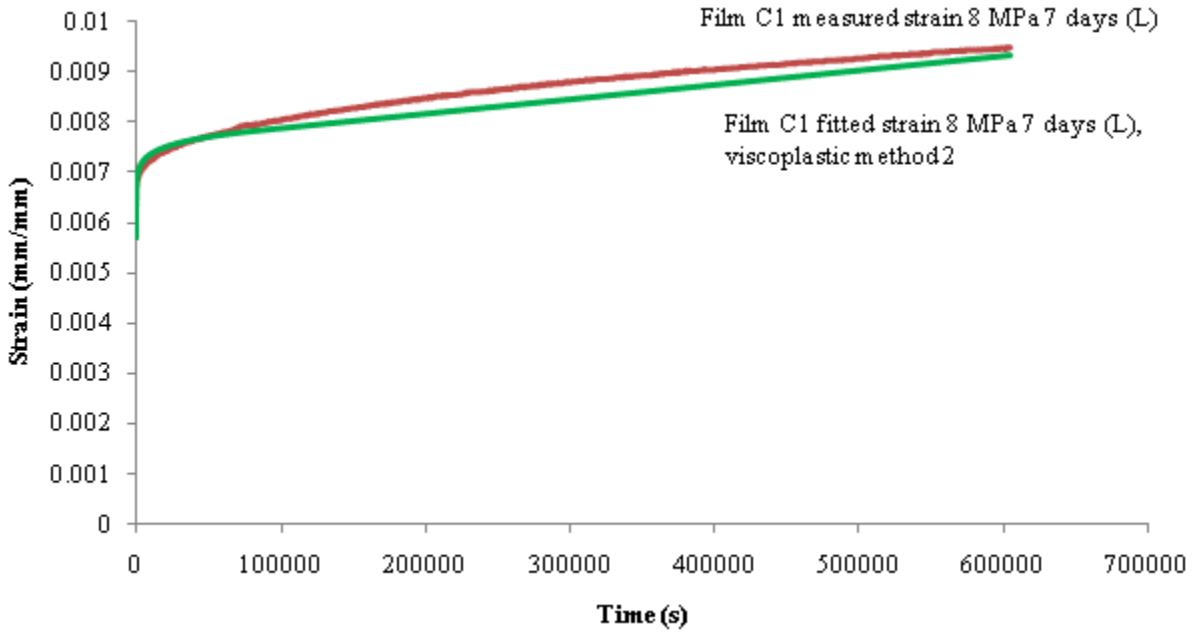

Figure 3.22 - Fitted viscoplastic/linear model for C1 tested at 8 MPa in the longitudinal direction for 7 days, based on first 24 hours of data and a straight line

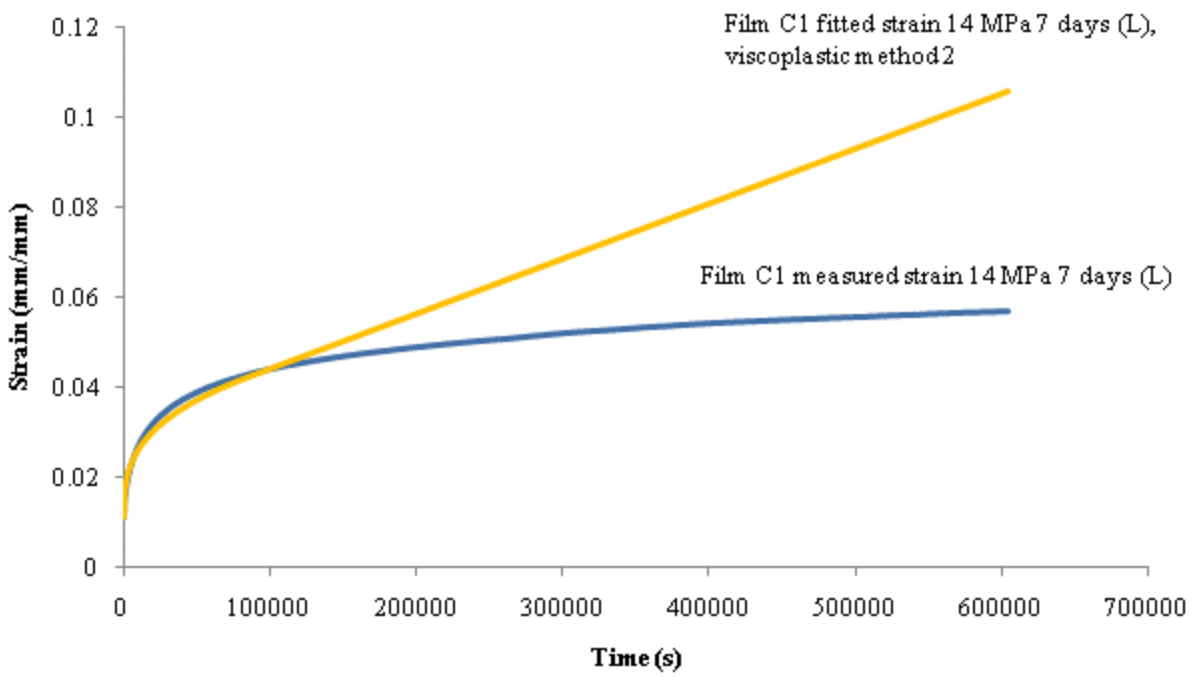

Figure 3.23 - Fitted viscoplastic/linear model for C1 tested at 14 MPa in the longitudinal direction for 7 days, based on first 24 hours of data and a straight line

Again, for the 8 MPa test, this model underestimates the seven day strain, but it is increasing at a greater rate than the actual strain, so if the data were to continue on for a short additional time interval the lines would likely cross, and the model would overestimate the strain from that point onwards. The 14 MPa model once again greatly overestimates the seven day strain.

The third method was to create the viscoplastic model based on the full seven days of data. The procedure was identical to that described in section 3.2.2. The corresponding fitted curves are shown in Figure 3.24 and Figure 3.25.

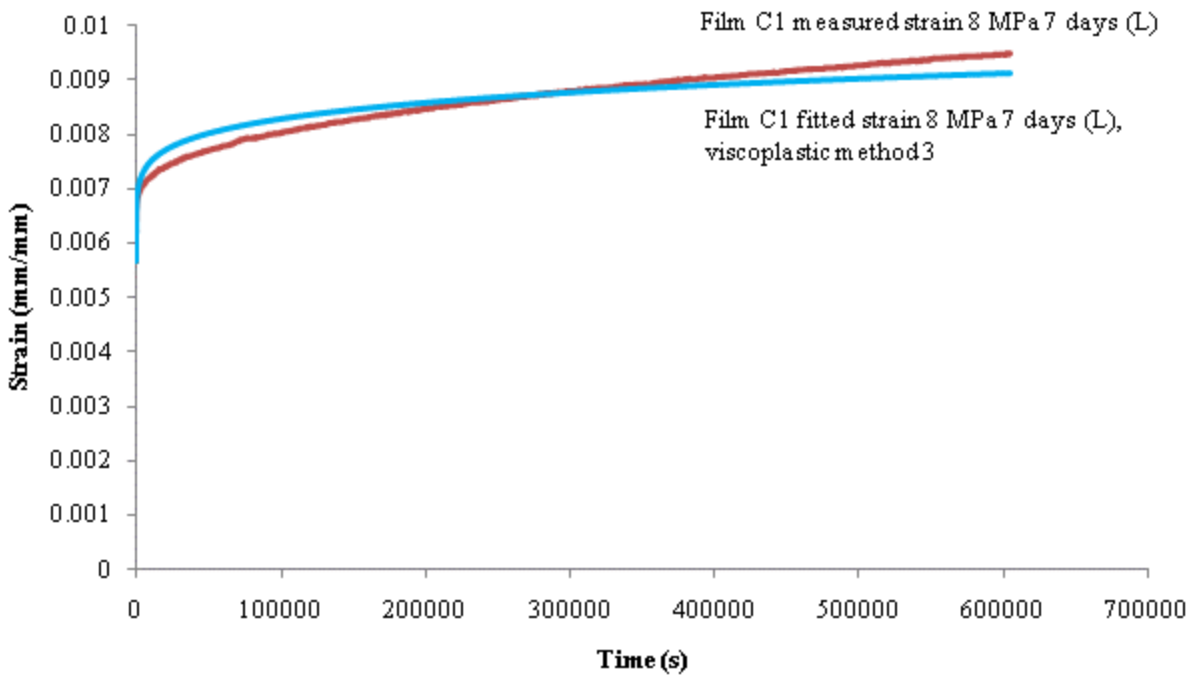

Figure 3.24 - Fitted viscoplastic model for C1 tested at 8 MPa in the longitudinal direction for 7 days, based on full 7 days of data

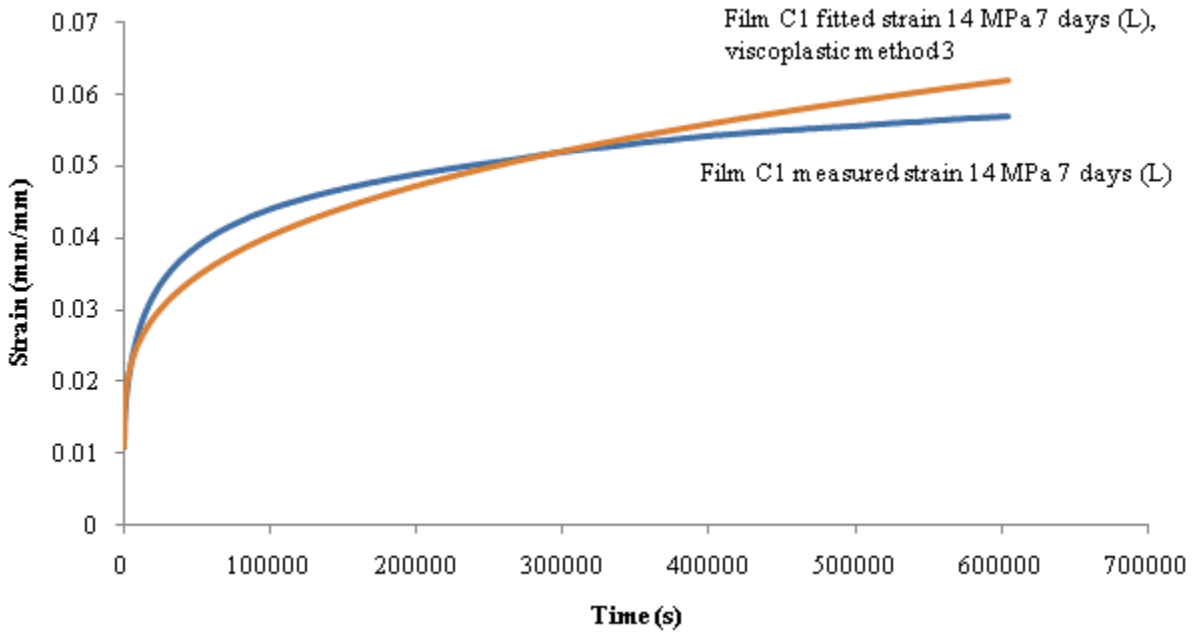

Figure 3.25 - Fitted viscoplastic model for C1 tested at 14 MPa in the longitudinal direction for 7 days, based on full 7 days of data

For the 8 MPa and the 14 MPa data, the fitted curve deviates from the measured results in a similar manner to the other viscoplastic models developed for the 24 hour data sets.

The applicability of these three modeling techniques will also be discussed further in section 3.3.

3.3 Discussion of models

While the viscoelastic models generally provide good fits to the data at all stress levels, the viscoplastic models provide good fits at low stress levels, but tend to deviate from the measured strain at higher stress levels. For the data corresponding to higher stress levels, the relationship between lnt and $\ln(\varepsilon(t)/\sigma_c - 1/E_0)$ was often highly nonlinear, so fitting the linear relationship in Equation (3-10) to the data resulted in a poor fit. For example, film A, tested in the transverse direction at 14 MPa resulted in the relationship between lnt and $\ln(\varepsilon(t)/\sigma_c - 1/E_0)$ shown in Figure 3.26.

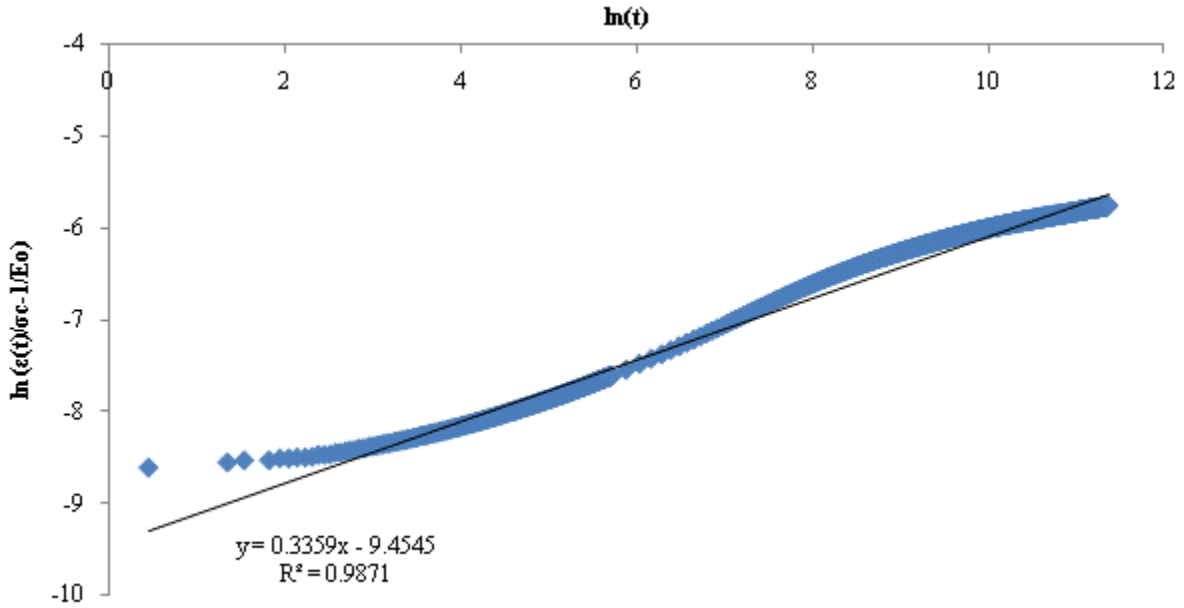

Figure 3.26 - Relationship between ln(t) and ln(ε/σ-1/Eo) for film A transverse 14 MPa creep test

Perhaps a better method for fitting the data to a viscoplastic model would be to divide the above curve into approximately linear segments, and fit a different linear relationship to each segment, or to create the model using nonlinear least squares fitting. In general, though, the viscoelastic models provide a much better fit to the creep data in this time scale, so that is the recommended modelling technique.

Of the three viscoelastic modeling techniques for the seven day creep curves, only the third method, using relaxation times that cover the full seven days of testing, provided a close fit to the data. Extending the 24 hour creep curves, whether it is by using the 24 hour equation for the full seven day period or developing a linear relationship extending from 24 hours to seven days, does not give a good estimation of the seven day behaviour. Method 1 can

either overestimate or underestimate the seven day strain, so it provides inconsistent results. Therefore, viscoelastic models based on 24 hours of creep data do not provide accurate predictions of long term creep behaviour. Models developed based on relaxation times covering the full range of time over which creep is to be predicted provide very close fits, but are not practical, as they require creep tests to be performed for the full time scale of prediction, which could be a very long time, in the range of years. Similarly, of the three viscoplastic modeling methods, only the third method provides a close estimate of the 24 hour strain data. However, as is the case for viscoelastic modeling, a viscoplastic model using the full time range to predict creep is not practical. It is desirable to have a model which is developed based on short-term creep tests, but which can accurately predict long-term creep behaviour. This should be the focus of future creep research on ETFE.

The rate of creep of the specimens slowed considerably by seven days, and would likely continue to slow beyond that, possibly reaching a constant value at some point in time. ETFE therefore appears to have a predominantly viscoelastic response, indicating that a viscoelastic constitutive equation is the best approach to modeling. Longer-term tests would be required to determine the length of time it takes for the creep to slow to a point where it could be considered approximately constant. This would indicate the optimal length of tests for developing accurate models.

Chapter 4 Conclusions

Twenty-four-hour creep tests were performed on three brands of ETFE. Two of the brands, A and B, were 50 μm thick, and the third brand C, had two thicknesses, C1, which was 150 μm thick and C2, which was 300 μm thick. All films were tested at four stress levels, 2, 8, 12 and 14 MPa, and in both the longitudinal and transverse directions of the material. Seven-day creep tests were also performed on the longitudinal direction of film C1, at 2 MPa, 12 MPa and 14 MPa. The seven-day tests were primarily done to determine how accurately the results of 24-hour tests can predict longer-term creep.

It is evident from the 24-hour creep test results that ETFE films do exhibit short term creep under levels of stress expected in structural applications. It is also evident that the amount of creep exhibited by the foils increases with stress level. At 2 MPa, very little creep strain, in the range of several hundredths of a percent, occurs in 24 hours. However, at 14 MPa, 24 hour creep strains reach values of several percent, an increase of over 100 times for only seven times the stress.

Differences were noted between the responses of films tested in the longitudinal direction and the transverse directions. In general, films tested in the transverse direction exhibited more creep strain. They also exhibited more strain initially upon loading, and therefore exhibited more total strain in 24 hours. Anisotropic mechanical behaviour of ETFE films has also been observed by other researchers. Possible reasons for this relate to the extrusion process of the films or to the molecular structure of ETFE.

The different brands of film also showed differences in creep behaviour. Films A and C were extruded from the same resin, and intended for structural applications, and as a result behaved very similarly. Films A and C1 experienced approximately the same levels of creep strain for the same stress levels, while film C2 experienced slightly higher strain, but had creep curves that were of the same shape as those belonging to films A and C1. Film B, a general purpose film, generally exhibited higher levels of creep, and had creep curves which increased at a greater rate in the 24 hour test period than the curves of the other films.

Films C1 and C2 were extruded from the same resin by the same manufacturer, and were therefore identical in everything but thickness. Film C2, the thicker film, always experienced higher levels of creep strain than film C1. This could be because the reduction in cross-section was more pronounced for the thicker film, making the increase in applied stress greater. This would lead to greater strains. It is possible that, for the same instantaneous stress levels, both films exhibited the same true strain, but since original applied stress and engineering strain were measured, the response of the films appears different.

Temperature effects were also observed during the seven-day 2 MPa creep test on film C1, when the heater regulating the temperature of the test chamber failed, causing fluctuations in temperature over the course of the test. Instead of the strain increasing continually with time, the strain instead increased and decreased as the temperature

rose and fell, meaning that the effect of the temperature fluctuations had a greater impact on creep than the stress did at this low stress level.

Constitutive models were developed to represent the observed creep behaviour. Nonlinear viscoelastic and viscoplastic models were developed for each creep test. For the 24 hour tests the viscoelastic models provided a very close representation of the data in all cases. The viscoplastic models provided a good representation at low stress levels, but often deviated from the results at the higher stress levels. For the seven day tests three modeling techniques were used: developing a model based on only the first 24 hours of data, and extending it to cover the full seven days, developing a model based on the first 24 hours, then using a linear relationship to model the remainder of the seven days, and developing a model based on the full seven days of data. In both the viscoelastic and viscoplastic cases, the first and second modeling techniques failed to provide an accurate representation of the seven day strain. The third technique provided a close fit to the full seven days of strain. This indicates that the models that have been developed based on the 24 hour creep data are not applicable for predicting long term strain. The third technique provides a good estimation, but requires experimental creep data for the full length of time for which the prediction is to be made, and this is impractical for long time scales. However, the seven-day data shows that the creep of ETFE follows more closely a viscoelastic model than a viscoplastic model, with strain slowing and possibly approaching an asymptote after a period of time. Viscoelastic models are therefore the most appropriate choice for representing creep behaviour of ETFE

Tensile tests were also done on the ETFE film. In general, the films yielded and failed at higher stresses in the longitudinal direction than the transverse direction, but were more ductile in the transverse direction. Average yield stresses for all the films ranged from 24 to 29 MPa, and average failure stresses ranged from 42 to 70 MPa. The results were close to those provided by the manufacturers.

Chapter 5 Recommendations

Based on the findings of this thesis the following steps are recommended for future work. They are organized by those related to testing and those related to modeling.

Testing:

- Based on the results of the seven-day 2 MPa test where the temperature fluctuated unintentionally, the strain of ETFE foils is highly sensitive to variations in temperature. Past research in temperature effects has mainly focussed on performing each test at a different, but constant temperature. Future research should include constant load tests done at fluctuating temperatures, similar to what would be experienced by ETFE cushions used in outdoor applications.
- More research should be done on the effects of very low temperatures on the mechanical behaviour of ETFE films, so that applications can extend to new colder areas, such as Canada and Northern Europe.
- More long-term creep tests should be done, such as 1000 hour tests, as recommended by ASTM D2990. These will provide a better indication of whether strain approaches a constant value after a period of time.

Modeling:

- The findings of the creep tests, particularly the 24 hour viscoelastic models, should be input into a finite element program used for designing ETFE cushions so that short-term creep behaviour can be taken into account in design.
- A model should be developed based on short term data which can accurately predict the long term creep behaviour of ETFE film. A viscoelastic model appears to be the best choice for this. This model should be implemented into a finite element program so that long-term creep can be accounted for in initial design.
- A model should be developed using nonlinear regression to estimate all the parameters including the relaxation times, as per Cheng et al. (2010). This would allow for different time scales to be considered using the same basic modeling technique, and could possibly assist in developing a model to accurately predict long-term behaviour.

References

Ahmad, J., Emery, A. F., Krishnaswamy, P., & Tuttle, M. E. (1992). Finite Element Modeling of the Time – Dependent Behavior of Nonlinear Ductile Polymers. *Polymer Engineering and Science, 32(16)*, 1086-1096.

All Weather Windows (n.d.). *Glass Performance.* Retrieved from http://www.allweatherwindows.com/area/corporate/prodguide/glass_terms.php

Ansell, M.P. (1985). *Acceptability of ET HOSTAFLON Film for Use in Buildings, Report of a Test Programme carried out for Buro Happold Consulting Engineers*. Bath: University of Bath. Cited in Moritz, K. (2007b). *ETFE-Folie als Tragelement* (Doctoral dissertation). Technische Universität München, Munich, Germany.

Architekten Landrel (n.d.). *ETFE Foil: A Guide to Design*. Retrieved from http://www.ribaproductselector.com/Docs/5/00435/external/COL1400435.pdf?ac

Arup. (n.d.a). *Eden Project Cornwall*. Retrieved from http://www.arup.com/unitedkingdom/project.cfm?pageid=187

Arup. (n.d.b). '*The Water Cube', National Aquatics Center, Beijing*. Retrieved from http://www.arup.com/china/project.cfm?pageid=11270

ASM International (2003). *Characterization and Failure Analysis of Plastics.* Materials Park: ASM International.

Barthel, R., Burger, N., & Saxe, K. (2003). Roof Structures with ETFE Foil. *Deutsche Bauzeitschrift, 4*, 72-75

Bobovitch, A., Gutman, E., Mogilansky, D. & Unigovski, Y. (2011). The creep behaviour of linear low-density polyethylene. *Society of Plastics Engineers Plastics Research Online*. doi: 10.1002/spepro.003571

Bögle, A. & Hartz, C. (2008). *Entwicklung beweglicher Strukturen für wandelbare Nutzungsmöglichkeiten von Sport- und Freizeitbädern*. Berlin: Technische Universität Berlin.

Borgart, A. (2007). Mechanical Behaviour of Multi Layered Air Inflated Cushions. In *International Conference on Textile Composites and Inflatable Structures: Structural Membranes, 2007* (pp. 340-343). Barcelona, Spain: CIMNE.

Broughton, T. (2004). Australian engineers SKM takes over Anthony Hunt. *Building*. Retrieved from http://www.building.co.uk/story.asp?storyCode=3036888

Buitink Technology (n.d.). *Examples of detailing of ETFE*. Retrieved from http://www.buitink-technology.com/co.uk/page.asp?menu_id=864

Campbell, D.M. (2010, January/February). BC Place Stadium Revitalization. *Construction Business*, 14-15.

Chawla, K.K. & Meyers, M.A. (1999). *Mechanical Behaviour of Materials.* Upper Saddle River: Prentice Hall.

Cheng, J. (2008). *Mechanical and Chemical Properties of High DensityPolyethylene: Effects of Microstructure on Creep Characteristics* (Doctoral dissertation). University of Waterloo, Waterloo, Ontario.

Cheng, J., Penlidis, A & Polak, M.A., (2010). An Alternative Approach to Estimating Parameters in Creep Models of High-Density Polyethylene. *Polymer Engineering and Science.* doi: 10.1002/pen

Cripps, A., Kolokotroni, M., Robinson-Gayle, S., & Tanno, S. (2001). ETFE foil cushions in roofs and atria. *Construction and Building Materials,* 15. 323-327.

Cygniak, K. (2011). BC Place Opened in 1983 – A New Beginning Coming September 30, 2011. *BuyRIC.com.* Retrieved from http://www.buyric.com/projects/2011/02/bc-place-opened-1983-new-beginning-coming-september-30-2011-004/

De Vries, J.W.J. (2003) *Tensile Foil – ETFE-Foil as Membrane Construction Material* (Master's thesis). Delft University of Technology, Delft, Netherlands.

Drobny, J.G. (2001). Blends and Composites Based on Fluoropolymers. *Macromolecular Symposium 170*. 149-156.

DuPont. (n.d.). *DuPont Tefzel Properties Handbook.* Wilmington, Delaware.

Dyneon. (2003). *Dyneon Fluorothermoplastics ET 6235.* Oakdale, Minnesota.

Ebnesajjad, S. & Khaladkar, P.R. (2005). *Fluoropolymers Applications in Chemical Processing Industries: The Definitive User's Guide and Databook*. Norwich: William Andrew, Inc.

ETFE General Properties. *Polymers: A Property Database*. Retrieved from http://www.polymersdatabase.com

Flugge, W. (1967). *Viscoelasticity*. Waltham, Massachusetts: Blaisdell.

Foster + Partners. (n.d.). *Khan Shatyry Entertainment Centre, Astana, Kazakhstan*. Retrieved from http://www.fosterandpartners.com/Projects/1438/Default.aspx

Fried, J.R. (1995). *Polmer Science and Technology.* Englewood Cliffs: Prentice Hall.

Glass Association of North America. (2008). Approximate Weight of Architectural Flat Glass. Retrieved from http://www.glasswebsite.com

Galliot, C. & Luchsinger, R.H. (2010). Biaxial testing of architectural membranes and foils. *TensiNet Symposium SOFIA 2010 – Tensile Architecture: Connecting Past and Future*. Sofia, Bulgaria: TensiNet.

Hadley, D.W. & Ward, I.M. (1993). *An Introduction to the Mechanical Properties of Solid Polymers.* West Sussex: John Wiley & Sons Ltd.

Hafner, A. & Moritz, K. (2010). Transparency Carried by Air – Pneumatic ETFE-Foil-Cushion Technology. *Structures Congress 2010*. Orlando, Florida: American Society of Civil Engineers.

Hinz, S., Schiemann, L., & Stephani, M. (2009). Tests of ETFE-foils under biaxial stresses. In: Kröplin B, Oñate E, editors. International *Conference on Textile Composites and Inflatable Structures, Structural Membranes 2009*. Barcelona: CIMNE.

Huntington, C.G. (2004). *The Tensioned Fabric Roof.* Reston: American Society of Civil Engineers.

Kennet, S. (2004, September). Clear Thinking. *Building Services Journal*. Retrieved from http://www.vector-foiltec.com/press/downloads/CIBSE%20Journal%20-%20Kingsdale.pdf

Koch, Klaus-Michael (2004). *Membrane Structures*. Munich: Prestel Verlag.

LeCuyer, A. (2008). *ETFE: Technology and Design*. Basel: Birkhauser Verlag AG.

Lehnert, S. & Schween, T. (2006). Bauen mit Folienkissen. *Bauingenieur* (5). 285-288.

Leonhardt, Andrä und Partner. (n.d.). *CityQuartier DomAquarée*. Retrieved from http://www.lap-consult.com/english/e_projekt.php?sp=00057&kat=_11

Lewis, W.J. (2003). *Tension structures: Form and behaviour*. London: Thomas Telford Publishing.

Liu, H. (2007). *Material Modelling for Structural Analysis of Polyethylene* (Master's thesis). University of

Waterloo, Waterloo, Ontario.

Liu, J.M., Mu, T., Wu, M.E. (2008). Cycle Loading and Creep Tests of ETFE Foil. *Journal of Building Materials, 11*(6). 690-694.

Lockett, F.J. (1972). *Nonlinear Viscoelastic Solids*. London: Academic Press.

Moritz, K. (2007a). Bauweisen der ETFE-Foliensysteme. *Stalbau 76 (5),* 336-342.

Moritz, K. (2007b). *ETFE-Folie als Tragelement* (Doctoral dissertation). Technische Universität München, Munich, Germany.

Otto, F. (1967). *Tensile Structures, Volume One: Pneumatic Structures*. Cambridge: The M.I.T. Press.

PCL. (n.d.). *BC Place Roof – Phase 2*. Retrieved from http://www.pcl.com/projects/Active/2200906/index.aspx

Roland, C. (1970). *Frei Otto: Tension Structures*. New York: Praeger Publications, Inc.

Schmid, G. (2009). Neues Bauen mit ETFE-Folien. *AB Archiv des Badewesens 5*, 245-256.

Schöne, L. (2007). Bauen mit ETFE-Folien – Ein Praxisbericht. *Stalbau 76 (5),* 305-313.

Seidel, M. (2009). *Tensile Surface Structures: A Practical Guide to Cable and Membrane Construction*. Berlin: Ernst & Sohn.

SKM. (2009). *Eden Project, St. Austell, Cornwall UK*. Retrieved from http://www.skmconsulting.com/Markets/buildings/Eden_Project_St_Austell_Cornwall_Europe.htm

Tanno, S. (1997). ETFE Cushions as an Alternative to Glass for Atriums and Rooflights. *The International Conference on Building Envelope Systems and Technologies '97*. Bath, UK: Centre for Window and Cladding Technology.

Vector Foiltec. (2011a). *Domaquarée*. Retrieved from http://www.vector-foiltec.com/projects/structure/steelcs.php?recordID=2

Vector Foiltec. (2011b). *Eden Project*. Retrieved from http://www.vector-foiltec.com/projects/location/ukcs.php?recordID=1

Vector Foiltec. (2011c). *Fire*. Retrieved from http://www.vector-foiltec.com/cms/gb/technical/fire.php

Vector Foiltec. (2011d). *Kingsdale School*. Retrieved from http://www.vector-foiltec.com/projects/location/ukcs.php?recordID=4

Vector Foiltec. (2011e). *Khan Shatyry Entertainment Centre*. Retrieved from http://www.vector-foiltec.com/projects/chronological/2009cs.php?recordID=127

Vector Foiltec. (2011f). *National Aquatics Centre*. Retrieved from http://www.vector-foiltec.com/projects/texlonfoil/texloncolouredcs.php?recordID=7

Vector Foiltec (2011g). *Variable Skins*. Retrieved from http://www.vector-foiltec.com/cms/gb/technical/variableskins.php

Wagner, R. (2007).Basics in Inflated Cushions. In *International Conference on Textile Composites and Inflatable Structures: Structural Membranes, 2007* (pp. 19-24). Barcelona, Spain: CIMNE.

Winkler, J. (2009). *Kriechverhalten von ETFE-Folien im konstruktiven Ingenieurbau* (Master's thesis). Technische Universität Berlin, Berlin, Germany.

Appendix A – Individual Creep Curves for Film A

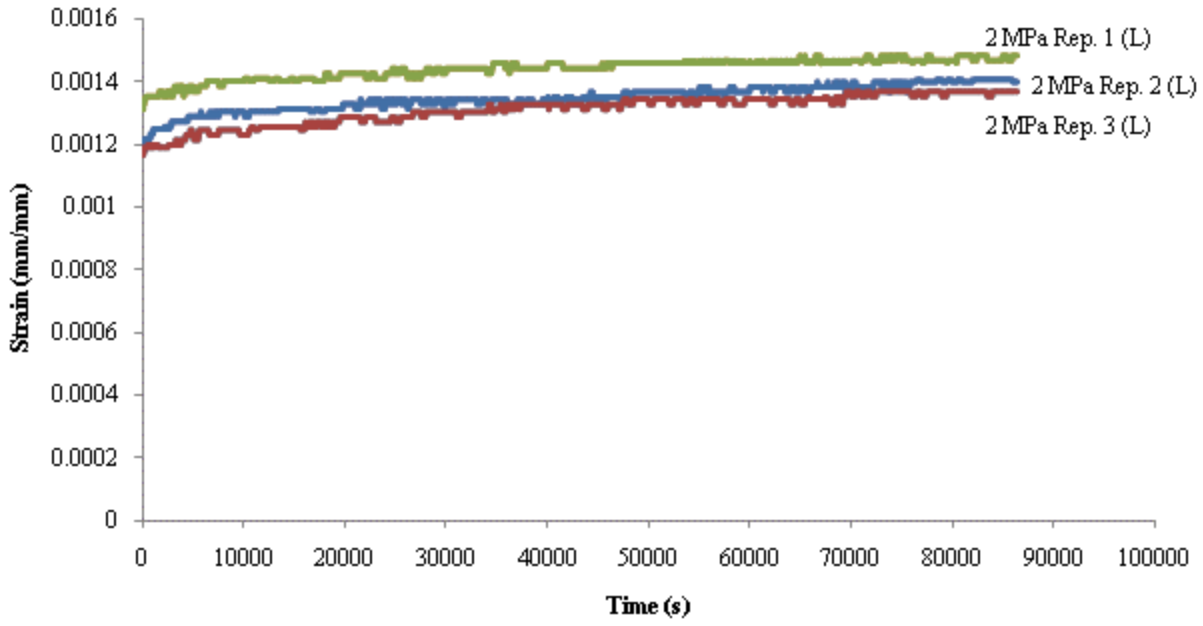

Figure A. 1 - Strain vs. time for film A subjected to 2 MPa in the longitudinal direction for 24 hours

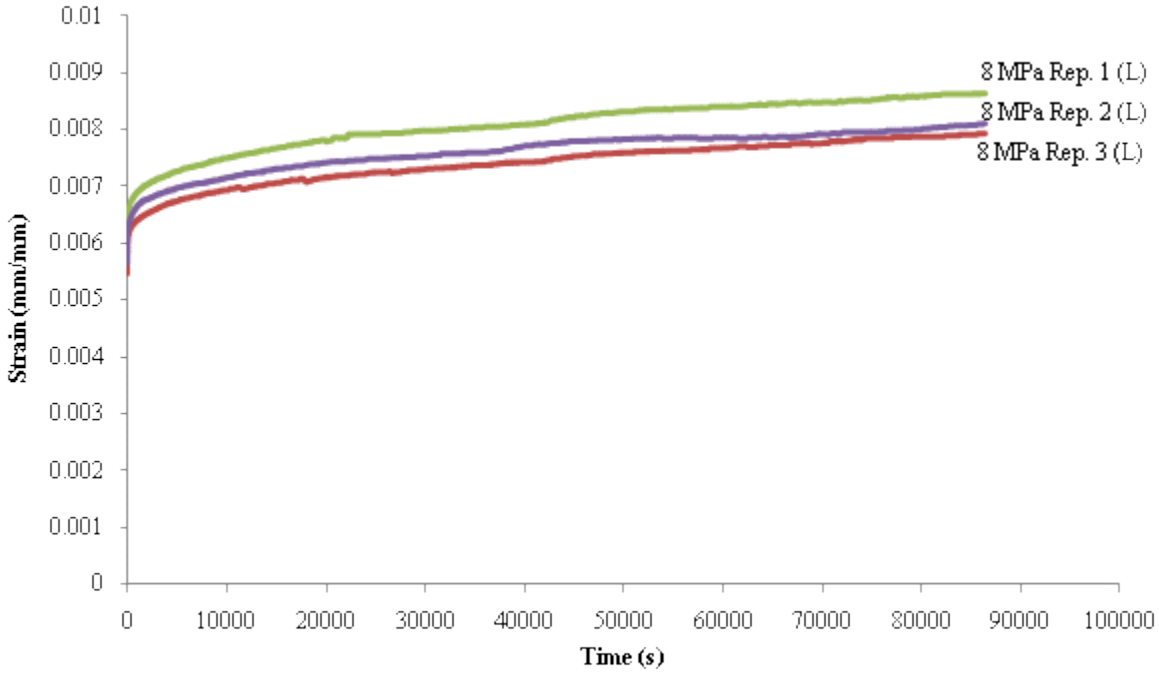

Figure A. 2 - Strain vs. time for film A subjected to 8 MPa in the longitudinal direction for 24 hours

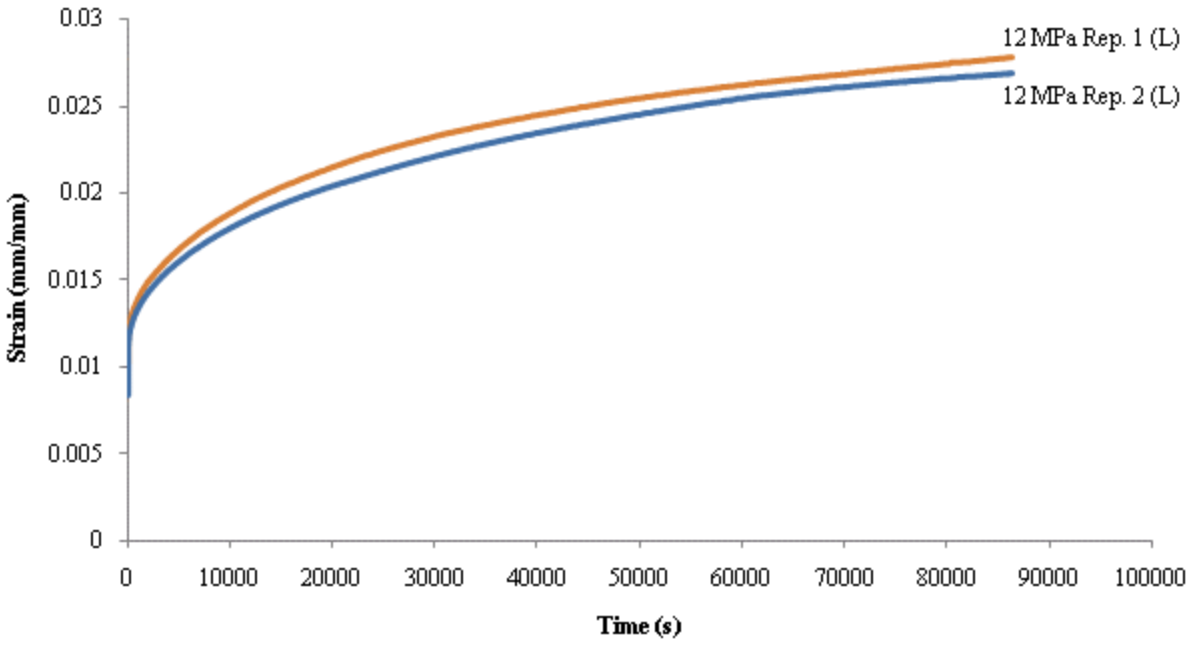

Figure A. 3 - Strain vs. time for film A subjected to 12 MPa in the longitudinal direction for 24 hours

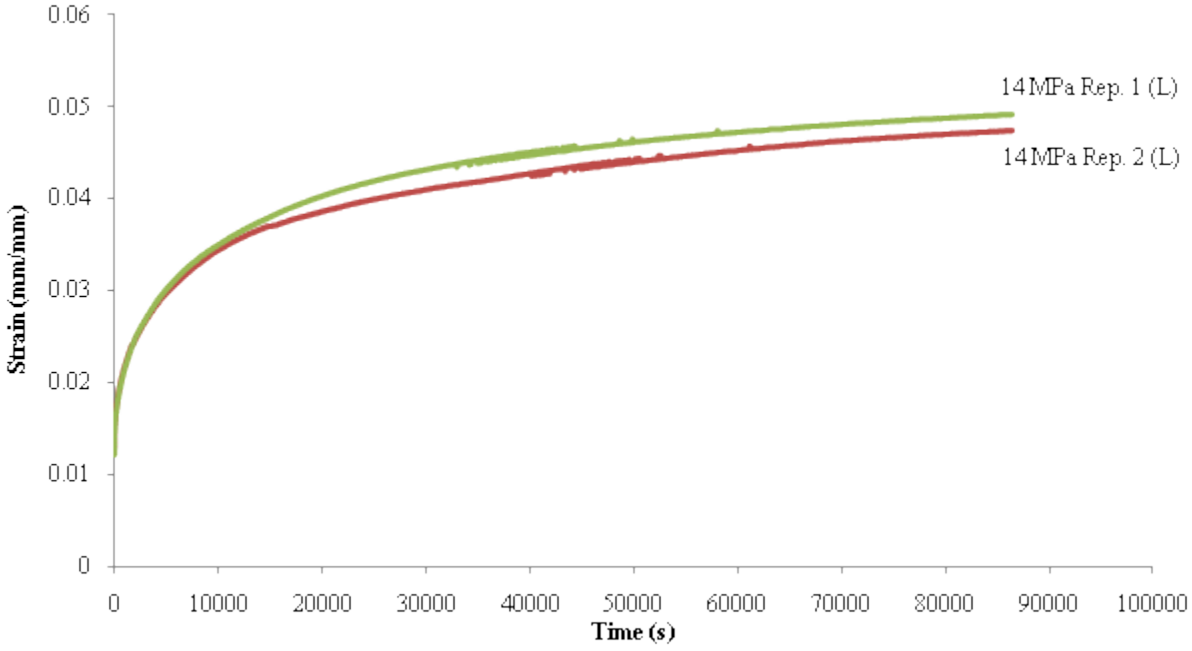

Figure A. 4 - Strain vs. time for film A subjected to 14 MPa in the longitudinal direction for 24 hours

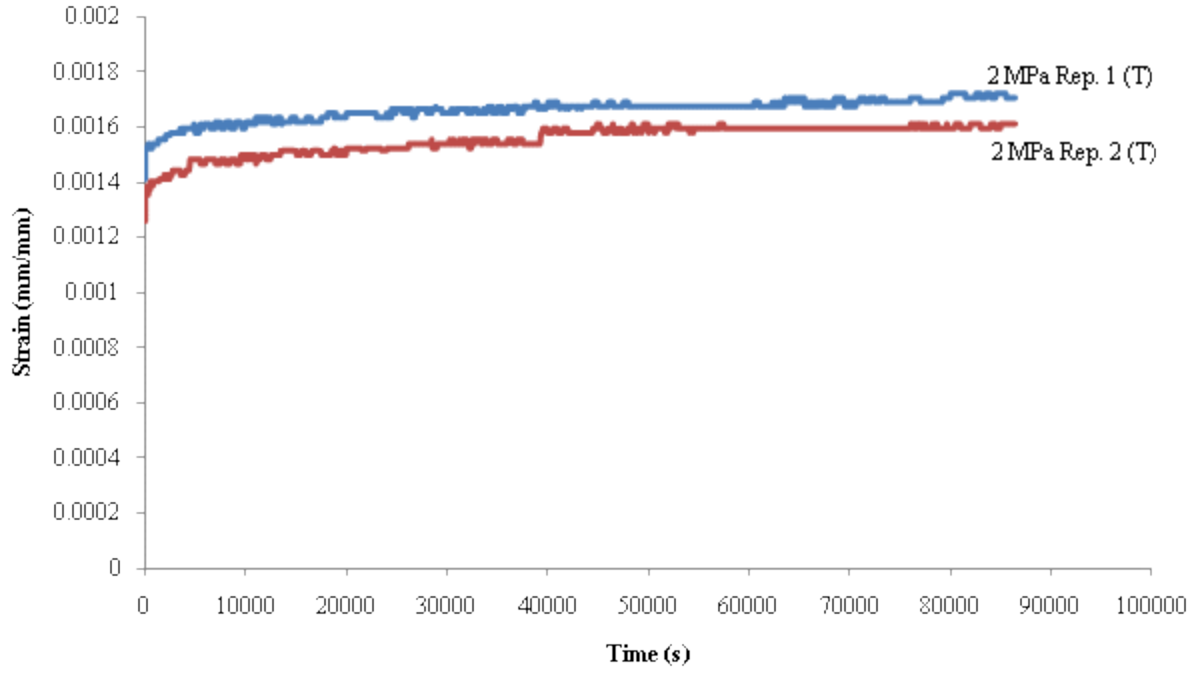

Figure A. 5 - Strain vs. time for film A subjected to 2 MPa in the transverse direction for 24 hours

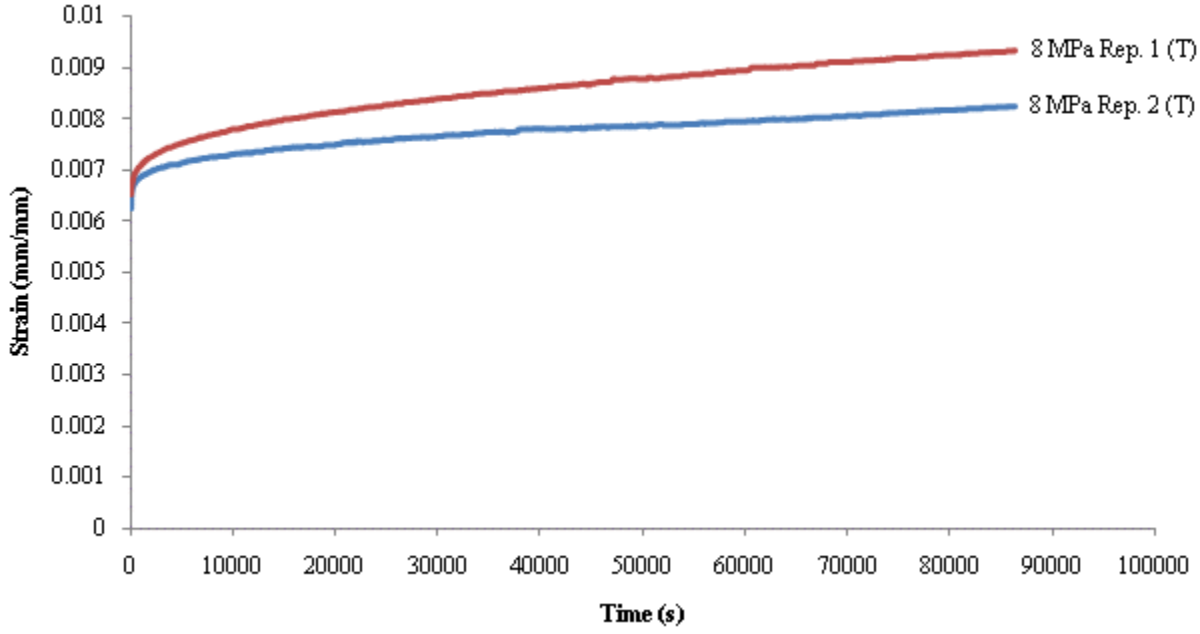

Figure A. 6 - Strain vs. time for film A subjected to 8 MPa in the transverse direction for 24 hours

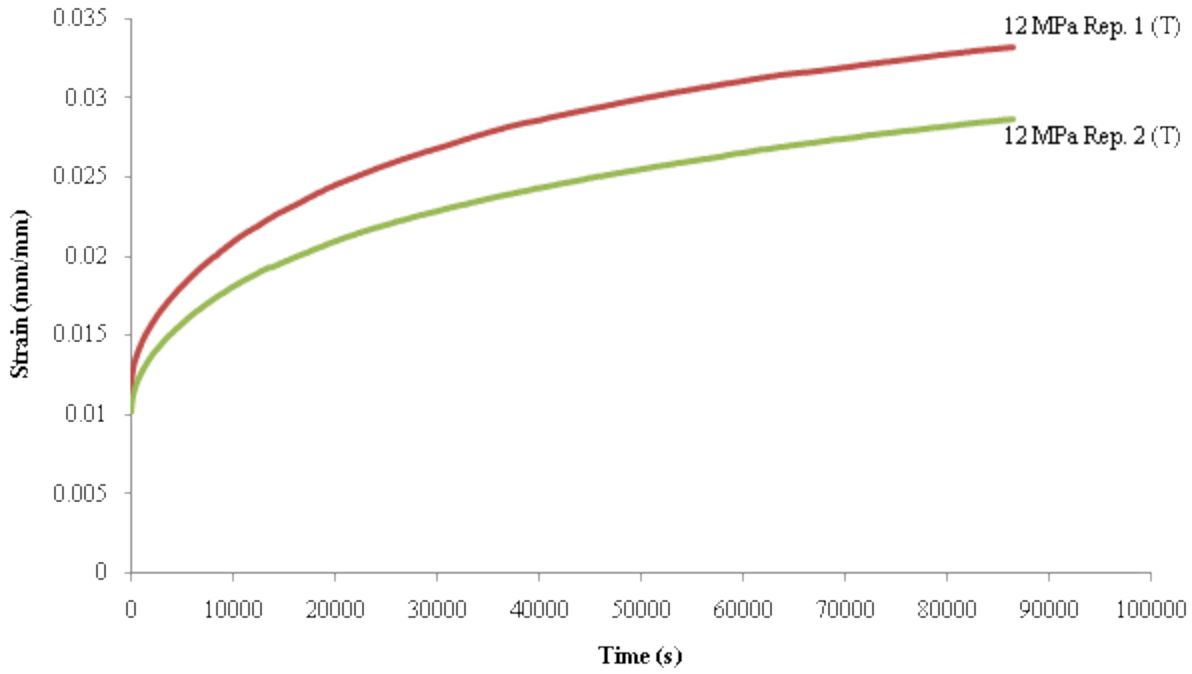

Figure A. 7 - Strain vs. time for film A subjected to 12 MPa in the transverse direction for 24 hours

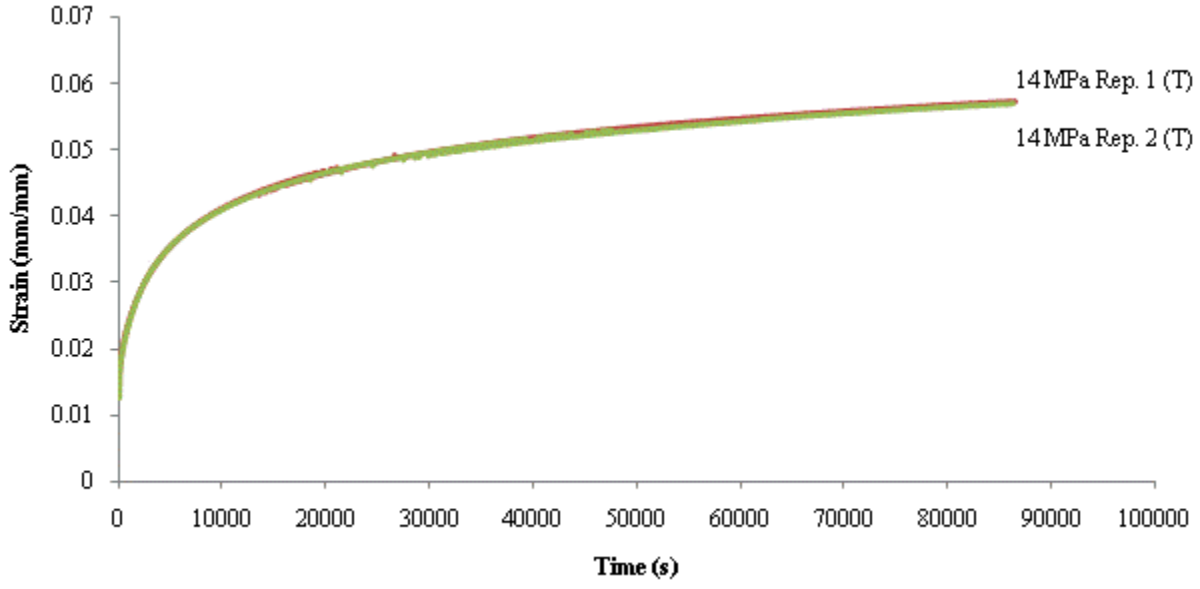

Figure A. 8 - Strain vs. time for film A subjected to 14 MPa in the transverse direction for 24 hours

Appendix B – Individual Creep Curves for Film B

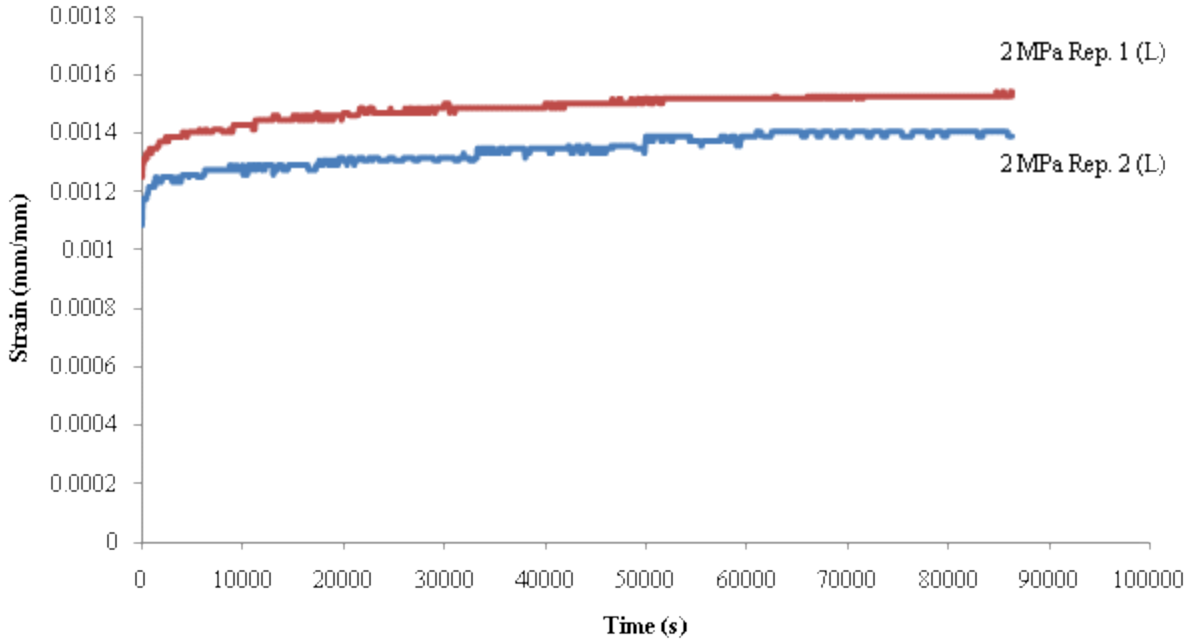

Figure B. 1 - Strain vs. time for film B subjected to 2 MPa in the longitudinal direction for 24 hours

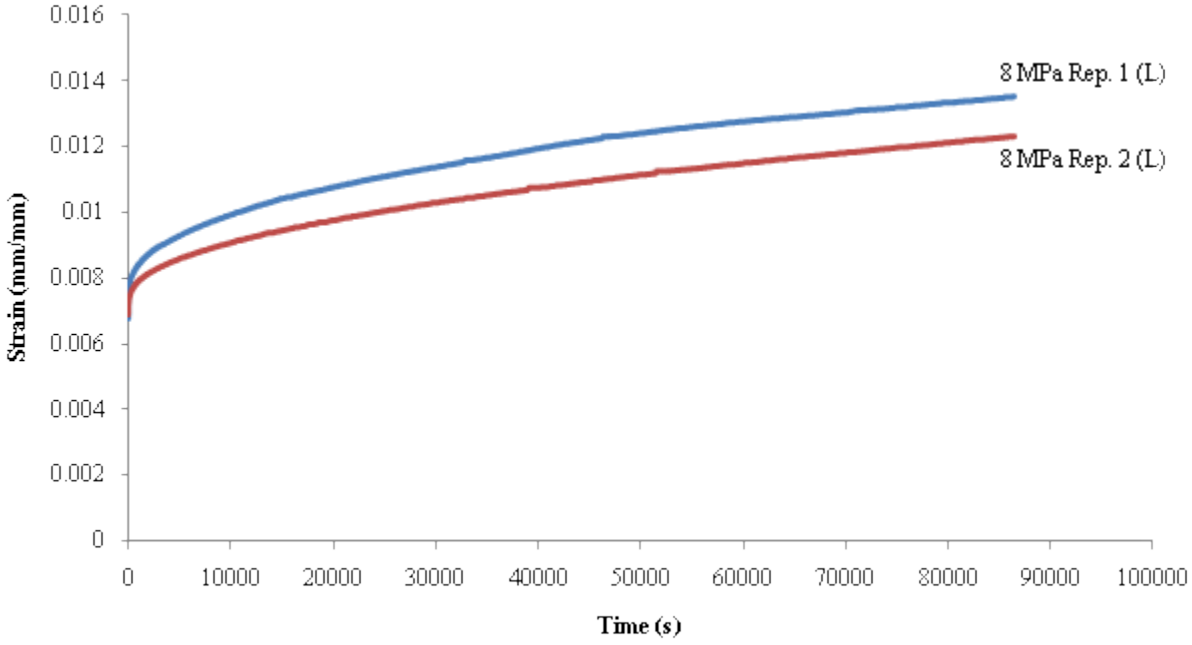

Figure B. 2 - Strain vs. time for film B subjected to 8 MPa in the longitudinal direction for 24 hours

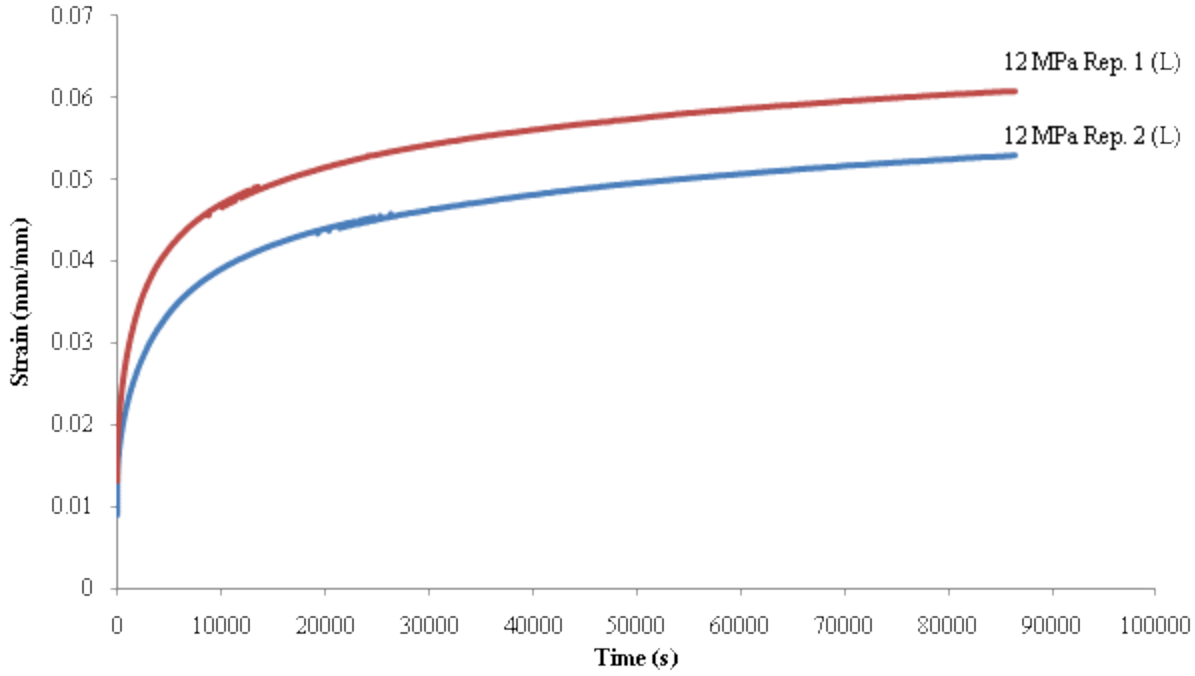

Figure B. 3 - Strain vs. time for film B subjected to 12 MPa in the longitudinal direction for 24 hours

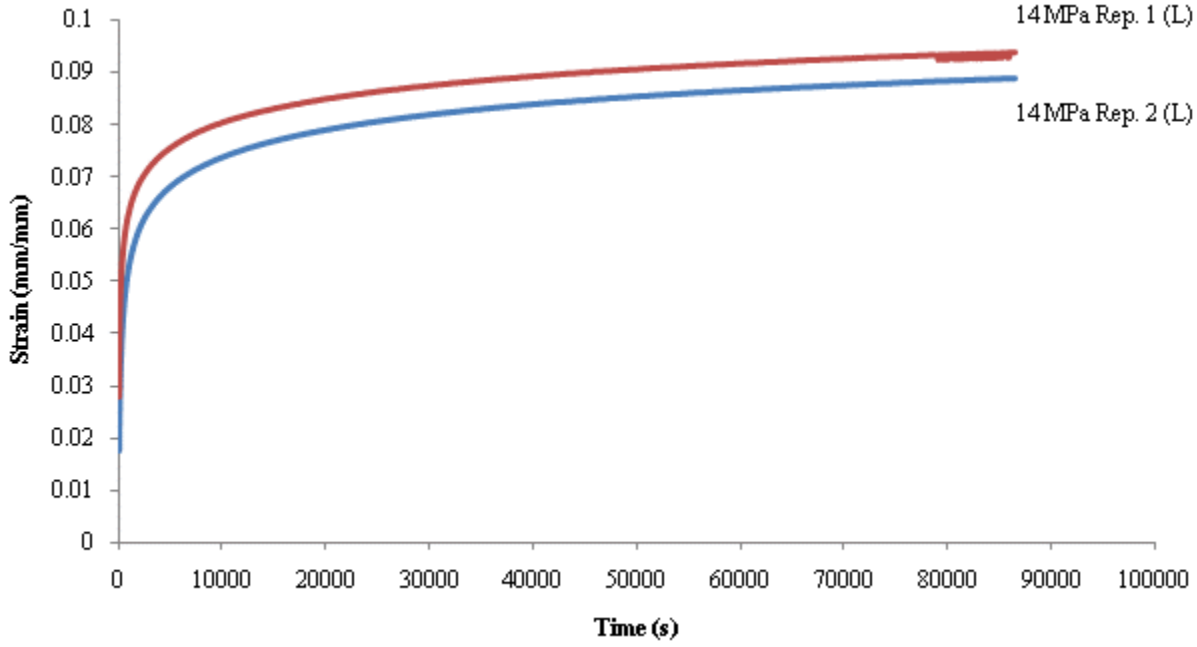

Figure B. 4 - Strain vs. time for film B subjected to 14 MPa in the longitudinal direction for 24 hours

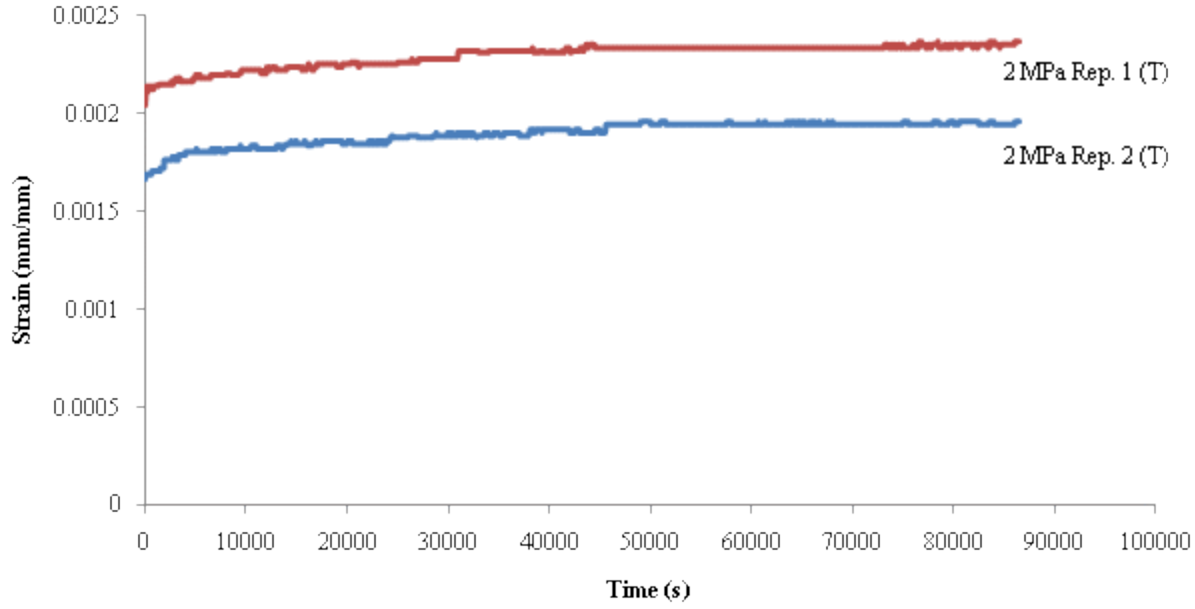

Figure B. 5 - Strain vs. time for film B subjected to 2 MPa in the transverse direction for 24 hours

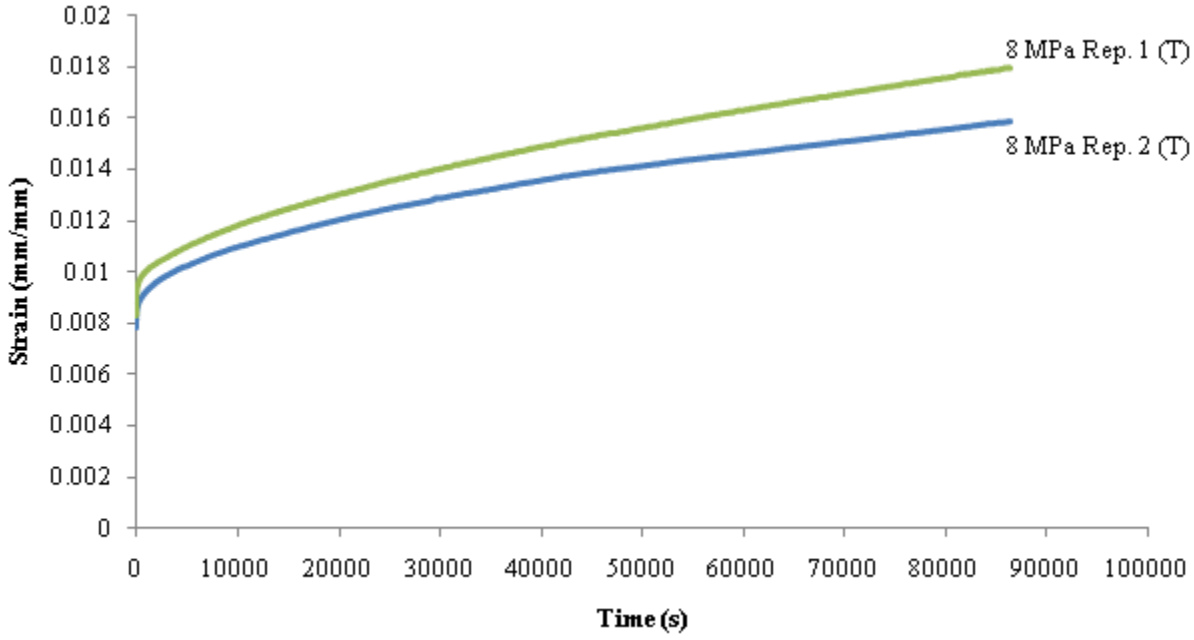

Figure B. 6 - Strain vs. time for film B subjected to 8 MPa in the transverse direction for 24 hours

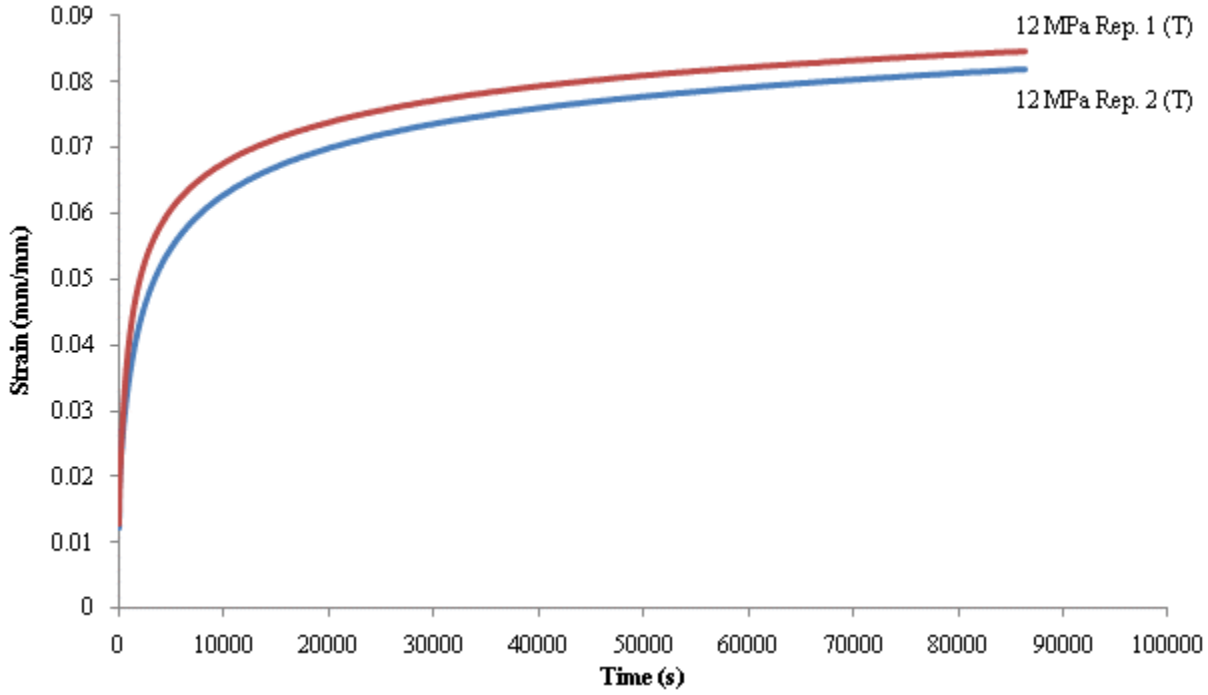

Figure B. 7 - Strain vs. time for film B subjected to 12 MPa in the transverse direction for 24 hours

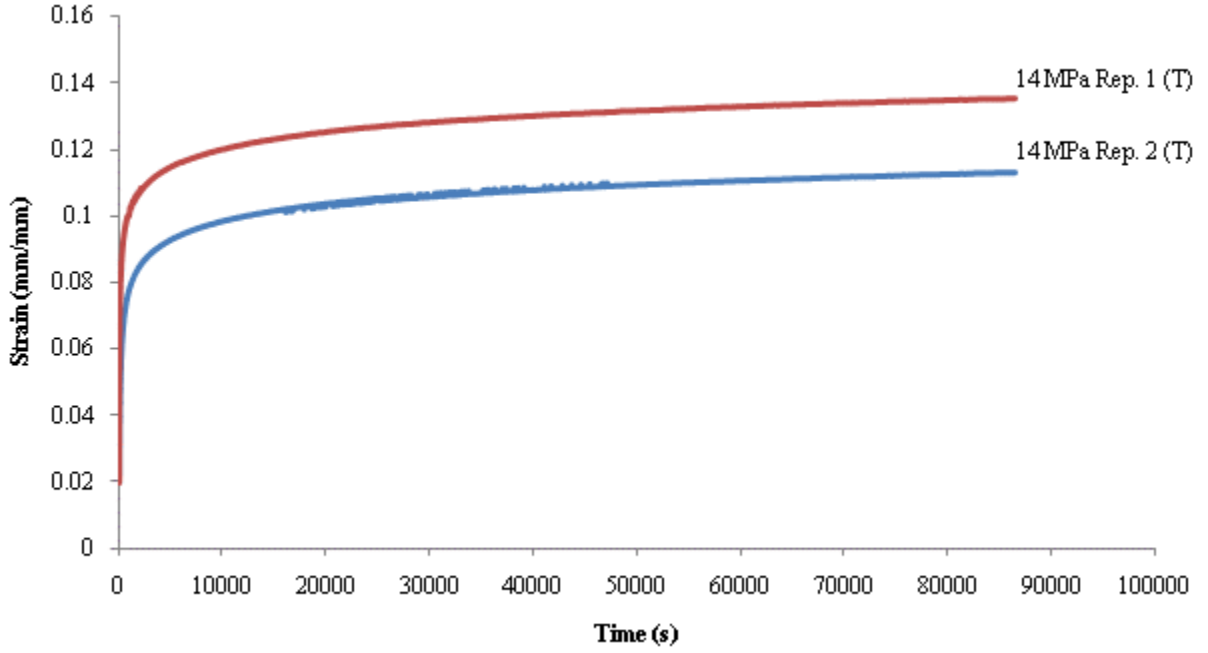

Figure B. 8 - Strain vs. time for film B subjected to 14 MPa in the transverse direction for 24 hours

Appendix C – Individual Creep Curves for Film C1

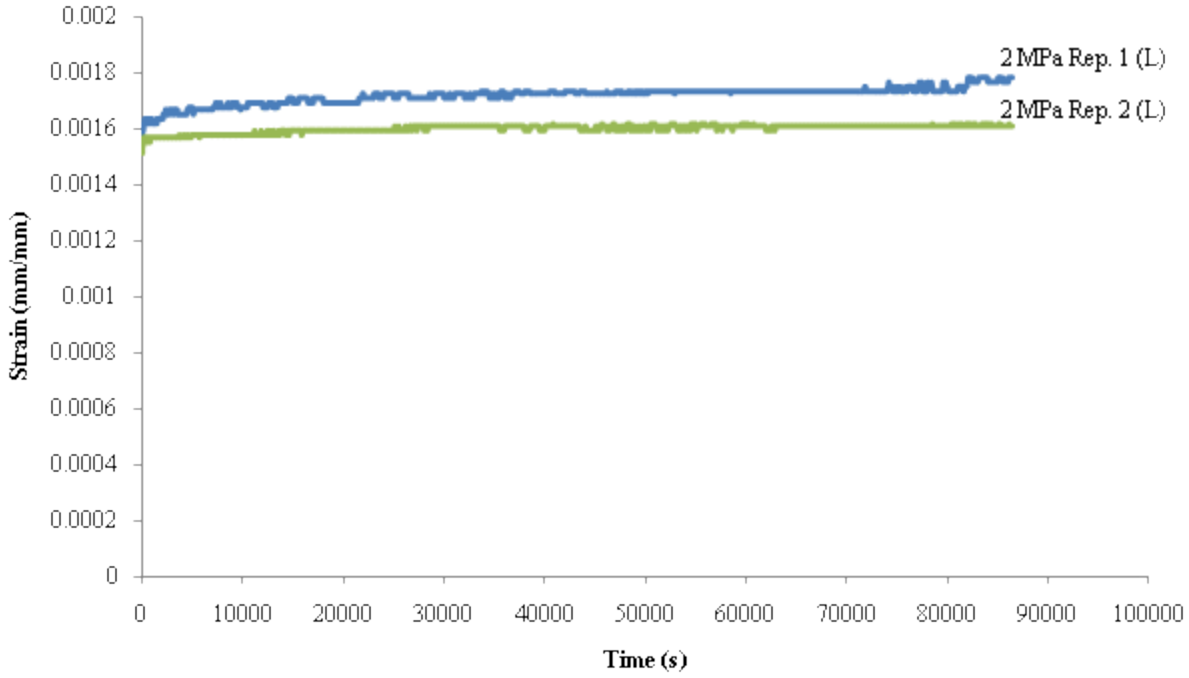

Figure C. 1 - Strain vs. time for film C1 subjected to 2 MPa in the longitudinal direction for 24 hours

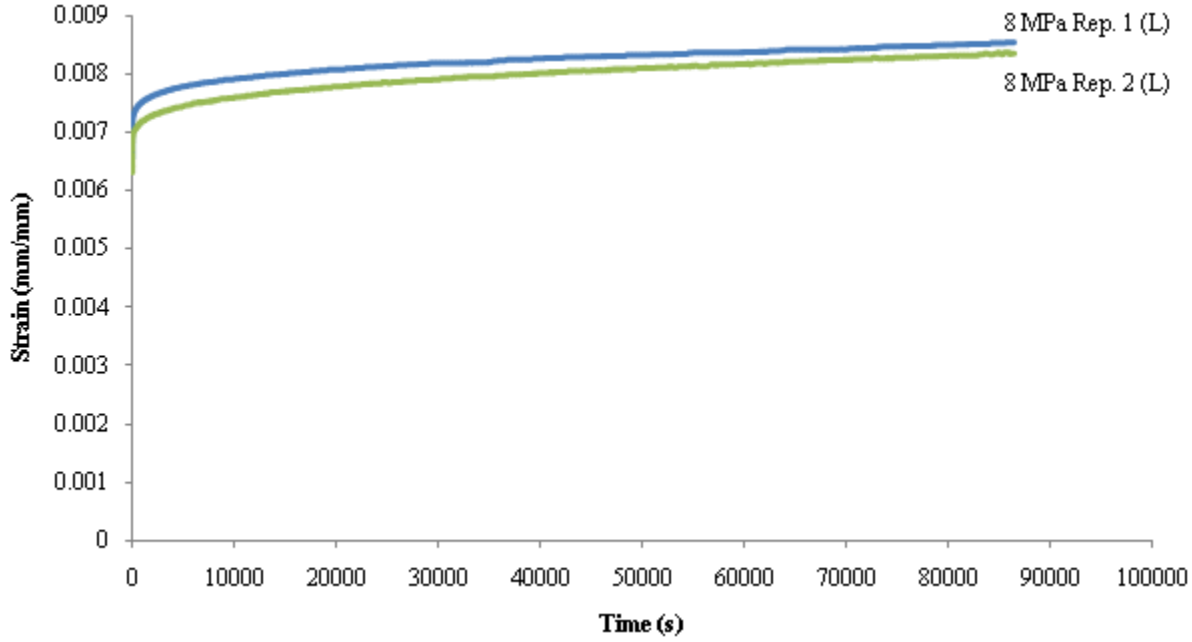

Figure C. 2 - Strain vs. time for film C1 subjected to 8 MPa in the longitudinal direction for 24 hours

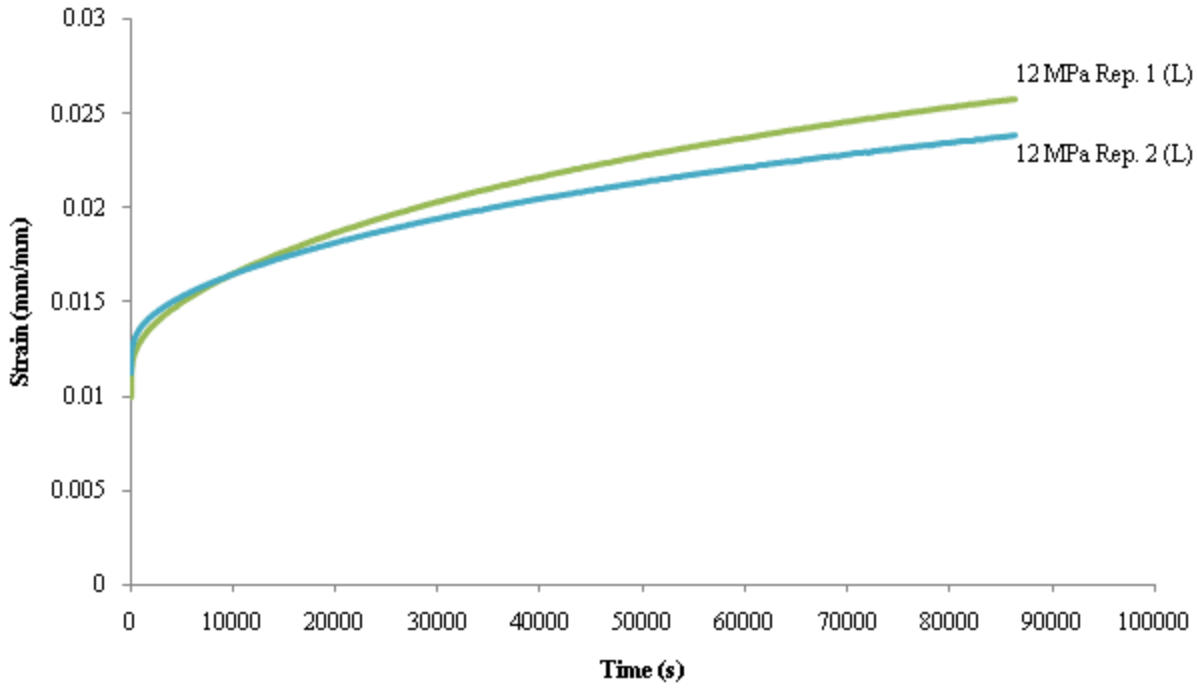

Figure C. 3 - Strain vs. time for film C1 subjected to 12 MPa in the longitudinal direction for 24 hours

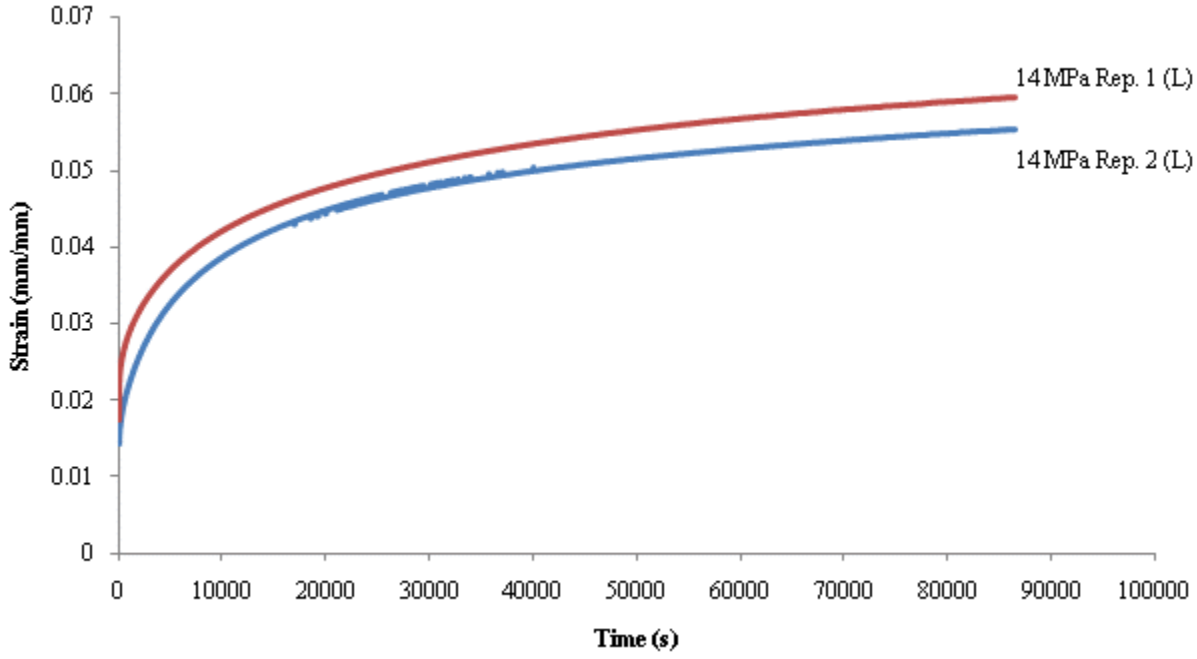

Figure C. 4 - Strain vs. time for film C1 subjected to 14 MPa in the longitudinal direction for 24 hours

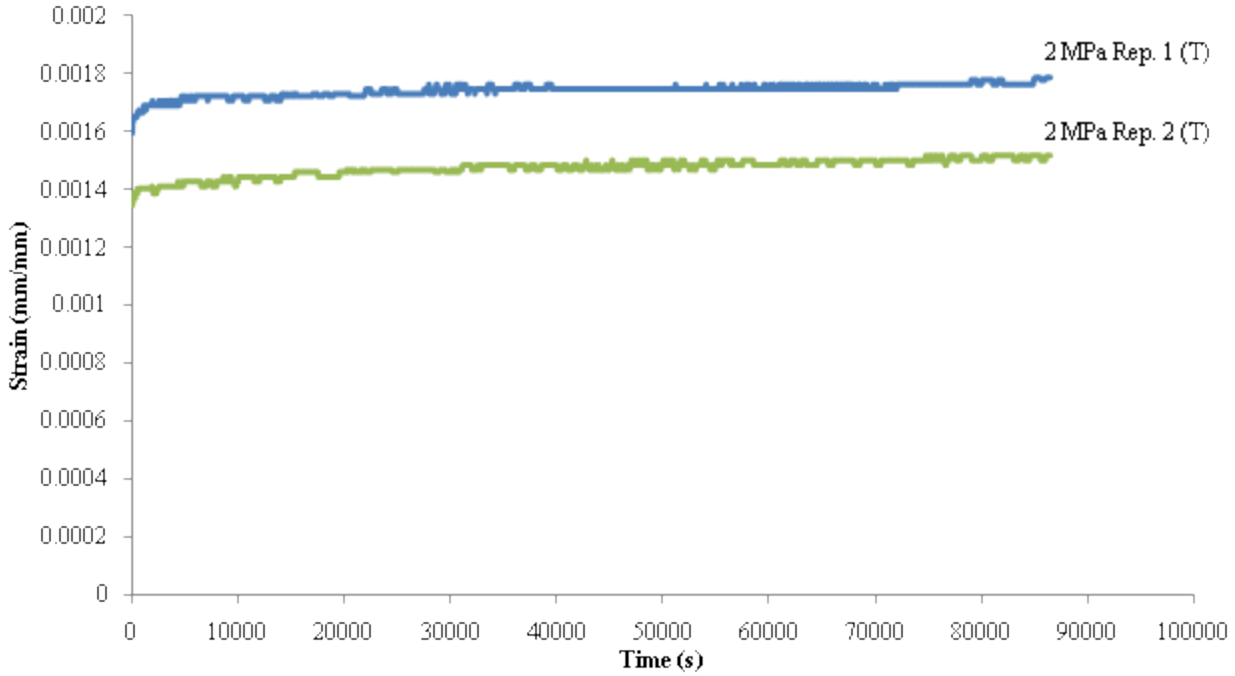

Figure C. 5 - Strain vs. time for film C1 subjected to 2 MPa in the transverse direction for 24 hours

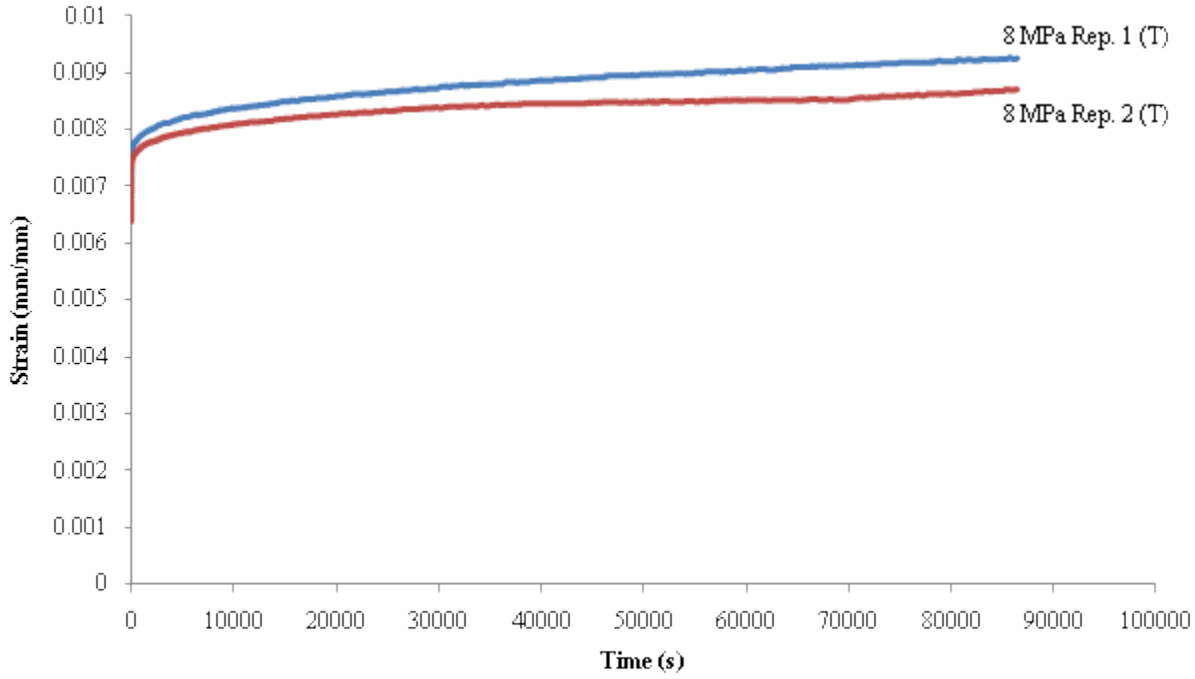

Figure C. 6 - Strain vs. time for film C1 subjected to 8 MPa in the transverse direction for 24 hours

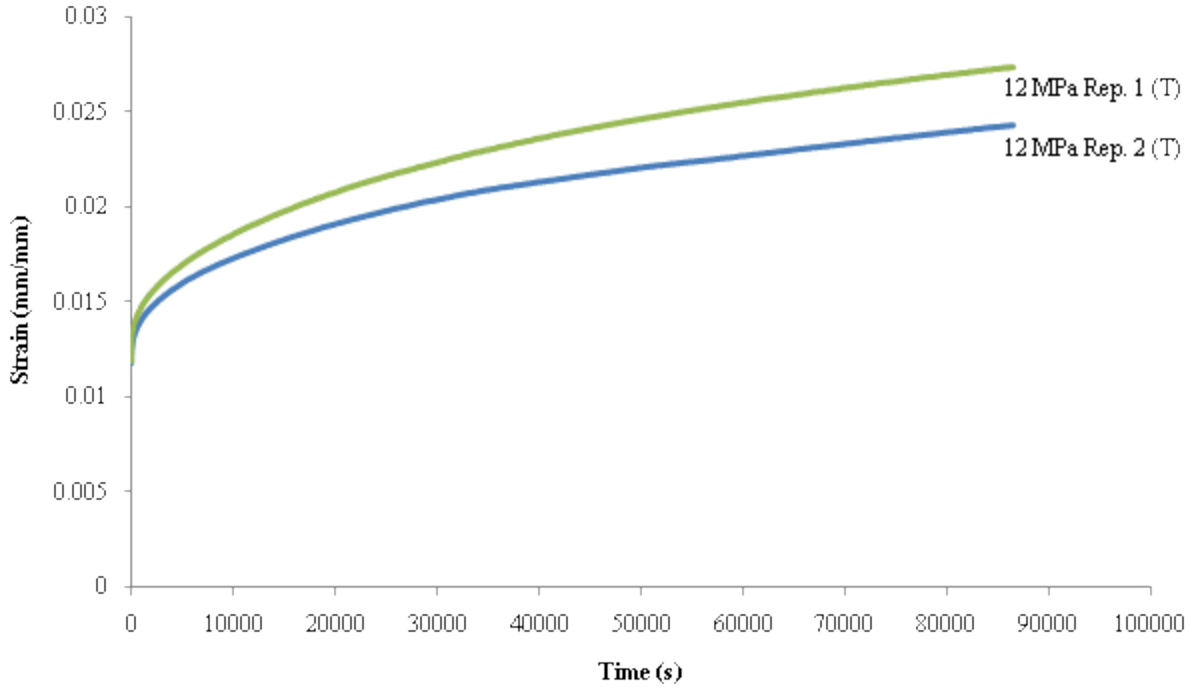

Figure C. 7 - Strain vs. time for film C1 subjected to 12 MPa in the transverse direction for 24 hours

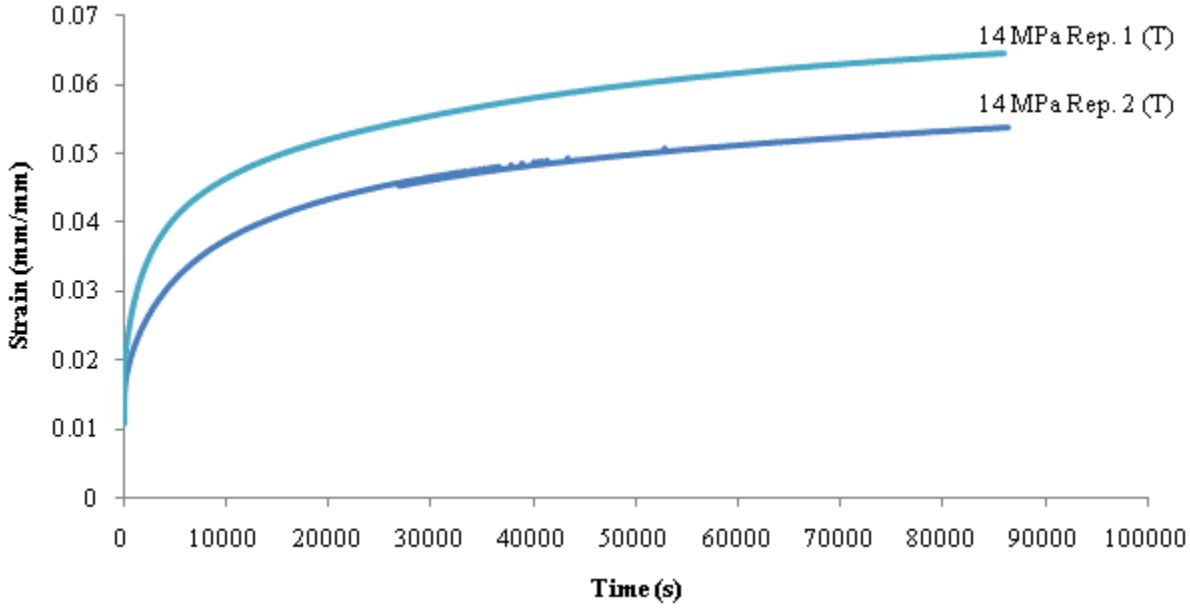

Figure C. 8 - Strain vs. time for film C1 subjected to 14 MPa in the transverse direction for 24 hours

Appendix D – Individual Creep Curves for Film C2

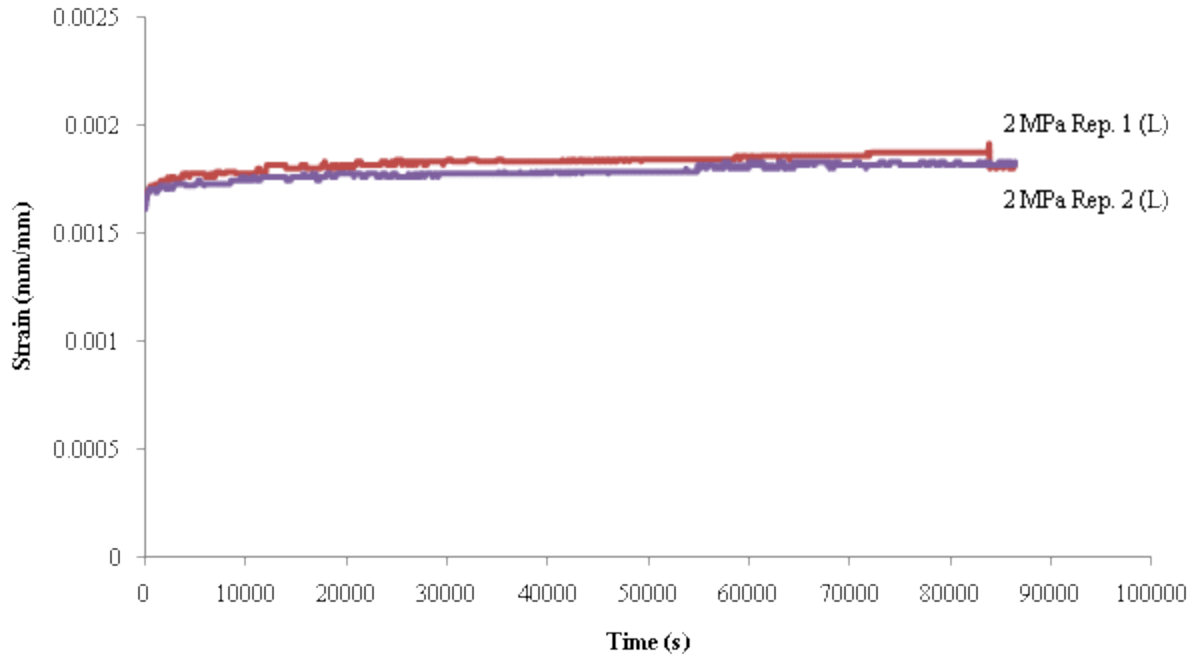

Figure D. 1 - Strain vs. time for film C2 subjected to 2 MPa in the longitudinal direction for 24 hours

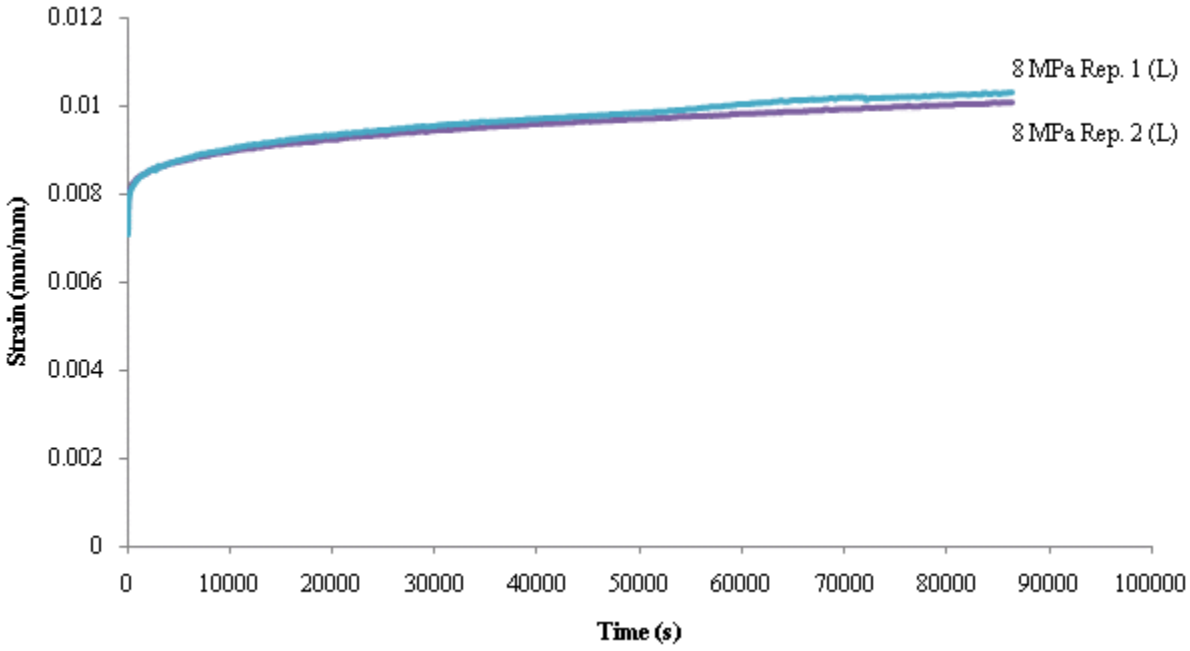

Figure D. 2 - Strain vs. time for film C2 subjected to 8 MPa in the longitudinal direction for 24 hours

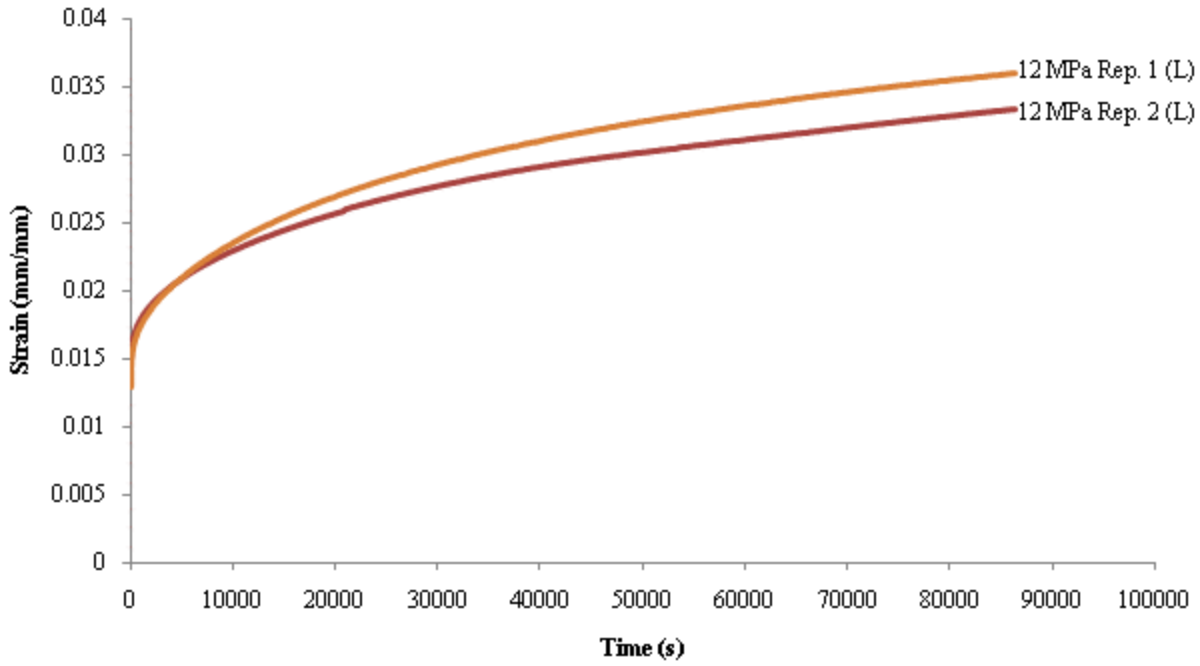

Figure D. 3 - Strain vs. time for film C2 subjected to 12 MPa in the longitudinal direction for 24 hours

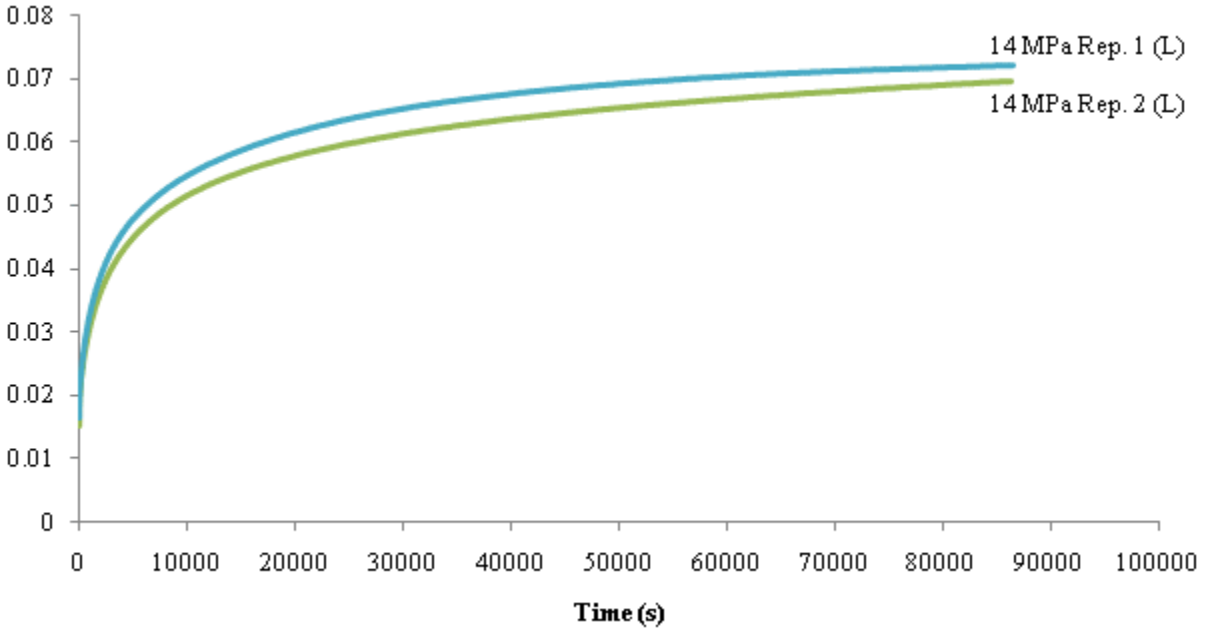

Figure D. 4 - Strain vs. time for film C2 subjected to 14 MPa in the longitudinal direction for 24 hours

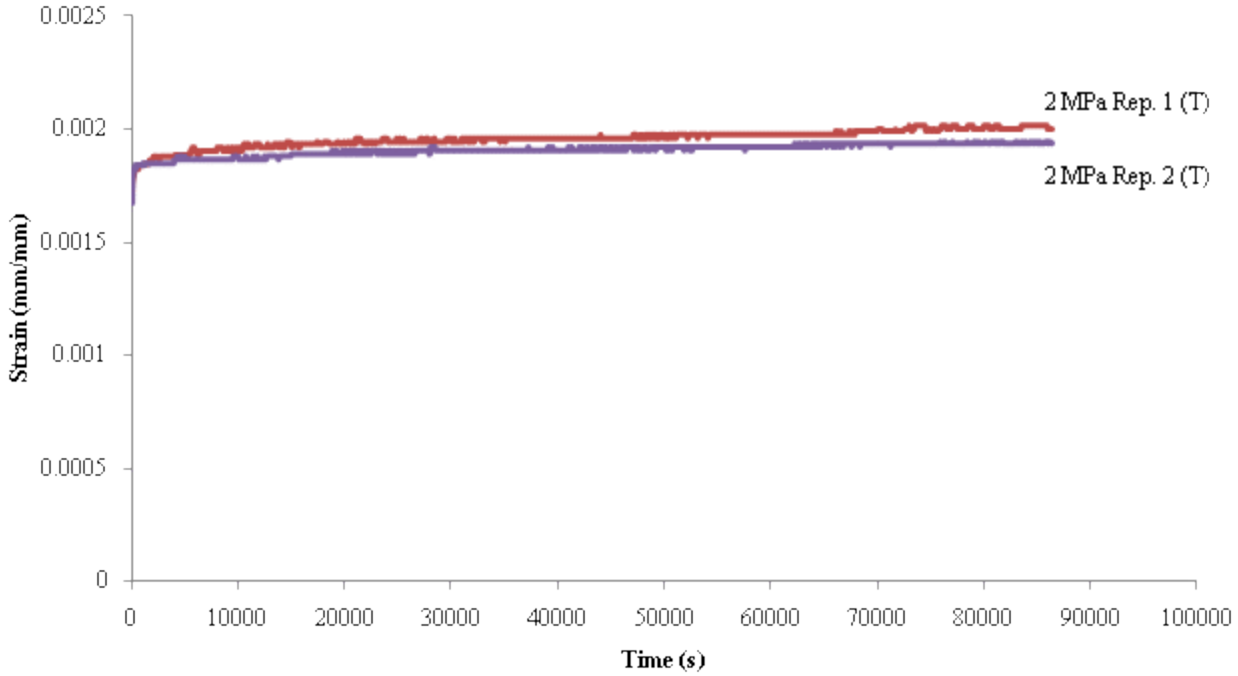

Figure D. 5 - Strain vs. time for film C2 subjected to 2 MPa in the transverse direction for 24 hours

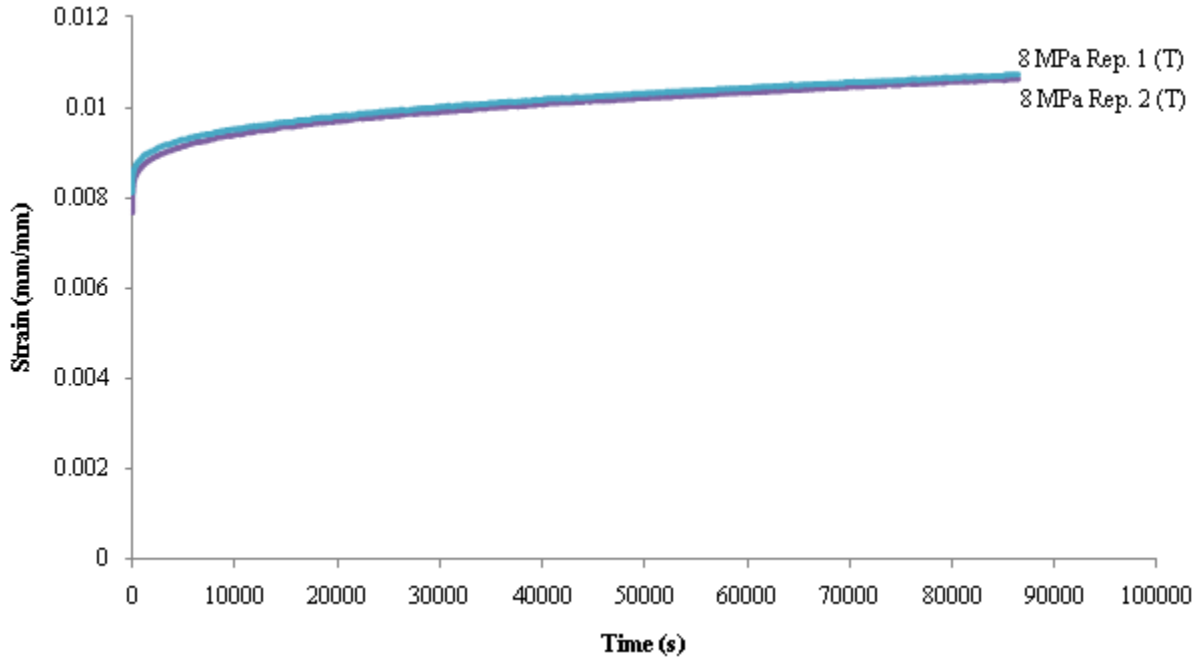

Figure D. 6 - Strain vs. time for film C2 subjected to 8 MPa in the transverse direction for 24 hours

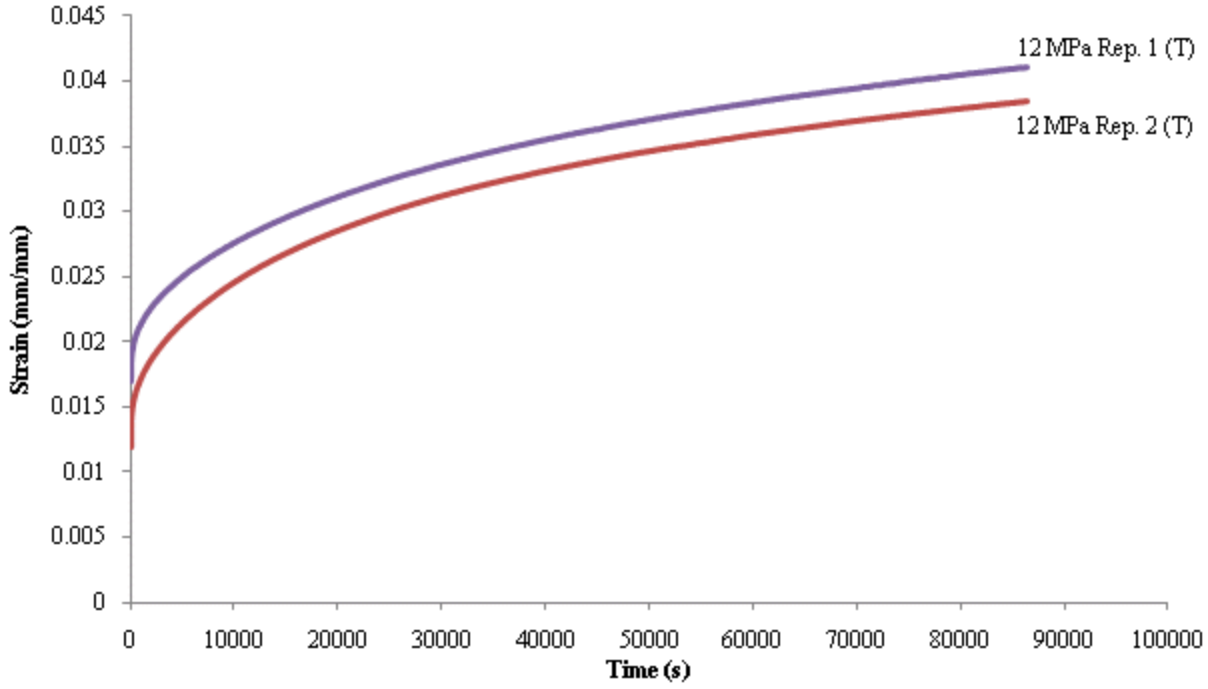

Figure D. 7 - Strain vs. time for film C2 subjected to 12 MPa in the transverse direction for 24 hours

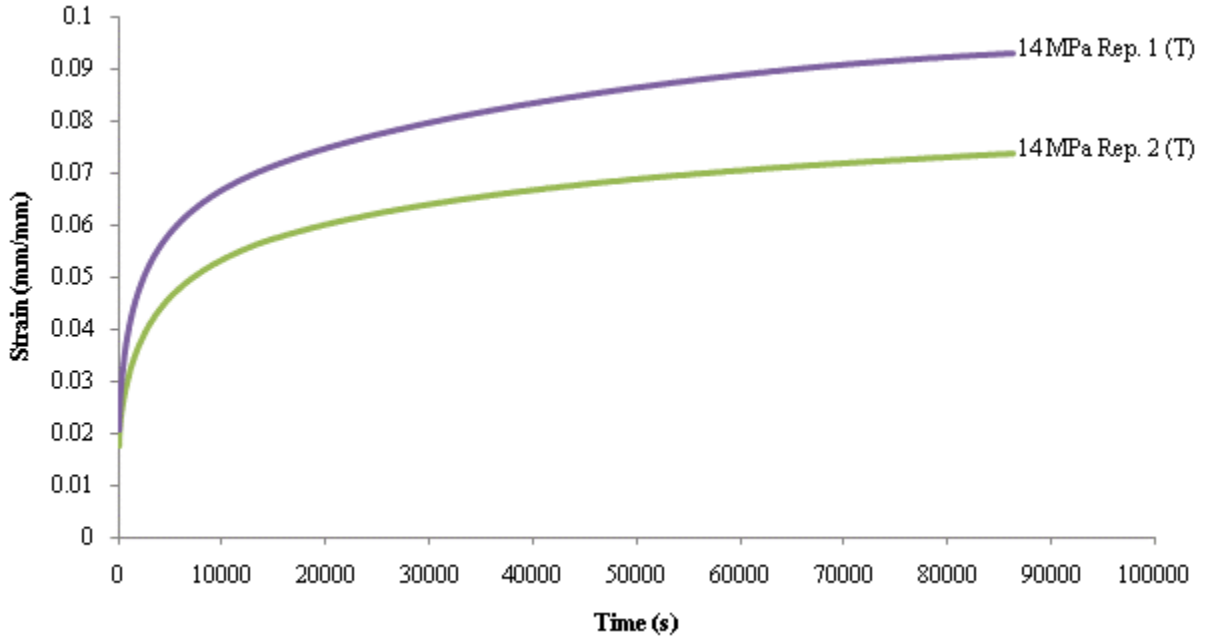

Figure D. 8 - Strain vs. time for film C2 subjected to 12 MPa in the transverse direction for 24 hours

Appendix E – Individual Viscoelastic Models

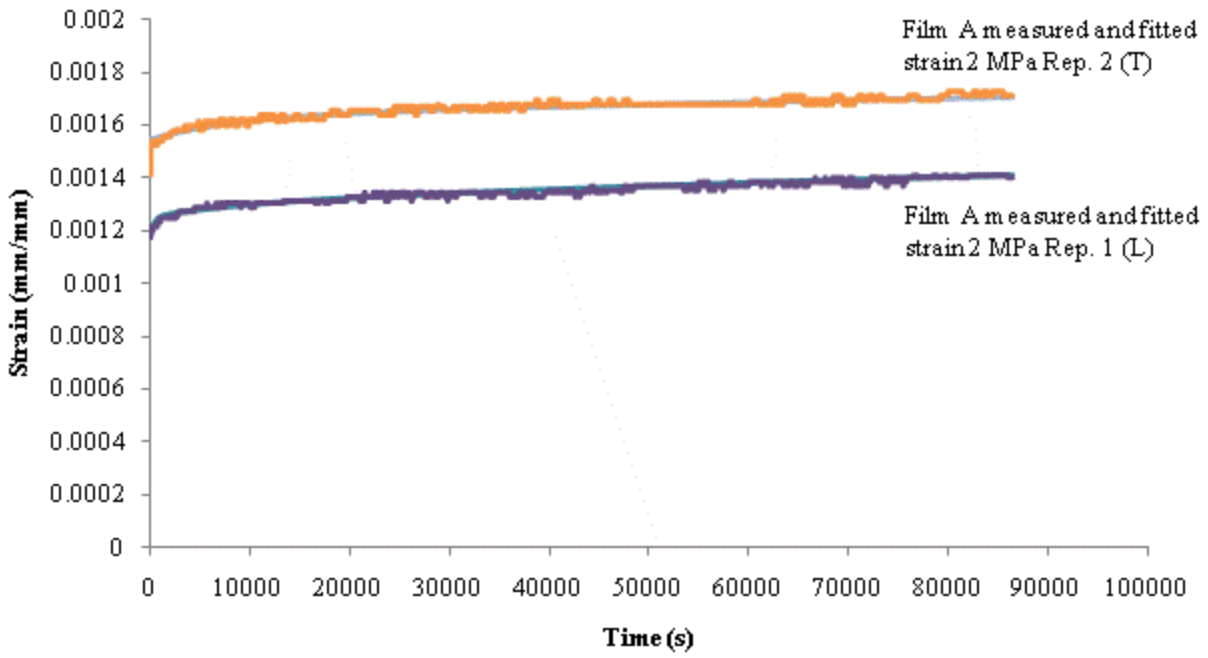

Figure E. 1 - Fitted viscoelastic strain curves for film A 2 MPa 24 hour tests

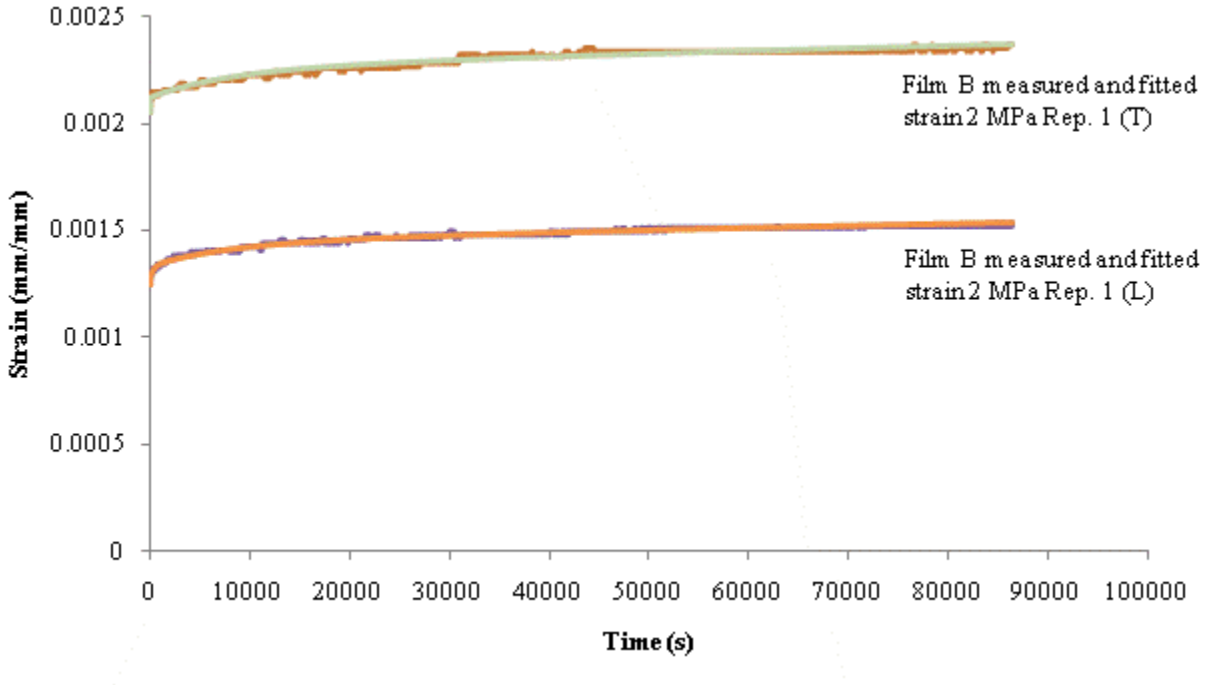

Figure E. 2 - Fitted viscoelastic strain curves for film B 2 MPa 24 hour tests

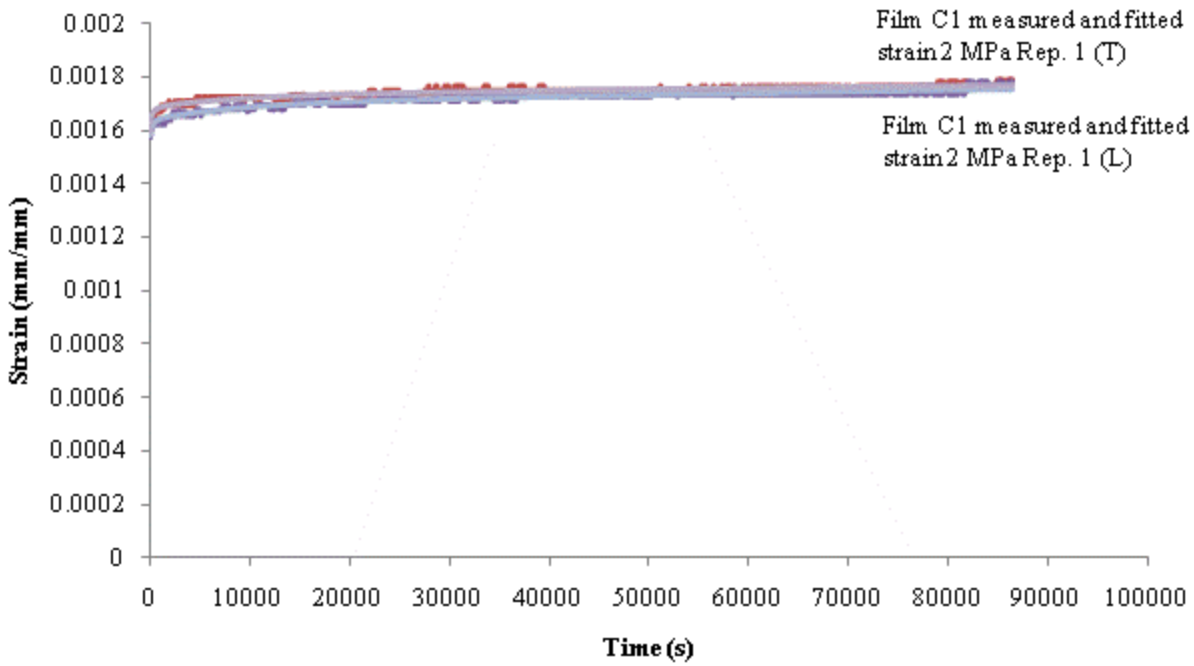

Figure E. 3 - Fitted viscoelastic strain curves for film C1 2 MPa 24 hour tests

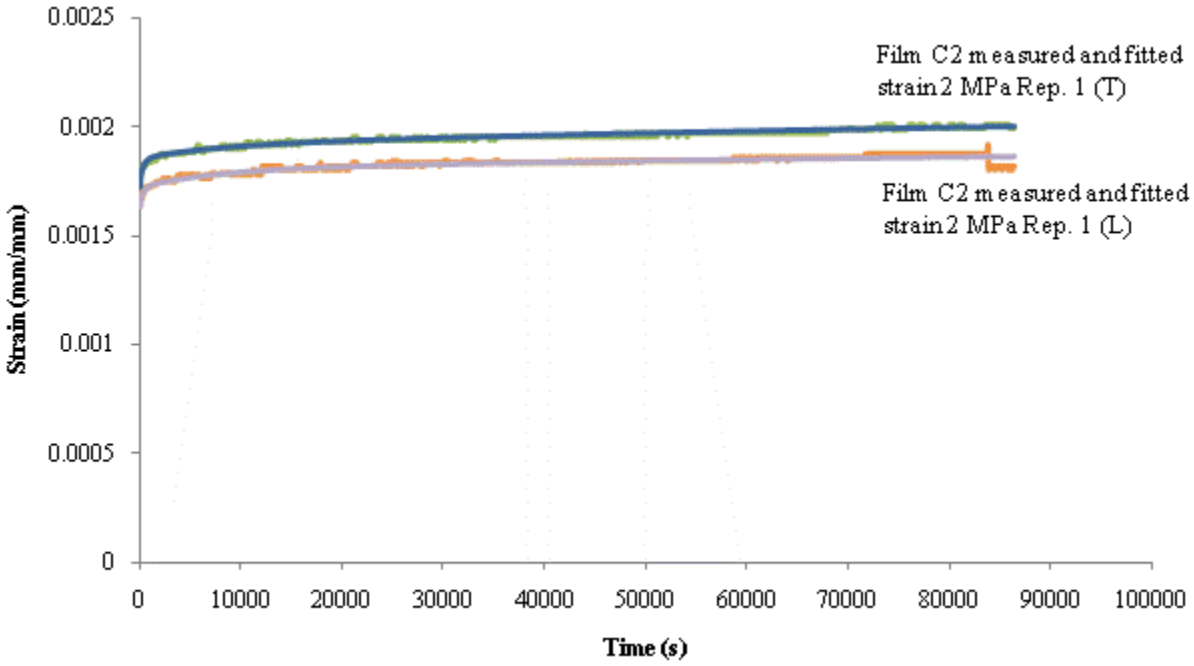

Figure E. 4 - Fitted viscoelastic strain curves for film C2 2 MPa 24 hour tests

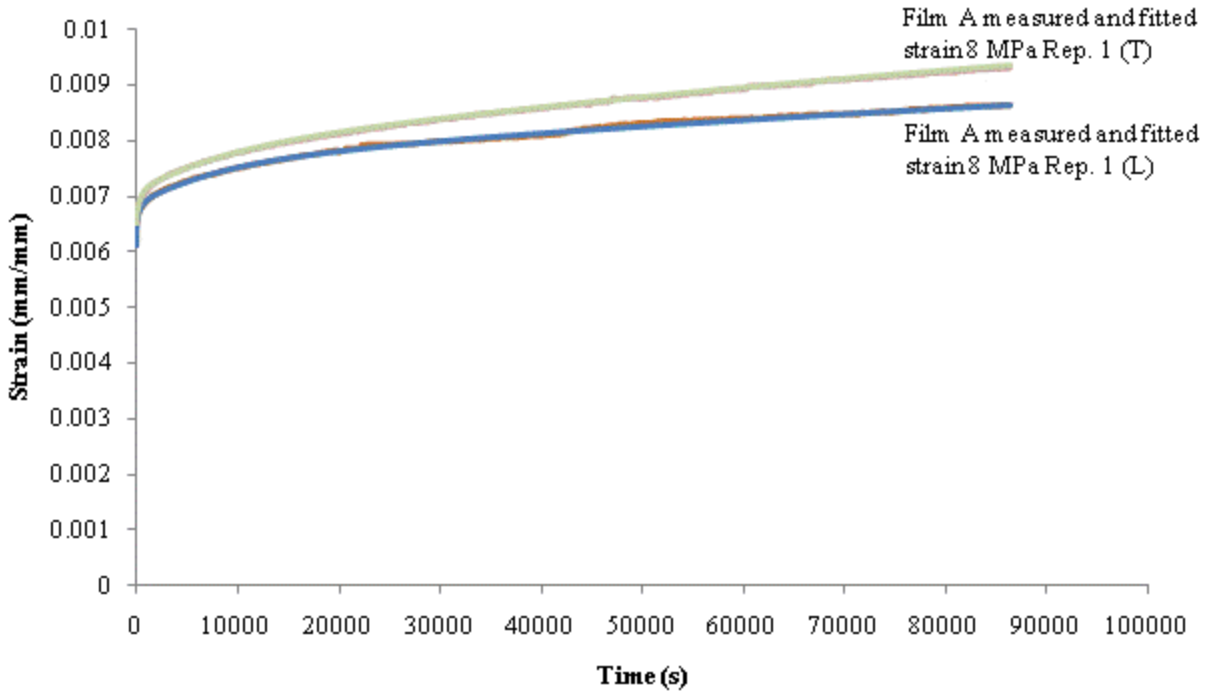

Figure E. 5 - Fitted viscoelastic strain curves for film A 8 MPa 24 hour tests

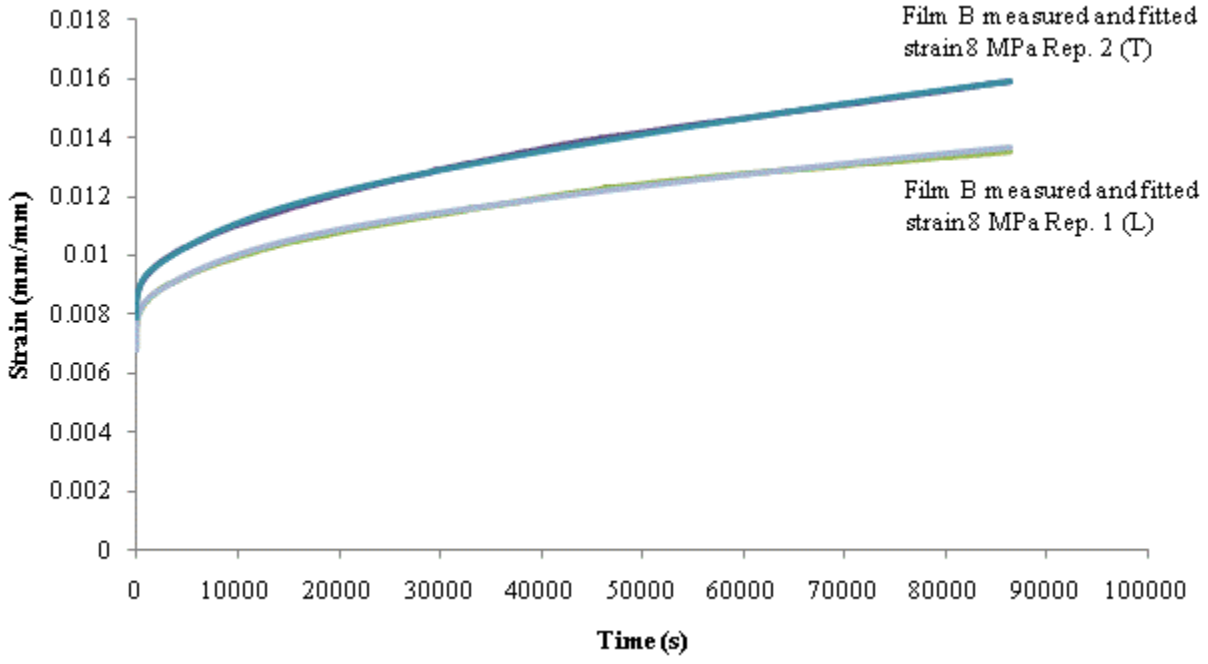

Figure E. 6 - Fitted viscoelastic strain curves for film B 8 MPa 24 hour tests

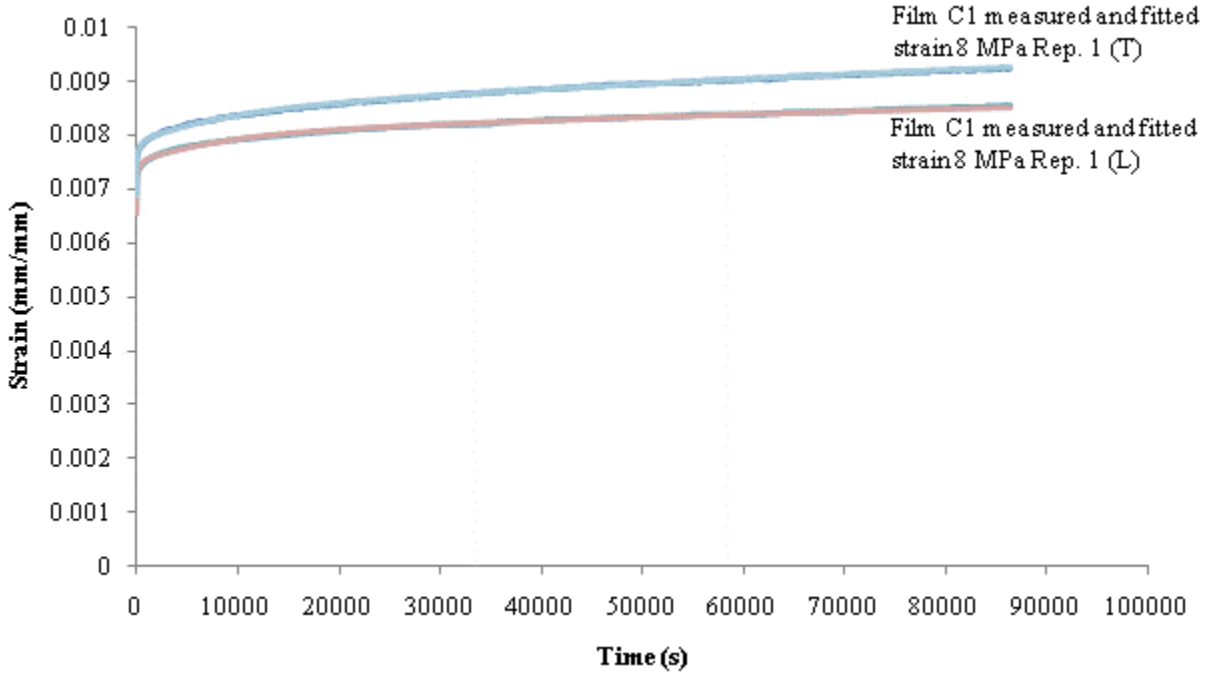

Figure E. 7 - Fitted viscoelastic strain curves for film C1 8 MPa 24 hour tests

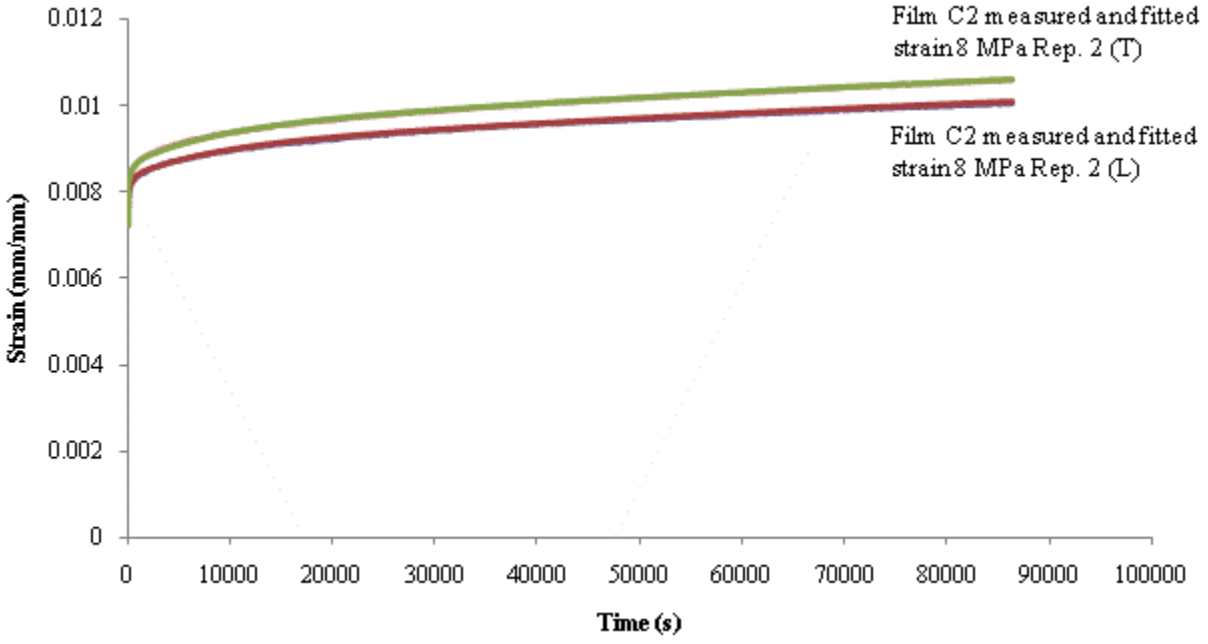

Figure E. 8 - Fitted viscoelastic strain curves for film C2 8 MPa 24 hour tests

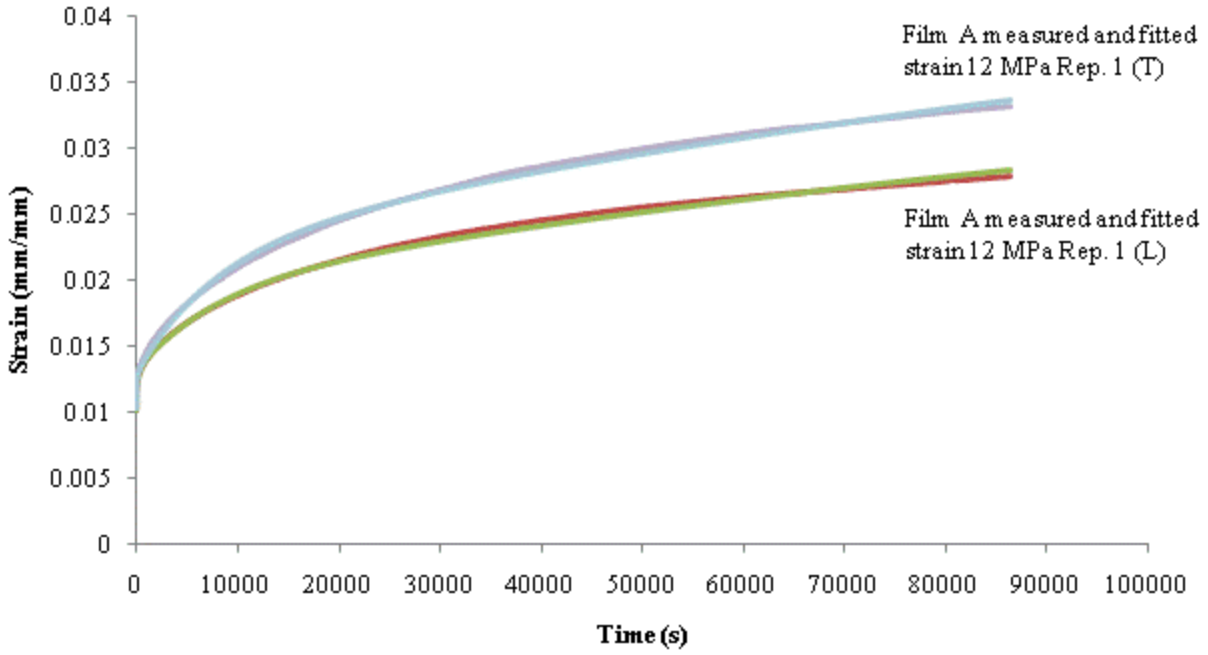

Figure E. 9 - Fitted viscoelastic strain curves for film A 12 MPa 24 hour tests

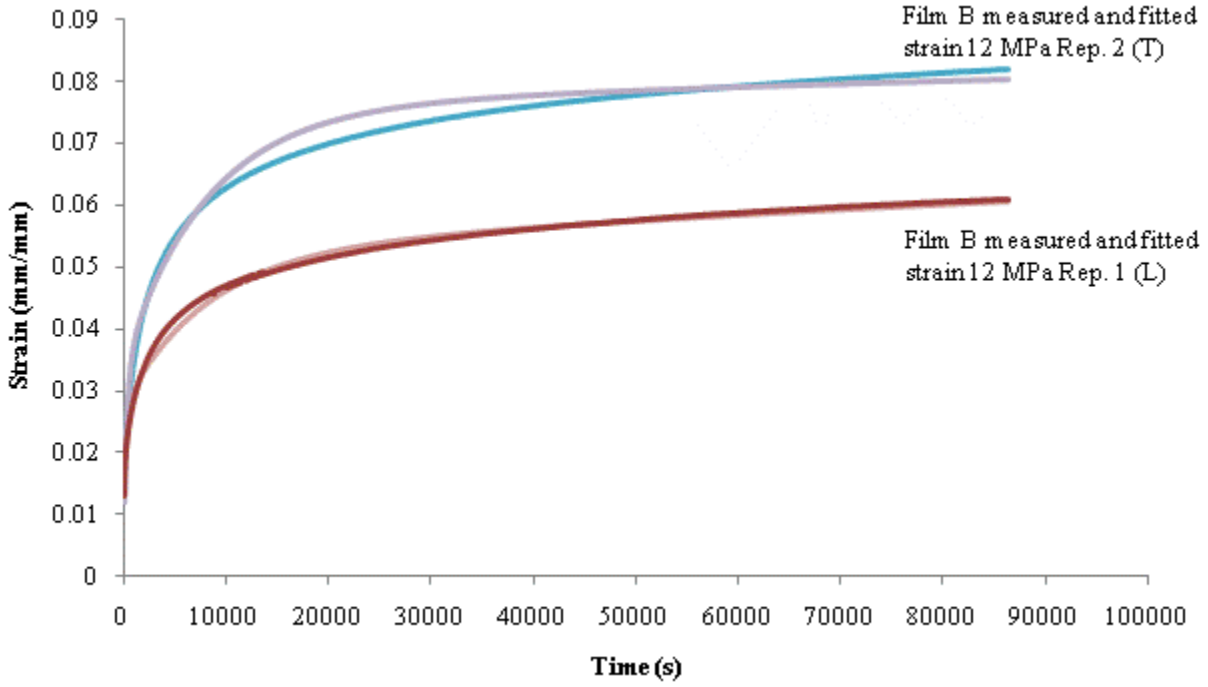

Figure E. 10 - Fitted viscoelastic strain curves for film B 12 MPa 24 hour tests

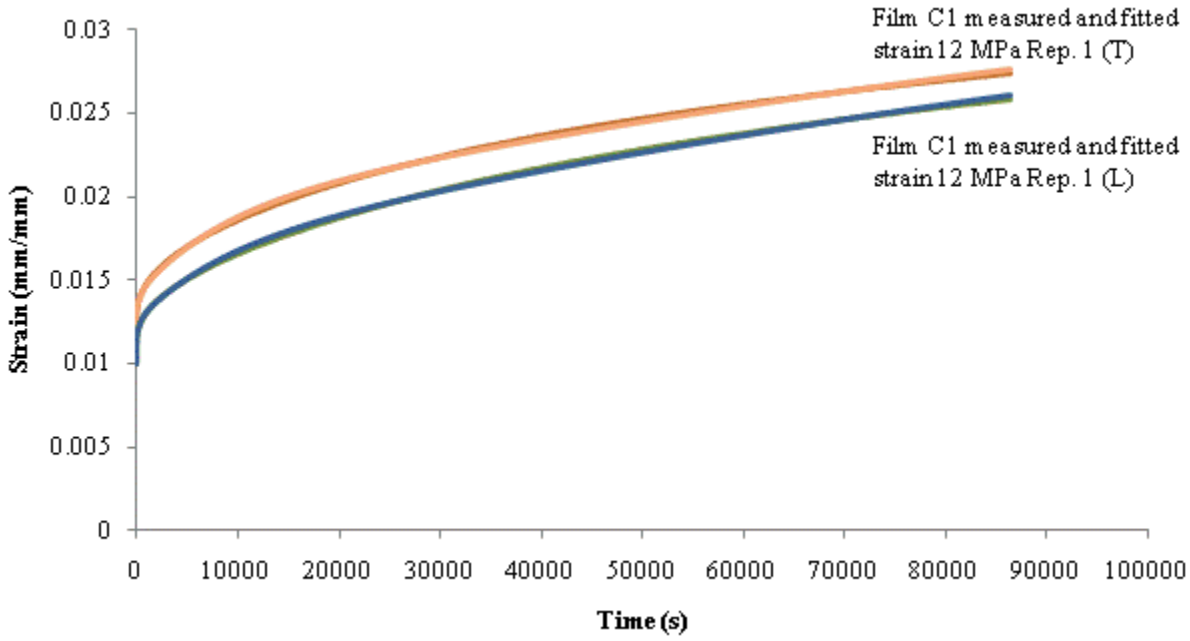

Figure E. 11 - Fitted viscoelastic strain curves for film C1 12 MPa 24 hour tests

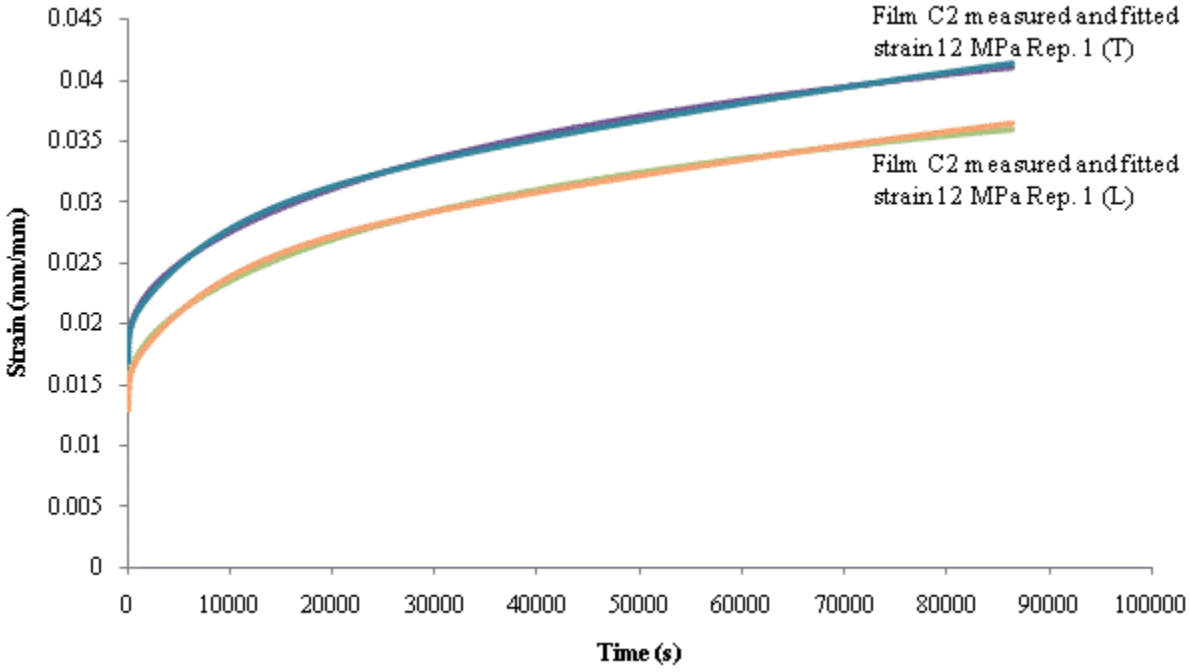

Figure E. 12 - Fitted viscoelastic strain curves for film C2 12 MPa 24 hour tests

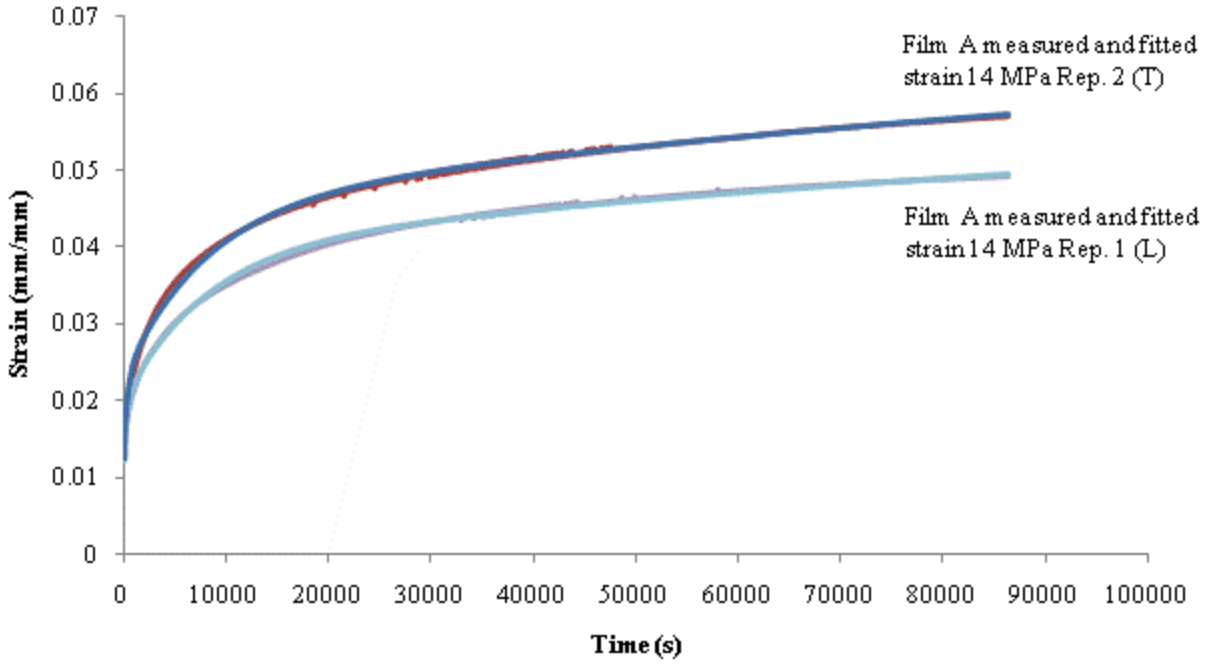

Figure E. 13 - Fitted viscoelastic strain curves for film A 14 MPa 24 hour tests

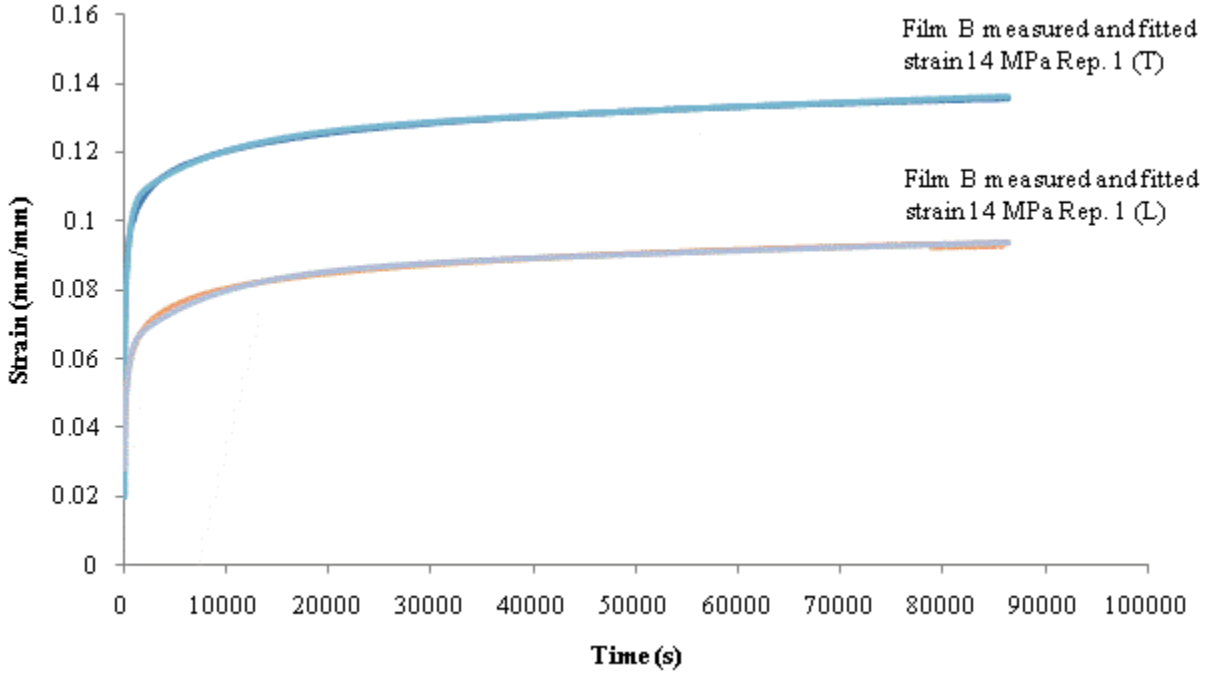

Figure E. 14 - Fitted viscoelastic strain curves for film B 14 MPa 24 hour tests

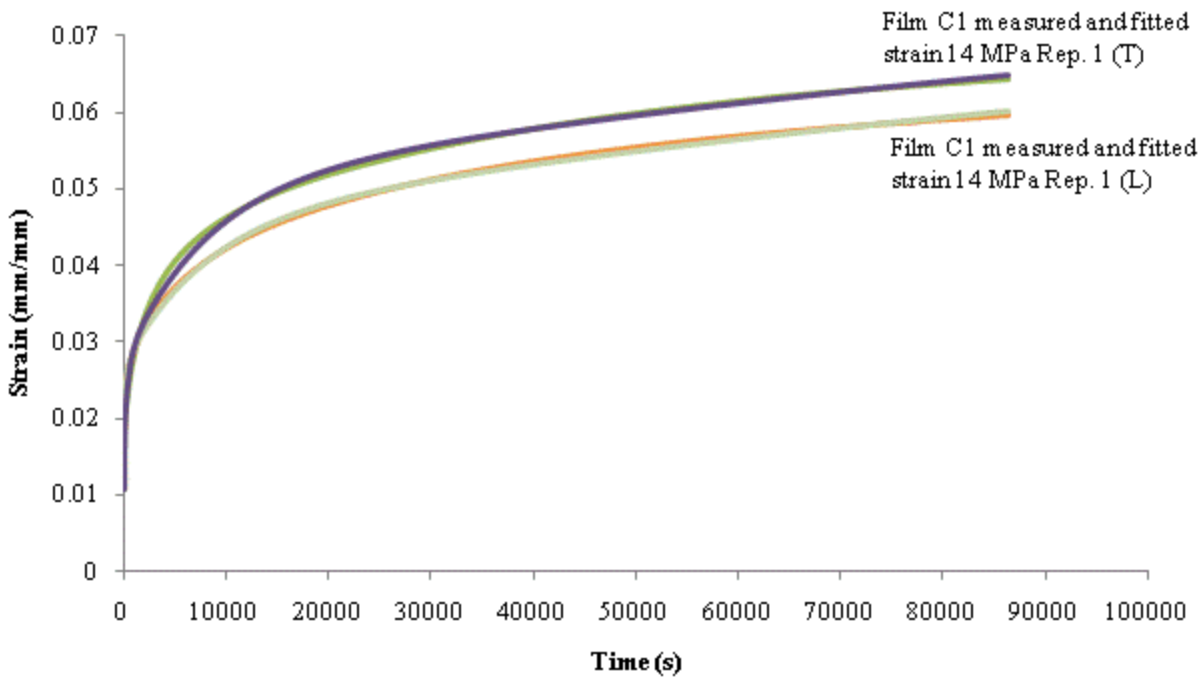

Figure E. 15 - Fitted viscoelastic strain curves for film C1 14 MPa 24 hour tests

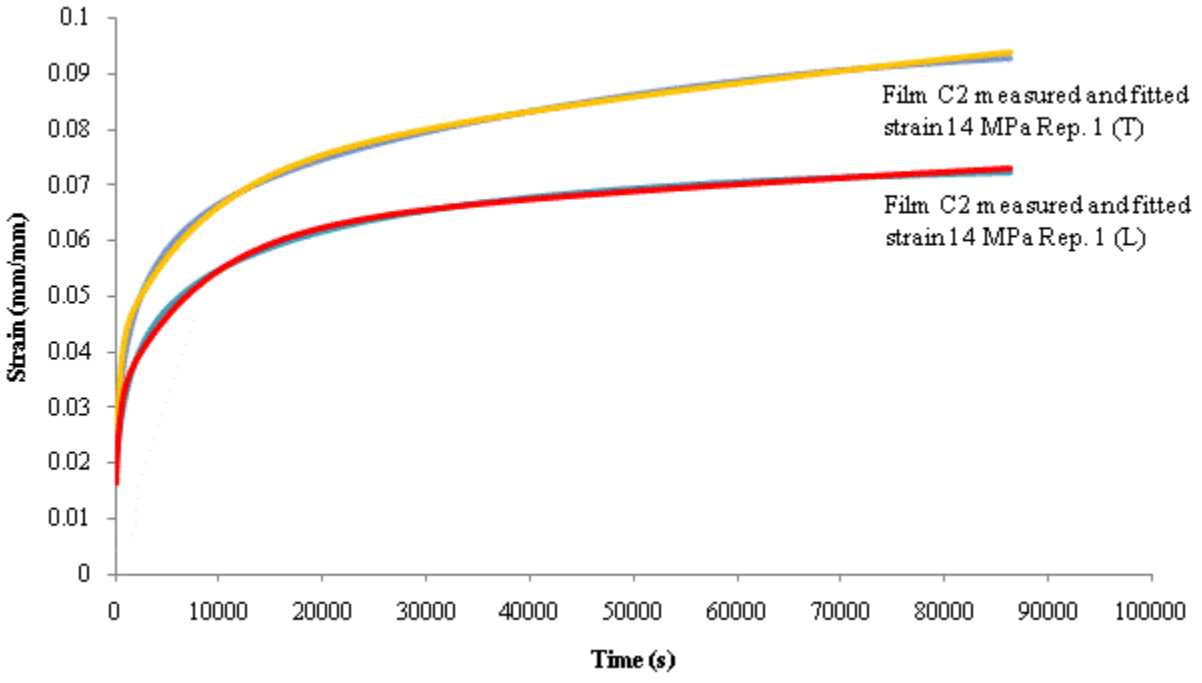

Figure E. 16 - Fitted viscoelastic strain curves for film C2 14 MPa 24 hour tests

Appendix F – Individual Viscoplastic Models

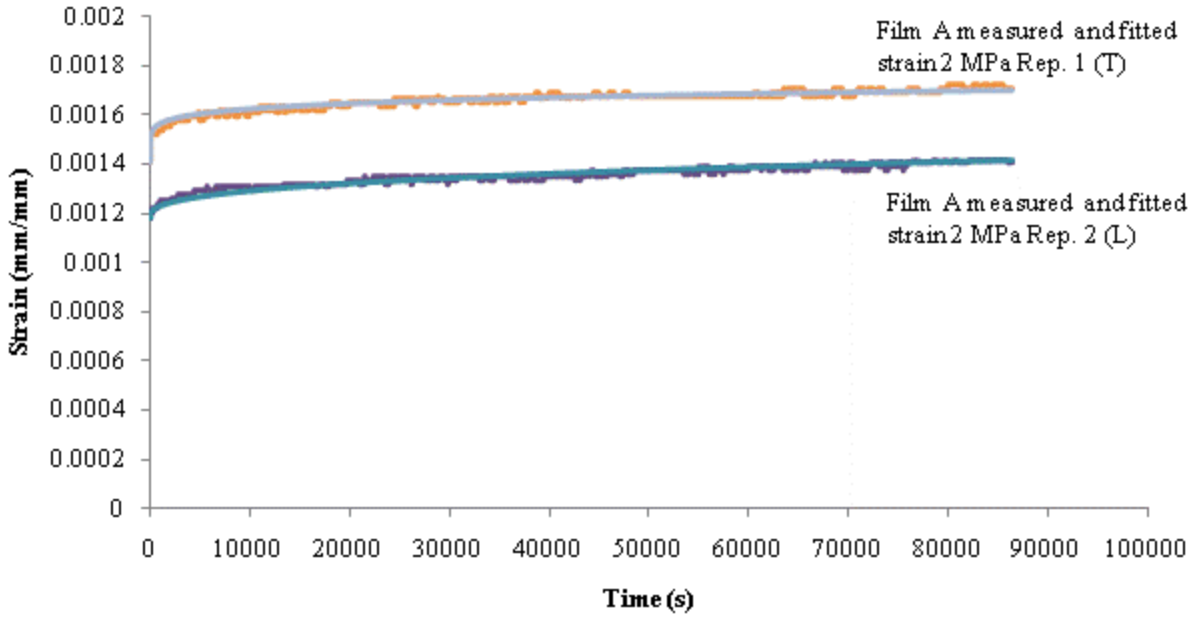

Figure F. 1 - Fitted viscoplastic strain curves for film A 2 MPa 24 hour tests

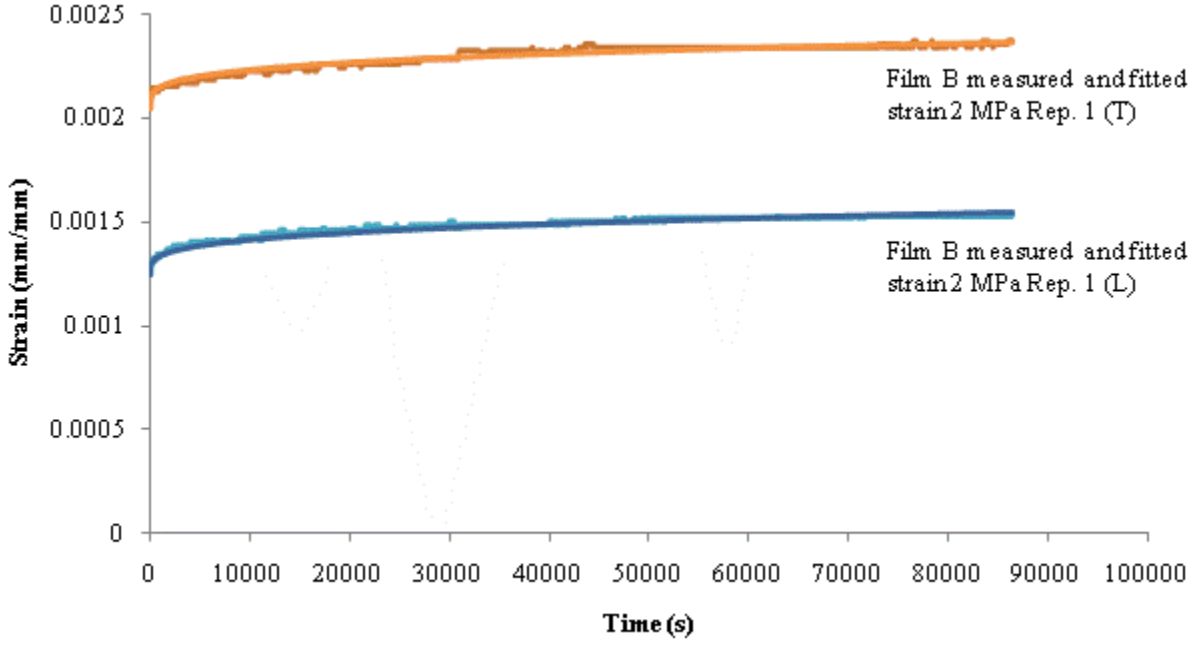

Figure F. 2 - Fitted viscoplastic strain curves for film B 2 MPa 24 hour tests

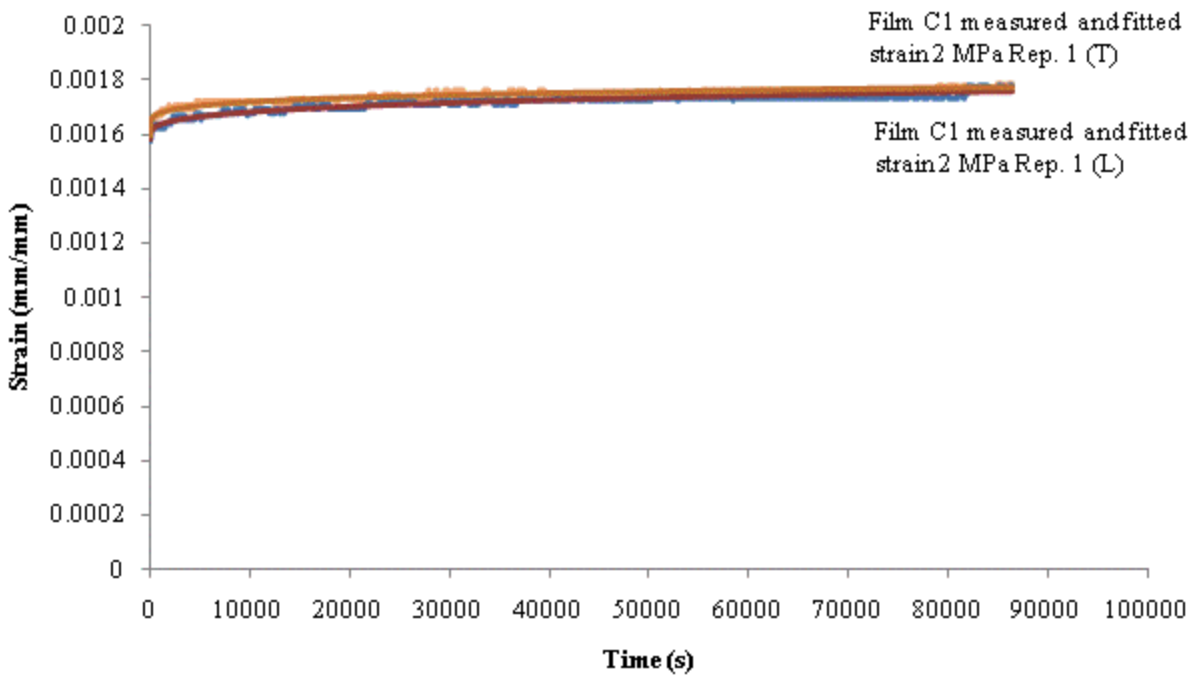

Figure F. 3 - Fitted viscoplastic strain curves for film C1 2 MPa 24 hour tests

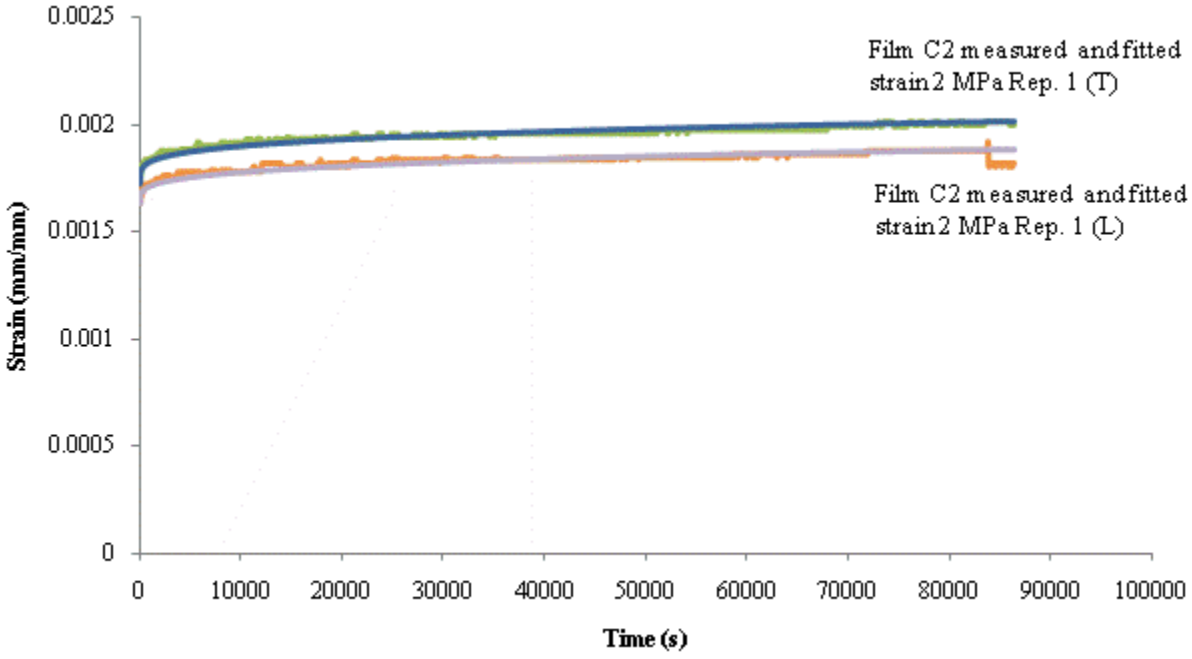

Figure F. 4 - Fitted viscoplastic strain curves for film C2 2 MPa 24 hour tests

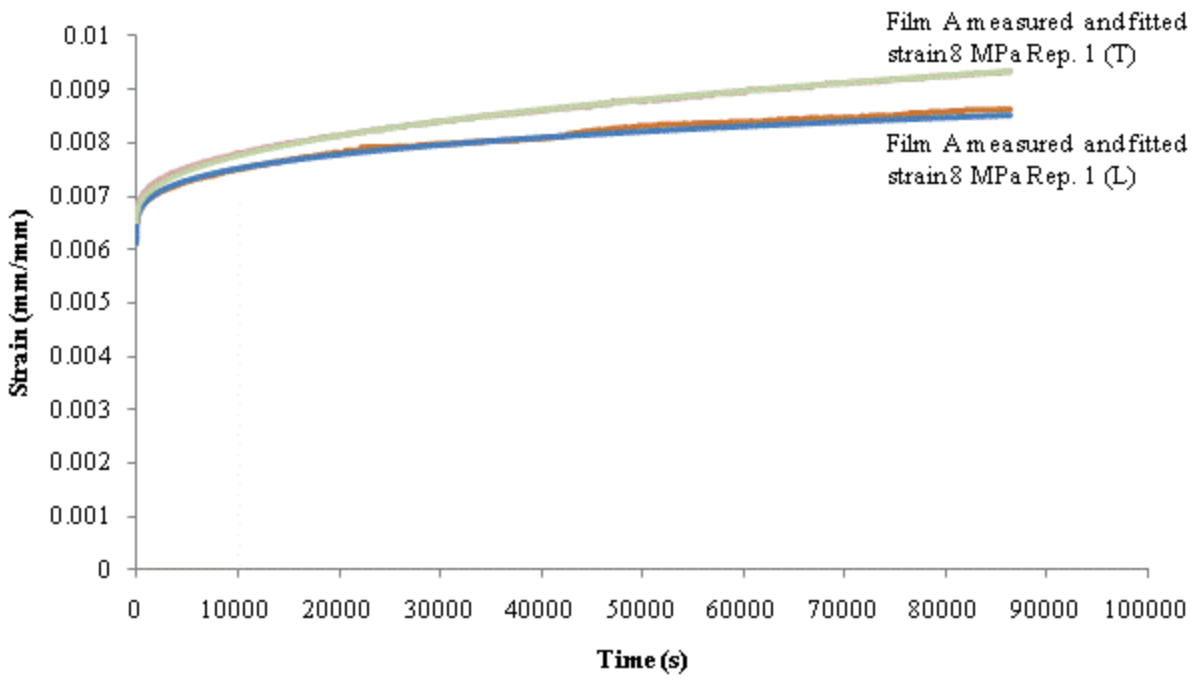

Figure F. 5 - Fitted viscoplastic strain curves for film A 8 MPa 24 hour tests

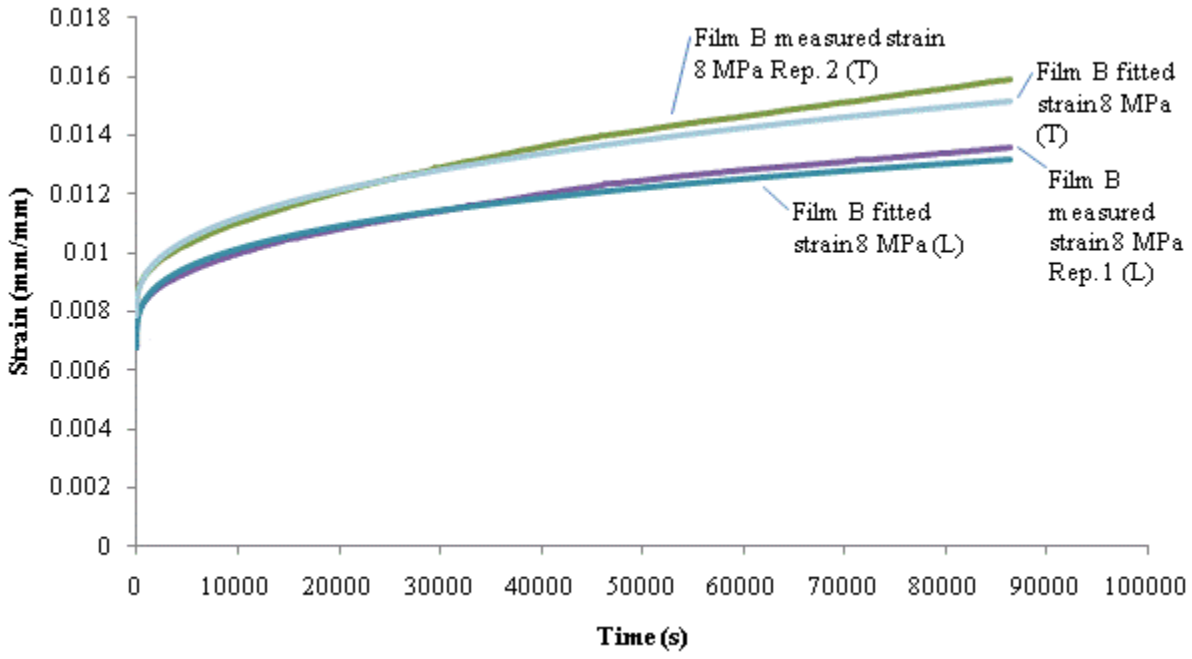

Figure F. 6 - Fitted viscoplastic strain curves for film B 8 MPa 24 hour tests

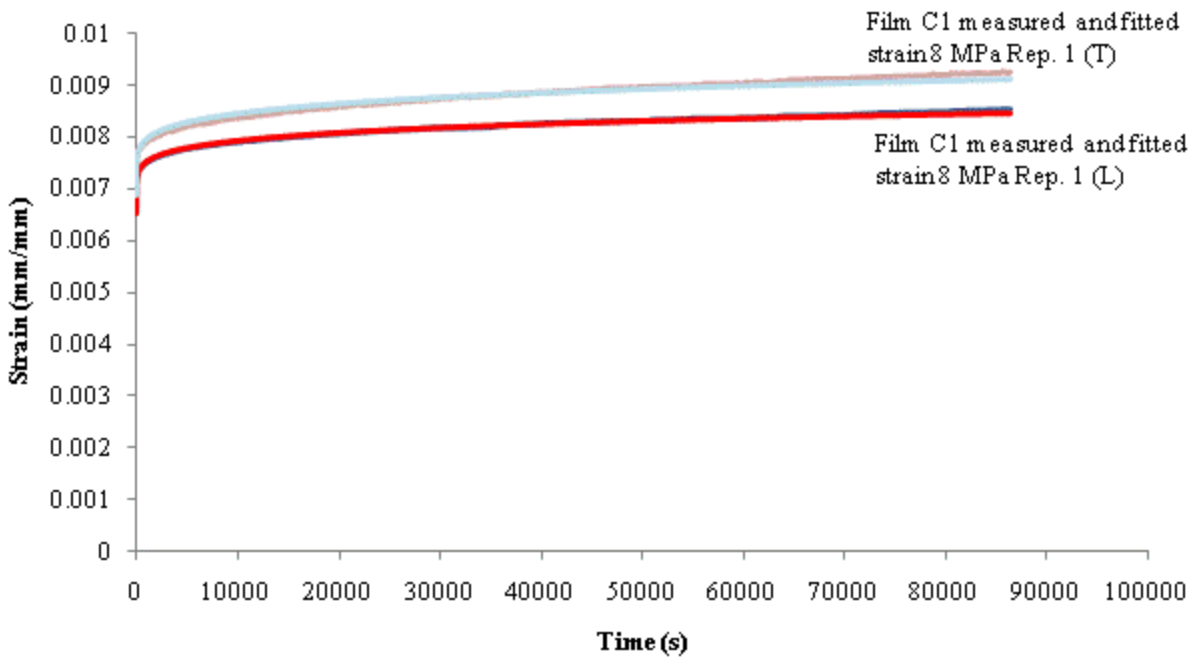

Figure F. 7 - Fitted viscoplastic strain curves for film C1 8 MPa 24 hour tests

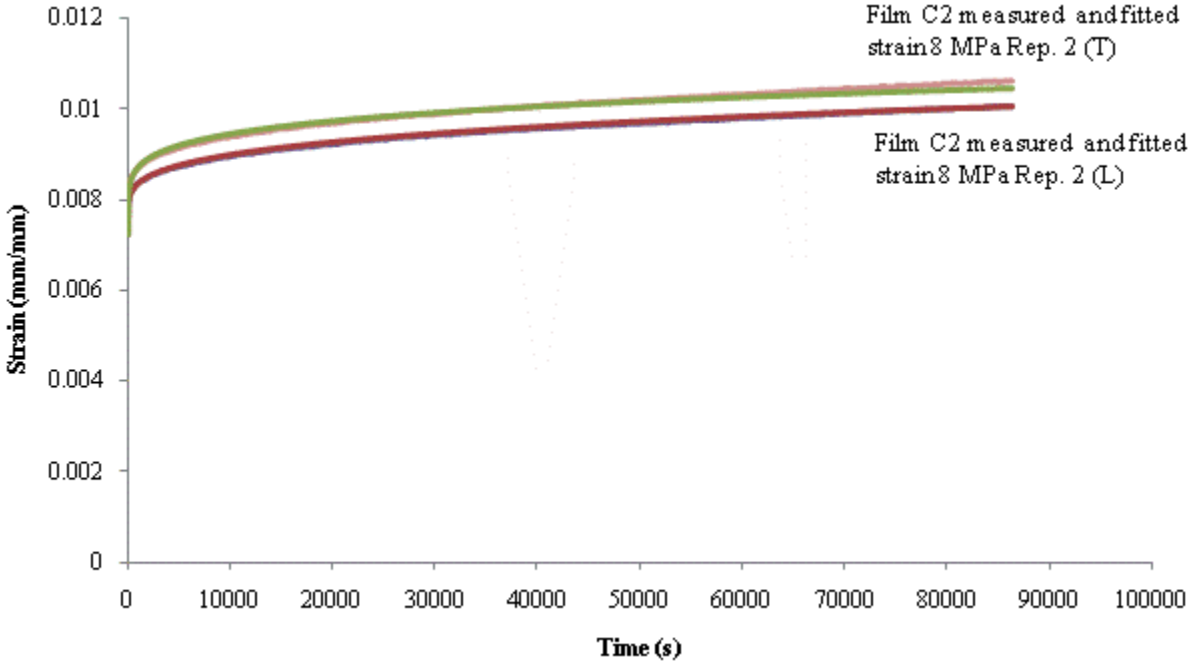

Figure F. 8 - Fitted viscoplastic strain curves for film C2 8 MPa 24 hour tests

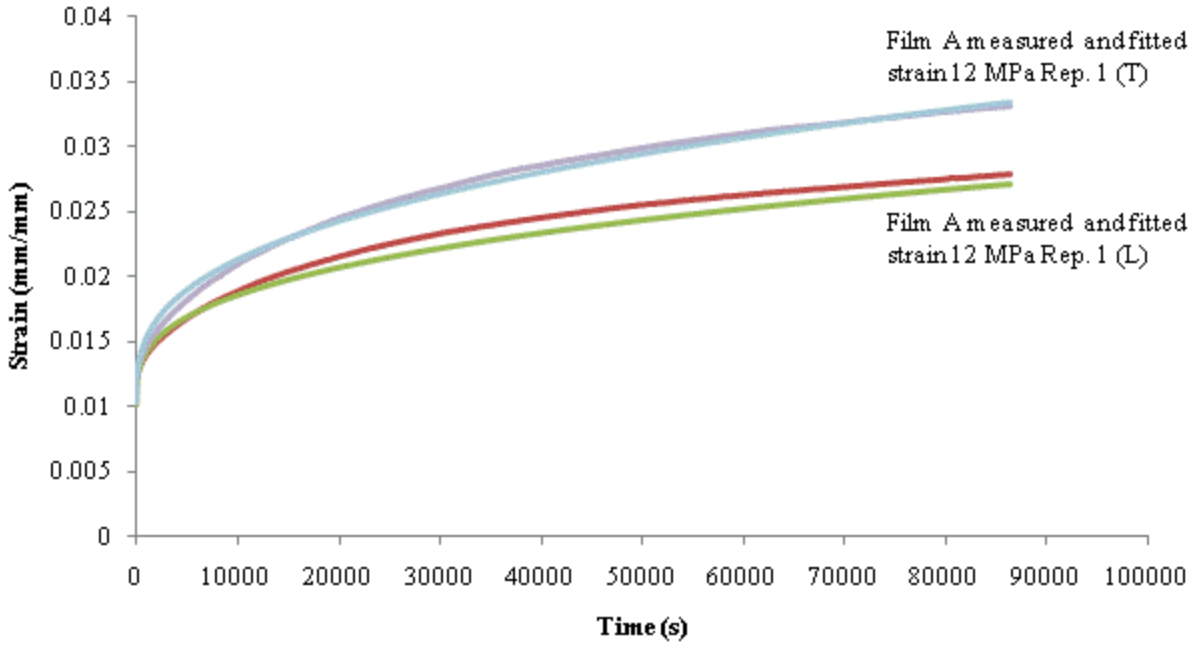

Figure F. 9 - Fitted viscoplastic strain curves for film A 12 MPa 24 hour tests

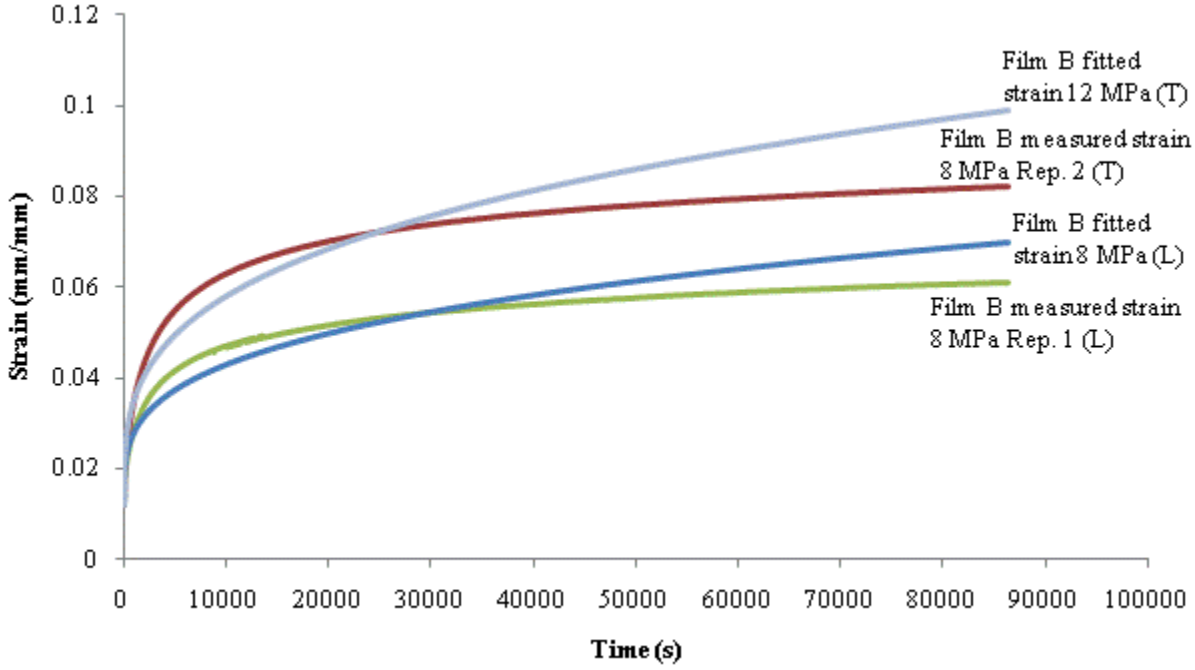

Figure F. 10 - Fitted viscoplastic strain curves for film B 12 MPa 24 hour tests

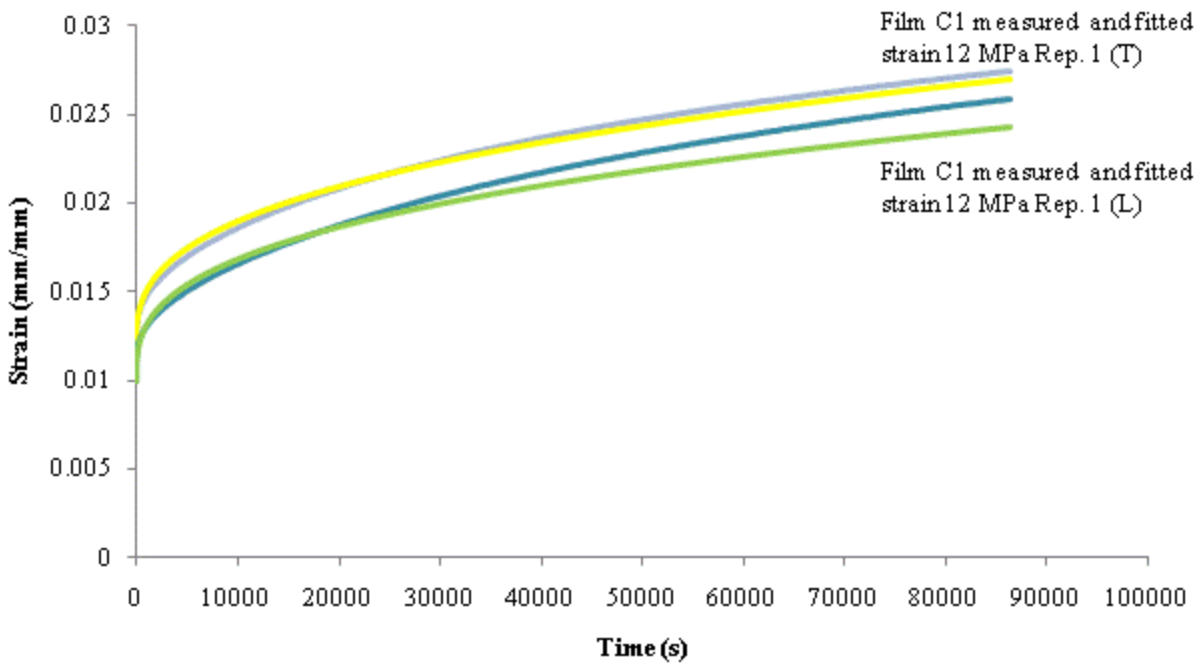

Figure F. 11 - Fitted viscoplastic strain curves for film C1 12 MPa 24 hour tests

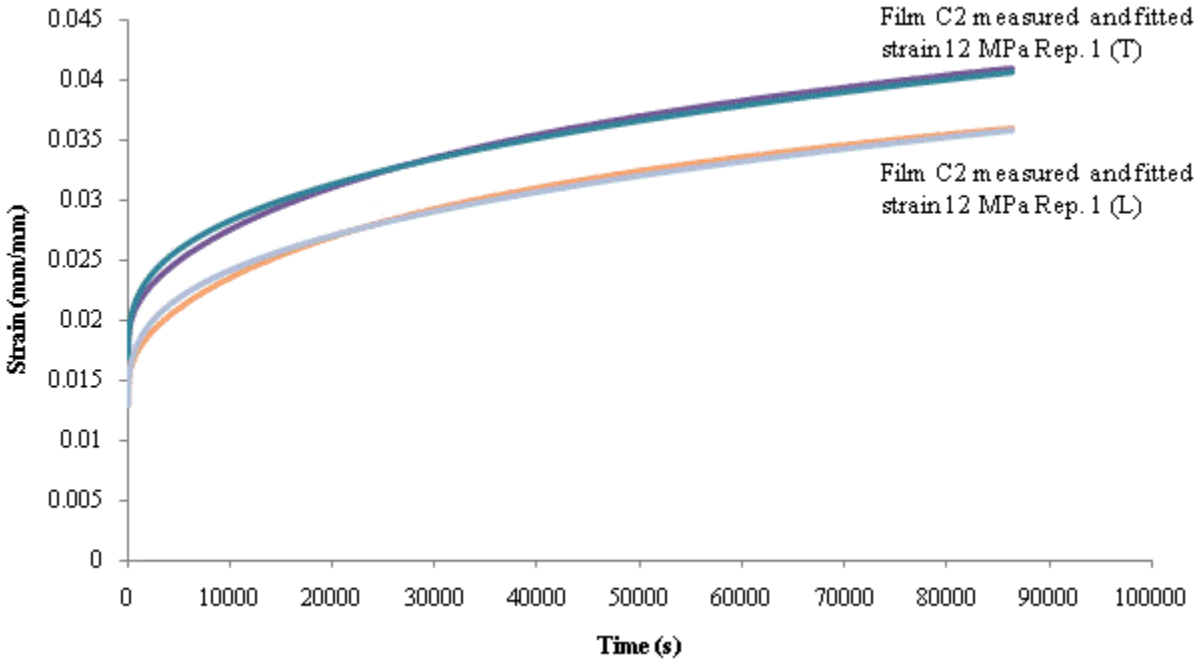

Figure F. 12 - Fitted viscoplastic strain curves for film C2 12 MPa 24 hour tests

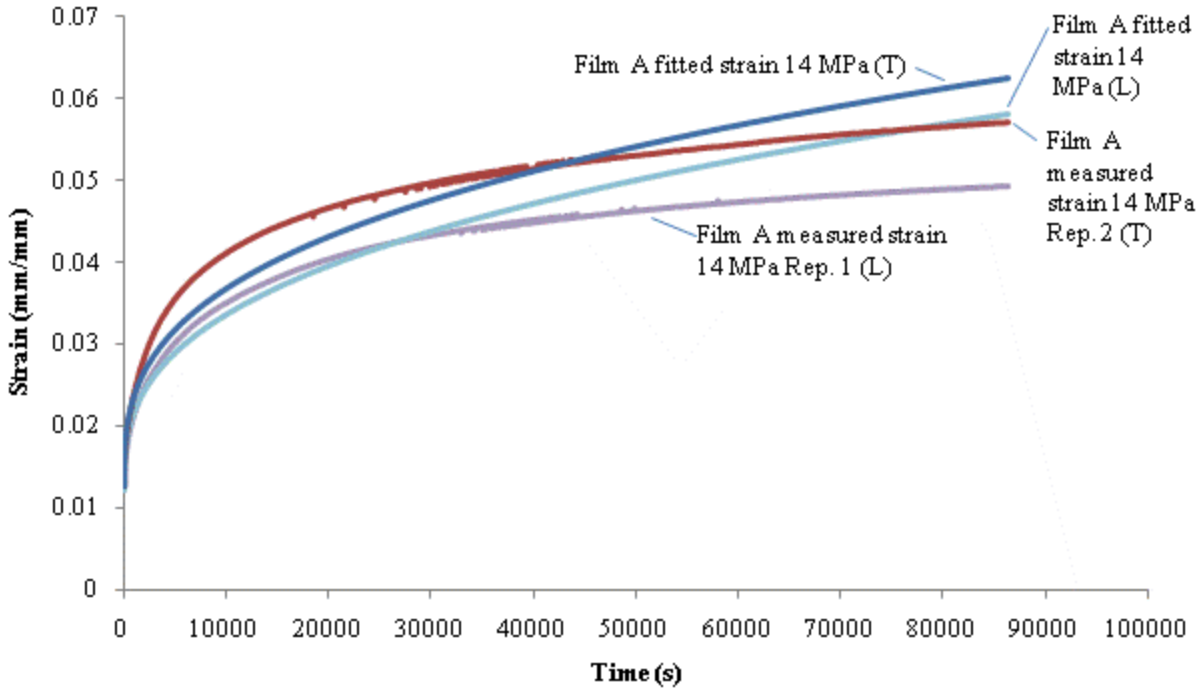

Figure F. 13 - Fitted viscoplastic strain curves for film A 14 MPa 24 hour tests

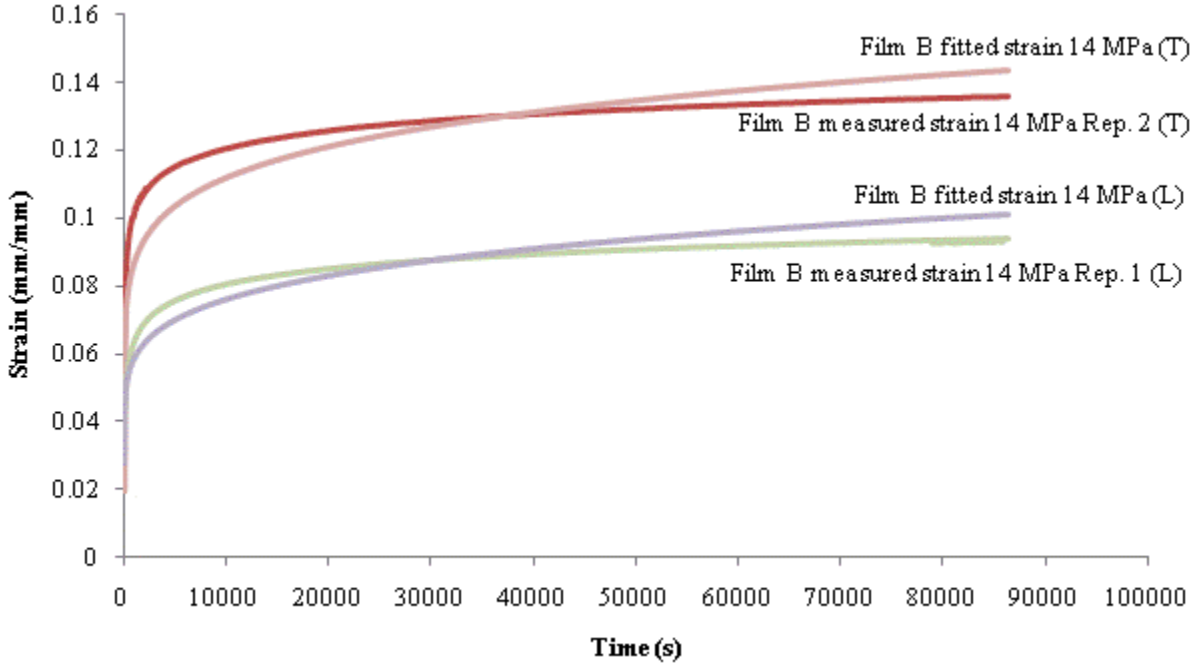

Figure F. 14 - Fitted viscoplastic strain curves for film B 14 MPa 24 hour tests

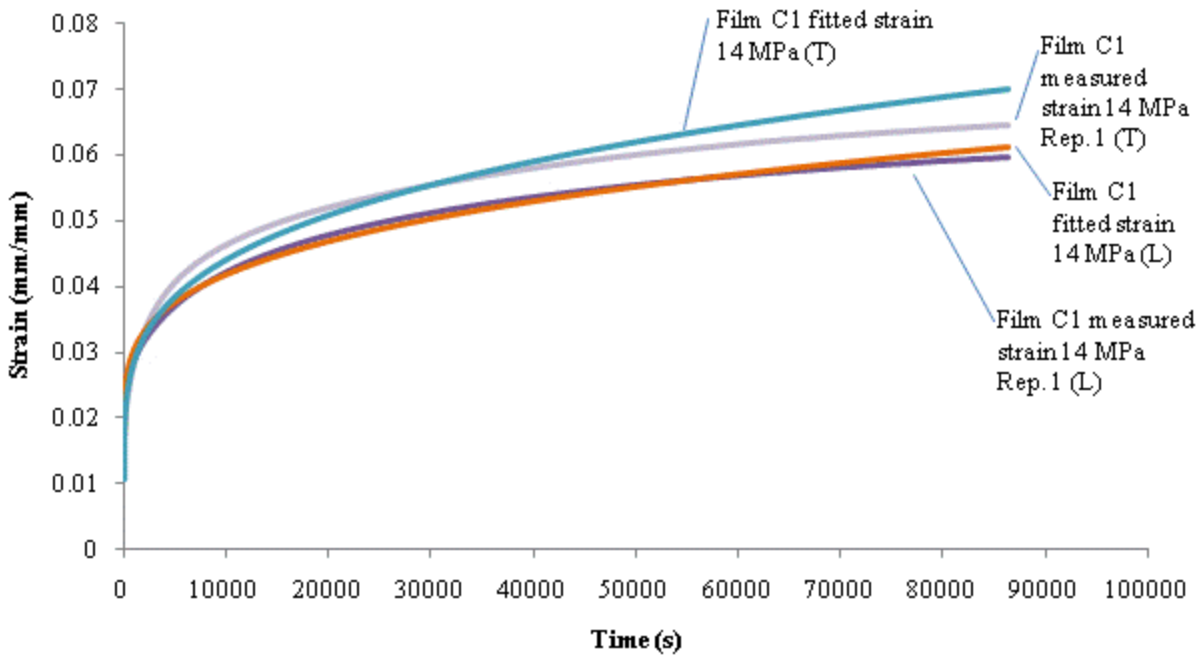

Figure F. 15 - Fitted viscoplastic strain curves for film C1 14 MPa 24 hour tests

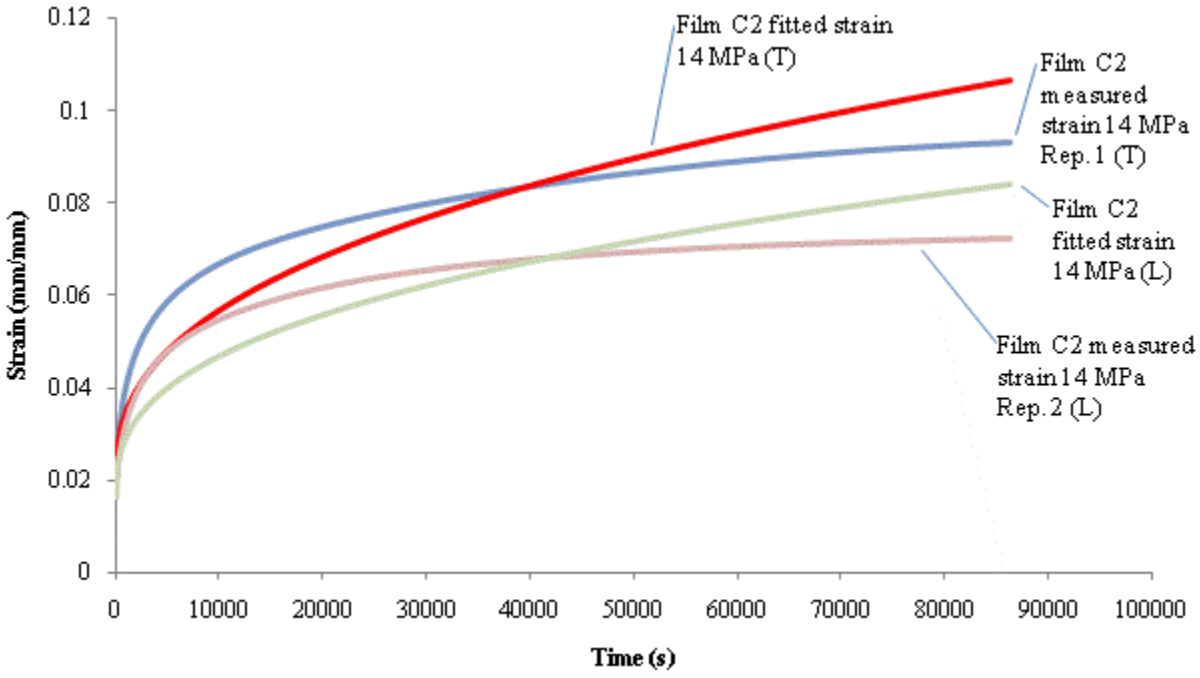

Figure F. 16 - Fitted viscoplastic strain curves for film C2 14 MPa 24 hour tests

Appendix G – Example of Viscoelastic Curve-Fitting Procedure

As an example, the viscoelastic fitting procedure will be shown for rep. 2 of the 8 MPa transverse tests on film C2. The data acquisition system returned the raw data in a text file which was imported into Excel. Table G. 1 is an excerpt from the start of the test.

Table G. 1 – Excerpt of data from rep. 2 of 8 MPa transverse creep test on film C2

Date	Time	Elapsed Time	CLIPGAUGE RAW
3/28/2011	1:59:25 PM	0.82	0.002
3/28/2011	1:59:26 PM	1.969	0
3/28/2011	1:59:27 PM	2.738	0
3/28/2011	1:59:27 PM	3.617	0
3/28/2011	1:59:28 PM	4.449	0
3/28/2011	1:59:29 PM	5.207	0
3/28/2011	1:59:30 PM	5.977	0
3/28/2011	1:59:31 PM	6.809	0
3/28/2011	1:59:31 PM	7.578	0
3/28/2011	1:59:32 PM	8.348	0
3/28/2011	1:59:33 PM	9.109	0
3/28/2011	1:59:34 PM	9.938	0
3/28/2011	1:59:35 PM	10.707	0
3/28/2011	1:59:35 PM	11.477	0.002
3/28/2011	1:59:36 PM	12.297	0
3/28/2011	1:59:37 PM	13.07	0.002
3/28/2011	1:59:38 PM	13.84	0
3/28/2011	1:59:39 PM	14.66	0
3/28/2011	1:59:39 PM	15.43	0
3/28/2011	1:59:40 PM	16.199	0
3/28/2011	1:59:41 PM	17.02	0
3/28/2011	1:59:42 PM	17.789	0
3/28/2011	1:59:42 PM	18.559	0
3/28/2011	1:59:43 PM	19.387	0
3/28/2011	1:59:44 PM	20.148	0.042
3/28/2011	1:59:45 PM	20.918	-0.007
3/28/2011	1:59:46 PM	21.688	0.059
3/28/2011	1:59:46 PM	22.52	0.896
3/28/2011	1:59:48 PM	24.047	0.952
3/28/2011	1:59:49 PM	24.82	0.954
3/28/2011	1:59:50 PM	25.648	0.959
3/28/2011	1:59:50 PM	26.418	0.962
3/28/2011	1:59:51 PM	27.18	0.964
3/28/2011	1:59:52 PM	27.949	0.967

The start of the data was then graphed so that the point where the initial elastic response of the material ends could be determined.

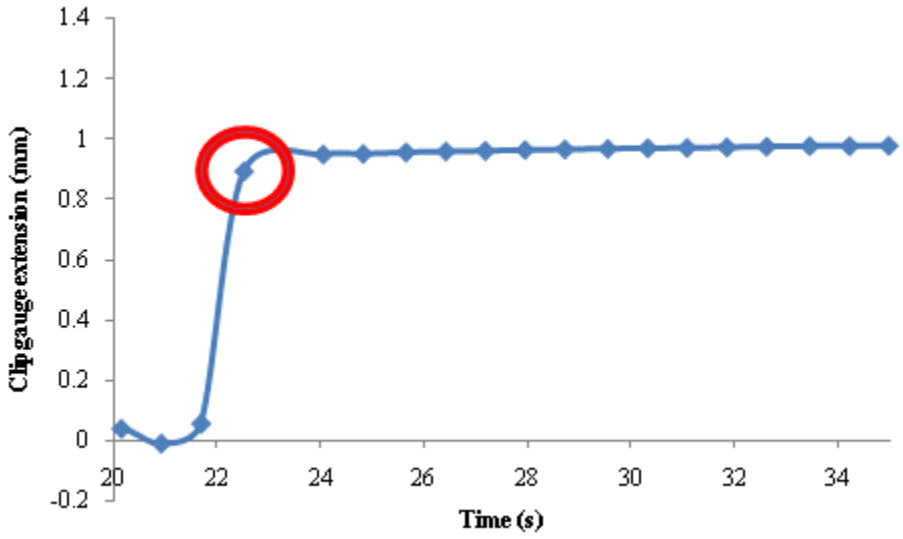

Figure G. 1 – Start of data for rep. 2 of 8 MPa transverse creep test on film C2

On this curve it can easily be identified as the point inside the circle, (22.52, 0.896). The time scale is then normalized to this point, setting it to (0, 0.896). The engineering strain is then calculated for each data point using the clipgauge extension and the original gauge length, 124 mm in this case. The creep compliance is then calculated for each point by dividing the strain by the stress. The compliance at t=0 is x_0, equivalent to $1/E_0$. Table G. 2 shows the initial few seconds of strain.

Table G. 2 – Strain and compliance for first few seconds of strain from rep. 2 of 8 MPa transverse creep test on film C2

Date	Time	Elapsed Time	CLIPGAGE RAW		gauge length		
					124		
					strain	compliance	xo
3/28/2011	1:59:46 PM	0	0.896		0.007226	0.000903226	0.000903
3/28/2011	1:59:48 PM	1.527	0.952		0.007677	0.000959677	
3/28/2011	1:59:49 PM	2.3	0.954		0.007694	0.000961694	
3/28/2011	1:59:50 PM	3.128	0.959		0.007734	0.000966734	
3/28/2011	1:59:50 PM	3.898	0.962		0.007758	0.000969758	
3/28/2011	1:59:51 PM	4.66	0.964		0.007774	0.000971774	
3/28/2011	1:59:52 PM	5.429	0.967		0.007798	0.000974798	
3/28/2011	1:59:53 PM	6.199	0.969		0.007815	0.000976815	
3/28/2011	1:59:53 PM	7.027	0.971		0.007831	0.000978831	
3/28/2011	1:59:54 PM	7.8	0.973		0.007847	0.000980847	
3/28/2011	1:59:55 PM	8.558	0.974		0.007855	0.000981855	

From this data, the A and F matrices can be calculated. Each individual Aij entry in the A matrix is calculated as the following equation summed up for all points in time.

$$A_{ij(tp=1,\ldots,86400s)} = \sigma_C \left[1 - \exp\left(-\frac{t_p}{\tau_j}\right)\right]\left[1 - \exp\left(-\frac{t_p}{\tau_i}\right)\right], i, j = 1, \ldots, N$$

Each individual Fi entry in the F matrix is calculated as the following equation added summed for all points in time.

$$F_i = \left(\hat{\varepsilon}_p - \frac{\sigma_C}{E_0}\right)\left[1 - \exp\left(-\frac{t_p}{\tau_i}\right)\right], i = 1, \ldots, N$$

The corresponding table of values appears in Table G. 3, split over the next two pages. Again, only the first portion of the test is shown. The sum of each Aij or Fi column was taken and the value was input into an A or F matrix, shown below.

$$A := \begin{pmatrix} 16900.23029 & 14230.0729 & 10672.01085 & 2631.131116 \\ 14230.0729 & 13104.34462 & 10589.64997 & 2626.920775 \\ 10672.01085 & 10589.64997 & 9934.792425 & 2569.89077 \\ 2631.131116 & 2626.920775 & 2569.89077 & 762.2151372 \end{pmatrix}$$

$$F := \begin{pmatrix} 4.816799534 \\ 4.423546051 \\ 3.770011609 \\ 0.987766214 \end{pmatrix}$$

The x matrix is found by multiplying A^{-1}*F. In this case it is as follows.

$$x = \begin{pmatrix} 1.199 \times 10^{-4} \\ 5.646 \times 10^{-5} \\ 9.918 \times 10^{-5} \\ 3.532 \times 10^{-4} \end{pmatrix}$$

Each xi values is then used to calculate the corresponding Ei value (1/xi). These values are then used to calculate the portion of the following equation inside the summation.

$$\varepsilon(t) = \sigma_C \left\{\frac{1}{E_0} + \sum_{i=1}^{N} \frac{1}{E_i}\left[1 - \exp\left(-\frac{t}{\tau_i}\right)\right]\right\}$$

They are then added and input into the equation to find strain. These results are shown in Table G. 4.

Table G. 3 - A and F matrix calculations

	N=4														i	j
	i	j	i	j	i	j	i	j	i	j	i	j	i	j	3	1
	1	1	1	2	2	1	2	2	1	3	2	3	3	3	8000	20
τ	20	20	20	400	400	20	400	400	20	8000	400	8000	8000	8000	Aij	Fi
	Aij	Fi	Aij	Fi	Aij	Fi	Aij	Fi	Aij	Fi	Aij	Fi	Aij	Fi	0.00E+00	0.00E+00
	0.00E+00	0.00E+00	0.00E+00	0.00E+00	0.00E+00	0.00E+00	0.00E+00	0.00E+00	0.00E+00	0.00E+00	0.00E+00	0.00E+00	0.00E+00	0.00E+00	1.12E-04	8.62E-08
	4.32E-02	3.32E-05	2.24E-03	3.32E-05	2.24E-03	1.72E-06	1.16E-04	1.72E-06	1.12E-04	3.32E-05	5.82E-06	1.72E-06	2.91E-07	8.62E-08	2.50E-04	1.34E-07
	9.44E-02	5.08E-05	4.98E-03	5.08E-05	4.98E-03	2.68E-06	2.63E-04	2.68E-06	2.50E-04	5.08E-05	1.32E-05	2.68E-06	6.61E-07	1.34E-07	4.53E-04	1.99E-07
	1.68E-01	7.36E-05	9.02E-03	7.36E-05	9.02E-03	3.96E-06	4.85E-04	3.96E-06	4.53E-04	7.36E-05	2.44E-05	3.96E-06	1.22E-06	1.99E-07	6.90E-04	2.59E-07
	2.51E-01	9.43E-05	1.37E-02	9.43E-05	1.37E-02	5.16E-06	7.52E-04	5.16E-06	6.90E-04	9.43E-05	3.78E-05	5.16E-06	1.90E-06	2.59E-07	9.68E-04	3.19E-07
	3.46E-01	1.14E-04	1.93E-02	1.14E-04	1.93E-02	6.35E-06	1.07E-03	6.35E-06	9.68E-04	1.14E-04	5.40E-05	6.35E-06	2.71E-06	3.19E-07	1.29E-03	3.88E-07
	4.52E-01	1.36E-04	2.56E-02	1.36E-04	2.56E-02	7.72E-06	1.45E-03	7.72E-06	1.29E-03	1.36E-04	7.32E-05	7.72E-06	3.68E-06	3.88E-07	1.65E-03	4.56E-07
	5.68E-01	1.57E-04	3.28E-02	1.57E-04	3.28E-02	9.05E-06	1.89E-03	9.05E-06	1.65E-03	1.57E-04	9.53E-05	9.05E-06	4.80E-06	4.56E-07	2.08E-03	5.31E-07
	7.02E-01	1.79E-04	4.13E-02	1.79E-04	4.13E-02	1.05E-05	2.43E-03	1.05E-05	2.08E-03	1.79E-04	1.22E-04	1.05E-05	6.17E-06	5.31E-07	2.52E-03	6.05E-07
	8.34E-01	2.01E-04	4.99E-02	2.01E-04	4.99E-02	1.20E-05	2.98E-03	1.20E-05	2.52E-03	2.01E-04	1.51E-04	1.20E-05	7.60E-06	6.05E-07	2.98E-03	6.73E-07
	9.70E-01	2.19E-04	5.90E-02	2.19E-04	5.90E-02	1.33E-05	3.58E-03	1.33E-05	2.98E-03	2.19E-04	1.81E-04	1.33E-05	9.15E-06	6.73E-07	3.47E-03	7.52E-07
	1.11E+00	2.40E-04	6.87E-02	2.40E-04	6.87E-02	1.49E-05	4.25E-03	1.49E-05	3.47E-03	2.40E-04	2.15E-04	1.49E-05	1.09E-05	7.52E-07	4.00E-03	8.34E-07
	1.26E+00	2.62E-04	7.90E-02	2.62E-04	7.90E-02	1.65E-05	4.97E-03	1.65E-05	4.00E-03	2.62E-04	2.52E-04	1.65E-05	1.27E-05	8.34E-07	4.60E-03	9.25E-07
	1.42E+00	2.85E-04	9.08E-02	2.85E-04	9.08E-02	1.83E-05	5.81E-03	1.83E-05	4.60E-03	2.85E-04	2.94E-04	1.83E-05	1.49E-05	9.25E-07	5.18E-03	9.90E-07
	1.57E+00	3.00E-04	1.02E-01	3.00E-04	1.02E-01	1.95E-05	6.65E-03	1.95E-05	5.18E-03	3.00E-04	3.37E-04	1.95E-05	1.71E-05	9.90E-07	5.77E-03	1.07E-06
	1.72E+00	3.18E-04	1.14E-01	3.18E-04	1.14E-01	2.10E-05	7.52E-03	2.10E-05	5.77E-03	3.18E-04	3.82E-04	2.10E-05	1.94E-05	1.07E-06	6.40E-03	1.13E-06
	1.87E+00	3.32E-04	1.26E-01	3.32E-04	1.26E-01	2.23E-05	8.47E-03	2.23E-05	6.40E-03	3.32E-04	4.30E-04	2.23E-05	2.18E-05	1.13E-06	7.09E-03	1.23E-06
	2.04E+00	3.54E-04	1.39E-01	3.54E-04	1.39E-01	2.42E-05	9.54E-03	2.42E-05	7.09E-03	3.54E-04	4.85E-04	2.42E-05	2.47E-05	1.23E-06	7.76E-03	1.33E-06
	2.19E+00	3.76E-04	1.52E-01	3.76E-04	1.52E-01	2.61E-05	1.06E-02	2.61E-05	7.76E-03	3.76E-04	5.39E-04	2.61E-05	2.74E-05	1.33E-06	8.43E-03	1.40E-06
	2.34E+00	3.89E-04	1.66E-01	3.89E-04	1.66E-01	2.74E-05	1.17E-02	2.74E-05	8.43E-03	3.89E-04	5.95E-04	2.74E-05	3.03E-05	1.40E-06	9.13E-03	1.50E-06
	2.50E+00	4.10E-04	1.79E-01	4.10E-04	1.79E-01	2.94E-05	1.28E-02	2.94E-05	9.13E-03	4.10E-04	6.55E-04	2.94E-05	3.34E-05	1.50E-06	9.84E-03	1.59E-06
	2.65E+00	4.27E-04	1.93E-01	4.27E-04	1.93E-01	3.11E-05	1.41E-02	3.11E-05	9.84E-03	4.27E-04	7.17E-04	3.11E-05	3.66E-05	1.59E-06	1.06E-02	1.66E-06

i	j	i	j	i	j	i	j	i	j	i	j	i	j	i	j
3	2	1	4	2	4	3	4	4	4	4	1	4	2	4	3
8000	400	20	160000	400	160000	8000	160000	160000	160000	160000	20	160000	400	160000	8000
Aij	**Fi**	**Aij**	**Fi**	**Aij**	**Fi**	**Aij**	**Fi**	**Aij**	**Fi**	**Aij**	**Fi**	**Aij**	**Fi**	**Aij**	**Fi**
0.00E+00	0.00E+00	0.00E+00	0.00E+00	0.00E+00	0.00E+00	0.00E+00	0.00E+00	0.00E+00	0.00E+00	0.00E+00	0.00E+00	0.00E+00	0.00E+00	0.00E+00	0.00E+00
5.82E-06	8.62E-08	5.61E-06	3.32E-05	2.91E-07	1.72E-06	1.46E-08	8.62E-08	7.29E-10	4.31E-09	5.61E-06	4.31E-09	2.91E-07	4.31E-09	1.46E-08	4.31E-09
1.32E-05	1.34E-07	1.25E-05	5.08E-05	6.59E-07	2.68E-06	3.31E-08	1.34E-07	1.65E-09	6.72E-09	1.25E-05	6.72E-09	6.59E-07	6.72E-09	3.31E-08	6.72E-09
2.44E-05	1.99E-07	2.26E-05	7.36E-05	1.22E-06	3.96E-06	6.11E-08	1.99E-07	3.06E-09	9.93E-09	2.26E-05	9.93E-09	1.22E-06	9.93E-09	6.11E-08	9.93E-09
3.78E-05	2.59E-07	3.45E-05	9.43E-05	1.89E-06	5.16E-06	9.49E-08	2.59E-07	4.75E-09	1.30E-08	3.45E-05	1.30E-08	1.89E-06	1.30E-08	9.49E-08	1.30E-08
5.40E-05	3.19E-07	4.84E-05	1.14E-04	2.70E-06	6.35E-06	1.36E-07	3.19E-07	6.79E-09	1.60E-08	4.84E-05	1.60E-08	2.70E-06	1.60E-08	1.36E-07	1.60E-08
7.32E-05	3.88E-07	6.45E-05	1.36E-04	3.66E-06	7.72E-06	1.84E-07	3.88E-07	9.21E-09	1.94E-08	6.45E-05	1.94E-08	3.66E-06	1.94E-08	1.84E-07	1.94E-08
9.53E-05	4.56E-07	8.26E-05	1.57E-04	4.77E-06	9.05E-06	2.40E-07	4.56E-07	1.20E-08	2.28E-08	8.26E-05	2.28E-08	4.77E-06	2.28E-08	2.40E-07	2.28E-08
1.22E-04	5.31E-07	1.04E-04	1.79E-04	6.12E-06	1.05E-05	3.08E-07	5.31E-07	1.54E-08	2.66E-08	1.04E-04	2.66E-08	6.12E-06	2.66E-08	3.08E-07	2.66E-08
1.51E-04	6.05E-07	1.26E-04	2.01E-04	7.53E-06	1.20E-05	3.80E-07	6.05E-07	1.90E-08	3.03E-08	1.26E-04	3.03E-08	7.53E-06	3.03E-08	3.80E-07	3.03E-08
1.81E-04	6.73E-07	1.49E-04	2.19E-04	9.06E-06	1.33E-05	4.57E-07	6.73E-07	2.29E-08	3.36E-08	1.49E-04	3.36E-08	9.06E-06	3.36E-08	4.57E-07	3.36E-08
2.15E-04	7.52E-07	1.74E-04	2.40E-04	1.08E-05	1.49E-05	5.43E-07	7.52E-07	2.72E-08	3.76E-08	1.74E-04	3.76E-08	1.08E-05	3.76E-08	5.43E-07	3.76E-08
2.52E-04	8.34E-07	2.00E-04	2.62E-04	1.26E-05	1.65E-05	6.37E-07	8.34E-07	3.19E-08	4.17E-08	2.00E-04	4.17E-08	1.26E-05	4.17E-08	6.37E-07	4.17E-08
2.94E-04	9.25E-07	2.30E-04	2.85E-04	1.47E-05	1.83E-05	7.46E-07	9.25E-07	3.73E-08	4.63E-08	2.30E-04	4.63E-08	1.47E-05	4.63E-08	7.46E-07	4.63E-08
3.37E-04	9.90E-07	2.59E-04	3.00E-04	1.69E-05	1.95E-05	8.55E-07	9.90E-07	4.28E-08	4.95E-08	2.59E-04	4.95E-08	1.69E-05	4.95E-08	8.55E-07	4.95E-08
3.82E-04	1.07E-06	2.89E-04	3.18E-04	1.91E-05	2.10E-05	9.69E-07	1.07E-06	4.85E-08	5.34E-08	2.89E-04	5.34E-08	1.91E-05	5.34E-08	9.69E-07	5.34E-08
4.30E-04	1.13E-06	3.20E-04	3.32E-04	2.15E-05	2.23E-05	1.09E-06	1.13E-06	5.47E-08	5.67E-08	3.20E-04	5.67E-08	2.15E-05	5.67E-08	1.09E-06	5.67E-08
4.85E-04	1.23E-06	3.55E-04	3.54E-04	2.43E-05	2.42E-05	1.23E-06	1.23E-06	6.18E-08	6.16E-08	3.55E-04	6.16E-08	2.43E-05	6.16E-08	1.23E-06	6.16E-08
5.39E-04	1.33E-06	3.88E-04	3.76E-04	2.70E-05	2.61E-05	1.37E-06	1.33E-06	6.87E-08	6.65E-08	3.88E-04	6.65E-08	2.70E-05	6.65E-08	1.37E-06	6.65E-08
5.95E-04	1.40E-06	4.22E-04	3.89E-04	2.98E-05	2.74E-05	1.52E-06	1.40E-06	7.59E-08	6.99E-08	4.22E-04	6.99E-08	2.98E-05	6.99E-08	1.52E-06	6.99E-08
6.55E-04	1.50E-06	4.57E-04	4.10E-04	3.28E-05	2.94E-05	1.67E-06	1.50E-06	8.36E-08	7.50E-08	4.57E-04	7.50E-08	3.28E-05	7.50E-08	1.67E-06	7.50E-08
7.17E-04	1.59E-06	4.93E-04	4.27E-04	3.59E-05	3.11E-05	1.83E-06	1.59E-06	9.17E-08	7.94E-08	4.93E-04	7.94E-08	3.59E-05	7.94E-08	1.83E-06	7.94E-08
7.87E-04	1.66E-06	5.32E-04	4.40E-04	3.94E-05	3.26E-05	2.01E-06	1.66E-06	1.01E-07	8.33E-08	5.32E-04	8.33E-08	3.94E-05	8.33E-08	2.01E-06	8.33E-08

Table G. 4 - Strain calculations

i			**i**			**i**			**i**			
1			2			3			4			
20			400			8000			160000			
xi	**Ei**	**inside Σ**	**xi**	**Ei**	**inside Σ**	**xi**	**Ei**	**inside Σ**	**xi**	**Ei**	**inside Σ**	**εj**
0.00012	8340.284	0	0.00005646	17711.6543	0	9.92E-05	10082.68	0	0.0003532	2831.257078	0	0.007226
		8.81362E-06			2.15125E-07			1.89292E-08			3.37084E-09	0.007298
		1.30252E-05			3.23713E-07			2.85102E-08			5.07721E-09	0.007333
		1.73595E-05			4.39795E-07			3.87718E-08			6.90499E-09	0.007369
		2.12323E-05			5.47531E-07			4.83137E-08			8.60473E-09	0.007401
		2.49208E-05			6.53942E-07			5.77555E-08			1.02868E-08	0.007431
		2.85034E-05			7.61126E-07			6.72832E-08			1.19843E-08	0.007461
		3.19553E-05			8.68244E-07			7.68223E-08			1.3684E-08	0.007489
		3.55219E-05			9.832E-07			8.7079E-08			1.55118E-08	0.007519
		3.87209E-05			1.0903E-06			9.66534E-08			1.72181E-08	0.007545
		4.174E-05			1.19513E-06			1.06041E-07			1.88913E-08	0.00757
		4.4692E-05			1.30141E-06			1.15576E-07			2.0591E-08	0.007595
		4.75288E-05			1.40735E-06			1.25099E-07			2.22884E-08	0.007618
		5.04777E-05			1.52174E-06			1.354E-07			2.41249E-08	0.007643
		5.30997E-05			1.6274E-06			1.44932E-07			2.58246E-08	0.007665
		5.5584E-05			1.73121E-06			1.54315E-07			2.74978E-08	0.007686
		5.80224E-05			1.83687E-06			1.63883E-07			2.9204E-08	0.007706
		6.05318E-05			1.94982E-06			1.74131E-07			3.10317E-08	0.007727
		6.27741E-05			2.05465E-06			1.8366E-07			3.27313E-08	0.007746
		6.49069E-05			2.15806E-06			1.93076E-07			3.4411E-08	0.007764
		6.69839E-05			2.26249E-06			2.02603E-07			3.61106E-08	0.007782
		6.89799E-05			2.36659E-06			2.12117E-07			3.7808E-08	0.007799
		7.10474E-05			2.47858E-06			2.22372E-07			3.96379E-08	0.007816

Appendix H – Example of Viscoplastic Curve-Fitting Procedure

The data for rep. 2 of the 8 MPa transverse tests on film C2 will again be used as an example. For the viscoplastic curve-fitting the data was normalized in time to the end of the elastic response in the same manner as for the viscoelastic procedure. The strain, compliance and x_0 were all also found in the same manner. The ln(t) values were then calculated, as were the $\ln(\varepsilon/\sigma - x_0)$ value. These two values were then plotted against each other, with ln(t) on the horizontal axis. A linear trendline was fitted to the resulting curve, shown below.

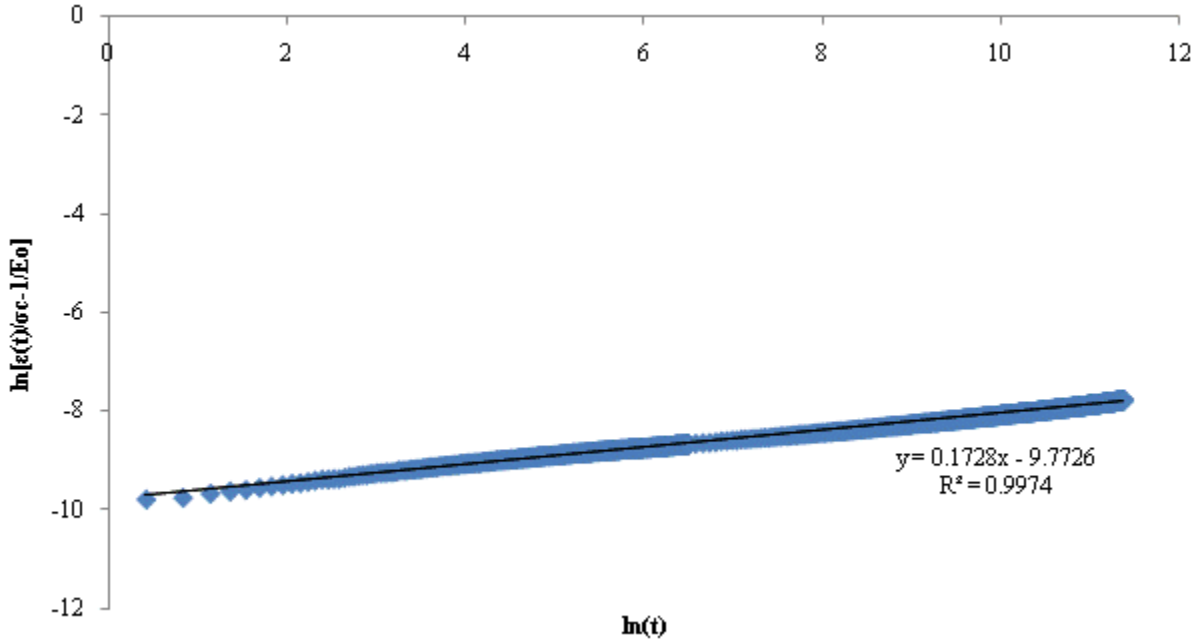

Figure H. 1 – ln(t) vs. $\ln(\varepsilon/\sigma - x_0)$, with linear trendline

The x-intercept, -9.7726, was taken as $\ln C_0$ and the slope, 0.1728, was taken as C_1. These values were input into the following equation for strain, which was used to develop the fitted viscoplastic curve.

$$\varepsilon(t) = \frac{\sigma_C}{E_0} + \sigma_C C_0 t^{C_1}$$